UNIVERSIDADE FEDERAL DE PERNAMBUCO
CENTRO DE TECNOLOGIA E GEOCIÊNCIAS
DEPARTAMENTO DE ENGENHARIA MECÂNICA
PROGRAMA DE PÓS-GRADUAÇÃO EM ENGENHARIA MECÂNICA

LARISSA DE FÁTIMA CHAVES PEREIRA

MULTIPHYSICS SIMULATION AND OPTIMIZATION OF THE CURING PROCESS OF THICK THERMOSETTING EPOXY SAMPLES: multi-objective genetic algorithm and a conversion rate driven approach

Recife
2022

LARISSA DE FÁTIMA CHAVES PEREIRA

MULTIPHYSICS SIMULATION AND OPTIMIZATION OF THE CURING PROCESS OF THICK THERMOSETTING EPOXY SAMPLES: multi-objective genetic algorithm and a conversion rate driven approach

Dissertation presented to the Graduate Program in Mechanical Engineering of Universidade Federal de Pernambuco in partial fulfillment of the requirements for the degree of Master of Science in Mechanical Engineering.

Area of concentration: Materials Engineering and Manufacturing Processes.

Supervisor: Prof. Dra. Nadège Sophie Bouchonneau da Silva.

Co-supervisor: Prof. Dr.-Ing. Habil Christian Jochum.

Recife

2022

Catalogação na fonte:
Bibliotecária Sandra Maria Neri Santiago, CRB-4 / 1267

P436m Pereira, Larissa de Fátima Chaves.
Multiphysics simulation and optimization of the curing process of thick thermosetting epoxy samples: multi-objective genetic algorithm and a conversion rate driven approach / Larissa de Fátima Chaves Pereira. – 2022.
201 f.: il., figs., tabs.

Orientadora: Prof. Dra. Nadège Sophie Bouchonneau da Silva.
Orientador: Prof. Dr. Christian Jochum.
Dissertação (Mestrado) – Universidade Federal de Pernambuco. CTG. Programa de Pós-Graduação em Engenharia Mecânica. Recife, 2022.
Inclui referências, apêndices e anexos.

1. Engenharia mecânica. 2. Termofixos. 3. Processo de cura. 4. Elementos finitos. 5. Otimização. 6. Estratégia impulsionada pela taxa de conversão. 7. Algoritmo genético multi-objetivo. I. Silva, Nadège Sophie Bouchonneau da (Orientadora). II. Jochum, Christian (Coorientador). III. Título.

UFPE

621 CDD (22. ed.) BCTG/2022-354

LARISSA DE FÁTIMA CHAVES PEREIRA

MULTIPHYSICS SIMULATION AND OPTIMIZATION OF THE CURING PROCESS OF THICK THERMOSETTING EPOXY SAMPLES: multi-objective genetic algorithm and a conversion rate driven approach

Dissertation presented to the Graduate Program in Mechanical Engineering of Universidade Federal de Pernambuco, Centro de Tecnologia e Geociências, in partial fulfillment of the requirements for the degree of Master of Science in Mechanical Engineering.

Area of concentration: Materials Engineering and Manufacturing Processes.

Approved in: 08/29/2022.

EXAMINATION BOARD

_____
Profa. Dra. Nadège Sophie Bouchonneau da Silva (Supervisor)
Universidade Federal de Pernambuco

_____
Prof. Dr.-Ing. Habil Christian Jochum (Co-supervisor)
École Nationale Supérieure de Techniques Avancées Bretagne

_____
Profa. Dra. Dayanne Diniz de Souza Morais (Internal Examiner)
Universidade Federal de Pernambuco

_____
Prof. Dr. Renato de Siqueira Motta (External Examiner)
Universidade Federal de Pernambuco

ACKNOWLEDGEMENTS

Firstly, to my parents, who always offered me unconditional love and all the support necessary for my development in every aspect of my life.

To my supervisor and co-supervisor, for the wonderful opportunity to be part of their research team, even in the adverse conditions experienced during the covid-19 pandemic season, without the possibility to meet in person and, thus, with the need to conduct all the research meetings online in different time zones. I really appreciate all the guidance and words of encouragement they gave me during my graduate research study. I should also thank them for always being understanding of my time restrictions due to my job at UFPE as a Mechanical Engineer. It was a pleasure to have such kind and knowledgeable Professors as my supervisors.

To my defense committee, for accepting to contribute to this research work even with short deadlines. I know that time is a scarce resource nowadays and, for that reason, I am grateful for the time they devoted to evaluate this work.

To my fellow graduates, for the fruitful discussions and the incentive they provided me throughout my academic journey.

To the *Coordenação de Aperfeiçoamento de Pessoal de Nível Superior* (CAPES), for the financial support provided during the first months of my graduate course.

Lastly, I am grateful to everyone who helped in some way to conduct this research and to face the challenges I have encountered in the way.

ABSTRACT

Over the last decades, due to higher specific strength and stiffness, low weight, and good resistance to corrosion, thermoset resin composite materials have been replacing conventional materials in aerospace, maritime, automotive and several other high performance engineering applications. These composites are usually produced in an autoclave by carrying out a cure schedule to crosslink the resin. However, for the case of thick thermosets, the manufacturer's recommended cure (MRC) schedule cannot be followed, once it is generally intended to thin parts. When applied to thick components, the MRC schedule usually results in cures either that are unnecessarily too long or that overheat the material internally, due to the thermoactived and exothermic aspects of the curing reaction associated to the thermal insulating property of the thermoset. This local overheating results in high gradients in the thermoset properties during the cure that may create residual stresses and structural defects, such as bubbles and cracks. To avoid this and find optimal cure schedules, this work simulated the cure process of a thermoset using the finite element software COMSOL Multiphysics and implemented two optimization methods in MATLAB, connected to the simulations via the COMSOL LiveLink for MATLAB. The first method is an authorial conversion rate driven (CRD) strategy based on cure kinetics, which has a single objective: minimize the cure time. The second one is a multi-objective genetic algorithm (GA) with three conflicting objectives: minimize cure time, minimize the gradient of degree of cure after gel point (AGP) and minimize the gradient of temperature AGP, reflecting the existing trade-off between manufacturing speed and product quality. As constraints for both methods, the minimum degree of cure in the final cured part was set as 0.854, in order to achieve the same material properties achieved by the MRC schedule; and the maximum temperature inside the composite during the cure was limited to 155°C, to avoid material degradation. Both methods searched for optimal two-step cure schedules with a constant heating rate of 3°C/min. The decision variables for the GA optimization and CRD strategy were the first and second plateau temperatures and the duration of the first plateau. The free MATLAB-based software package GOSET was used as the basis to execute an elitist GA, with 20 generations and 50 individuals per generation. The thermoset polymer selected for the study was the LY-556 epoxy resin system, cured in a cylindrical geometry with a height of 60 mm and a diameter of 32 mm. It was found that, in comparison to the MRC schedule, the CRD strategy and GA reduced the cure time by almost the same amount: 87% and 88%, respectively; whereas the gradients of degree of cure and temperature AGP were reduced by the GA by 6%

and 31%, respectively. Thus, the methods presented in this work were shown to be effective tools to optimize the cure schedule of thermosets, depending on the objective selected.

Keywords: thermosets; curing process; finite element; optimization; conversion rate driven strategy; multi-objective genetic algorithm.

RESUMO

Ao longo das últimas décadas, devido à maior resistência e rigidez específicas, baixo peso e boa resistência à corrosão, os materiais compósitos de resina termofixa vêm substituindo os materiais convencionais em aplicações aeroespaciais, marítimas, automotivas e diversas outras aplicações de engenharia de alto desempenho. Esses compósitos geralmente são produzidos em autoclave, executando-se um cronograma de cura para reticulação da resina. No entanto, para o caso de termofixos espessos, o perfil de cura recomendado pelo fabricante (PCRF) não pode ser seguido, uma vez que geralmente é destinado a peças finas. Quando aplicado a componentes espessos, o PCRF geralmente resulta em curas desnecessariamente muito longas ou que superaquecem o material internamente, devido às características exotérmica e termoativada da reação de cura associadas à propriedade isolante térmica do polímero termofixo. Esse superaquecimento local resulta em altos gradientes nas propriedades do termofixo durante a cura que podem criar tensões residuais e defeitos estruturais, como bolhas e rachaduras. Para evitar isso e encontrar cronogramas de cura ótimos, este trabalho simulou o processo de cura de um termofixo usando o software de elementos finitos COMSOL Multiphysics e implementou dois métodos de otimização no MATLAB, conectados às simulações via COMSOL LiveLink for MATLAB. O primeiro método é uma estratégia autoral impulsionada pela taxa de conversão (ITC), que se baseia na cinética de cura e tem um único objetivo: minimizar o tempo de cura. O segundo é um algoritmo genético (AG) multi-objetivo com três objetivos conflitantes: minimizar o tempo de cura, minimizar o gradiente de grau de cura após o ponto de gel (APG) e minimizar o gradiente de temperatura APG, refletindo o conflito existente entre velocidade de fabricação e qualidade do produto. Como restrições para ambos os métodos, o grau mínimo de cura na peça final curada foi fixado em 0,854, a fim de alcançar as mesmas propriedades do material alcançadas pelo PCRF; e a temperatura máxima no interior do termofixo durante a cura foi limitada a 155°C, para evitar a degradação térmica do material. Ambos os métodos buscaram perfis de cura de duas etapas com uma taxa de aquecimento constante de 3°C/min. As variáveis de decisão para o AG e estratégia ITC foram as temperaturas do primeiro e do segundo platô e a duração do primeiro platô. O pacote de software gratuito GOSET, baseado em MATLAB, foi utilizado como base para executar um AG elitista, com 20 gerações e 50 indivíduos por geração. O polímero termofixo selecionado para o estudo foi o sistema de resina epóxi LY-556, curado em geometria cilíndrica com altura de 60 mm e diâmetro de 32 mm. Verificou-se que, em comparação com o ciclo de cura recomendado pelo fabricante, a estratégia ITC e o AG reduziram o tempo de cura em quase a

mesma quantidade: 87% e 88%, respectivamente; enquanto que os gradientes de grau de cura e temperatura APG foram reduzidos pelo AG em 6% e 31%, respectivamente. Assim, os métodos apresentados neste trabalho mostraram-se ferramentas eficazes para otimizar o perfil de cura de materiais termofixos, dependendo do objetivo selecionado.

Palavras-chave: termofixos; processo de cura; elementos finitos; otimização; estratégia impulsionada pela taxa de conversão; algoritmo genético multi-objetivo.

LIST OF FIGURES

LIST OF TABLES

CONTENTS

1 INTRODUCTION

In many applications, plastics and composites are taking the place of conventional structural metals like steel and aluminum (ANDERSON, 2005; RATNA, 2009). Engineering plastics have a variety of advantages, such as corrosion resistance and low cost, while composites provide excellent strength-to-weight ratios and allow for the creation of materials with specific mechanical and thermal properties.

Over the past decades, there has been a significant increase in the use of polymer matrix composites (PMC), particularly fiber-reinforced plastic (FRP) composites, and this trend is expected to continue (RATNA, 2009; GOODMAN & DODIUK, 2014; COHERENT MARKET INSIGHTS, 2022). Thermoset resin composites, particularly, have been widely used in a variety of field, including civil infrastructure, the automotive, aerospace, and renewable energy sectors (STRUZZIERO et al., 2019; DAI et al., 2019; TEIJIN CARBON, 2022). Several advantages, such as accessibility, good flow properties and low material cost, make thermoset resins be the predominant material in the composite industries (RATNA, 2009).

Thermoset polymers are materials that undergo a chemical reaction called "curing", which transforms them into an insoluble and infusible substance. The infusibility and insolubility of the cured polymer are induced by the formation of a three-dimensional network structure. Thermosets cannot be resoftened by heat once they have fully cured. A resin cures as a result of an exothermic and thermoactived reaction (BLEST et al., 1999; CIRISCIOLI et al., 1991; PITCHUMANI & YAO, 1993; HOJJATI & HOA, 1994; SURATNO et al., 1998 apud STRUZZIERO et al., 2019; PAIVA, 2018). All polymers are naturally thermal insulators, so the exothermic heat cannot easily escape the curing mass during the reaction, increasing the heat input and the temperature of the inner parts of the composite (GOODMAN & DODIUK, 2014; PAIVA, 2018). When the thermoset is thick (i.e. thickness larger than 10 mm), the mass effect is stronger, which results in high internal gradients of temperature and degree of cure within the curing material. Those strong internal property gradients can result in defects like bubbles, cracks, and wavy fibers that will reduce the product's mechanical performance (PAIVA, 2018). Additionally, defects like matrix deterioration, non-homogeneous curing, and internal residual stress can be seen (YUAN et al., 2021).

Typically, thermoset resin composites are made in an autoclave by applying a cure schedule in order to start and maintain the resin's irreversible crosslinking (GUTOWSKI, 1997 apud ALEKSENDRIĆ et al., 2016; YUAN, 2021). A two-step cure schedule is the typical process cycle for polymer-matrix composites (WHITE & HAHN, 1993), which is the cure schedule usually recommended by the polymer resin manufacturer. In this type of cure schedule, the material's temperature is raised from ambient to the first dwell temperature and then kept constant. The temperature is then increased to the second dwell temperature and kept there. This kind of cure schedule is referred to as a two-step cure schedule because there are two dwell times.

1.1 RESEARCH ISSUE

The thermoset manufacturer usually recommends a cure schedule to produce only thin parts. The manufacturing of thick parts are more challenging due to the potential generation of defects, as previously mentioned. Since the manufacturer's recommended cure schedule seems acceptable for the production of thin components but less successful when dealing with thick work pieces, significant research works have been focusing on the adoption of tools that are useful in optimizing the design of the curing process (ALEKSENDRIĆ et al., 2016).

By carefully selecting the temperature profiles, it is possible to optimize cure schedules and create materials that are fully cured with little residual stress (GOPAL et al., 2000; RUIZ & TROCHU, 2006; STRUZZIERO et al., 2019). However, trial and error methods, whether through numerical simulations or experiments, are incredibly inefficient and ineffective when it comes to processing composites due to the complexity of the phenomena involved (STRUZZIERO et al., 2019). For instance, processing at low temperatures would decrease the material's internal gradients and thermally induced stresses. Nevertheless, the degree of the cure affects the material's mechanical properties, and cross-linking cannot begin until a minimum temperature is reached. In addition, longer cure schedules at low temperatures raise the cost of production.

Therefore, it is extremely important to implement a method that optimizes the cure schedule, taking into account many conflicting variables that evolve during the cure process, affecting the material quality and cure time.

1.2 RESEARCH MOTIVATION

In order to meet the demand for the highest possible product quality at the lowest possible production cost, cure simulation (COSTA & SOUSA, 2003; MAWARDI & PITCHUMANI, 2003; CARLONE & PALAZZO, 2009 apud ALEKSENDRIĆ et al., 2016; PAIVA, 2018) and optimization of thick thermosets (CARLONE & PALAZZO, 2013; STRUZZIERO & SKORDOS, 2017; STRUZZIERO & TEUWEN, 2018; TIFKITSIS et al. (2018); DOLKUN et al., 2018; YUAN, 2021) have been the subject of several studies due to the expansion in the use of thermosetting matrix composite materials and the increased geometrical complexity.

Due to its well-known capacity to provide precise and effective predictions of the physical behavior of a component or system subjected to various physical phenomena, the Finite Element Method (FEM) is one of the most used numerical methods that the scientific community has applied to this problem. Based on this method, commercial software has been constantly developed and improved, with a focus on improving the efficiency of material design. This type of software is particularly good at simulating the curing process (PAIVA, 2018).

Among the existing FEM software, COMSOL Multiphysics is one that is designed to run coupled phenomena problems, producing results relatively quickly in these cases. Thus, it has shown to be extremely appropriate for the simulation of the thermochemical phenomenon of the cure (PAIVA, 2018). Besides, COMSOL has very useful modules, like the COMSOL LiveLink for MATLAB®, which allows automatizing all the steps of a simulation model and optimize the process simulated from a script in MATLAB (COMSOL INC., 2019a).

The successful implementation of the cure process of a thermoset resin systems and thermoset composites using a COMSOL model has stimulated the authors to develop of a strategy to find a cure schedule that minimized the cure time, while assuring that the material was not thermally degraded during cure and that the whole part reached a minimum degree of cure required by a given application. This strategy was developed by the authors of the present research, purely based on the kinetics of the cure process. No similar method was found in the literature. The strategy is based on a simple aspect of the cure process: the moment when the average conversion rate within the sample reaches its maximum value. Due to its simplicity, it was thought of as a highly efficient method to minimize the cure time, which could be

implemented manually in COMSOL, or in an automated way using COMSOL LiveLink for MATLAB® to run multiple cure schedules in a single script run (COMSOL INC., 2020).

On the other hand, a literature review on recent optimization methods for engineering problems demonstrated that one of the prevailing trends in composite manufacturing optimization is multi-objective optimization, which takes into account the trade-offs related to this problem (STRUZZIERO et al., 2019). Additionally, due to the complexity of the problem, nature-inspired algorithms are preferred, particularly Evolutionary Algorithms (EAs), such as Genetic Algorithms (GAs), which are able to explore a large portion of the objective space without getting trapped in local minima or maxima (STRUZZIERO et al., 2019). GAs are well suited for multi-objective optimization, due to its population-based approach, meeting the needs of real-world problems with conflicting objectives. In the specific problem of cure optimization, the three conflicting objectives that this work aimed to achieve using the GA, taking into account the trade-off between cure speed and product quality, were: minimize the cure time, minimize the gradient of degree of cure AGP and minimize the gradient of temperature AGP.

Although Genetic Algorithm require high computational resources, this optimization method has received a lot of recent attention from researchers due to the quick advancement of computer technology, which includes the development and accessibility of user-friendly software and fast, parallel processors (SUDHOFF, 2021).

A GA optimization can be performed using different software and programming languages. Among the existing possibilities, the Genetic Optimization System Engineering Tool (GOSET) is one of the most attractive and accessible tools, which is a free MATLAB® based algorithm package for solving single- and multi-objective optimization problems (SUDHOFF, 2014). It is a direct result of three research awards from the Office of Naval Research (ONR) and does not require the use of any additional MATLAB toolboxes (SUDHOFF, 2014). Therefore, through COMSOL LiveLink for MATLAB® and the development of some MATLAB scripts and functions, a multi-objective cure optimization can be successfully performed using a bi-directional link between the COMSOL model and GOSET/MATLAB.

1.3 OBJECTIVES

In this section, the general objective of the present research work is presented and the specific objectives taken in order to achieve it are detailed.

1.3.1 General objective

Simulate and optimize the cure of thick thermosets, providing better solutions than the MRC schedule, in terms of cure time and/or final product quality. Two methods will be used for the optimization: an authorial conversion rate driven (CRD) strategy, which is single-objective, and a multi-objective Genetic Algorithm (GA).

1.3.2 Specific objectives

- Study thermoset characteristics, classifications, curing process and learn how this material has been applied in the composite industry.
- Implement the cure simulation of an epoxy matrix on the FEM software COMSOL Multiphysics based on previous experimental and numerical studies, in order to monitor variables of interest related to the cure optimization (cure time x product quality).
- Simulate the MRC cure schedule to analyze its results and use them a reference for the cure optimization.
- Configure the COMSOL simulation model manually to perform the CRD strategy.
- Learn how to use the module COMSOL LiveLink for MATLAB in order to establish a bidirectional link between the cure simulation model in COMSOL and a code in MATLAB.
- Develop a MATLAB script to automate and run the CRD strategy efficiently in a loop, so that multiple solutions are computed and stored in a single script run.
- Review optimization methods available in literature and compare the efficiency of the results obtained by them for the problem of curing thick thermoset matrices.

- Study multi-objective Evolutionary Algorithms, specifically Genetic Algorithms.
- Study the software package GOSET for GA implementation in MATLAB. Then, develop a MATLAB script and function to initialize the multi-objective GA optimization of the cure schedule and compute the respective fitness values.
- Execute the automated single-objective CRD strategy and the multi-objective GA optimization, storing the solutions obtained.
- Analyze the CRD and GA results, comparing them with each other, with the MRC schedule results and with the literature as well.

2 LITERATURE REVIEW

This literature review presents the essential background of the research in four domains: thermoset polymers; modeling of the cure of thermosets; numerical simulation; optimization; and state of the art. The background outlines the broad assumptions for this research work and reviews the data required to support the work's motivation, while the state of the art summarizes the most recent research in the related fields.

2.1 THERMOSET POLYMERS

Due to advancements in polymer science and technology, polymers have been employed in a variety of applications as replacements for conventional materials (ANDERSON, 2005; RATNA, 2009). This is motivated by their remarkable advantages, such as lightweight, low cost and extensive range of customizable properties (RATNA, 2009).

A polymer (from the Greek poly, meaning many, and meros, meaning part) is a long molecule consisting of many small units (monomers) joined end-to-end (MCCRUM, 1997). The process of synthesizing these large molecules is termed polymerization, and many different types of monomers can be polymerized.

Depending on the method used for polymerization, the final products can be divided into two categories: addition polymers and condensation polymers (CALLISTER, 2007). Addition polymerization is a process by which monomer units are attached one at a time in a chainlike way to form a linear macromolecule. The composition of the molecule formed by the addition reaction is an exact multiple of the initial reactant monomer. Condensation polymerization, on the other hand, is the synthesis of polymers by stepwise intermolecular chemical reactions that may involve more than one monomer species. Usually, a tiny molecular weight byproduct, like water, is eliminated (or condensed). No reactant species has the chemical formula of the repeat unit, and every time the intermolecular reaction takes place, a repeat unit is produced.

Whether produced by a condensation or an addition reaction, the synthesized polymer might be linear, branched or cross-linked, as illustrated by Figure 1. A network polymer is

produced when linear polymer chains interact chemically or when a three-dimensional fish-net configuration is built up from monomeric resinous reactants (GOODMAN & DODIUK, 2014).

Using the biological analogy, thermoset polymers, or thermosets, fit into the family of materials as shown in Figure 2, according to Goodman and Dodiuk (2014).

Instead of being genuine straight lines, linear polymers are made up of carbon atoms that form a single, uninterrupted path from one end of the chain to the other. As the name implies, a branched polymer molecule consists of a number of smaller chains that branch off from a main "backbone", while a cross-linked polymer has a network structure. A highly cross-linked structure is the main distinguishing element of a thermoset polymer.

Figure 1 - Three types of polymer chains: (a) linear polymer, (b) branched polymer, and (c) cross-linked polymer

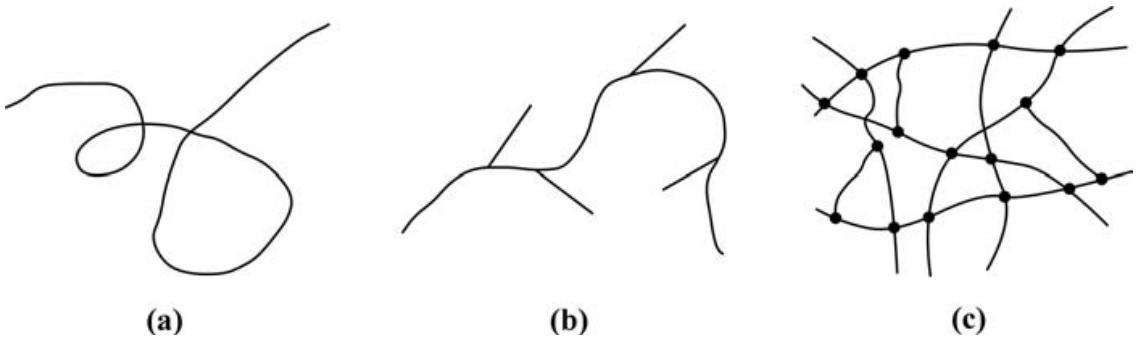

Source: Anderson (2005)

Thermoplastic and thermoset polymers are two categories of synthetic polymers, usually called plastics. The former gets softer with heating and stiffer with cooling. When heated, thermoset polymers go through a chemical reaction known as "curing", which turns them into an insoluble and infusible substance. The creation of a three-dimensional network structure is what causes the infusibility and insolubility of the cured polymer. After being fully cured, thermosets cannot be resoftened by heat. The term "thermo" suggests that heat energy input influences how cross-linking occurs, while the term "setting" denotes the occurrence of an irreversible reaction on a macro scale. A network polymer is produced when linear polymer chains interact chemically or when a three-dimensional fish-net configuration is built up from monomeric resinous reactants (GOODMAN & DODIUK, 2014).

Using the biological analogy, thermoset polymers, or thermosets, fit into the family of materials as shown in Figure 2, according to Goodman and Dodiuk (2014).

Figure 2 - Relationship of thermosets in chemistry

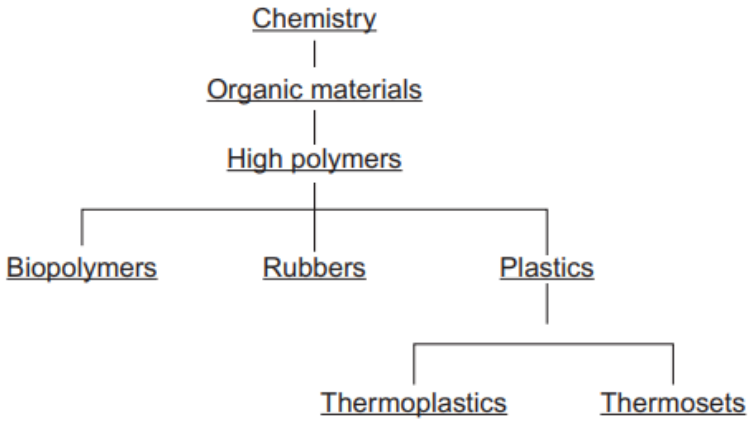

Source: Goodman & Dodiuk (2014)

2.1.1 Classifications

Thermoset polymers can be categorized as general purpose, engineering, and specialty (high-temperature) plastics, as explained below (GOODMAN & DODIUK, 2014):

- **General-purpose thermosets** have mechanical properties that are considered average (for thermosets), they exhibit greater coefficients of expansion, poorer temperature resistance, low cost manufacturing and high production and sales volume (tons/year).
- **Engineering thermosets** are thought to be more durable since they have better mechanical and thermal resistance qualities. They cost more and have a moderate production volume (kilograms/year).
- **High-temperature/specialty thermosets** can withstand temperatures over 200°C for extended periods of time while retaining their strength, adhesiveness, thermal resistance, and electrical resistance. Costs are frequently greater, and production processes can be highly complex. Specialty thermosets are helpful because they possess one or more incredibly unique and specialized property that offsets any lack of other good properties. They are typically made in little amounts (a few kilograms each batch) and are quite costly. A general-purpose phenolic frequently competes with an engineering polyimide, and there is frequently overlap between the three groups.

Some of the existent thermosets families can be broadly classified as seen in Table 1 (GOODMAN & DODIUK, 2014).

Table 1 - Categories of thermosets

General Purpose	Phenolics, aminos, polyesters
Engineering	Epoxy, polyurethane
High Temperature Thermosets Specialty	Silicones, Polyimides, Polybenzimidazoles Allyls, cross-linked thermoplastics

Source: Goodman & Dodiuk (2014)

2.1.2 Degree of polimerization

A measurement of the quantity of units (mers) in a specific molecule is the degree of polymerization (ANDERSON, 2005). Typical engineering plastics have extremely long chains, with the degree of polymerization on the order of several thousand. Heat input, catalyst, as well as reagents that may be added to aid the polymerization process can control the degree of polymerization (ANDERSON, 2005).

2.1.3 Molecular weight

The molecular weight is a measure of the length of a polymer chain. Since a polymer sample often contains a range of molecule sizes, it is convenient to measure the average molecular weight, which can be described in one of two ways (ANDERSON, 2005):

1) *The number average molecular weight*, which is the total weight divided by the number of molecules; and
2) *The weight average molecular weight*, which places more focus on the larger molecules (whereas the number average molecular weight attaches equal importance to all molecules).

Based on their molecular weight, thermoset polymers can be divided into rubber or elastomer (high molecular weight) and thermoset resins (low molecular weight) (RATNA, 2009). Low molecular weight thermoset polymers, i.e., thermoset resins, are the subject of this study. Commonly used thermosetting resins typically have molecular weights between 200 and

400 g/mole (WANG et al., 2011), which means they have a low softening temperature and viscosity as well as high fluidity like other low molecular weight compounds. However, the molecular weight of the resin increases during the curing reaction, when cross-linking occurs, viscosity of the resin rises and fluidity decreases.

2.1.4 Cross-linking density

Cross-link density can be defined as the number of effective cross-links per unit volume of the thermoset material, in inverse relation to the molecular weight between cross-links (GOODMAN & DODIUK, 2014). There are several factors that affect this parameter (GOODMAN & DODIUK, 2014):

1. Functionality: the number of reactive functional sites on the reactants (monomers);
2. Actual number of functional sites that react (depends on the process);
3. Chain length: the length between one crosslink and another;
4. Chain mobility between cross-links (depends on the chain structure).

2.1.5 Thermoset resin composites

Over the last decades, in several fields, such as the aerospace, automotive, and renewable energy sectors, composite materials have become a viable and preferred high performance material solution (STRUZZIERO et al., 2019). In this context, thermosetting resin composites have been extensively adopted, due to their favorable properties.

According to the traditional definition of the literature, a composite material, also known as a composition material or simply composite, is made up of two or more elements or phases that produce a superior combination of attributes than each substance or phase could provide on its own (ASKELAND et al., 2011; CALLISTER, 2008). A composite material is produced when two or more materials are combined on a macro, micro or nano scale (ASKELAND & WRIGHT, 2014). Regardless of the scale, to be considered a composite, the combination must have a distinguishable interface (RATNA, 2009).

Based on the matrix nature, four broad categories may be used to classify composites (RATNA, 2009): polymer matrix composite (PMC), metal matrix composite (MMC), ceramic matrix composite (CMC) and carbon matrix composite or carbon carbon composite. The usage of PMC, particularly fiber-reinforced plastic (FRP) composites, has dramatically increased over the past decades, and this trend is expected to continue (RATNA, 2009; GOODMAN & DODIUK, 2014; COHERENT MARKET INSIGHTS, 2022). This high interest in PMC is because they possess many useful properties, such as high specific stiffness and strength (properties-to-density ratios), dimensional stability, adequate electrical properties and excellent corrosion resistance (RATNA, 2009). Because of the easy transportability, high payload for vehicles, low stress on rotating parts, and high ranges for rockets and missiles, they are desirable for both civilian and military applications When a composite material is used instead of metal to create a component, the weight is significantly lower for a given design load. With regard to passenger aircraft, PMC's high specific stiffness and strength may result in a reduction in fuel consumption and an extension of range. It also improves military aircraft's stealth performance (DRZAL, 1986; MIDDLETON, 1990 apud RATNA, 2009). Besides, PMC can be processed at a much lower temperature compared with MMC and CMC (RATNA, 2009). Wang et al. (2011) lists other advantages of composites with polymer matrix:

a) Fatigue resistance: It is equivalent to 30% to 50% of tensile stress for metal matrices, 70% to 80% of tensile strength for carbon fiber/polyester composites, and a percentage between these aforementioned proportions for fiberglass composites.
b) Damage tolerance: While common materials show the unstable propagation of the primary crack and its rapid failure, composite failure results from a variety of damages including matrix failure, fiber extraction, splitting or rupture, and interface separation;
c) Damping characteristics: Composite materials vibrate at high frequencies that are proportional to the square root of a particular Young's modulus, and the interface between the fiber and matrix in these materials is good at absorbing vibrational energy;
d) Multifunctional performance: among them, good friction properties, high resistance to chemical corrosion and superior electrical insulation performance;
e) Good processing techniques: The material can be designed by choosing its components based on the conditions and demands of its intended usage. The product's molding enables the processing technique to be chosen in accordance with its physical properties

and can decrease the number of mounting parts, reducing the product's weight and the time and resources required to produce it.;

f) Capacity of property design and anisotropy: For instance, fiber-reinforced composites increase the material's resistance in the direction of dispersed phase orientation. Thus, the material is created in a way that satisfies the design specifications, and optimizing the design of the material involves strengthening it in the desired direction.

According to the types of polymer matrices, PMC are further classified as thermoset resin composites or thermoplastic resin composites (RATNA, 2009). Thermoset resins are the dominant material in the composite industries, due to their accessibility, relative simplicity of processing, less cost of processing capital equipment, and low material cost (RATNA, 2009). Due to their availability in low-viscosity oligomeric or monomeric liquid forms, thermosetting resins offer good flow properties that make it easier to impregnate fiber bundles with resin and properly wet the surface of the fiber with resin (RATNA, 2009). As mentioned before, they are characterized by a crosslinking reaction or curing, which transforms them into a three-dimensional (3D) network form (insoluble, infusible). In comparison to many thermoplastics, thermoset composites have better creep properties and environmental stress cracking resistance due to the crosslinked structure (JANG, 1991 apud RATNA, 2009).

However, because to the inability of remolding, thermosetting resins must be manufactured with the appropriate care and supervision to attain their final qualities. With the required heat supply, a thermosetting chemical reaction causes the crosslinking effect, which is what defines the material curing. The manufacture of thermosetting polymeric matrix composites must have the requisite control during curing, so that the desired matrix performance is obtained and the reinforcement is not negatively impacted (SMAALI, 2005).

Composites are also generally classified according to the shape of the reinforcement and to the matrix material. Depending on the shape of the reinforcement, they can be divided into composites reinforced by particles, continuous fibers, staple fibers (long or short), and fabric fibers. Continuous fiber reinforcements, which can be used in numerous ways such as continuous random mats, woven fabrics, stitched fabrics, unidirectional or bidirectional fabrics, often offer high improvements in mechanical properties such as stiffness and strength (ADVANI & HSIAO, 2012). The fiber material is usually glass, carbon or aramid. Natural fibers such as kenaf, flax, jute, hemp and sisal have been intensely studied in the last years as

alternatives to artificial fibers due to their clearly positive environmental impact (BIAGIOTTI et al., 2008).

Often these composite materials are introduced in a precursor form in the manufacturing process, where the precursor form usually mixes the fibers and resin in the form of prepregs (continuous fibers with resin attached to them in terms of a powder or pre-impregnated partially cured resin) or of a pellet (short fibers embedded in a solid matrix) (ADVANI & HSIAO, 2012).

Because they provide a distinctive mix of properties that is not possible to achieve with other thermoset resins, epoxy resins are a kind of material that is widely employed in structural and specialty composite applications (MIRACLE & DONALDSON, 2001; RATNA, 2009; GOODMAN & DODIUK, 2014). Epoxies provide great electrical insulation, high strength, low shrinkage, chemical and solvent resistance, low cost, and low toxicity (MIRACLE & DONALDSON, 2001). They are easily cured without evolution of volatiles or by-products by a broad range of chemical species (MIRACLE & DONALDSON, 2001; RATNA, 2009; GOODMAN & DODIUK, 2014). Epoxy resins are also chemically compatible with most substrates and tend to wet surfaces easily, making them particularly well suited to composites applications (MIRACLE & DONALDSON, 2001; RATNA, 2009; GOODMAN & DODIUK, 2014).

For years now, glass fiber-reinforced epoxies have been widely used for many years as important parts of boats, cars, airplanes, medical prosthesis, and sporting goods (RATNA, 2009). Besides, glass, graphite, and polyaramid-reinforced epoxy composites continue to find major use in such industries as space, printed circuitry, tanks, pressure vessels, and pipes (RATNA, 2009). In recent years, the epoxy resin is also widely used to produce carbon fiber and boron fiber composite materials (WANG et al., 2011). Epoxy composites are compatible with every reinforced plastics process (RATNA, 2009).

The main components of thermosetting molding compounds are a resin system - which typically includes curing agents, hardeners, inhibitors, and plasticizers - and fillers and/or reinforcements - which can be made of mineral or organic particles, inorganic or organic fibers, inorganic or organic chopped cloth, or inorganic or organic paper (BERINS, 1991). In composites made of thermosetting resin, the reinforcing agent undergoes no chemical reactions, but the resin experiences a complicated chemical transformation, moving from a viscous flow state via a high elastic state to a glass state (WANG et al., 2011).

2.1.5.1 Manufacturing process of thermoset resin composites

There are several ways to process composite materials, and there are significant variations among the various molding techniques (WANG et al., 2011). One of the important processes, which are used to produce high-performance laminated composites out of thermosetting-matrix composites, is the autoclave curing of the prepreg lay-ups (GOPAL et al., 2000). In general, this procedure entails subjecting a multi-layered fiber-resin combination to high temperatures and pressures for predetermined lengths of time. High temperatures start and promote the crosslinking of polymers, and pressure applied to the mixture makes any gases and cavities to be removed, which allows the specimen to be compacted (GOPAL et al., 2000).

In fact, nowadays, most of thermal curing processes are realized in autoclave (YUAN, 2021). Although out-of-autoclave procedures are given a lot of attention, they do not yet seem to be at a stage where they are ready for productions that are competitive (CENTEA et al., 2015 apud ALEKSENDRIĆ et al., 2016). As a result, significant research has been focused on the adoption of tools that are useful in optimizing the design of the autoclave curing process, while manufacturer's recommended cycle seem acceptable for the production of thin components but less successful when dealing with thick work pieces (ALEKSENDRIĆ et al., 2016; STRUZZIERO et al., 2019).

2.1.6 The curing process

Knowledge of the material properties and fabrication process must be mastered in order to produce materials with the desired performance, optimize designs, and reduce costs. An important phenomenon to consider of thermosetting polymer matrix composites manufacturing is the process of curing of such matrix.

When thermosetting resins are exposed to high temperatures, ranging from room temperature to about 230 °C, they go through the process of curing, or polymerization, which is a permanent chemical reaction in which the structure's cross-linking causes the resin to harden (WRIGHT, 2002 apud PAIVA, 2018). After curing, the substance transforms into a solid that is insoluble, three-dimensional, and incapable of melting from its initial viscous flow state (WANG et al., 2011).

The reaction that causes a resin to cure is both thermoactivated and exothermic (BLEST et al., 1999; CIRISCIOLI et al., 1991; PITCHUMANI & YAO, 1993; HOJJATI & HOA, 1994; SURATNO et al., 1998 apud STRUZZIERO et al., 2019; PAIVA, 2018), and it often involves a combination of three ingredients: prepolymer, hardener, and accelerator (PAIVA, 2018). Commercial prepolymers are widely available. The Bisphenol A Diglycidyl Ether (DGEBA, or BADGE) epoxy resin, one of the most frequently used prepolymers for thick epoxy composites in the naval and offshore industries, was the one chosen for this work. They exhibit a linear structure at first. When hardeners (amines and anhydrides are examples of this group) react with epoxy, the three-dimensional network is produced. They exhibit a rather diverse chemical nature and control the kind of chemical bonding and the degree of cross-linking in the network, which affects the final product's properties and cure characteristics (MAZUMDAR, 2002 apud PAIVA, 2018). Finally, accelerators shorten the reaction's overall duration by promoting the cross-linking of the prepolymer/hardener mixture. They do not alter the glass transition temperature or the overall enthalpy of polymerization, for example. Additionally, the reaction's final degree of cross-linking is unaffected (RABEARISON, 2009).

Cure kinetics must be comprehended, examined, and established in order to model, simulate, and optimize the cure process of thermoset materials. The polymer's quality may be described using predictions of the local temperature and degree of conversion. Therefore, an overview of the cure kinetics is presented below.

2.1.6.1 Degree of cure

During curing, the thermosetting resin's state changes. A low molecular weight monomer undergoes a significant transformation into a strongly cross-linked polymer. The development of curing is usually defined by the degree of cure, which can be computed from the ratio of the heat generated at a certain time during the process to the total heat generated over the whole cure (BARAN, 2017).

As a thermoset resin cures, a chemical reaction causes the progressive conversion of functional groups (RATNA, 2009). As a result, the first stage in the study of cure kinetics is to specify the degree of conversion, also known as the degree of cure (α), which is used to describe and track the cure process. Theoretically, the degree of cure ranges from zero - the resin's initial liquid state - to one, or 100% - fully cured resin.

Using nuclear magnetic resonance (NMR) spectroscopy analysis or Fourier-transform infrared, as well as differential scanning calorimetry (DSC), the degree of cure is determined by the disappearance of functional groups and the heat of reaction (DSC) (RATNA, 2009). When processing DSC observations, the degree of cure at a particular time t is defined as the ratio between the reaction's enthalpy at that instant – (t) –, and the reaction's total enthalpy for a fully cross-linked resin – H_U (PAIVA, 2018). It is expressed by Equation (1):

$$\alpha(t) = \frac{H(t)}{H_U} = \frac{1}{H_U}\int_0^t \left(\frac{dH}{dt}\right) dt \qquad ((1)$$

Where dH/dt is the measured heat flux, in power units.

The degree of cure can also be expressed in terms of the cure/conversion rate $d\alpha/dt$/ $[s^{-1}]$, which measures how quickly polymerization occurs and α increases, as follows:

$$\frac{d\alpha}{dt} = \frac{1}{H_U}\left(\frac{dH}{dt}\right) \qquad ((2)$$

The higher the cure rate, the shorter the process cycle. Additionally, a higher cure temperature results in a resin that has a higher degree of cure and that is denser. In practice, degree of cure seldom reaches 100% (PAIVA, 2018). Hence, it is assumed that the curing process reaches its end as the degree of cure – and material properties since they depend on α – are stabilizing.

Resin begins the chemical process of curing in a viscous liquid form, transitions to a solid rubbery state, and then solidifies into a glassy state. These phase shifts are illustrated by the Time-Temperature-Transformation (T.T.T.) Diagram in Figure 3, along an isothermal cure, for instance, at 120°C.

Figure 3 - LY 556 epoxy T.T.T Cure Diagram.

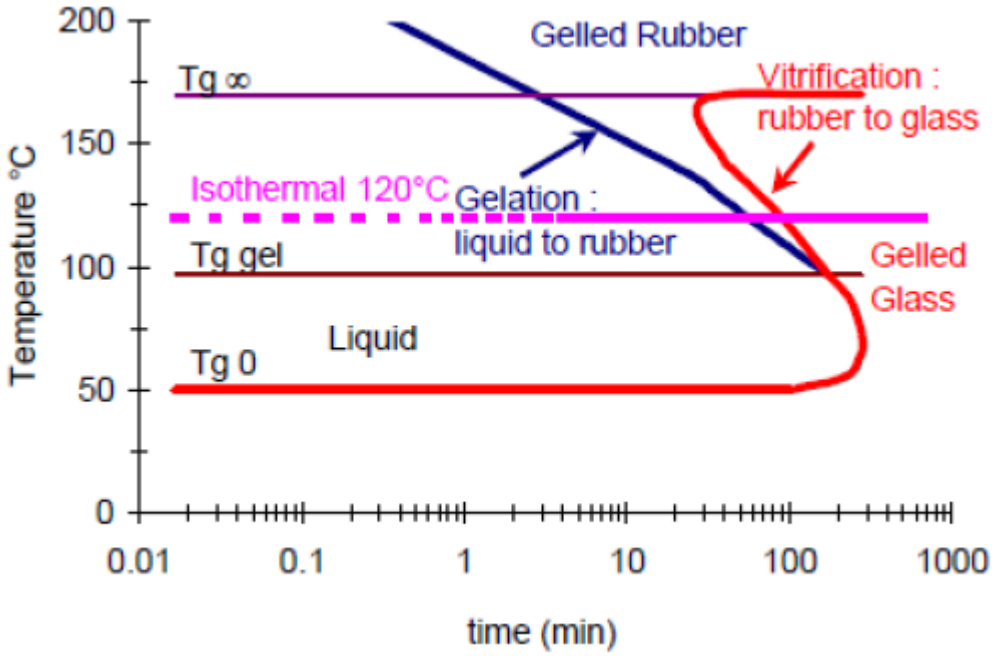

Source: Jochum et al. (1999)

The diagram displays the thermosetting system curing processes of gelation and vitrification. The temperature where they coexist and happen concurrently is represented by Tg gel. Gelation and vitrification are crucial to the curing process and, consequently, to the material's ultimate properties. In order to accurately predict the thermoset properties, the cure process must be characterized, and these phenomena should be investigated.

2.1.6.2 Gelation

When a thermoset resin cures, it runs into the phenomenon of gelation, which refers to the change of the material under curing from liquid to a cross-linked gel, or rubber (RATNA, 2009; PAIVA, 2018). At the gel point, all the units in a polymerizing mixture are linked together to create a single network (RATNA, 2009). The degree of polymerization (weight average) tending to infinite is the most widely accepted criteria for gelation. At gel point, the material is a combination of a soluble phase losing way to the insoluble one as it forms—a macroscopic-sized gel—and is neither liquid nor fully solid (PAIVA, 2018).

After gelation, due to the increase in cross-linking density, the cure process slows down, reducing system mobility. Cross-linking density rise also enlarges glass transition temperature

and mechanical properties (COSTA et al., 1999 apud PAIVA, 2018). Moreover, the material cannot be processed above the gel point. The gelation process is, therefore, irreversible (PAIVA, 2018). The gel point can be seen in Figure 4 from the starting increase of viscosity (μ) to its divergence to considerably greater values. After the gel point, a significant rise in the elastic modulus can also be seen in Figure 4.

Figure 4 - Viscosity and Elastic Modulus evolutions of the epoxy resin in the chemical reaction of polymerization.

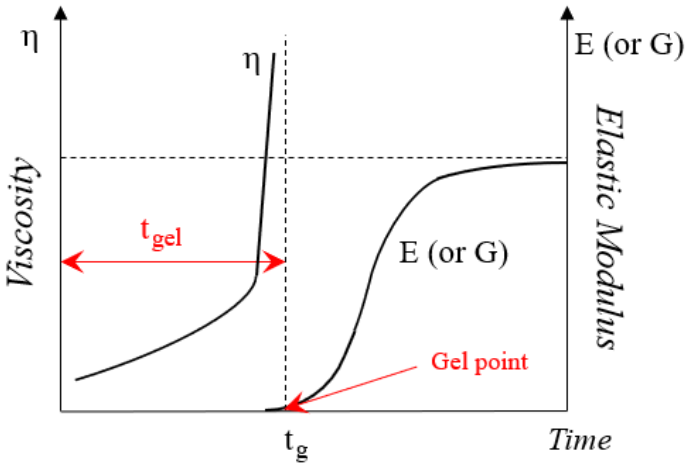

Source: Adapted from Rabearison (2009) by Paiva (2018)

Flory's gel theory states that the degree of cure for any cross-linking reaction is a constant at gel point, independent of reaction temperature or experimental conditions (Wang et al., 2011). According to Rabearison (2009), the degree of cure at gel point, for epoxy systems, ranges from 40% to 80%. Jochum et al. (2008) determined that the initiation of gelation for the LY 556 epoxy blend, which is the subject of the present work, occurs at a degree of conversion (α_{gel}) = 55%.

2.1.6.3 Vitrification

During the initial stage of curing, the cure is reactivity-controlled (RATNA, 2009). Unlike the reaction for synthesis of small molecules, a polymerization reaction is linked to an increase in the medium's viscosity. As the viscosity of the medium increases and the rate at which molecules diffuse slows, there will be a competition between reactivity-controlled and diffusion-controlled reactions (RATNA, 2009; PAIVA, 2018).

The reaction becomes completely diffusion controlled at a critical level of degree of cure (RATNA, 2009; PAIVA, 2018). This stage is known as "vitrification" and it marks the

transition from a rubbery gel to a glassy gel. The rate of diffusion will be greatly slowed down at this point due to a large reduction in free volume (RATNA, 2009). Tg is the term used to describe the temperature at which the transition to a glass occurs. Glass transition is not abrupt, in contrast to melting. For this reason, this range of temperatures is referred to as the "glass transition region".

After cured, polymer materials are glassy at temperatures below the Tg (hard and strong). The polymer softens and loses its dimensional stability when the service temperature exceeds the Tg. The Tg area has a considerable shift in modulus (rigidity). The Tg of a thermoset is therefore extremely important when designing the materials for a certain application.

The substance remains in a rubbery form as long as the glass transition temperature, Tg, is lower than the reaction temperature. However, during curing, Tg eventually approaches (and then surpasses) the system temperature, allowing vitrification to take place. The change in the material's condition from rubbery to glassy is the transformation associated to this phenomenon. In contrast to gelation, vitrification is reversible with heating, allowing a glassy state to transform back into a rubbery one (PAIVA, 2018).

At glassy state, as the forming network's densification rises and thermal agitation declines, system mobility is further decreased. Diffusion of reactants increasingly controls reactions. Therefore, maintaining reaction temperature above Tg allows curing to continue in a rubbery condition, resulting in a faster reaction rate and the fullest possible degree of cure. A post cure is a step in a typical manufacturing process that raises the cure temperature to increase cross-linking density and, as a result, the degree of cure and mechanical and physical qualities (PAIVA, 2018).

2.1.6.4 Cure (chemical e thermal) shrinkage

Throughout the curing process, thermosetting resin systems shrink due to cross-linking and temperature changes, increasing their density (WANG et al., 2011). The shrinkage will be greater at higher curing temperatures, which will result in increased internal stresses (WANG et al., 2011). Shrinkage significantly lower the quality of a fiber-reinforced composite since resin shrinkage has been shown to be correlated with the production of residual stresses and,

consequently, fiber waviness (RABEARISON et al., 2008; LORD & STRINGER, 2009; MSALLEM et al., 2010 apud PAIVA, 2018). Besides, several works have shown that a viscoelastic behavior of the resin induces stress relaxation effects (WISNOM et al., 1999; EOM et al., 2000; JOCHUM et al., 1999; 2007; 2008; RABEARISON et al., 2009; PATHAM, 2009; 2013 apud PAIVA, 2018).

When segment displacement is fixed, internal stress is difficult to release. Furthermore, because resin has a limited heat conductivity, the curing exothermic peak increases as the curing process progresses. Different heat diffusion conditions during the curing process or a quick heating rate will result in an uneven temperature field in some portions of the thermoset, especially in thick components (WANG et al., 2011). Additionally, it will result in internal stresses due to varying curing temperatures and shrinkages at different sites (WANG et al., 2011).

Uneven temperature, particularly during shrinkage after gelation, will result in varying rates of stress relaxation at different locations, producing different stresses, which in turn generates more internal stress (WANG et al., 2011). Therefore, the faster the reaction happens and the thicker the pieces are, the higher the temperature gradient will be and the more the resin system shrinks when it cures. Then, the pieces will be more likely to distort and warp as a result of the higher internal stress created during the curing process.

According to Wang et al. (2011), because the resin is in its liquid condition before the gel point, only a portion of curing, following gelation, influences internal tensions. The same is supported by Jochum et al. (2007; 2008), Rabearison (2009), and other authors: internal stresses first manifest during gelation, a process during which chemical shrinkage is generated, the polymer structure starts to take shape, and the elastic modulus of the resin changes (PAIVA, 2018).

In a single fiber carbon/epoxy composite, the mechanism of fiber waviness was observed by Jochum et al. (1999). They determined that it was a result of the shrinkage of the resin during the hot phase of curing, which caused the fiber microbuckling phenomena. The experiments were conducted at various cure cycles, but with the same cooling phase. The conclusion that thermal stresses do not cause the fiber microbuckling phenomenon during cooling was made as a result of the sample with a fast cure exhibiting fiber instability whereas the sample with a slow cure did not. This is proof that internal strains are mostly caused by the

matrix's chemical shrinkage during the curing reaction, which occurs before the cured composite is exposed to room temperature, and its thermal shrinkage during the cooling stage.

Thereafter, Jochum et al. (2007) measured fiber instability experimentally at the hot stage of cure. The undulation evolution of a long carbon fiber in a LY 556 epoxy resin was captured on camera in real time, and the wavelengths measured from a sinusoidal-like behavior were used to characterize the undulations. At the hot stage of cure, recordings reveal lower wavelengths and, consequently, higher amplitudes, which demonstrate the emergence of strains. According to a subsequent study (JOCHUM et al., 2008), the maximum chemical shrinkage seen just before the transition to glass coincides with local heating rates exceeding 3°C/min, which is when fiber instability is said to be induced.

Hence, internal stresses are decreased through more uniform shrinkage, temperature distribution, and cure rates at lower temperatures. The authors continued to look into the development of internal residual stresses during the curing of thick epoxies, where there is more heterogeneity (JOCHUM et al., 2013; 2014; 2016). They used simulations of samples subjected to laser-induced shock waves to estimate internal stresses and forecast damage, recording internal strains of about 10 MPa.

While further examining the evolution of fiber undulations, Jochum et al. (2007) observed a modest increase in fiber wavelength before and during the cooling stage to room temperature. The authors point to the matrix's viscoelastic behavior as the root reason, which enables matrix tensile relaxation and, as a result, a reduction in fiber compressive stress, thereby increasing the fiber's wavelength. Therefore, compared to a solution in the elastic framework, residual stresses are lower.

The specific volume-T curve in Figure 5 depicts the volume change of an epoxy resin system as an example (WANG et al., 2011). The unreacted liquid epoxy resin system is heated from room temperature to curing temperature, and its volume expands from point X to point A and reaches gel point C due to curing shrinkage in curing temperature. Its volume decreases to point B as cure progresses. Then cooling from curing temperature to room temperature, it reaches point Y through point D (glass transition temperature Tg) due to cooling shrinkage. Two stages make up cooling: high elastic state (BD) above glass transition temperature (Tg), and glass state (DY) below Tg. According to Figure 5, two different line slopes, the thermal expansion coefficients in the two stages are different.

Figure 5 - The shrinkage of epoxy in curing process.

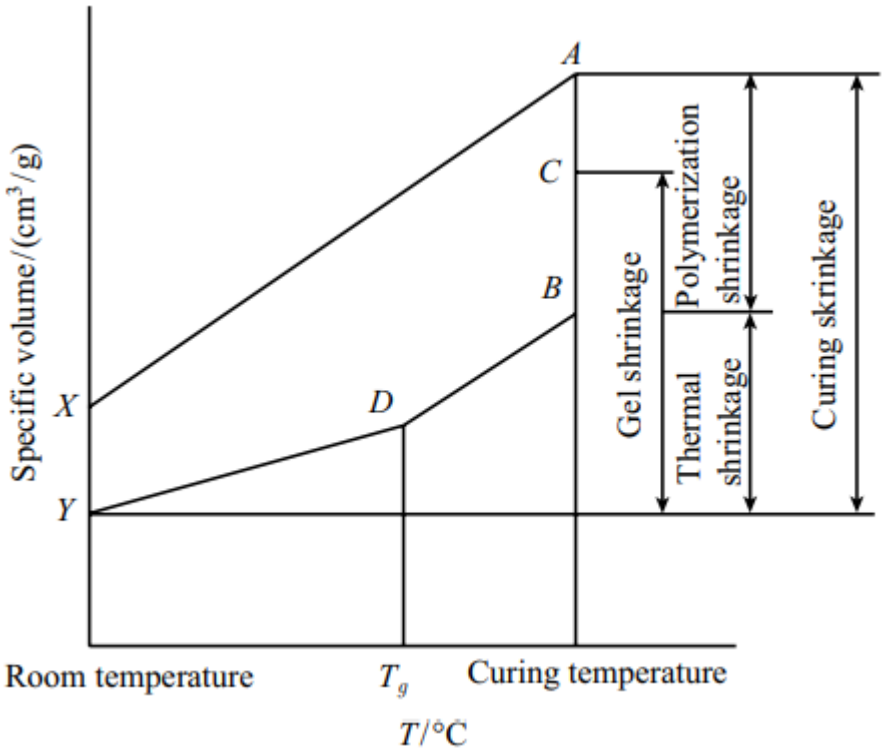

Source: Wang et al. (2011)

From point X to point A, it is the thermal expansion of non-curing system. From point A to point B, it is the shrinkage caused by curing reaction within given curing time at curing temperature, which is called polymerization shrinkage. From point B to point Y, it is the thermal shrinkage of cured system. The volume change between point A and point Y is the total curing shrinkage of system (curing shrinkage = polymerization shrinkage + thermal shrinkage). The volume change between point X and point Y is the volume change before and after curing, which is usually used to calculate the actual volume shrinkage after the system cured (WANG et al., 2011).

2.1.6.5 Cure schedule

Manufacturing of polymer composites using a curing process requires the specification of the temperature as a function of time, i.e., the temperature profile, also called cure schedule. It is extremely important that the selected cure schedule satisfies a number of criteria which include the minimum residual stresses, minimum cure cycle time, full degree of cure and no thermal degradation for the final cured material.

The cure schedule must take into account a realistic time-temperature profile that will produce an optimal mix of properties when more than one material property is important. Figure 6 describes such a circumstance. Besides, the cure schedule that is chosen to manufacture a component is influenced by heating and cooling rates, volatiles release, part design, and many other aspects (GOODMAN & DODIUK, 2014).

Figure 6 - Optimization of cure schedule for thermosetting plastics. Optimum properties occur at point A.

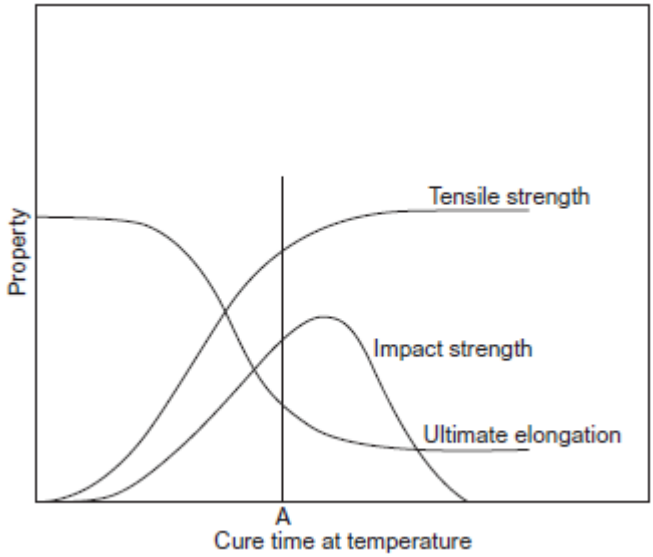

Source: Goodman & Dodiuk (2014)

Practical considerations generally dictate that the cure time be chosen at some fractional level of the ultimate properties (GOODMAN & DODIUK, 2014). This is because the time scale can often be logarithmic (GOODMAN & DODIUK, 2014). Thus 90% of, say, ultimate tensile strength, may be achieved in a few hours at 25°C. The remaining 10% (often not needed for use) may require months to years for achievement.

If firstly pre-cure at a low temperature (then cure at a high temperature), macromolecules can move around during the slow-moving curing reaction, and the curing agent has time to fully react with the surrounding resin to create more reaction centers, which results in a more uniform structure and cross-linking density. If directly cure at high temperature, as a result of the high reaction speed and the curing agent's encapsulation, which prevents it from reacting with farther away macromolecules, there is a structural heterogeneity, greatly inhomogeneous crosslinking density, and significant internal stress. Therefore, stepped-curing from low to high temperature is frequently used in advanced composite material components, and autoclave process in particular (GOODMAN & DODIUK, 2014).

As previously mentioned, a two-step cure cycle is the typical process cycle for polymer-matrix composites. The first dwell's goal is to let gases (such as trapped air, water, or volatiles) escape the matrix material and to let the matrix flow, which will aid in the part's compaction, while the second dwell's purpose is to allow the polymer crosslink (WHITE & HAHN, 1993). In this second stage, the composite's strength and other mechanical characteristics grow.

2.1.6.6 Influence of temperature and mass/thickness on gel time

Essentially, the temperature dependence of cross-linking reactions follows a conventional Arrhenius relationship (GOODMAN & DODIUK, 2014; PAIVA, 2018). Therefore, cross-linking rate is greatly influenced by ambient temperature. A mass effect affects the rate of reaction because all commercial thermosetting reactions are exothermic.

The heat produced by the exothermic reaction brings on a typical viscosity decrease. The resultant increase in mixed viscosity outpaces and quickly surpasses any reduction brought on by heat as the mass' molecular weight rises. Over time, the molecular growth continues until a macroscopic gel-like "lump" is discernible: this is the gel time, also known as the gel point, or t_{gel} (GOODMAN & DODIUK, 2014). The viscosity increases infinitely after this point. In other words, the polymeric mass transforms into a plastic, a macroscopic solid (GOODMAN & DODIUK, 2014).

All polymers are naturally thermal insulators, so the exothermic heat cannot easily escape the mass curing during the reaction, increasing the heat input (GOODMAN & DODIUK, 2014).

Figure 7 demonstrates this effect. Curve 1 represents a normal room temperature cure. With added heat (T2 > T1, Curve 2) the gel time decreases. Curve 3 (T3 < T1) shows the effect of decreasing the temperature (i.e. t_{gel} increases). Curve 4 (T4 << T1) describes a stable situation wherein the cure is arrested because the temperature is below the activation level necessary for the start of the reaction.

Figure 7 - Influence of ambient cure temperature on the gel time of thermosets.

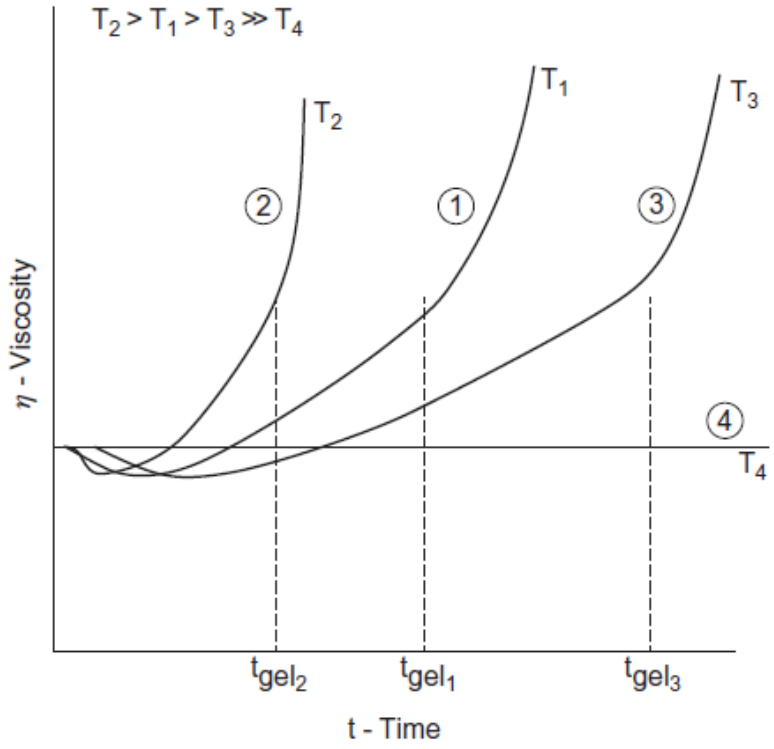

Source: Goodman & Dodiuk (2014)

The temperature influence on gelation is paralleled by the mass effect (GOODMAN & DODIUK, 2014; PAIVA, 2018). Because polymers are thermal insulators, as a cross-linking mass grows larger, the ability to transmit the exothermically produced heat away from the reaction site is dramatically reduced. Curve A in Figure 8 shows the typical gel profile for a given mass. Curve B represents the doubling of the mass, whereas curve C represents a halving of the mass. A situation when the mass is below a crucial threshold size, which stops the cross-linking and creates an effective latency, is described by Curve D.

Figure 8 - Influence of mass on the gel time of thermosets

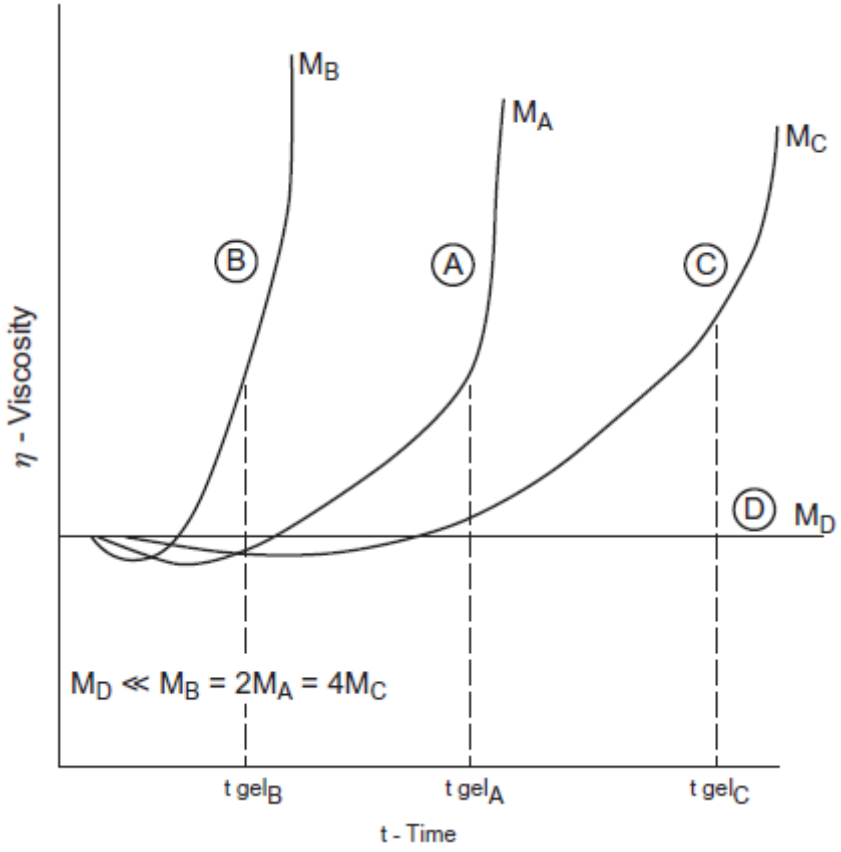

Source: Goodman & Dodiuk (2014)

The gel duration can be increased from minutes to hours, because of the temperature/thickness dependency, which is quite relevant in practice (GOODMAN & DODIUK, 2014). For instance, a 5-gallon mixture of urethane flooring varnish compound may gel in 20 to 30 minutes with an often-abrupt exotherm (GOODMAN & DODIUK, 2014). The gel time, however, may increase to 4 to 8 hours if the same amount is immediately poured and distributed over a cool surface (GOODMAN & DODIUK, 2014).

2.1.6.7 Influence of temperature on conversion rate and degree of cure evolution

Figure 9 and Figure 10, respectively, depict typical plots illustrating how temperature affects conversion rate and degree of conversion of a thermoset (in this case, a polyester) (RATNA, 2009).

Figure 9 - Isothermal reaction rate versus time plot of a free radical-polymerized unsaturated polyester resin

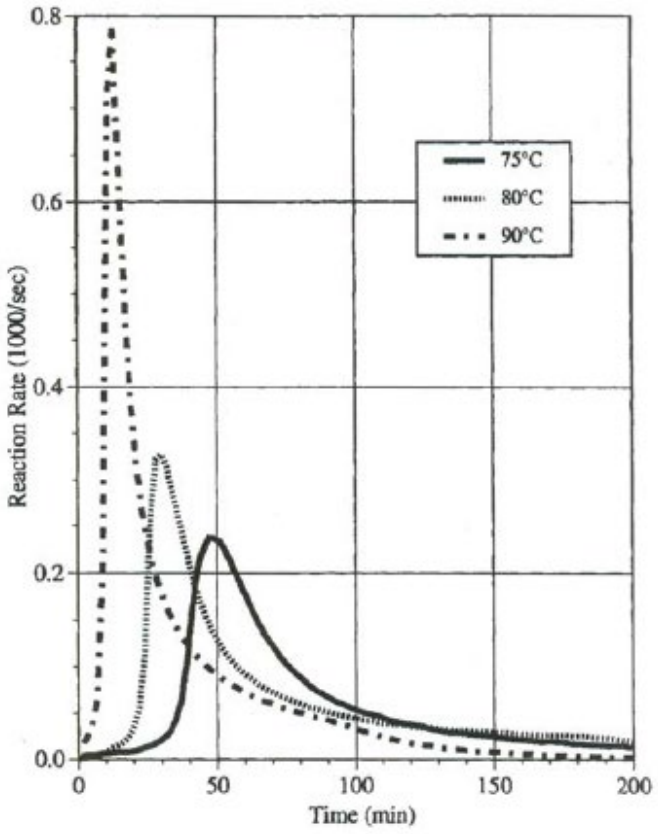

Source: Ratna (2009)

Figure 10 - Conversion profile versus time plot of a free radical-polymerized unsaturated polyester resin.

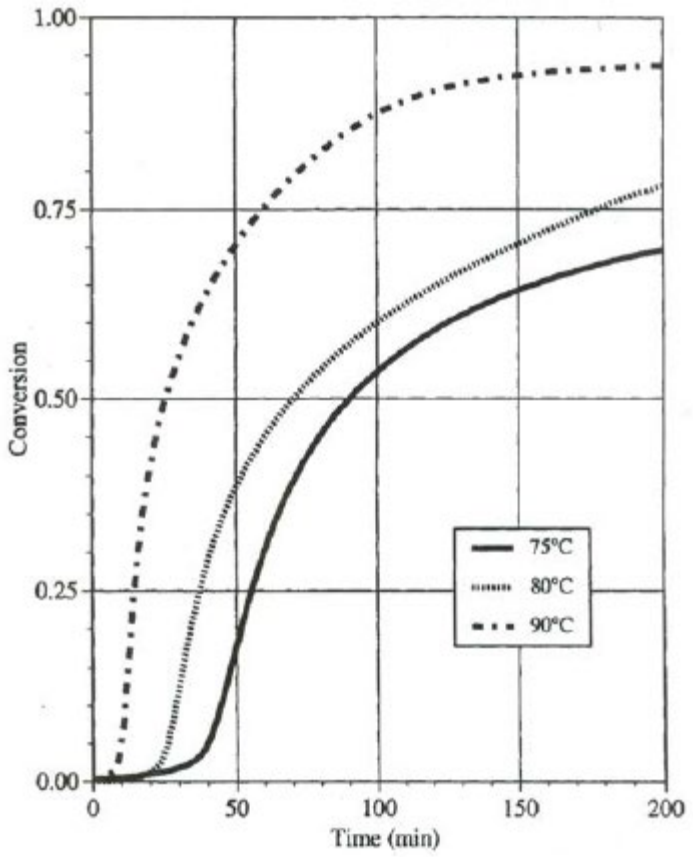

Source: Ratna (2009)

2.1.6.8 Internal gradients and defects

A thermochemical, chemical, and mechanical coupling occurs during an exothermic process during the curing of thermosetting polymers and composites. The curing procedure affects the final product's material qualities. However, internal tensions produced during the curing process can also result in the formation of quality defects including bubbles, cracks, and wavy fibers, which will lower the product's mechanical performance (PAIVA, 2018).

Figure 11 depicts the use of a carbon/epoxy composite to construct pipelines (risers) for the extraction of petroleum from deep wells. The composite exhibits flaws throughout its thickness, including bubbles, pores, fissures, and local dislocations. This illustrates the process of material stress generation during curing, which degrades the final product's mechanical quality.

Figure 11 - Defects through thickness in a carbon/epoxy composite riser (80-mm thickness).

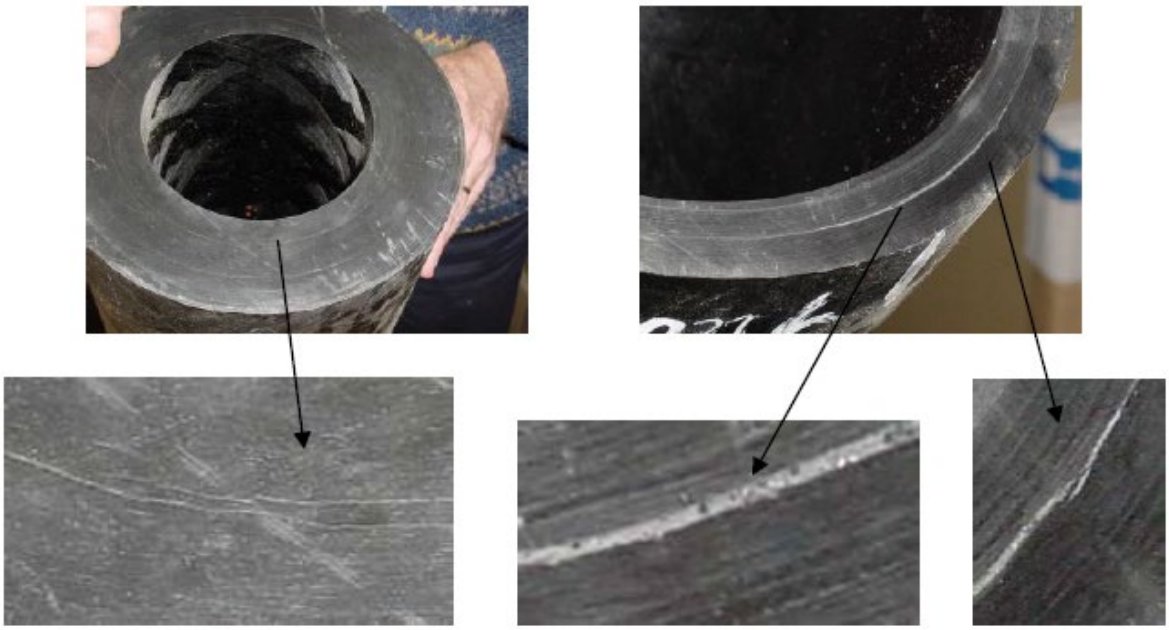

Source: Jochum (2009)

Such defects become more significant in the production of thick laminates for structural purposes, which are increasingly being used in naval and offshore applications and typically have thicknesses above 4-5 mm (RABEARISON et al., 2009).

Viscoelasticity and thermal degradation brought on by internal overheating are further aspects of the process that have an impact on the polymer's final state (PAIVA, 2018). Therefore, research has been done to optimize the cure cycle, avoid overheating and high internal gradients and assure higher mechanical properties for the composites during manufacture (PAIVA, 2018).

2.1.6.9 Residual stresses

Residual stress is the stress experienced without the presence of external or thermal loading (CALLISTER & RETHWISCH, 2007). In other words, residual stresses are those stresses that persist in a structural material or component after the original source of the stresses (external forces, heat gradient) has been eliminated.

A thorough understanding of the process-induced residual stresses and their effects is necessary given the increased use of polymer composites in load-bearing applications. This is extremely necessary in order to have more reliable composite manufacturing since residual

stresses change the internal stress level of the composite part during service life and residual shape distortions may result in failure to meet the desired geometrical tolerances (BARAN, 2017).

Residual stresses may be created through the manufacturing process or working conditions (TEIMOURI & SAFARABADI, 2019). The development of residual stresses during the manufacturing process is inevitably accompanied by a variety of interactions between the physical phenomena that are primarily involved with material flow, heat transfer, and polymerization or crystallization (BARAN, 2017).

Process-induced residual stresses have been linked to a number of different mechanisms, including thermal anisotropy, chemical resin shrinkage, tool-part interaction, resin flow, consolidation and compaction, gradients in fiber volume fraction, moisture swelling, prepreg variability, gradients of temperature and degree of cure or crystallization (BARAN, 2017). Other factors may govern the evolution of the residual stresses and deformation of thermoset composite structures during the fabrication process, the mismatch of thermal and chemical properties of constitutive materials, material degradation or viscoelastic effects during curing (ERSOY et al., 2005; WISNOM et al., 2006; FERNLUND et al., 2002 apud LIU & SHI, 2018). Therefore, accurate predictions of residual stresses in thermoset resins and composites require detailed accounting of multiple phenomena, such as the kinetics of resin cure, the evolution of the resin properties with temperature and degree of cure, cure shrinkage strains, thermal strains and mold-part interaction (PATHAM, 2013).

Large temperature gradients across the thickness caused by the exothermic heat of reaction have an additional impact on residual stress generation and shape distortions in thick thermoset sections (PATHAM, 2013). The matrix material experiences differential polymerization, shrinkage, and modulus development in the throughthickness direction as a result of these high thermal gradients, which cause residual stresses (BARAN, 2017). Due to the reduced thermal conductivity of thermoset composites, thicker sections may experience considerable temperature and cure gradients even though through-thickness temperature gradients are relatively tiny for thin parts and can be disregarded (JOHNSTON, 1997 apud BARAN, 2017). The evolution of macroscopic in-plane residual stresses caused by temperature and degree of cure gradients in thick thermoset laminates was examined in (BOGETTI & GILLESPIE, 1989, 1992; RUIZ & TROCHU, 2005 apud BARAN, 2017).

When residual stresses have the same sign as those brought on by external loads, they can have a negative effect on composites (SAFARABADI & SHOKRIEH, 2014 apud AGIUS et al., 2016). Matrix cracking and/or excessive shape distortion can be caused by residual stresses (BARAN, 2017). Besides, residual stresses are very effective at reducing the strength of a composite structure because they cause structural delamination, fiber tear, and twist of asymmetrical multilayers (TEIMOURI & SAFARABADI, 2019)

In fact, residual stresses can be high enough to cause matrix cracking even before mechanical loading is applied (WHITE & HAHN, 1990 apud GOPAL et al., 2000). This microcracking weakens the material's strength and exposes the fibers to chemical deterioration (HAHN, 1984 apud GOPAL et al., 2000). Even though they might not reach this level, residual stresses still have a negative impact on strength because the component was preloaded during the curing process (HAHN, 1984 apud GOPAL et al., 2000).

Nevertheless, according to Liu and Shi (2018), residual stresses are inevitable in the composite structures during the manufacturing process (LIU & SHI, 2018). These process-induced residual stresses may lead to undesirable shape distortions when the cured components are released from the mold and such distortions are often large enough to render the part unserviceable (LIU & SHI, 2018). Moreover, residual stress during fabrication greatly decreases the fatigue life and dimensional accuracy of composite parts (ERSOY et al., 2005; SALOMI et al., 2008; KAPPEL et al., 2013 apud LIU & SHI, 2018). Consequently, it is important to accurately predict the development of residual stresses and deformations during curing (ZHU et al., 2001; CAPEHART et al., 2007; WUCHER et al., 2014 apud LIU & SHI, 2018).

Researchers have put in a lot of work to predict residual stresses and distortions in composites using analytical and numerical methods in the extensive published literature (BARAN, 2017). Although analytical expressions are frequently preferred to predict residual stresses in composite materials, numerical analysis must be used if higher accuracy is desired (SAFARABADI & SHOKRIEH, 2014). Generally, numerical methods include finite element method (FEM), finite difference method (FDM) and boundary element method (BEM) (SAFARABADI & SHOKRIEH, 2014). The FE method is more effective than the other two methods for predicting micro- and macro- residual stresses (SAFARABADI & SHOKRIEH, 2014). FE analysis has been widely utilized to investigate the process induced stresses and deformations for different shaped parts, in composite manufacturing processes (ANTONUCCI

et al., 2006; CLIFFORD et al., 2006; ERSOY et al., 2010; CINAR et al., 2014; TAVAKOL et al., 2013; CINAR, 2014; WUCHER et al., 2014 apud BARAN, 2017).

To forecast how the residual stress will evolve in composites, the viscoelastic model, the cure hardening instantaneously linear elastic (CHILE) model, and the elastic model are frequently used (LIU & SHI, 2018). These three models each have unique advantages and disadvantages, as well as varying degrees of adoption. Undoubtedly, during the curing process, particularly during the heat-up and hold phases, the polymer acquires viscoelasticity (LIU & SHI, 2018). The elastic model can only be used to predict how the internal stress will change during the cool-down period; however, it ignores how the stress will change during the curing process (ARAFATH, 2007; ABOUHAMZEH et al., 2015 apud LIU & SHI, 2018). In this regard, the CHILE model is the model suggested by some researchers to effectively assess the deformation and residual stress of the composite laminates (WISNOM et al., 2007; DING et al., 2017; KAPPEL, 2016; BELLINI & SORRENTINO, 2018 apud LIU & SHI, 2018). This is because the model considers the variation of elasticity modulus as a function of degree of cure and temperature during the cure period.

According to Paiva (2018), many studies on thermosetting polymer curing have been shown that residual stresses appear during the hot stage of the curing. A prediction tool for a unidirectional AS4 carbon fiber embedded in a Hexcel 8552 epoxy, which is frequently used in aerospace composite structures, was created by Lord & Stringer (2009). Taking into account the resin chemistry and structural analysis, a 3D model was simulated on Abaqus with its subroutines for the prediction of residual stresses and distortions during and after cure. Experimental data were used to model cure kinetics. Both a one-step cure at 180°C and a two-step cure with isotherms at 210°C and 180°C were applied to the U-shaped geometries. Similar parts were created using an autoclave process to validate mathematical outcomes. The authors stress the significance of modeling the entire cure cycle because distortions are significantly increased if the expansion and cure shrinkage that have accumulated in the fiber and resin up to the gel point are ignored in analyses that begin at the gel point. Finally, there was good agreement between the numerical and experimental results; however, the numerical results were more accurately predicted as the simulation's element through-thickness number increased.

Msallem et al. (2010) also looked into the issue of residual stress generation during curing, which is more important in thick resin parts. FEMLAB (now COMSOL Multiphysics®) was used to simulate the cure of a 1D simple plate thermosetting resin using coupled thermal, chemical, and mechanical phenomena. According to the authors, the gel point is typically used as a criterion for

residual stress formation, which is primarily caused by chemical shrinkage. However, they believe that stresses should be considered to start forming when the resin has a yield stress.

Patham (2009) studied the evolution of cure-induced stresses in a thick viscoelastic thermosetting polymeric resin using multiphysics simulations on COMSOL® that incorporated heat transfer and cure kinetics. In cure kinetics, diffusion effects were also taken into account. The attraction of a thick matrix stems from the exothermic reaction's larger temperature gradients across the thickness, which result in the growth of residual stresses and shape distortions. According to the author, thermal stresses and chemical shrinkage both contribute to the isotropic stresses that are produced. On the other hand, due to viscoelasticity, there is a time-dependent stress relaxation during cure. Viscoelastic model estimates of the first case were significantly lower than equivalent elastic model estimates, according to a comparison the authors made. The instantaneous stresses, which in a linear elastic material are only controlled by the instantaneous states of temperature and degree of cure, were another topic of discussion in the paper. It was found that locations with higher temperatures allowed quick relaxation of stresses caused by thermal shrinkage, resulting in a slower build-up of stresses. For a viscoelastic material, these stresses are also influenced by the resin's thermal history.

Patham (2013) continues the study of cure-induced stresses in a viscoelastic epoxy/amine thermosetting resin system in a subsequent work. Heat transfer and a semi-empirical cure kinetics model were both included in COMSOL Multiphysics®, which made it easier to implement the model without making any simplifying assumptions. Two other equivalent material models, one with a constant elastic modulus and the other with a cure-dependent, time-invariant elastic modulus, were compared to the simulation results. The author observed lower estimates of generated stresses for the viscoelastic model, but found no differences in the stress response between the two elastic models.

The internal stress growth during curing of a thermosetting system was also studied by Rabearison et al in consecutive researches using FE simulations on Abaqus and its subroutines, where thermal, chemistry, and mechanics were coupled within the framework of elasticity with small strains. The heat generated by the exothermic polymerization reaction was included in the heat transfer equation as a heat source, causing the resin to expand thermally before shrinking due to the transition between the liquid and solid states. The chemical shrinkage and property evolutions were accounted for by the degree of cure computed at each stage of curing. The evolution of the material's characteristics (temperature and degree of cure dependents) was inferred from DMA-TMA and DSC experiments, and the cure kinetics parameters for Kamal and Sourour's phenomenological model were obtained.

In their initial study (RABEARISON et al., 2008), the rule of mixtures was used to predict the coefficient of thermal expansion and the specific heat capacity according to the degree of conversion of the reaction. The chemical shrinkage followed Li et al. (2004)'s bi-linear relationship. They also took into account how DiBenedetto's equation would change the glass temperature. Two simulations were run, each with associated experiments to validate the models. The first one was an epoxy resin filled steel tube with a 32 mm diameter and 30 mm height that was heated in an oven using a 3°C/min ramp before reaching an isotherm of 100°C. The second model was a 20 mm Pyrex test tube filled to a height of 25 mm with epoxy resin and heated at a ramp rate of 3 °C/min before reaching an isothermal plateau of 120 °C in the oven. The authors draw attention to the significant internal stress development that was witnessed during a resin's cure cycle as well as the strong strain and stress gradients that were seen inside the matrix during formation and that, after gelation, were around 7-8 MPa. In conclusion, it is stated that stresses are caused by different thermal and chemical strains that manifest within the matrix as a result of gradients of curing caused by thermal heterogeneity.

The results of a subsequent investigation (RABEARISON et al., 2009) were compared to the first one. Once more, Abaqus simulations were compared to experimental data, demonstrating that local temperature predictions were consistent with the data. Shear elastic modulus and loss modulus values for a typical curing at 120°C were obtained from DMA-TMA tests. It was discovered that the shear elastic modulus appeared to be sensitive to the frequency of the tests, indicating that the matrix exhibited viscoelastic behavior during the cure cycle and should be taken into account in future research for more accurate predictive models of the internal stress state estimation. Additionally, authors claimed that as thickness increases, the exothermic reaction's contribution to the curing process' heterogeneity becomes more pronounced. There are mass effects on the exothermically generated heat during the curing of thick matrices, which can decrease the composite quality. Because of this, the understanding of the gradients that arise within the material properties is a strategic point for thermoset composite manufacturing, particularly for thick matrices.

2.1.6.10 Thermal degradation

Manufacturing components out of thermosetting resins requires performing an exothermic chemical reaction in addition to shaping the material. In order to achieve an acceptable rate of reaction without overheating and causing unwanted reactions that result in thermal degradation, proper temperature control is necessary (MCCRUM, 1997).

According to Thermogravimetric Analysis (TGA), show in Figure 12, the thermal degradation temperature of the LY 556 epoxy system studied in this research work is around 155 °C. When this temperature is exceeded, the epoxy starts to loose mass, followed by the formation of gases and bubbles, which increases the internal pressure of the component and generate cracks.

It is important to note that TGA analysis indicates mass loss appearance quite early, at around 75°C. However, until temperature reaches around 120°C, the loss observed in the TGA plot is related to the release of gases (such as trapped air, water, or volatiles), not to the epoxy thermal degradation.

Figure 12 - Mass loss evolution of the LY 556 epoxy according to TGA, indicating the material thermal degradation temperature

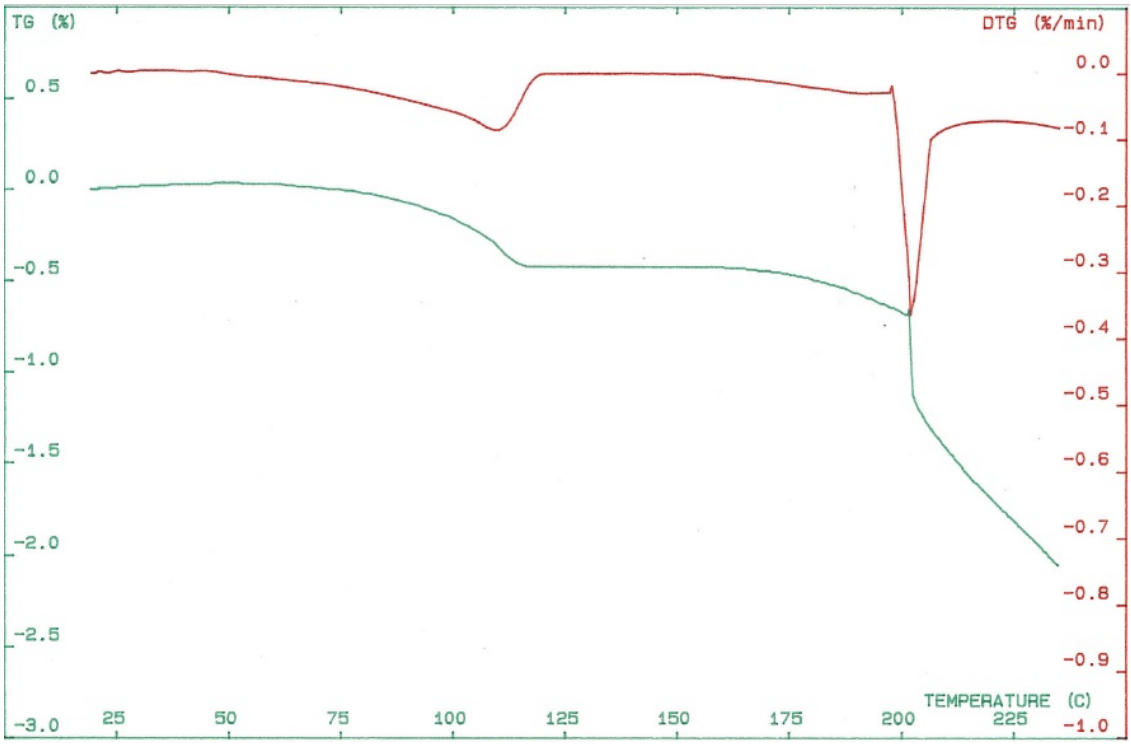

Source: The author (2022)

2.1.7 Mechanical properties

The mechanical properties of thermoset resin composite components are largely affected by the cure cycle, which must be designed and optimized based on the component geometry.

Because of the molecular structure of polymers, they experience rate-dependent viscoelastic deformation (ANDERSON, 2005). The ability of materials to exhibit both viscous and elastic properties when deformed is known as viscoelasticity. Time affects how stress and strain are related (or frequency, for a frequency domain). Thus, the strain rate affects the stress-strain plot's slope. Van der Waals bonds are weak attractive forces that act between two nearby molecules or various pieces of a single folded-back molecule (ANDERSON, 2005). These secondary bonds will resist any external force that tries to pull the molecules apart. Because the Van der Waals bonds in most polymers are much weaker than primary bonds, their elastic modulus is significantly lower than the Young's modulus for metals and ceramics. It takes coordinated motion between molecules to deform a polymer. If the imposed strain rate is sufficiently low to give molecules enough time to move, the material is considered relatively compliant. Higher stresses are needed to deform the material at higher strain rates due to friction caused by the forced molecular motion. The material tries to return to its original shape after the load is removed, but molecular entanglements stop this from happening instantly. If the strain is significant enough, yielding processes like crazing and shear deformation take place, and a significant portion of the induced strain becomes essentially permanent.

Viscoelasticity is a still growing subject in composites studies, and recent works show relations between viscoelasticity and generated residual stresses in fiber-reinforced composites (PAIVA, 2018). The elastic shear modulus and loss modulus for a LY 556 epoxy system, which is the focus of this study, was determined through DMA-TMA experiments in accordance with the evolution of degree of cure shown in works by Jochum & Grandidier (2004), Smaali (2005), Rabearison (2009), and Rabearison et al. (2009) in Figure 13. The values were tabulated for a loading frequency of 0.1 Hz.

Figure 13 - Elastic shear modulus evolution with degree of cure.

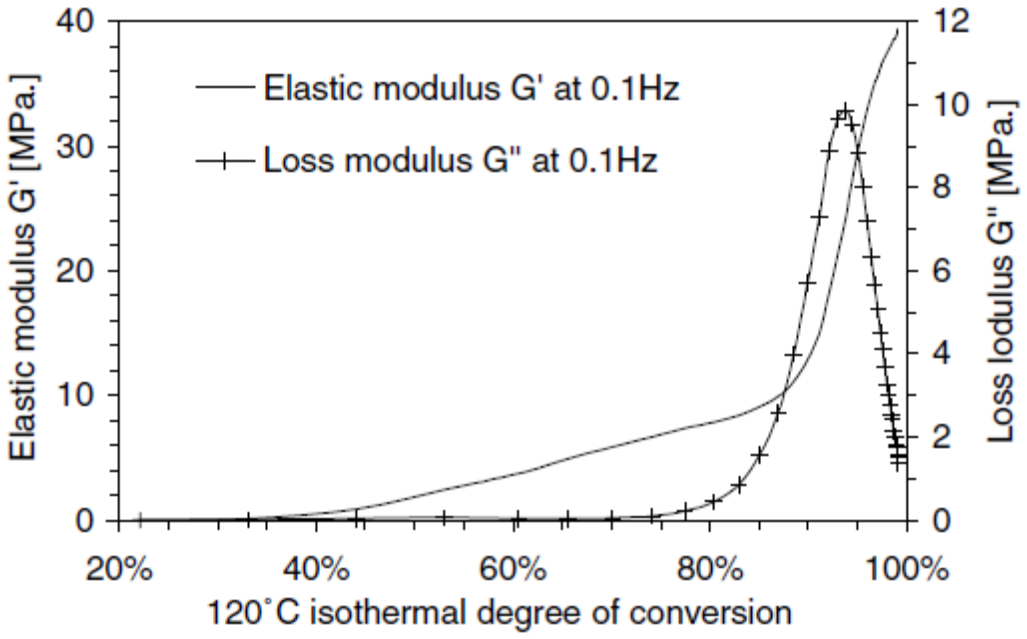

Source: Jochum & Grandidier (2004)

Critical factors that affect the cured resin's properties, especially its mechanical properties, include cross-link density and degree of conversion (GOODMAN & DODIUK, 2014). A thermoset resin that has a high cross-link density or degree of conversion tends to be harder but brittle, whereas one with a low density/degree of cure is more flexible, has better impact strength, and has a higher elongation. This general principle enables one to adjust the degree of conversion to enhance the performance of the final material (GOODMAN & DODIUK, 2014).

2.1.8 Epoxy resins

Epoxies are a class of polymers that are essential to modern industry (GOODMAN & DODIUK, 2014). Indeed, these materials are so common that researchers and engineers from a variety of fields are likely to come across them in a variety of settings.

Epoxy resin synthesis began in the 1930s (WANG et al., 2011). Industrial usage of epoxies became widespread with the first commercial production beginning in 1947 (GOODMAN & DODIUK, 2014). Since then, several applications have made the market of epoxy resins expand.

Epoxy resins are a subcategory of thermosetting resins distinguished by the presence of two or more oxirane rings or epoxy groups in their molecular structure (RATNA, 2009). These epoxy groups are situated terminally, cyclically, or internally in a molecule (GOODMAN & DODIUK, 2014).

Typically, two compounds that are liquid at room temperature are combined to create epoxy resin, which upon curing solidifies into a cross-linked lattice (ANDERSON, 2005). Amines and anhydrides are the main hardeners for reinforced epoxies (BERINS, 1991). The choice of compounds in a formulation, their relative proportions, the processing of the recipe, and the configuration and environment of the finished part can all affect the properties of epoxy resins. The most popular form of epoxy resin, and the one selected for this work, is called diglycidyl ether of Bisphenol A (DGEBA), which is created when Bisphenol A (BPA) and epichlorohydrin (ECD) react (RATNA, 2009).

There are undoubtedly more articles and reports based on fundamental and applied research on epoxy resins than any other thermosetting resin that is marketed today (RATNA, 2009). The versatility of the epoxy group toward a variety of chemical reactions and the practical properties of the network polymers are the sources of epoxy resins' widespread interest, such as high strength, very low creep, excellent corrosion and weather resistance, elevated temperature service capability, and adequate electrical properties apud (LEE & NEVILLE, 1967; BAUER, 1979; RATNA, 2007 apud RATNA, 2009).

This material is extensively used in the mechanical, electrical, chemical, aerospace, automotive, building, and other industrial sectors (WANG et al., 2011). It can be used as adhesives, coatings, fluxes, casting plastics, and the matrix resin of fiber-reinforced composites (WANG et al., 2011). Some of their most interesting applications are found in industries where resins and fibers are combined to produce complex and sometimes thick composite structures, such as in naval and offshore industries.

High-performance epoxies were developed in response to the needs of the structural composites sector. These demands were satisfied by increasing functionality (number of epoxide groups per molecule), altering curing agents, and substituting rigid bonds for the thermally weak aliphatic linkages in glycidyl groups (GOODMAN & DODIUK, 2014).

2.2 MODELING OF THE CURE OF THERMOSETS (GOVERNING EQUATIONS)

A model is a mathematically idealized representation of the system or physical process. When developing new products, the manufacturing of composites has relied on intuition based on experience and trial and error methods (MIRACLE & DONALDSON, 2001). However, when creating new prototype geometries, this method has shown to be costly in terms of both time and money. The use of composite materials in numerous potential industrial applications has been hindered by the associated risks (MIRACLE & DONALDSON, 2001). These materials and their processing operations can become cost competitive with metals and other materials by using process simulation models to speed up the development of prototypes from concept to completion.

Physically based models are used in process simulations of thermoset resins and composites curing in order to simulate the process and forecast the cure time and other properties of the finished part. The process model uses two governing equations. One is a cure kinetics equation, and the other is the heat transfer equation. A transient multiphysics-coupled problem is composed by these two equations.

2.2.1 Kinetics model

The curing process, which involves thermoset state change of the matrix from liquid to glass, is a heat transfer problem with heat generation due to the chemical reaction occurring in the resin during the process (BLEST et al., 1999; CIRISCIOLI et al., 1991; PITCHUMANI & YAO, 1993; HOJJATI & HOA, 1994; SURATNO et al., 1998 apud STRUZZIERO et al., 2019; PAIVA, 2018).

Several models have been proposed to describe the curing of thermoset resins (HORIE et al., 1970; DUSEK et al., 1975; MUZUMDAR & LEE, 1996 apud RATNA, 2009; PAIVA, 2018). There are two types of modelling approaches: mechanistic models and phenomenological models. Both of them have the purpose of determining the degree of cure and temperature distribution within the studied sample during the cure process and allowing the evaluation of its properties.

Mechanistic models consider the mechanisms of reaction that take place during curing. There may be two of them: mechanism of addition and mechanism of etherification and

homopolymerization (PAIVA, 2018). Horie's model (HORIE et al., 1970) considers these mechanisms while taking into account chemical species concentrations.

According to Ratna (2009), the mostly used model for isothermal kinetic analysis is the phenomenological model developed by Kamal (KAMAL & SOUROUR, 1973). In many curing reactions, the new groups that are created as a result of curing act as catalysts (RATNA, 2009).

Kamal and Sourour's equation (KAMAL & SOUROUR, 1973) for an autocatalytic curing reaction can be represented as:

$$\frac{d\alpha}{dt} = (K_1 + K_2\alpha^m)(1-\alpha)^n \qquad ((3)$$

Where $d\alpha/dt$ is the rate of degree of conversion α, and K_1 and K_2 the rate constants of the catalytic and auto-catalytic processes, respectively. Exponents m and n are, respectively, the orders associated with the auto-catalytic and catalytic reactions. The sum $(m + n)$ gives the overall order of the curing reaction.

The formula demonstrates that reaction rate depends on the amount of resin that has not yet been reacted – factor $(1-\alpha)^n$, catalytic – and the amount of resin that has been reacted (reaction product) – factor α^m, auto-catalytic. According to Rabearison (2009), in most studies on epoxy systems, n varies between 1 and 2, while m typically takes values between 0.67 and 1. For m=1 and n=2, Kamal and Sourour's model is identical to Horie's mechanistic model.

The Arrhenius equation shown below (Equation 4) can be used to correlate the kinetic rate constants K_1 and K_2 to temperature (RATNA, 2009; PAIVA, 2018).

$$K_1 = A_1 exp\left(\frac{-E_1}{RT}\right)$$
$$K_2 = A_2 exp\left(\frac{-E_2}{RT}\right) \qquad ((4)$$

Where the activation energy is denoted by E_i, R is the universal gas constant (8.314 J/(mol.K), T is the absolute temperature at the reaction site, and A is a pre-exponential constant.

2.2.1.1 Diffusion factor

The final degree of cure predicted by Kamal and Sourour's model is 100%. However, experimental results rarely achieve such conversion (PAIVA, 2018). Kamal and Sourour's model is appropriate at the start of the evolution of the degree of conversion, where the molecules' reactivity is dominant, but not in a moment near the end of the thermosetting reaction, beginning the vitrification (PAIVA, 2018). As curing progresses, reaction becomes increasingly governed by diffusion of reactive species and has less molecule mobility, slowing the reaction rate.

In order to incorporate diffusion effects into the cure kinetics model, which cannot be ignored, Fournier et al. (1996) added a diffusion factor f_d to Kamal's model. f_d is a function of degree of conversion and a semi-empirical relationship. The following equation represents the extended model:

$$\frac{d\alpha}{dt} = (K_1 + K_2\alpha^m)(1-\alpha)^n . f_d(\alpha) \qquad ((5)$$

The diffusion factor is expressed by:

$$f_d(\alpha) = -1 + \frac{2}{1 + exp\left(\frac{\alpha - \alpha_f}{b}\right)} \qquad ((6)$$

Where b is an empirical diffusion constant of the material and parameter αf is the conversion at the conclusion of the isothermal cure. Therefore, eight parameters must be determined in order to fully characterize the cure kinetics using the extended model: m, n, $A1$, $A2$, $E1$, $E2$, αf and b.

2.2.2 Glass transition temperature

The glass transition temperature must be properly described because, according to earlier discussions, this parameter is a reference to rubbery state and glassy state

transformations that directly affect material properties. However, the temperature at which glass transitions occur varies over the course of the curing process. With the increase in conversion, the concentration of reactive functionalities decreases and crosslinks or junction points are formed. Thus, the glass transition temperature of the resin will rise as the curing reaction progresses (RATNA, 2009).

To correlate the glass transition temperature with the degree of conversion (α), several models have been proposed. The models are constructed using statistical analysis of network formation and calculations of the concentration of junction points for various functionalities as a function of degree of cure (RATNA, 2009). The following equation, also referred to as the DiBenedetto's equation, has been successfully used to correlate the experimental values of the Tg as a function of degree of conversion for numerous thermosetting resins, including epoxy (DIBENEDETTO, 1987; PASCAULT et al., 2002 apud PAIVA, 2018; RATNA, 2009):

$$\frac{T_g - T_{g0}}{T_{g\infty} - T_{g0}} = \frac{\lambda\alpha}{1-(1-\lambda)\alpha} \qquad ((7)$$

Where T_{g0} is the T_g of the resin mixture before the cure ($\alpha = 0\%$), $T_{g\infty}$ is the T_g obtained after maximum possible curing (α = 100%), and λ is an adjustable parameter that typically assumes values between 0.46 and 0.58 for the majority of epoxy/amine systems (SMAALI, 2005).

2.2.3 Heat transfer equation

Curing is an exothermal reaction, whose activation is aided by the heat produced by itself. Thus, the model of heat transfer includes both internal and external heat sources, with a coupling of two physics: thermal and chemical (PAIVA, 2018; DAI et al., 2019).

Since the interest is on the evolution of degree of cure and temperature within the thermoset rather than how chemical species are reacting, a straightforward coupling of these physics can be represented by the addition of a heat flow (ϕ) equivalent to that released by the chemical reaction (PAIVA, 2018). The resulting heat transfer equation is the following:

$$\rho \boldsymbol{c_p} \frac{\boldsymbol{dT}}{\boldsymbol{dt}} = \boldsymbol{div}\{\boldsymbol{k}[\boldsymbol{grad}\, \boldsymbol{T}]\} + \boldsymbol{q} + \boldsymbol{\phi} - \boldsymbol{T}\{(\boldsymbol{3k} + \boldsymbol{2}\mu)\alpha_{\boldsymbol{T}}\}\boldsymbol{tr}\dot{\varepsilon} \quad (8)$$

The local temperature T of the matrix during curing is defined by Equation (8). Parameters ρ, C_p, k and α_T are the density, specific heat capacity, thermal conductivity and coefficient of thermal expansion of the forming matrix. The heat flow imposed by the oven is represented by term q. The fourth and last term of the equation is the heat produced by the mechanics as a function of the bulk modulus κ, shear modulus μ, and second-order strain tensor $\dot{\boldsymbol{\varepsilon}}$, which can be considered to be neglected in comparison to the others.

The heat flow generated by the chemical reaction (ϕ), which corresponds to the thermochemical coupling, can be expressed as follows (PAIVA, 2018):

$$\boldsymbol{\phi} = \boldsymbol{\rho}\, \boldsymbol{\Delta H^r} \frac{\boldsymbol{d\alpha}}{\boldsymbol{dt}} \quad (9)$$

Where the term ΔH^r stands for the enthalpy of the reaction.

2.2.4 Cure modelling variables

Table 2 provides a summary of all the parameters and properties needed for thorough characterization and monitoring of the thermochemical cure process.

Table 2 - Cure process variables

Field	Variables
Material Properties	k,ρ,c_p
Cure Kinetics	$A_1,A_2,E_1,E_2,m,n,\alpha_f,b$
Chemistry	ϕ
Environmental Conditions	q
Glass Transition Temperature	$T_{go}, T_{g\infty},\lambda$
State variables	$\boldsymbol{\alpha},\boldsymbol{T},\boldsymbol{t}$

Source: Adapted from Paiva (2018)

2.3 NUMERICAL SIMULATION

Several studies have focused on the numerical simulation of the curing process of thermoset matrices or composites in an effort to elucidate various aspects of the process (COSTA & SOUSA, 2003; MAWARDI & PITCHUMANI, 2003; CARLONE & PALAZZO, 2009 apud ALEKSENDRIĆ et al., 2016; PAIVA, 2018). Among the numerical methods that have been applied to this problem by the scientific community, the Finite Element Method (FEM) is one of the most used method, due to its widely known capacibilty of delivering accurate predictions of the physical behavior of a component or system subjected to different conditions.

Thus, this section focuses on explaining the principles of the FEM and how it can be implemented thorough a commercial software.

2.3.1 Finite Element Model

The Finite Element Method is a numerical technique for solving partial differential equations that was developed in the 1950s by the aerospace industry (FISH, 2009). As the equations that describe the behavior of materials are written in terms of partial differential equations, and the solution of these equations through analytical methods for arbitrary geometries is extremely difficult, this method has been widely applied in Engineering in recent

decades. Millions of engineers and scientists around the world use FEM to predict the mechanical, structural, thermal, electrical and chemical behavior of systems (FISH, 2009).

The FEM is implemented by a software in order to perform a Finite Element Analysis (FEA) of a physical phenomenon. The first steps in using FEA software are to create a computer-aided design (CAD) model of the real-world components being simulated and to insert the material's properties, the loads, and the constraints that have been placed on it. With the help of this information, real-world behavior can be predicted, frequently with astounding levels of accuracy.

The FEA methodology entails dividing the component (the domain of the differential equation) into finite elements connected to one another, which form a mesh (Figure 14). To obtain the equations for each element, an integral form of the differential equation is deduced through the principle of virtual work (PTV). In stress analysis, the field variable of the equations is the displacement (u). This variable is then approximated by a linear combination (series expansion) of known functions (N) with unknown coefficients (a), called interpolation functions, also known as shape functions. The choice of these functions is conveniently made so that the unknown coefficients represent the nodal displacements.

Figure 14 – A finite element mesh over a rectangular region with a central hole

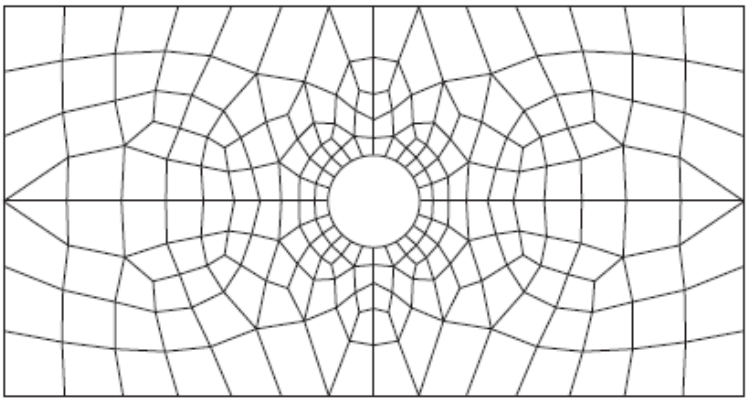

Source: Hutton (2004)

The equations obtained for the elements are combined, resulting in the following global system of equations for the component:

$$[\boldsymbol{K}][\boldsymbol{a}] = [\boldsymbol{P}] \qquad ((10)$$

Where $[K]$ is the stiffness matrix, $[P]$ is the force vector applied to the body and $[a]$ is the vector of the nodal displacements. The stiffness matrix contains information about the

geometry and behavior of the material, and indicates the element's resistance to deformation when subjected to loading. Applying the boundary conditions, the system of equations is solved to find the vector [a], and then the displacement approximation function [u] is obtained by:

$$[\boldsymbol{u}] = [\boldsymbol{N}][\boldsymbol{a}] \tag{11}$$

Having found the displacement field for the component, it is possible to calculate the stress and strain tensors at any point on the elements. The deformation components are obtained through the Equations (12). Moreover, the stress components are given by the constitutive equations of the material, which for a linear material are expressed by the generalized Hooke's law.

$$\begin{aligned}
\varepsilon_{11} &= \frac{\partial u_1}{\partial x_1} = \epsilon_1 \; ; \quad 2\varepsilon_{12} = 2\varepsilon_{21} = \left(\frac{\partial u_1}{\partial x_2} + \frac{\partial u_2}{\partial x_1}\right) = \gamma_6 = \epsilon_6 \\
\varepsilon_{22} &= \frac{\partial u_2}{\partial x_2} = \epsilon_2 \; ; \quad 2\varepsilon_{13} = 2\varepsilon_{31} = \left(\frac{\partial u_1}{\partial x_3} + \frac{\partial u_3}{\partial x_1}\right) = \gamma_5 = \epsilon_5 \\
\varepsilon_{33} &= \frac{\partial u_3}{\partial x_3} = \epsilon_3 \; ; \quad 2\varepsilon_{23} = 2\varepsilon_{32} = \left(\frac{\partial u_2}{\partial x_3} + \frac{\partial u_3}{\partial x_2}\right) = \gamma_4 = \epsilon_4
\end{aligned} \tag{12}$$

2.3.1.1 Types of finite element mesh

The type of mesh that is selected for the simulation strongly affects the modeling computational requirements and the accuracy of the results. In fact, when it comes to setting up and resolving a finite element problem, meshing is one of the memory-intensive steps. The correct element types and sizes must be chosen, taking into account the trade-off between accuracy and computational cost, in order to determine the mesh that is best suited for a specific model.

Depending on the nature of the problem, elements can take on a variety of forms, such as: bars for 1D elements; triangles or quadrilaterals, for 2D elements; and tetrahedrons, pyramids, prisms or hexahedrons, for 3D elements.

The interpolation functions are related to the number of nodes in the element. The higher the geometric order of the interpolation functions, the higher the number of nodes per element, which imply greater accuracy in the solutions, as shown in Figure 15 for 1D elements. However,

the costs in terms of computational time also increase. Besides, Figure 15 shows that more elements (mesh refinement) also lead to solutions that are more exact, and that are more computationally expensive as well.

Figure 15 – Discretization errors for 1D Finite Elements

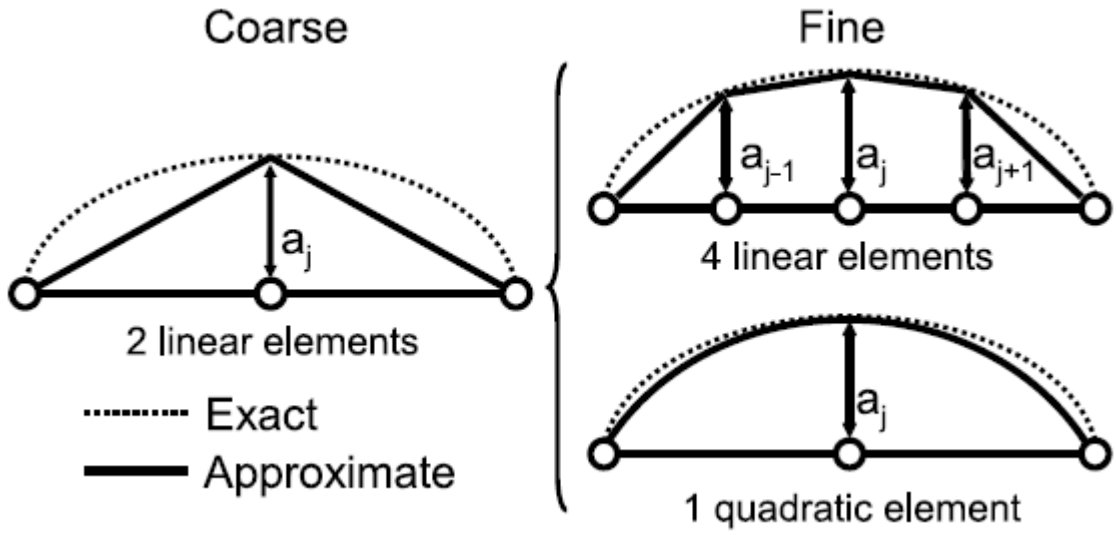

Source: Adapted from Barbero (2013)

In order to validate a FEA model, increasing the element order is one approach but it is likely that refining the mesh instead will lead to better results (COMSOL INC., 2019e).

2.3.1.2 Timestep refinement

Transient simulations need to compute a discrete solution that reflects the time evolution. The unknown transient degrees of freedom are calculated using time-integration techniques starting from initial data. If the computed solution meets the predefined error boundaries within the specified tolerances, the time step's computed solution is approved.

When working with transient FE models, in addition to the mesh refinement, it is necessary to perform a timestep refinement, by comparing the model against other models run with finer timesteps, to gain confidence in the simulation results (COMSOL INC., 2019f)

2.3.1.3 Steps of the Finite Element Analysis

Finite Element Analysis consists of three main steps:

1) Pre-processing: where the model is configured before performing the calculations, by specifying geometry, material properties, loading and boundary conditions, and the Finite Element mesh characteristics.
2) Processing: this is the step where the calculations are actually performed by the Finite Element software.
3) Post-processing: In this step, the calculation results are displayed. A critical analysis of the results obtained must be carried out, judging whether they are coherent or not.

2.3.1.4 Finite Element Software

Currently, there are several Finite Element software available on the market, each with its advantages and disadvantages in terms of graphical interface, performance, types of analysis, among others. Some popular commercial Finite Element software are: COMSOL®, Abaqus®, ANSYS®, ADINA®, Cosmos®, Nastran® and LS DYNA®.

COMSOL Multiphysics® is a simulation platform that provides fully coupled multiphysics and single-physics modeling capabilities (COMSOL INC., 2019c). The entire modeling workflow is covered by COMSOL® Model Builder, from specifying geometry, material properties, and the physics that characterize particular phenomena to solving and postprocessing models to generate precise results (COMSOL INC., 2019c). In several areas of engineering, manufacturing, and scientific research, engineers and scientists simulate designs, devices, and processes using the COMSOL Multiphysics® program. The main capabilities and functionalities of this software is the following (COMSOL INC., 2019a):

- The program provides a multiphysics interface that makes it simple to configure variant input parameters and solve coupled physics problems in a user-friendly interface.
- There are several modules in COMSOL®, including those for math, acoustics, electrical, chemical, mechanical, fluid, and heat applications.

- It works with several space dimensions – 3D, 2D Axisymmetric, 2D, 1DAxissymmetric, 1D and 0D – and types of study – stationary, time dependent, frequency domain, etc.
- Given that the program was designed to run coupled phenomena problems, it produces results relatively quickly in these cases.
- Everything is incorporated into the program, which reduces the need for computer memory and processing time.
- The program has an Application Programming Interface (API) for Java and LiveLink for CAD software, MATLAB® and Excel®, which effectively integrates them with COMSOL® simulations.

COMSOL LiveLink for MATLAB® is one of the most interesting features of COMSOL because it allows automatizing all the steps of a simulation model from a script in MATLAB. The tasks that can be performed with COMSOL LiveLink for MATLAB® are detailed below (COMSOL INC., 2021):

- Create models using a script. The COMSOL® Application Programming Interface (API), which is part of the LiveLink™ for MATLAB®, has all the required methods and functions to create models from scratch. There is a command entered at the MATLAB prompt that corresponds to every action taken in the COMSOL Desktop®. It is a streamlined syntax built on the Java® platform and does not require any prior Java expertise.
- Use MATLAB functions when configuring models. To use a MATLAB function to set model properties, use LiveLink™. Define boundary conditions or material properties, for instance, as a MATLAB routine that is assessed as the model is solved.
- Interactive modeling using the same model in MATLAB and COMSOL Desktop. Every change made at the MATLAB prompt updates the COMSOL Desktop at the same time.
- Utilize MATLAB's features to improve program flow. To manage the progression of your programs, combine MATLAB functionality with API syntax. For instance, use the for or while commands to implement nested loops, the if or switch statements to implement conditional model settings, or the try and catch syntax to handle exceptions.

- Analysis of the simulation results in MATLAB. It is simple to extract data at the command line thanks to the included API wrapper functions. Functions are available to access results at arbitrary or node points. Additionally, it possible to obtain detailed information about the extended mesh, such as the coordinates of the finite element mesh and details about the connections between the elements and nodes. Extracted information is available as MATLAB variables that are prepared for use with any MATLAB function.

- Create models with unique interfaces. To combine a user-defined graphical interface with a COMSOL model, use the MATLAB Guide or the App Designer functionality. Create graphical user interfaces that are specifically designed to expose the settings and parameters of one's choice to make the models accessible to others.

- COMSOL Server™ and COMSOL Multiphysics Server can both be accessed through LiveLink for MATLAB®. This implies that any user with access to COMSOL Server™ can receive and use MATLAB scripts and GUIs that make use of COMSOL functionality.

2.4 NUMERICAL OPTIMIZATION

The broad field of optimization has drawn the intense and continuous attention of a number of researchers in recent years, primarily as a result of the quick development of computer technology, including the creation and availability of user-friendly software, fast and parallel processors, and artificial neural networks (SUDHOFF, 2021). Optimization is a vital tool in both decision science and the analysis of physical systems.

The process of optimization involves comparing viable solutions until no better one can be found (DEB, 2001). Solutions are classified as good or bad in terms of an objective, which is frequently the price of fabrication, the quantity of harmful gases, the efficiency of a process, the dependability of the product, or other factors. Mathematically speaking, optimization is the minimization or maximization of one or more objective functions under restrictions on their variables (GOPAL et al., 2000).

Prior to performing an optimization, we must first choose an objective, which is a numerical evaluation of the effectiveness of the system under investigation (NOCEDAL & WRIGHT, 2006). This objective could be any quantity or combination of quantities that can be represented by a single number, including money, time, potential energy, and many others. The problem can be classified as a Single Objective (SO) optimization problem, which only considers one objective, or a Multi Objective (MO) optimization problem, which considers two or more objectives.

The objective is dependent on specific system properties known as decision variables or unknowns. Finding decision variable values that optimize the objective is the optimization goal. The decision variables are frequently restricted or constrained in some manner. For example, a material's density is a quantity that cannot be negative.

Identifying the objective, decision variables, and constraints for a specific problem is a process known as optimization modeling. The first step in the optimization process is the creation of a suitable optimization model. The model will not provide useful insights into the real-world problem if it is overly simplistic. On the other hand, it might be too difficult to solve if it is too complex.

Once the model has been created, its solution can be found using an optimization algorithm, typically with the aid of a computer. There is not a single algorithm that can be used to solve all optimization problems; rather, there is a variety of algorithms, each of which is designed to solve a specific kind of optimization problem (NOCEDAL & WRIGHT, 2006). It is frequently the user's responsibility to select the algorithm that is best for a given application. This decision is crucial because it could affect how quickly the problem is solved, or even whether a solution is ever found (NOCEDAL & WRIGHT, 2006).

After an optimization algorithm has been applied to a given model, the solution's interpretation in terms of the application may suggest ways that the model can be improved or refined (NOCEDAL & WRIGHT, 2006).

2.4.1 Numerical optimisation methods

According to (STRUZZIERO, 2019), there are two broad categories that can be used to classify optimization methods:

1) **Gradient-based techniques**: Optimization methods that use an objective function's derivatives to try to minimize or maximize the objective function. When the problem's landscape is relatively straightforward, this family of techniques (gradient-based) can be successfully applied. These techniques have the advantage of fast convergence. However, they take the approach of beginning with a single estimated solution and attempting to refine that estimate, which makes them vulnerable to being stuck at a local maximum or minimum, as the ones displayed in Figure 16(a). The single estimate will tend to converge to the local extrema if it is close to them. Thus, the success of gradient-based methods in situations where the landscape is filled with local minima and/or maxima depends heavily on the choice of the initial values of the optimization variables, requiring a priori knowledge of the landscape, which is frequently unavailable.
2) **Zero-order methods**: Methods that do not require continuity of the objective function and of its derivatives. Hessians and gradients are not even used or estimated. This characteristic is advantageous when operating in a discrete search space or with discontinuities, as shown in Figure 16(b). The objective function must only be able to be assessed at any location within the chosen search space. Nevertheless, there is no guarantee that the solution found is strictly optimal and they are computationally expensive. Zero order methods can also be referred to as stochastic algorithms or evolutionary strategies (ES) and are most frequently nature-inspired. These techniques typically begin with the generation of a population, a first random set of solutions, and progress toward better sets of solutions with each algorithm iteration (generation) by assessing the fitness of the solutions and employing stochastic operators. These population-based techniques are less likely to converge to a local extrema because they work with several potential solutions at a single simulation run.

Figure 16 – Function properties that are detrimental to gradient-based optimization techniques

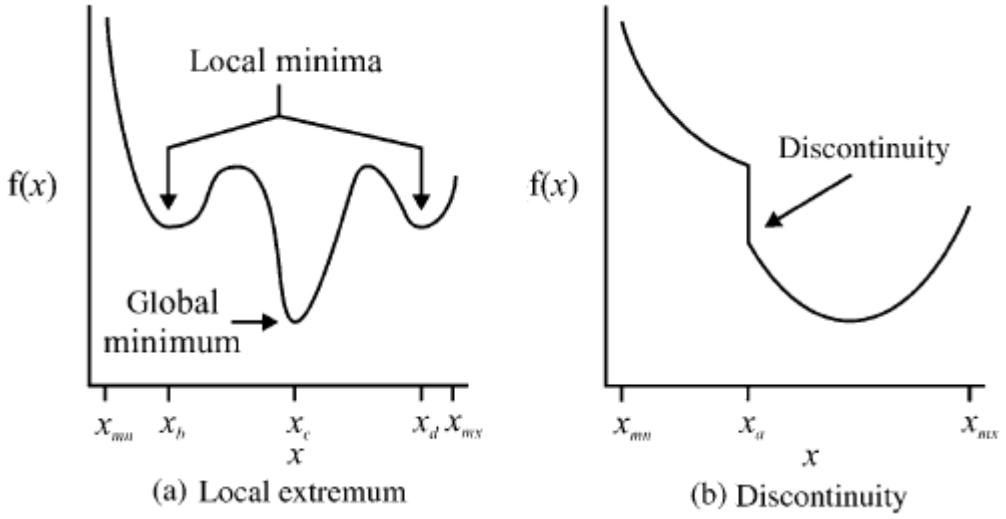

Source: Sudhoff (2021)

Deb (2001) claims that gradient-based methods are a subset of what he calls **“**classical optimization methods”, which are defined as optimization algorithms that use a single solution update in every iteration and that mainly use a deterministic transition . Yet according to Deb (2001), classical optimization methods can be classified into two distinct groups: direct search methods and gradient-based techniques. In direct search methods, the search strategy is determined solely by the objective function and the constraint values. Because derivative information is not utilized, direct search methods are typically slow and require numerous function evaluations before convergence. However, direct search methods present many difficulties that are common to most classical methods (including gradient-based techniques), as follows:

- Most algorithms tend to be *stuck* to a suboptimal solution (local minimizer or maximizer).
- The initial solution that is selected determines the convergence to an optimal solution.
- An algorithm that works well to solve one optimization problem might not work well to solve another one.
- When dealing with problems with a discrete search space, theses algorithms are ineffective.
- A parallel machine cannot be used to run these algorithms effectively.
- Algorithms are inconvenient for solving multi-objective optimization problems because they can only find, at best, one solution in one simulation run.

Some examples of classical optimization methods are weighted sum, ε-constraint, weighted metric, Benson's, value function and goal programming methods (DEB, 2001). Among the zero-order methods, the most widely used evolutionary strategies are Genetic Algorithms (GA), Particle Swarm Optimization (PSO), and Ant Colony Optimization (ACO) (STRUZZIERO, 2019).

2.4.2 Multi-objective optimization

In most disciplines, problems with multiple objectives naturally arise, and finding solutions to these problems has long been a problem for researchers (COELLO et al., 2014).

The key distinction between single-objective optimization and multi-objective optimization is that the latter searches a set of points that describe the best tradeoff between competing objectives, whereas the former looks for a single point associated to the maximum or minimum of a single objective function (SUDHOFF, 2014).

2.4.2.1 Definitions

A multi-objective optimization problem has a number of objective functions that are to be minimized or maximized. Similar to the single-objective optimization problem, there are a number of constraints that any feasible solution must meet. The general form of multiobjective optimization problem can be formally defined as (DEB, 2001):

$$\begin{aligned} \text{min/max} \quad & f_m(\boldsymbol{x}), && m = 1, 2, \cdots, M \\ \text{subject to} \quad & g_j(\boldsymbol{x}) \geq 0, && j = 1, 2, \cdots, J \\ & h_k(\boldsymbol{x}) = 0, && k = 1, 2, \cdots, K \\ & \underset{\text{lower bound}}{x_i^{(L)}} \leq x_i \leq \underset{\text{upper bound}}{x_i^{(U)}}, && i = 1, 2, \cdots, n \end{aligned} \tag{13}$$

where a solution $\boldsymbol{x}$ is a vector of n decision variables:

$$x = [\boldsymbol{x_1}, \boldsymbol{x_2}, \boldsymbol{x_3}, \dots, \boldsymbol{x_n}] \quad (14)$$

The last set of constraints are called variable bounds, restricting each decision variable x_i to take a value within a lower and an upper bound ($x_i^{(L)}$ and $x_i^{(U)}$, respectively). These bounds delimit a decision variable space, or simply the decision space. In the present work, to refer to a solution vector $\boldsymbol{x}$, the terms point and solution were used interchangeably. J inequality and K equality constraints are related to the optimization problem, where $g_j(\boldsymbol{x})$ and $h_k(\boldsymbol{x})$ and the constraint functions. The inequality constraints are handled as "greater-than-equal-to" types, though the above formulation also addresses a "less-than-equal-to" type inequality constraint (DEB, 2001). The constraint must be changed into a "greater-than-equal-to" type constraint in the latter situation by multiplying the constraint function by -1 (DEB & KUMAR, 1995 apud DEB, 2001).

A solution $\boldsymbol{x}$ is said to be infeasible if it fails to satisfy each of the above-mentioned $2n$ variable bounds and *(J + K)* constraints. On the other hand, a feasible solution is one that satisfies all restrictions and variable bounds (DEB, 2001).

2.4.2.2 Goals in multi-objective optimization

A multi-objective optimization has the following two goals (DEB, 2001):

1) **To identify a set of solutions that is as near the Pareto-optimal front as possible**. Given the significance of each objective in a multi-objective optimization, a diverse set of obtained solutions that are close to the Pareto-optimal front offers a range of optimal solutions that trade objectives in various ways. The Pareto-optimal front is explained in next section.
2) **To identify a set of solutions that is as diverse as possible.** If a multi-objective optimization algorithm is unable to identify a diverse set of feasible solutions to a problem, it is just as effective as a single-objective algorithm.

In order to achieve those two goals, a multi-objective optimization algorithm must include explicit or implicit mechanisms to emphasize convergence near the Pareto-optimal front and the maintenance of a diverse set of solutions (DEB, 2001). Multi-objective optimization is more challenging than single-objective optimization because of those two goals.

2.4.2.3 Pareto-optimal front

In the single-objective optimization problem, it is easy to choose which solution is better than the others, by comparing the respective values of the objective function. However, in multiple-objective optimization problem, it is necessary to redefine what is good in a solution.

With this in mind, the concept of domination was introduced. Assume that there are two possible solutions, x^1 and x^2 (here the superscript denotes only the solution number). The following two requirements must be met for the solution x^1 to be considered to dominate x^2 (or for x^2 to be dominated by x^1) (SUDHOFF, 2014):

1) The solution x^1 is no worse than x^2 in all objectives.
2) The solution x^1 is strictly better than x^2 in at least one objective.

The non-dominated solution set, given a set of solutions, consists of all the solutions that are not dominated by any of the members of the solution set (SUDHOFF, 2014). The Pareto-optimal solution set is the non-dominated set of all feasible solutions (feasible decision space) (SUDHOFF, 2014). Each solution in the feasible decision space can be mapped to the feasible objective space, as shown in Figure 17 for an optimization problem that possess two conflicting objectives, $f_1(\boldsymbol{x})$ and $f_2(\boldsymbol{x})$, that need to be minimized. The Pareto-optimal front is the set of all the points mapped from the Pareto-optimal solution set, which is shown in Figure 17 as a bold line in the feasible objective space.

Figure 17 - The Pareto-optimal front

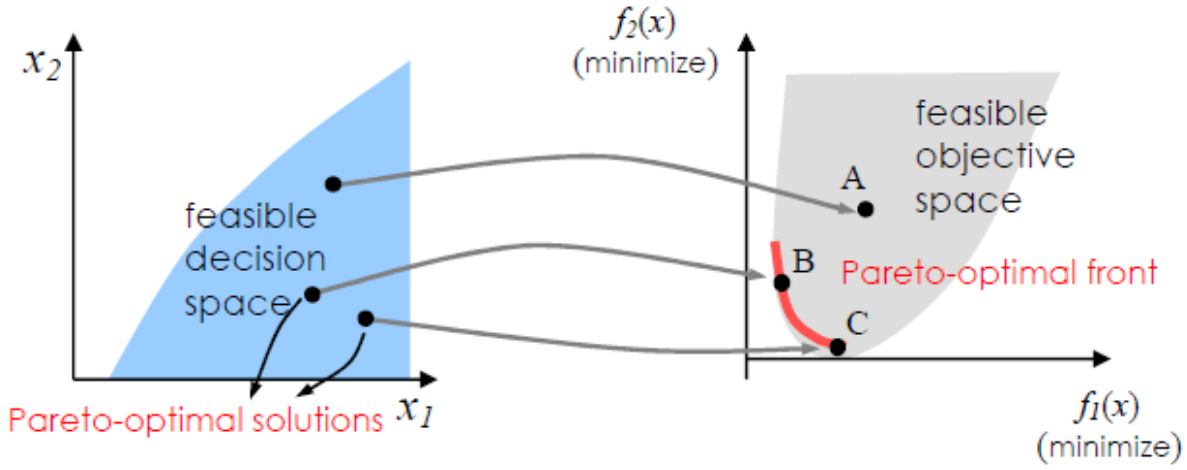

Source: Sudhoff (2014)

2.4.2.4 Diversity control

For a given multi-objective optimization problem, there are several possible solutions, and any solution found in the set of Pareto-optimal solution set can be the best one according to the application (SUDHOFF, 2014). Finding as many Pareto-optimal solutions as possible is therefore necessary, but also finding solutions that are as diverse as possible on the Pareto-optimal front.

Five points in the Pareto-optimal front are shown in Figure 18 for cases (a) and (b). The solutions of (a) are concentrated on a particular area of the Pareto-optimal front, whereas (b) are evenly distributed throughout the Pareto-optimal front. For the given problem (a), there is a chance that the best solution is hidden in the Pareto-optimal front's neglected area. Thus, having a diversity of solutions is important.

Figure 18 - Different distributions of solutions: (a) concentrated on a specific part of the Pareto-optimal front and (b) evenly distributed over the Pareto-optimal front

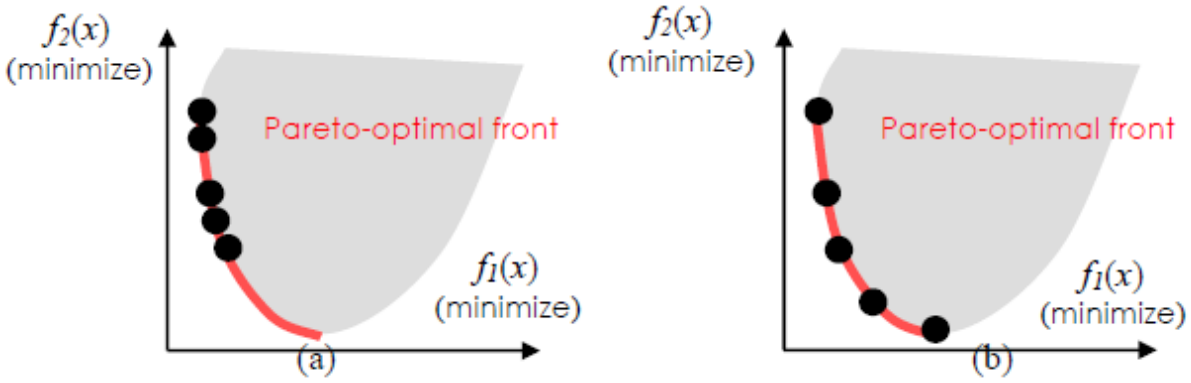

Source: Sudhoff (2014)

There are several different techniques that can be applied in multi-objective optimization algorithms to control the diversity of solutions (DEB, 2001; COELLO et al., 2014).

2.4.3 Evolutionary Algorithms

Among the existing optimization algorithms, Evolutionary algorithms (EAs) EAs are ideal candidates for solving multi-objective optimization problems (DEB, 2001). This is because they can find multiple optimal solutions in one single simulation run due to their population-approach.

Evolutionary algorithms (EAs) are search and optimization techniques that mimic natural evolutionary principles (DEB, 2001). They are a subclass of Evolutionary Computation, which work with the concept of populations, and correspond to the set of general stochastic search algorithms (VIKHAR, 2016).

Other population-based optimization methods, such as particle swarm optimization, have also been used successfully in literature (SUDHOFF, 2021). Nevertheless, here the emphasis is given to the study of EAs and, specifically, Genetic Algorithms (GAs), which are Evolutionary Algorithms that have proven to be very effective in solving design optimization problems (SUDHOFF, 2021).

Although the use of traditional multi-objective optimization methods to address issues in a variety of fields - such as management, engineering, and science - dates back to 1951, it wasn't until the middle of the 1980s that Multi-Objective Evolutionary Algorithms (MOEAs) were used for the first time (ITO et al., 1983; SCHAFFER, 1985; FOURMAN, 1985 apud COELLO et al., 2014). However, the number of MOEA applications has significantly increased since the late 1990s (COELLO et al., 2014). This was largely stimulated by MOEAs' success in resolving real-world problems. MOEAs have produced results that are either competitive to or superior to those obtained using other search strategies (COELLO et al., 2014).

2.4.3.1 Advantages when compared to classical methods

The main advantages that an Evolutionary Algorithm has over classical search and optimization techniques, which stimulate its wide use in complex problem solving, are the following (WHITLEY, 2001; AL-SALAMI, 2009 apud VIKHAR, 2016):

1) It is conceptually simple and flexible because it is inspired by natural evolution;
2) It is representation independent, while there are some numerical optimization techniques that can only be used in applications with continuous values or with constrained sets.
3) Evolution is a parallel process. Each evaluation in an EA performs parallel operations, only operations carried out during the selection process requires serial processing.
4) Evolutionary Algorithms are robust and develop to adapt the solution in a changing environment, while classical optimization methods change with dynamic variation that takes place in problem environment;
5) EAs are capable of solving problems without the aid of any human expertise. If human expertise is available, an EA can use it; however, human expertise may not be reliable, qualified, or accurate.

The advantage number 3 must be highlighted. The objective functions and constraints of many real-world optimization problems are usually computed using simulation software involving the finite element method, the computational fluid mechanics approach, nonlinear equation solving, or other computationally intensive methods (DEB, 2001). Since most classical methods use the point-by-point approach, where a single solution is updated to a new solution in one iteration, the benefits of parallel systems cannot be fully utilized. On the other hand, Evolutionary Algorithms can use parallelism, which highly reduces the computational

time and also increases the quality of the solutions found (SUDHOLT, 2007 apud VIKHAR, 2016). This is a relevant benefit considering that parallel computing systems are now practical to use due to their availability and affordability.

2.4.3.2 Difficulties of evolutionary algorithms

In spite of having many advantages, EA possesses some drawbacks, such as (VIKHAR, 2016):

1) Inability to always provide the optimal solution to a given problem in a predictable amount of time;
2) Potential need for parameter tuning through trial and error or another method; and
3) High computational resource requirements.

There are two basic reasons for the large amount of computational resources that can be required by EAs (VIKHAR, 2016). The first one is that the evaluation of the objective (and fitness) functions may be complex and slow. The second one is that the size of the population may need be too large. To tackle this drawback, the natural solution is to split up the workload among several computers and run all computations in parallel.

2.4.3.3 Operators and parameters tuning

When implementing an Evolutionary Algorithm, two optimization problems are faced (YU & GEN, 2010):

1. Finding the optimal solution(s) of the original optimization problem, which is associated to the *problem parameter*;
2. And finding the optimal optimization operators and their respective optimal parameters, which is associated to the *strategy parameter*.

The second problem can occasionally be even more challenging than the first one because of the nonlinear intrinsic properties of EAs (YU & GEN, 2010). That explains why there are so many papers on how to optimize the performance of optimization algorithms (YU & GEN, 2010).

The factors affecting the results of optimization can be roughly divided into two categories: local factors and global factors (YU & GEN, 2010). Those factors that will only have effects at the individual (solution) level are *local factors,* such as crossover and mutation operators and their parameters. On the other hand, factors that will have effects at the population (set of solutions per iteration) level are *global factors*, such as selection type and its parameters, stop criteria and population size. Local factors have less of an impact on population diversity and selective pressure than do global factors (YU & GEN, 2010). Consequently, they are more difficult to set.

An extensive study on *strategy parameter* setting was performed by Eiben et al. (1999) apud Yu and Gen (2010). Much effort has been dedicated to fine-tuning the strategy parameters for most problems in a numerical way. The most well-known work is De Jong's experiments in his Ph.D. thesis (DE JONG, 1975 apud YU & GEN, 2010), where he suggested that the following optimization operators and parameters were proper strategy parameters for his test functions: population size = 50, crossover probability = 0.6, mutation probability = 0.001, and elitism. Grefenstette, in turn, used a meta-level GA to handle the strategy parameter optimization problem (GREFENSTETTE, 1986 apud YU & GEN, 2010). The optimal solution of the meta-level GA, that is, the best strategy parameters for a given performance criteria were population size = 30, crossover probability = 0.95, mutation probability = 0.01, and elitism.

As can be seen from the above studies, suggestions from different researchers are achieved by different test functions and different performance criteria, which makes it difficult to choose the best strategy parameters for a specific problem based on literature data, because different problems might require different optimal strategy parameters.

Therefore, sometimes EAs users need to do the *parameter tuning* on their problems, thorough trial-and-error or another method, such as the meta-GA (YU & GEN, 2010). Both of these methods can be very time consuming because the possible value number of the strategy parameters might be large and the coupling between strategy parameters might be tight (YU & GEN, 2010).

2.4.3.4 Types of evolutionary algorithms

There are numerous Evolutionary Algorithms available nowadays. As displayed in Figure 19, they can be divided into four categories: Evolutionary Strategies (ES), Genetic Algorithm (GA), Genetic Programming (GP) and Evolutionary Programming (EP) (DE JONG, 1997; WHITLEY, 2001 apud VIKHAR, 2016).

Figure 19 - Classification of Evolutionary Algorithms

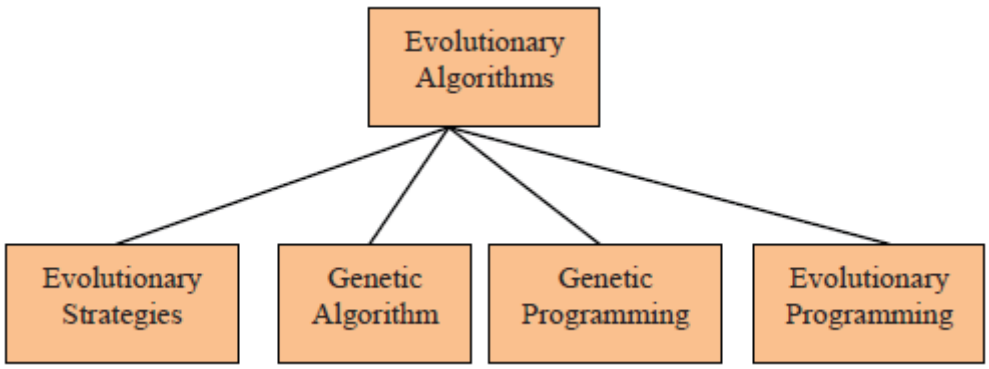

Source: Vikhar (2016)

According to Vikhar (2016), the most popular type of EA is the Genetic Algorithm (GA) because it presents the most accurate computer mapping of the natural evolution process. It is frequently used for machine learning, pattern recognition and optimization problem (COELLO, 2005 apud VIKHAR, 2016). In the next sections, we will discuss in detail the canonical and real-coded genetic algorithms.

2.4.3.5 Genetic Algorithm

A century after the work of Mendel and Darwin on genetics and evolution, by the mid-1960s, John Holland, a professor at the University of Michigan, developed a computation algorithm for optimization using biological genetics principles, the Genetic Algorithm (GA) (HOLLAND, 1992 apud SUDHOFF, 2021). In 1984, Schaffer implemented the first multi-objective Genetic Algorithm (SCHAFFER, 1984 apud SUDHOFF, 2014). However, researchers did not start working on this topic actively until the middle of the 1990s (SUDHOFF, 2014).

2.4.3.5.1 Review of Biological Genetics

By going over some fundamental concepts of biological genetics, this section will prepare the ground for the use of GAs as optimization engines.

Every living thing is built according to a specific set of instructions. Deoxyribonucleic acid (DNA), found in each living thing's cell, contains these instructions (SUDHOFF, 2021). A sequence of compounds in a DNA molecule forms a gene of a living being (SUDHOFF, 2021). In terms of optimization, the gene is seen as a decision variable, also called design parameter, of a living organism. Chromosome is the name given to each DNA molecule found in a living thing. Most living things have several chromosomes. Humans, for instance, have 46 chromosomes per cell (SUDHOFF, 2021). In contrast, the number of chromosomes in artificial GAs is much lower and frequently consists of just one chromosome per individual (SUDHOFF, 2021).

In addition to having a basic understanding of DNA, chromosomes, and genes, one also needs to take into account sexual reproduction, especially the development of gametes (sperm and egg cells). Meiosis is the process by which gametes are created. The pairing of the chromosomes provided by the mother and father initiates meiosis. It is possible for the chromosome arms to switch places during this pairing process, creating a new chromosome with a mixture of genes from the mother and the father. The crossover point typically occurs between genes (SUDHOFF, 2021). All chromosomes are capable of multiple crossovers. Numerous additional genotypes of gametes can be produced as a result of the crossover. In fact, the number of genotypes that can be produced is related to the number of genes because of crossover. Consequently, crossover is crucial for achieving genetic diversity (SUDHOFF, 2021).

In addition to the diversity of gametes brought about by genetic crossover, mutation also results in additional diversity. Errors in the DNA copying process lead to mutation. It is usually for the worse when mutation has a noticeable effect. However, occasionally advantageous mutations take place that increase an individual's (and eventually a species') capacity for survival.

The idea of natural selection and the survival of the fittest, which originated during Charles Darwin's travels, is the final biological concept that will serve our needs for an optimization engine (SUDHOFF, 2021). GAs directly employ the notion that only the

population's fittest members survive to reproduce. The individuals who "survive" and are inserted into a mating pool will be chosen using these algorithms, based on an explicit fitness function (SUDHOFF, 2021).

2.4.3.5.2 The Canonical Genetic Algorithm

In this section, the canonical GA, similar to Holland's original vision, will be explained. The first concept that needs to be established in a GA is that it operates on a population, not an individual, just like evolution does (SUDHOFF, 2021). The population of the GA will be represented by the symbol $\mathbf{P}[k]$, where k is the generational number. There are many individuals in the kth generation, as shown below:

$$\mathbf{P}[k] = \{\boldsymbol{\theta}^1, \boldsymbol{\theta}^2, \cdots \boldsymbol{\theta}^{N_P}\} \tag{15}$$

Where $\boldsymbol{\theta}^i$ is the genetic code for the ith individual in the kth generation of the population and N_p represents the number of individuals in the population, which should be an even number. The ith individual's genetic code may be structured as:

$$\boldsymbol{\theta}^i = \begin{bmatrix} \text{chromosome } 1 & \begin{Bmatrix} \boldsymbol{\theta}_1^i \\ \boldsymbol{\theta}_2^i \end{Bmatrix} \\ \text{chromosome } 2 & \begin{Bmatrix} \boldsymbol{\theta}_3^i \\ \boldsymbol{\theta}_4^i \\ \boldsymbol{\theta}_5^i \end{Bmatrix} \\ & \vdots \\ \text{chromosome } N_c & \begin{Bmatrix} \boldsymbol{\theta}_{N_g}^i \end{Bmatrix} \end{bmatrix} \tag{16}$$

Where N_c is the number of chromosomes, N_g is the number of genes, and $\boldsymbol{\theta}_j^i$ is the jth gene of the ith individual, related to the kth generation. Every gene, in the canonical GA, is a binary string sequence. Thus, $\boldsymbol{\theta}^i$ is represented by a binary number. It should be noted that many GAs only allow for the existence of one chromosome per individual, in which case genetic diversity is only produced through crossover and mutation (SUDHOFF, 2021).

A decoding function *d* is associated with the genetic code of the individuals, in order to translate the genetic code into a parameter vector (SUDHOFF, 2021):

$$\mathbf{x}^i = \mathrm{d}(\boldsymbol{\theta}^i) \tag{17}$$

Where $\mathbf{x}^i$ is the parameter vector of the ith member of the population and is structured as

$$\mathbf{x}^i = \begin{bmatrix} x_1^i \\ x_2^i \\ \vdots \\ x_{N_g}^i \end{bmatrix} \tag{18}$$

As can be seen, $\mathbf{x}^i$ has one element for each gene, denoted with a subscript, but it is not divided into chromosomes (SUDHOFF, 2021). Based on the parameter vector of ith population member, the objective function $f(\mathbf{x}^i)$ can be evaluated:

$$f^i = \mathrm{f}(\mathbf{x}^i) \tag{19}$$

The objective function in a GA is referred to as a fitness function (SUDHOFF, 2021). It will be used to decide which members of the population will mate to create the following generation in the "survival of the fittest" sense. Fitness is viewed positively in the context of a GA, so it is assumed that we want to maximize the fitness function. Fortunately, converting between a function's maximization and minimization is a simple process (SUDHOFF, 2021).

The canonical GA has a simple algorithm composed of three operators: selection, crossover and mutation (GOLDBERG, 1989). The fundamental aspects of a GA are illustrated in Figure 20.

Figure 20 – Canonical Genetic Algorithm

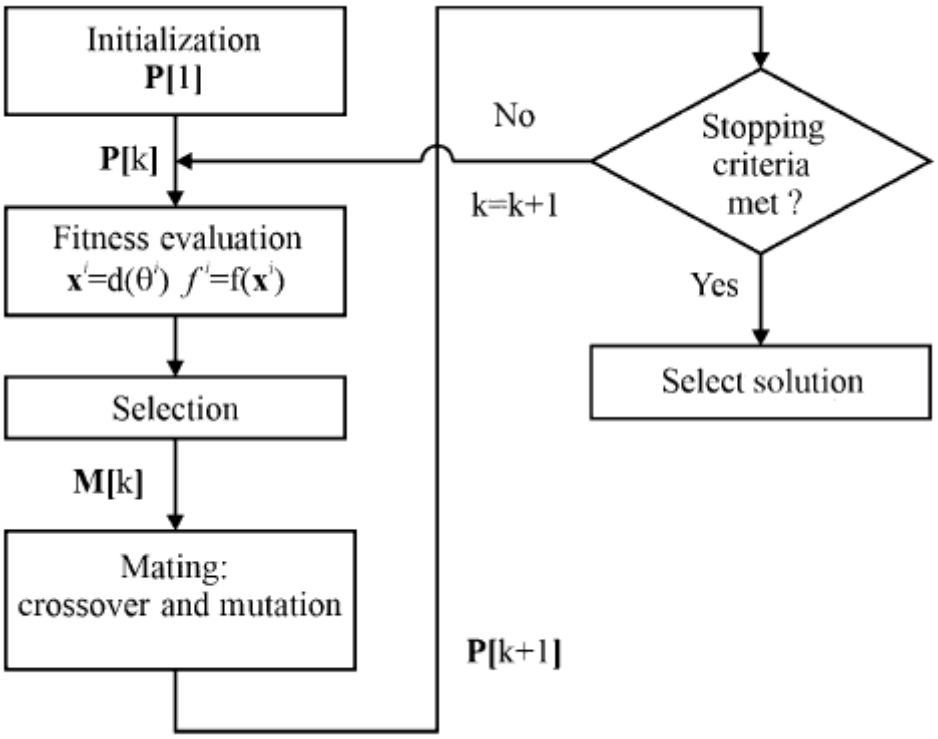

Source: Adapted from Sudhoff (2021)

Initialization

Initialization, the first process in the GA, results in the initial population. Every individual's genetic code is given a random initialization (SUDHOFF, 2014). This yields an initial population of designs, designated **P**[1].

Fitness Evaluation

The genes are then encoded, and the fitness of each population member is assessed (SUDHOFF, 2021). The fitness value is a measure of an individual's worth (SUDHOFF, 2014). An individual is typically more optimal when their fitness value is higher .

Selection

Based on the fitness, the selection process establishes a mating pool **M**[k]. In nature, the more adapted individuals have a higher chance of surviving and procreating. In order to simulate this scenario, the selection operator makes sure that individuals with higher fitness values have a higher likelihood of surviving and reproducing. The roulette wheel and

tournament selection algorithms are typically used to create a mating pool, among the many different selection techniques (SUDHOFF, 2014):

a) **Roulette wheel selection:** It is one of the most widely used methods of selection (SUDHOFF, 2021). Let's assume that each individual has been evaluated and given a fitness value. Then, one can picture a roulette wheel with sections whose total number is equal to the total number of individuals and whose areas are proportional to the corresponding individual's fitness levels. After that, a chromosome is chosen and copied to the mating pool by turning the wheel. The mating pool is complete after several repetitions of this process.
b) **Tournament selection:** According to the name, two or more individuals are randomly selected from the population, and the one who has the highest fitness value is chosen and reproduced in the mating pool. Compared to the roulette wheel method, this one is easier to implement (SUDHOFF, 2021).

In order to create the children who will make up the following generation, P[k + 1], the individuals chosen from the population will mate. Genetic operators like crossover and mutation will then be used to create the offspring.

Crossover

The crossover operator simulates the reproduction of living organisms by transferring genes between chromosomes. New individuals created through crossover have traits inherited from both of their parents. Crossover is performed on the mating pool Mk and it can be of two types (SUDHOFF, 2014):

a) **Single-point crossover:** in which a random crossover point is chosen, and after that point, the genes of the parents are switched; and
b) **Multiple-point crossover:** where the parents' genes are switched in between a number of crossover points that are randomly selected.

Mutation

A mistake in copying the gene information leads to mutation in natural evolution. Similar to this, the process of mutation in GA involves changing a random subset of genes in chromosomes. Maintaining the population's diversity is the primary role of the mutation operator. In the canonical GA with binary representation, mutation operator acts by flipping the chosen bit value (SUDHOFF, 2014).

Following mutation, a stopping criterion is then checked. An easy way to do this is to check the generation number. When the stopping criterion is satisfied, the algorithm comes to an end by choosing the optimizer from the final population who is the most fit.

2.4.3.5.3 Enhanced Real-Coded Genetic Algorithm

Real-coded GAs are very similar to canonical GAs except that instead of each gene being represented as a binary string, each gene is represented by a real number (SUDHOFF, 2021). Beyond the change of the way in which a gene is represented, there are many other algorithms that can be employed in real-coded GAs to achieve crossover and mutation (SUDHOFF, 2021). Additional genetic operators are also used in real-coded GAs, aiming to enhance the performance of the algorithm (SUDHOFF, 2021). These operators were introduced below and placed into the diagram of Figure 21, so that the relationships between them can be made clear and, consequently, an enhanced real-coded GA is well understood.

Figure 21 - Enhanced real-coded genetic algorithm.

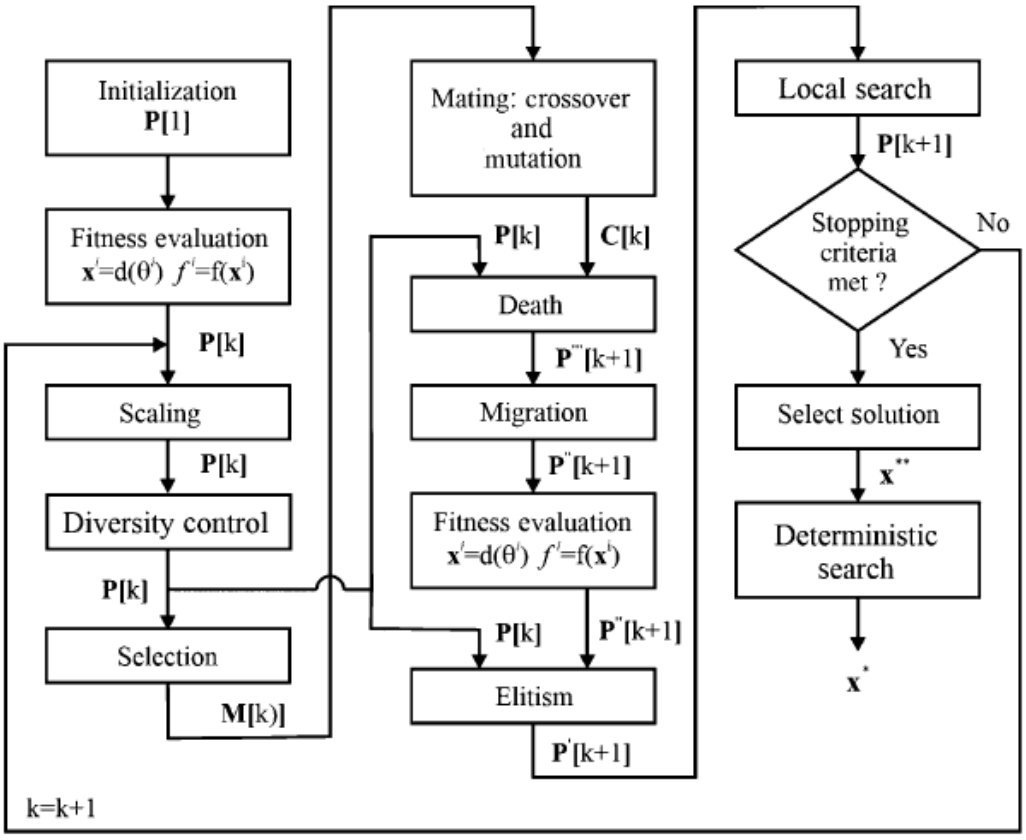

Source: Adapted from Sudhoff (2021)

Scaling

If there are only a few individuals with very high fitness values in the early stages of evolution, these powerful individuals will quickly dominate the entire population, which can result in convergence to some local optimum without thorough exploration of the search space. This is called as premature convergence. The evolution process slows down as the population approaches convergence, with the majority of individuals having similar fitness values. At this point, there is little competition among individuals. Scaling can be used to address these issues by preserving the proper evolution pressure throughout the evolution process (SUDHOFF, 2014).

In multi-objective optimization problems, where the objective functions have different scales, scaling is also helpful (SUDHOFF, 2014). Several different scaling methods are available and can be applied to the fitness values (SUDHOFF, 2014). As the first step in the scaling operation, the fitness values are scaled using a chosen method. After scaling, all negative fitness values are clipped to zero, and the fitness values in the multi-objective optimization are then scalarized using a normalized objective function weight vector (SUDHOFF, 2014). Finally, a penalty vector is applied and the scalarized fitness values are penalized to yield the aggregated fitness values that are used in the selection operation (SUDHOFF, 2014).

Diversity Control

There are multiple optimal solutions for some optimization problems. However, the solutions may converge to one optimal solution as a result of naive GA application (SUDHOFF, 2014). Even when there is only one optimal solution, it is undesirable to have multiple solutions that all explore the same area of the solution space. As a result, a diversity control needs to be employed (SUDHOFF, 2014).

In the diversity control algorithms, the underrepresented solutions are highlighted, and similar solutions are punished by lowering their fitness values (SUDHOFF, 2014). To maintain the diversity of the solutions, many algorithms are available (SUDHOFF, 2014). These algorithms determine each individual's fitness weight value, which is the fitness penalty vector that is used for generate an aggregated fitness in the scaling process. Individuals with a large number of close neighboring individuals are given a low fitness weight value, which lowers

their effective fitness, while those with a small number of neighbors are given a fitness weight value that is close to unity (thus, the fitness is less penalized).

Either the parameter (or decision) space or the fitness function (or objective) space can be subject to the diversity control (SUDHOFF, 2014).

Death

Children replace the whole population in the canonical GA (SUDHOFF, 2014). However, in some GAs, a mating pool that is only a fraction of the size of the population is formed, giving rise to a population of offspring that is only a fraction of the size of the population (SUDHOFF, 2014). The children replace members of the existing population, creating a new population that includes the children as well as some individuals from the previous population.

Then, it becomes necessary to choose which members of the current population will "die" to make room for the arrival of children maintaining the population size constant. The individuals who will be replaced can be chosen based on factors other than those used for selection, such as diversity (or, more specifically, a lack of it) or another property (SUDHOFF, 2014).

Migration

Only when a multiple-region (or multiple-population) scheme is used does this operator function (SUDHOFF, 2014). The population is split into n distinct populations by increasing the number of regions, n, above one. These populations typically develop independently (SUDHOFF, 2014). Some of the individuals occasionally move from one region to another and are redistributed.

Elitism

Elitism serves as a measure to prevent the best individual from being damaged and lost through genetic operations. The simplest way to implement elitism is to transfer the best

member of the current population to the following one without using any genetic manipulations (SUDHOFF, 2014). Elitism ensures that the maximum fitness in the population will never decrease.

Random (local) search

By randomly mutating the best individual, random search is a method of exploring the area around the best individual in search of a better solution. It may shorten the time needed for the GA to reach the optimal solution (SUDHOFF, 2014).

To create mutants, the best individual is randomly perturbed. The fitness of the created mutants are then assessed. If the best mutant has a higher fitness value than the current best individual, the current best individual is replaced by the best mutant. Otherwise, the original best individual is placed back to the population.

Deterministic search

When initialized close to the solution, many traditional optimization techniques are very effective. Although GAs are frequently very effective at approaching a global optimum, they might not always converge quickly from a good approximation of a solution to the exact solution (SUDHOFF, 2021). This suggests combining the two strategies, initializing a classical optimization method with the best member of the final population of a GA (SUDHOFF, 2021). The Nelder-Mead simplex method (CHONG & ZAK, 2008 apud SUDHOFF, 2021) is particularly appealing in this regard because it does not call for gradients or Hessians.

Given the extensive use of optional operators, the algorithm shown in Figure 21 is probably more complex than is typical (SUDHOFF, 2021). Diversity control and scaling are not always required. If the population is entirely replaced by children, no separate death algorithm is required either. Random and deterministic search routines are frequently not used (SUDHOFF, 2021). On the other hand, elitism is a fairly important algorithm among the optional ones (SUDHOFF, 2021).

Despite not being used as frequently as elitism, the migration operator has been shown to significantly affect performance (SUDHOFF, 2021). There are undoubtedly many different types of GA operators, and there are numerous books that discuss them. Several references

(ZBIGNIEW, 1999; GOLDBERG, 1989; 2002; OSYCZKA, 2002 apud SUDHOFF, 2021) for genetic operators can be found in the literature. The good news is that nearly all variations are effective optimizations: they differ mainly in their rates of convergence and likelihood of discovering global solutions (SUDHOFF, 2021).

2.4.3.5.4 Genetic algorithms for multi-objective optimization

GAs are well suited for multi-objective optimization, and there are a large number of multi-objective genetic algorithms that have been developed over the years (SUDHOFF, 2021). The goal in all of these methods is to evolve the population so that it becomes a Pareto-optimal set. Some of the multi-objective GAs are listed below (SUDHOFF, 2014):

- Vector Evaluated GA (Schaffer, 1984)
- Non-Dominated Sorting GA – NSGA (Goldberg, 1989)
- Vector-optimized ES ((Frank Kursawe, 1990)
- Multiple objective GA (Fonseca & Fleming, 1993)
- Weighted-Based GA (Hajela and Lin, 1993)
- Niched-Pareto GA (Horn et al., 1994)
- Random Weighted GA (Murata & Ishibuchi, 1995)
- Distance-based Pareto GA (Osyczka & Kundu., 1995)
- Strength Pareto EA (Zitzler & Thiele., 1998)
- Elitist NSGA – NSGA-II (Deb et al., 2000)
- Pareto-archived ES (Knowles & Corne., 2000)
- Rudolph's elitist MOEA (Rudolph, 2001)

There are two main types of multi-objective GAs: non-elitist and elitist.

Elitist strategies are particularly effective because they explicitly identify and preserve, when possible, the nondominated individuals (SUDHOFF, 2021). Elitist strategies include the elitist nondominated sorting GA (NSGA-II), distance-based Pareto GA, and the strength Pareto GA (DEB, 2001 apud SUDHOFF, 2021).

In fact, the studies have demonstrated that the elitist NSGA (NSGA-II) finds more non-dominated solutions in the obtained non-dominated front than the non-elitist NSGA for a

number of problems (DEB, 2001). This result is expected because an elitist algorithm should preserve and propagate more non-dominated solutions than its non-elitist counterpart. Better offspring are generated when there are more non-dominated solutions in the parent population. Furthermore, once a set of non-dominated solutions is identified, it is only possible to get rid of them if a better set is found.

Observations made in many studies suggest that the use of elitist algorithms is also advantageous in the case of multi-objective optimization problems (ZITZLER, 1999 apud DEB, 2001; SUDHOFF, 2021). Thus, in the present work, the focus was placed on the elitist GA.

2.4.3.5.5 GOSET (MATLAB TOOTBOX)

A GA optimization can be performed using different software and programming languages. Among the existing possibilities, the Genetic Optimization System Engineering Tool (GOSET) is one of the most attractive and accessible tools.

GOSET is a MATLAB® based algorithm package for solving single- and multi-objective optimization problems (SUDHOFF, 2014). It is a free software, thus, it can be redistributed and/or modified under the terms of the GNU Lesser General Public License as published by the Free Software Foundation, either version 3 of the License, or any later version (SUDHOFF, 2014). Besides, GOSET runs on MATLAB® without requiring the use of any other MATLAB toolboxes, although the MATLAB Paralleling Computing Toolbox can be used to enable GOSET to execute parallel computing (SUDHOFF, 2014).

GOSET is a direct result of three research awards from the Office of Naval Research (ONR), which an organization within the United States Department of the Navy responsible for the science and technology programs of the U.S. Navy and Marine Corps (SUDHOFF, 2014). GOSET allows the user to become deeply involved in its algorithms and the parameters used in these algorithms. In other words, it gives the user a powerful tool for automating the engineering design process. The GOSET algorithm's execution involves a lot of information. In order to facilitate the organization of the information, GOSET stores it in the following the three data structures shown in Table 3:

Table 3 - Data structures of GOSET

MATLAB Structure Name	Contents
P	Population information: All the information related to the current population.
GAP	Genetic Algorithm Parameters: All the parameters about genetic operations.
GAS	Genetic Algorithm Statistics: The best fitness values, median fitness values, average fitness values, and best chromosomes over the generations are stored in GAS. Current generation number and the number of total objective function evaluations are also stored.

Source: Sudhoff (2014)

Its algorithm execution flow is depicted in Figure 22, which contains a short description of each step and the respective GOSET function names. As it can be seen from the images, various genetic operators act on the current population to generate a new one. Once the new population has been produced, the best fitness value, the average fitness value, and the gene values of the individuals are stored in the data structure named GAS. This task is referred to as post-processing. At the completion of the genetic operations, GOSET reports the information on the new population in the gene distribution plot and/or the Pareto plot. In the gene distribution plot, the normalized gene values of the individuals are plotted and also the best fitness value, the average fitness value, the average fitness value, and the worst fitness value over the generations are plotted. In the Pareto plot, the population is plotted in the objective function space. The Trim GA step is executed only in single objective optimization problem. This step utilizes the Nelder-Mead simplex algorithm and carries out an optimization to enhance the best solution after the evolution process is complete. The detailed descriptions of all operators present in GOSET can be found in SUDHOFF (2014).

Figure 22 - GOSET algorithm execution flow

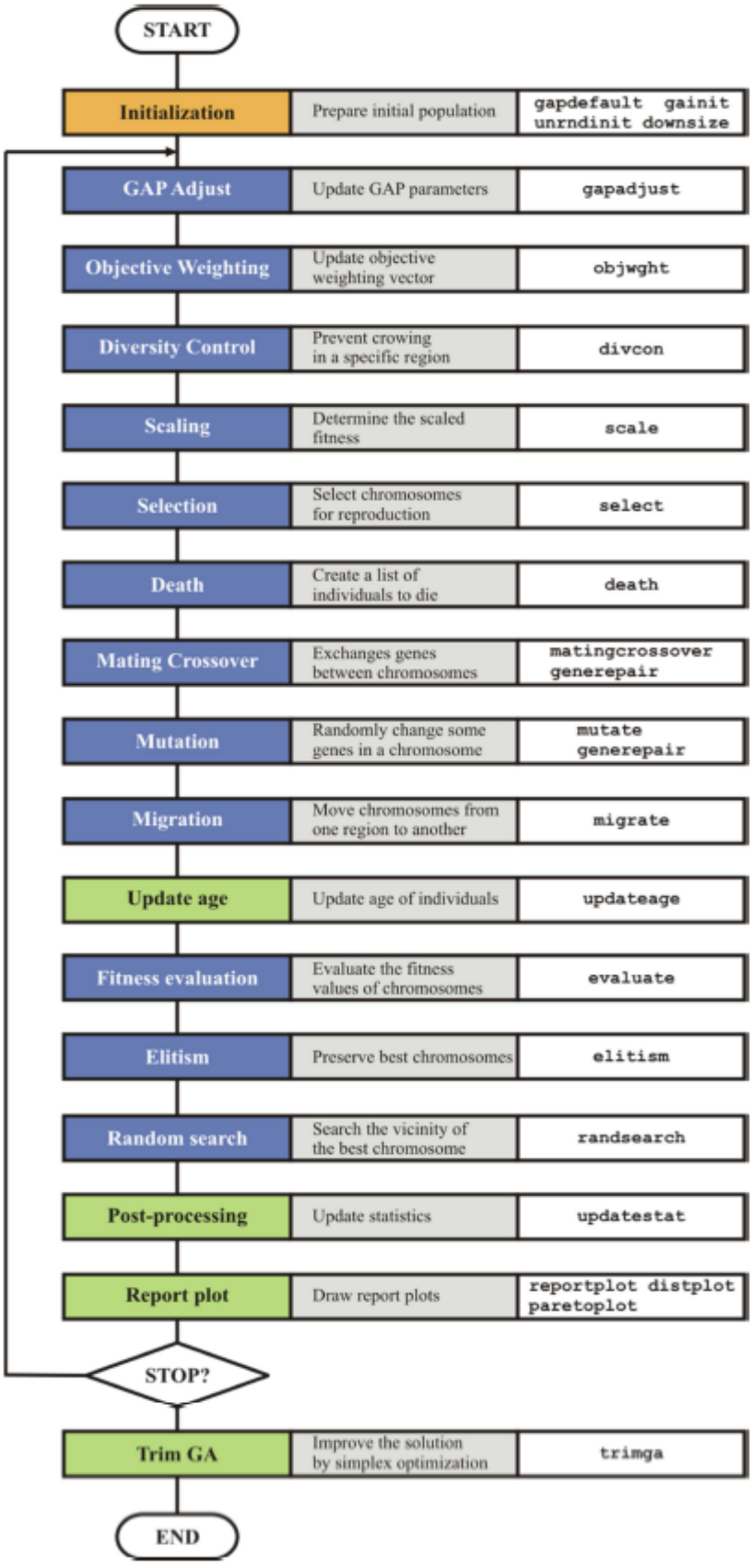

Source: Sudhoff (2014)

GOSET was heavily employed during its development at a number of universities, companies, and laboratories to address many engineering issues, particularly those involving the design optimization of inductors, brushless dc motors, power supplies, and inverters, and those related to the parameter identification of synchronous machines, induction machines, gas turbines, etc. (SUDHOFF, 2014).

In the literature, many research works have employed GOSET together with COMSOL, through the COMSOL LiveLink for MATLAB, to optimize different systems. Some of them are cited next.

Subbiah and Laldin (2016) developed a framework consisting of a genetic algorithm coupled with the finite element method to perform the multi-objective optimization of an electromagnetic actuator design. The optimization framework was set forth with a MATLAB implementation of a GA, the Genetic Optimization System Engineering Tool (GOSET), used in conjunction with an FE model implemented in the COMSOL AC/DC module. Ten design parameters were selected aiming to achieve two objectives: minimizing the actuator volume and minimizing losses, with the constraint of producing a minimum electromagnetic force of 2500 N. The GA was responsible to invoke a fitness function in MATLAB that computed objectives values and verified all the constraints. By using COMSOL LiveLink for MATLAB, this function transmitted geometry, material, and winding parameters to the COMSOL AC/DC module. The GA was initialized with 200 individuals and was run for 200 generations. The optimization process took approximately 30 hours on a computer containing 24 CPU cores, clocked at 2.5 GHz, and 128 GB RAM. A resulting family of designs containing approximately 70 optimal choices was available for consideration based on system-level requirements.

Adomanis et al. (2017) also implemented a multi-objective GA optimization, but with the goal of improving the design of a metasurface. As an example of a single-objective GA optimization performed with GOSET and COMSOL that can be found in the literature is the one developed by Pierrick et al. (2019). In this work, presented a method based on GOSET to design a high efficient klystron, operating in the X band, through the optimization of a bunching circuit and a multi-cell output cavity.

2.4.3.6 No Free Lunch Theorem

When working with optimization and Evolutionary Algorithms, it is important to learn about the No Free Lunch (NFL) theorem, which was developed by Wolpert and Macready (1997) regarding the performance of optimization algorithms. According to the NFL theorem, it is impossible to develop a general-purpose, universal optimization strategy; one strategy can only outperform another one if it is customized for the configuration of the particular problem being studied. In their work, Wolpert and Macready (2005) state that "any two optimization algorithms are equivalent when their performance is averaged across all possible problems".

The interpretation of the No Free Lunch theorem can be illustrated by Figure 23. Different problem types are represented on the horizontal axis, and we assume that they have been skillfully arranged so that those with similar properties are closer to one another. Concerning Figure 23, a few things should be mentioned (YU & GEN, 2010):

1) The more we comprehend the optimization problem, the more customized a technique we can develop to address it and the better it will perform, but the less robust it will be to other problems.
2) General purpose EAs are reliable methods when a blind or near blind search is performed, in most cases.
3) If problem information could be incorporated into the encoding and decoding process, as well as into the EA operators, together with a problem-dependent local search method, the algorithm's performance would be enhanced (at the expense of decreased adaptability for other problems).

Figure 23 - One kind of interpretation of the No Free Lunch theorem

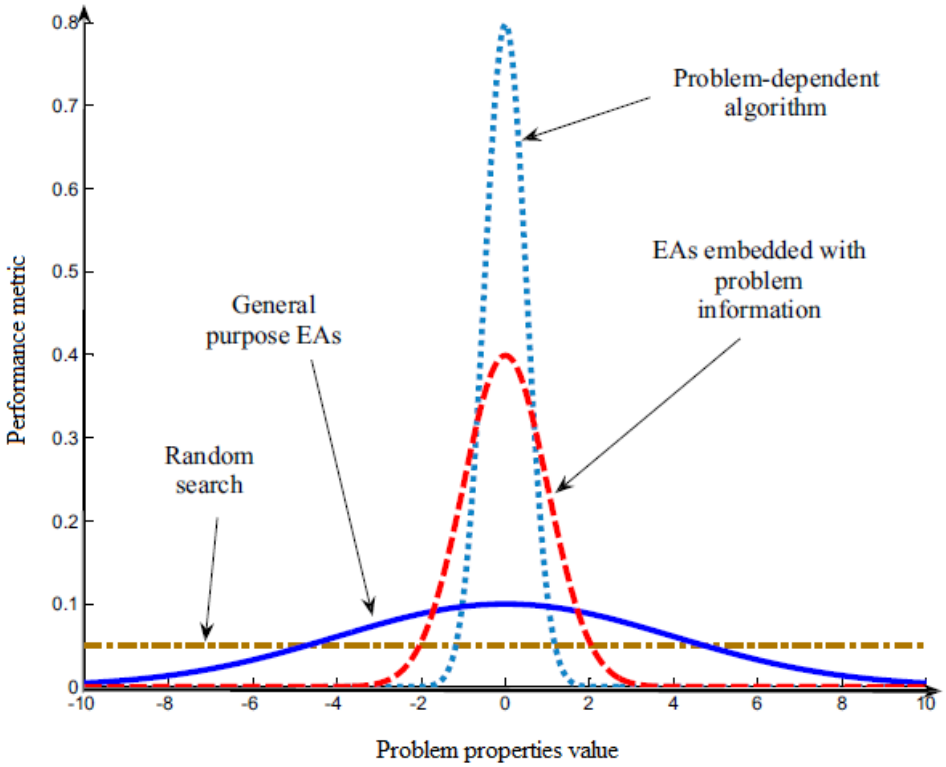

Source: Yu & Gen (2010)

2.4.3.7 Enhancements in Evolutionary Algorithms

Although Evolutionary Algorithms are widely applicable to many fields, it delivers only marginal performance (YU & GEN, 2010; VIKHAR, 2016), as mentioned in the previous section. Therefore, current efforts are concentrated on applying some complementary algorithms to EA that may enhance its performance (YU & GEN, 2010). Hybridizing two or more algorithms or improving the ones that already exist is a current trend (YU & GEN, 2010).

Table 4 shows some recent enhanced EAs along with their descriptions.

Table 4 - Enhancements in EAs

No	Enhanced EA	Description
1	Genetic Swarm Optimization (GSO) (CHAKRADEO et al., 2014)	Combines GA and PSO to solve electromagnetic problem
2	Hybrid PSO (CHAKRADEO et al., 2014)	It reduces probability of trapping local optima using Cauchy mutation for PSO
3	Self-adaptive differential evolution (SaDE) (SUN et al., 2012)	It adaptively search for suitable strategy and associated parameter setting
4	Immune self-adaptive differential evolution (ISDE) (SUN et al., 2012)	Scale and crossover factors of DE are adaptively modified by information process mechanism of biological immune system
5	Multi-objective Evolutionary algorithm (MOEAs) (LI et al., 2015; HE et al., 2014)	Extension to simple evolutionary multi-objective optimizer
6	Multi-objective Evolutionary algorithm based on decomposition (MOEA/D) (LIU et al., 2015)	Based on simple evolutionary multi-objective optimizer and decomposition
7	Dynamic multi-agent GA (LIU et al., 2015)	Integrates dynamic multi-agent with Genetic algorithm
8	Multi-objective Particle Swarm Optimization (MOPSO) (ZENG & SUN, 2014)	Given multi-objective functions to solve optimization problem

Source: Vikhar (2016)

2.5 STATE OF THE ART

In this section, the current state of the art regarding the numerical simulation and optimization of the cure of thick thermosets is presented. For the design of the curing process of thick parts, computational procedures, primarily based on numerical simulation (COSTA & SOUSA, 2003; MAWARDI & PITCHUMANI, 2003; CARLONE & PALAZZO, 2009 apud ALEKSENDRIĆ et al., 2016; PAIVA, 2018) and optimization (JAHROMI et al., 2012 apud ALEKSENDRIĆ et al., 2016; STRUZZIERO & SKORDOS, 2017; STRUZZIERO & TEUWEN, 2018; TIFKITSIS et al. (2018); DOLKUN et al., 2018; YUAN, 2021) have recently been proposed as an alternative to empiric approaches. The aforementioned studies highlighted some benefits offered by simulation-based optimization procedures due to the numerous potential solutions that could be investigated, regardless of the computational method used (ALEKSENDRIĆ et al. 2016).

The goal here is to gather the most updated scientific knowledge and methods applied to this problem, as well as the respective results, to serve as the basis for the development and analysis of the present research work. The main aspects of the optimization that were observed were the following: the decision variables, the constraints, the objective(s), whether the optimization was single or multi-objective, and the types of algorithms used.

The literature research focus was placed on cure simulation and optimization to address the demand for maximum product performance/quality at a minimum production cost/time. Simulation of the curing is a necessary step towards the optimization of thermosets and thermoset composites manufacturing. Therefore, several simulation tools have been created to address the curing process. The commercial FE software shows a great capacity in composites simulation, especially in coupled predictions of the cycle of cure, constantly providing reliable results (PAIVA, 2018).

Although the majority of real-world problems involve multiple objectives, prior to the 2000s, a significant portion of optimization research focused on a single objective (DEB, 2001). However, SO optimization does not address the challenges of the manufacturing process as a whole and its results do not consider the trade-offs between the variables involved, even though it is possible to restrict the outcomes of the objectives not specifically addressed by the optimization (STRUZZIERO et al., 2019). Because of this, recent research efforts have shifted from SO optimization to MO optimization.

A timeline of the significant events in the field of numerical optimization of composite curing is shown in Figure 24. The earliest works in the field focused on SO optimization problems, which were then followed by the simultaneous treatment of competitive objectives in a MO optimization framework (STRUZZIERO et al., 2019). The most recent trend involves taking variability into account in a stochastic modeling framework, which results in robust MO optimization (STRUZZIERO et al., 2019).

Figure 24 - Time line depicting the milestones in numerical optimization of composite curing

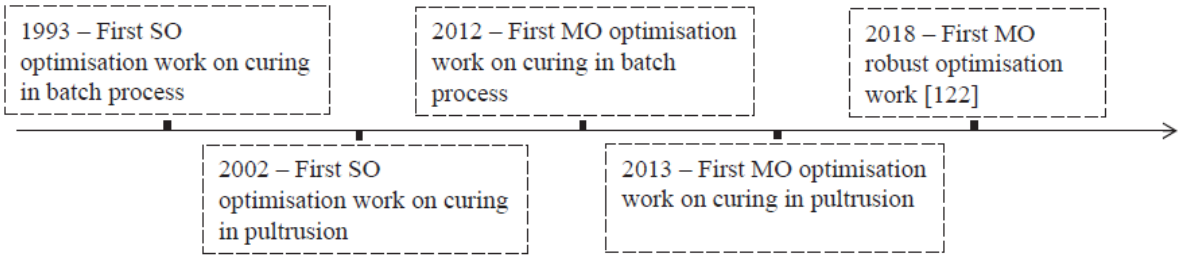

Source: Adapted from Struzziero et al. (2019)

The optimization of the cure of thermoset composites has been addressed as a minimization problem for cost related objectives (such as cure time) and quality related objectives (e.g. temperature overshoot or residual stresses) (STRUZZIERO et al., 2019).

SO optimization of thick components indicated that the use of a three dwell cure profile can reduce the process time in 60% when compared to a two dwell profile (LI et al., 2001 apud STRUZZIERO et al., 2019) In the process of curing, weighted objectives have been used in SO problems to take both quality- and cost-related objectives into account. Ruiz & Trochu (2005; 2006) developed a weighted fitness function to take into account the shortest cure time, the greatest degree of final cure, and the fewest residual stresses. VAFAYAN et al. (2015) used a GA optimizer with a weighted fitness function taking into account cure time, temperature and cure gradients through the thickness to determine optimal cure cycle; and execution of the cure schedule found led to negligible temperature and degree of cure gradients through thickness. However, since prior understanding of the problem's requirements is necessary, SO optimization through the definition of weighted fitness functions is only applicable in certain circumstances.

On the other hand, MO optimization releases the designer from the need for a priori process knowledge and offers a collection of optimal solutions that can be used in a variety of applications. Using a MO optimization method, Matsuzaki et al. (2019) minimized curing time

and degree of cure inhomogeneity, and also identified relevant trade-offs. Struzziero and Skordos (2012; 2017), as well as Struzziero and Teuwen (2018), carried out a MO optimization of the curing process, with GA, taking cure time and overshoot temperature as the objective variables, and obtained a Pareto-optimal set of cure schedules with significant improvements in both objectives. Compared to the other thermoset composite manufacturing steps, the concept of MO optimization for optimal cure process solutions is more well established (STRUZZIERO et al., 2019).

Typical constraints for the cure optimization of thermoset composites are minimum degree of cure reached within the part at the end of the process and the maximum temperature permitted throughout the cure (STRUZZIERO et al., 2019).

The implementation of a gradient based technique by Rai and Pitchumani (1997) to a cure optimization problem resulted in a 60% reduction in cure time. Kennedy and Hansen (2010) identified optimal parameters for curing of thermoset composite laminates to maximize material properties via gradient-based techniques and achieved improvements in the order of 10–20%.

Nevertheless, according to (STRUZZIERO et al., 2019), the use of zero order search methods (GA, for example) is required to avoid becoming trapped in local minima because the design search space of a cure process optimization contains multiple local minima. Pillai et al., (1994; 1996) apud STRUZZIERO et al. (2019) found a near optimal cure profile using a zero-order search algorithm for thick composite laminates resulting in a roughly 40% process time reduction and a roughly 60% reduction in overshoot temperature, taking a recommended cure profile as a reference.

It has been common practice to combine two different algorithms, such as a gradient-based algorithm and a zero-order algorithm (STRUZZIERO et al., 2019). This is done to combine the best aspects of each method, such as the EA solution's global optimality and a gradient-based technique's quick convergence to local optimal points. To design the best cure profiles with the shortest process times, Carlone and Palazzo (2011), as well as Mawardi and Pitchumani (2003), investigated various combinations of zero order search algorithms.

Pagano (2014), Skordos and Partridge (2004) applied GA and PSO to minimize the cure time and reduced its time by about 25% compared to standard cure schedules, whereas a GA combined with ANN implemented Aleksendrić et al. (2016) reduced the cure time by about 40%. In order to minimize a weighted fitness function, which included cure time and uniformity

through the thickness, Pantelelis et al. (2003) compared gradient-based techniques and Evolutionary Strategies to identify the best cure cycles. The results showed that the hybrid algorithm produces better overall performance in terms of CPU time.

Furthermore, several works in literature tried to find the best cure profiles to reduce residual stress and/or temperature overshoot (STRUZZIERO et al., 2019). Investigations into the impact of various cure profiles on residual stress formation resulted in residual stress reductions of 25-30% (WHITE & HAHN, 1993). Gopal et al. (2000), Olivier and Cottu (1998) identified optimal cure profiles to minimize residual stresses using graphical methods and the sensitivity of process stresses to cycle parameters, achieving a reduction of approximately 30%. The minimization of residual stress was also addressed by Bailleul et al. (2003) and Jahromi et al. (2012), that configured SO problems using different gradient based techniques aimed to minimize the temperature gradients in the through thickness direction. A quasi-uniform temperature distribution through the thickness was achieved by successfully implementing those techniques. According to Struzziero et al. (2019), research efforts in the optimization of composites cure should move towards direct minimization of residual stresses.

Yuan et al. (2021) optimized the cure process of thick composites using a multi-field coupled FE model, surrogate model and genetic algorithm. The non-dominated sorting genetic algorithm-II (NSGA-II) was combined with the surrogate model to search for global optimum solution. To reduce the computational cost, the radial basis function (RBF) surrogate model was developed to substitute the FE model in the optimization procedure. Their model took into account the interaction between heat transfer and resin flow during the cure. The polymer matrix composite studied was a carbon fiber-reinforced epoxy. The composite laminate was a plate 157.6 mm × 157.6 mm with a thickness of 35.76 mm. The design variables in the model were the first and second dwell temperatures, the first and second dwell time, and the first and second heating rates. The three optimization objectives of the work were to select the two-step cure profile that: minimize the cure time, minimize the gradient of temperature after gel point (AGP) and minimize the gradient of degree of cure AGP. The definition of gradient used in the referred work was the difference between the maximum and minimum values of a variable within the sample at a given time, regardless of the distance between the material points that possess those values. As constraints for the optimization, the minimum degree of cure in the final cured part was set as 0.96 in order to keep the desired mechanical properties and the maximum temperature inside the thermoset during the cure was limited to 220°C to avoid resin degradation and exceeding the capacity of the equipment. The parameters of the NSGA-II

algorithm are set as: population size 100, crossover fraction 0.9, section process tournament and stop generations 5000. To select the best solution from the Pareto-Optimal set, the authors used the TOPSIS method (Technique for Order Preference by Similarity to Ideal Situation), putting more emphasis on the reduction of the gradients of temperature and degree of cure AGP than on the reduction of cure time, with the following weight factors: 0.4, 0.4 and 0.2, respectively. The resulting optimal cure profile derived from the Pareto-optimal set reduced the maximum gradient of degree of cure by 16.88%, decreased the maximum gradient of temperature by 45.76%, and cut down the cure time by 30.9%.

Tifkitsis et al. (2018) developed a stochastic multi-objective cure optimization methodology and applied to the case of thick flat carbon fibre/epoxy laminate. The thickness considered for the composite laminate was 15.6mm. A Finite Element (FE) model was applied for the cure simulation. The cure kinetics model applied to the resin system of study took into account the combination of the catalytic and autocatalytic processes. Kriging was used to construct a surrogate model of the cure substituting Finite Element (FE) simulation aiming to increase computational efficiency. The surrogate model was coupled with Monte Carlo and integrated into a stochastic multi-objective optimization framework based on Genetic Algorithms. The individual (or chromosome) was a two-dwell cure profile, whose genes (optimization variables) were the first dwell temperature, the second dwell temperature, the duration of the first dwell and the heating rate. Two optimization objectives were selected: minimize the cure time and minimize the maximum temperature overshoot. Cure time was defined as the time at which the minimum degree of cure of the part is greater than 88%. The temperature overshoot was defined as the maximum difference between the tool control temperature and the temperature in the composite during the process. The optimal cure profiles results were compared to the results of a standard one-dwell cure profile and a standard two-dwell cure profile. The average temperature overshoot of a short dwell optimal profile was lower by about 40%. The same short dwell optimal profile resulted in an approximately 40% reduction of cure time in comparison with the standard two dwell profile and a slightly faster cure time than the standard one-dwell profile.

Struzziero and Skordos (2017) addressed the multi-objective optimization of the cure stage of composites manufacture using a Genetic Algorithm implemented in C++. The methodology developed combined the GA with a finite element (FE) model of the cure process and was applied to the case of thick (24 mm) and ultra-thick (60 mm) characteristic composite component geometries. The materials utilized were a pseudo unidirectional carbon fabric and

an epoxy resin. Six test geometries in total were taken into account. A flat panel, an L-shape, and a T-joint were the components that were chosen with an increasing level of complexity. In the case of thick components, a two-dwell cure profile was considered and parameterized using four design parameters: the temperatures of the first and second dwell, the duration of the first dwell and the heating rate. In the case of ultrathick components, the complexity of the cure profile was increased by incorporating a third dwell, and the profile was parameterized using six parameters: the temperatures of the first, second and third dwell, the durations of the first and second dwell and the heating rate. The optimization objectives were to minimize the cure time and maximum temperature overshoot within the curing part. In the case of ultra-thick components, improvements of up to 70% in terms of overshoot and 14 h in terms of process time, compared to conventional cure profiles for ultra-thick components, can be achieved. In the case of thick components reduction up to 50% can be achieved in both temperature overshoot and process duration. The analysis did not take into account residual stress and distortion effects.

Summarizing, residual stresses and the maximum temperature overshoot within the composite part have been addressed with regard to the cure stage as quality-related objectives to be minimized, while the cure time has been minimized to try to minimize manufacturing cost. In some cases, residual stresses have been indirectly addressed by the minimization of the gradients of temperature and/or degree of cure. The maximum temperature overshoot within the part has been considered in some studies as an optimization constraint rather than an objective. Other common optimization constraint set was the minimum degree of cure reached within the part at the end of the process. As for the design decision variables, all the studies found in the literature intended to optimize the composite cure of batch processes, such as autoclave, considered the properties of the cure temperature profile as those variables. Therefore, the decision variables were the isothermal temperatures, the duration of the isotherms and sometimes the heating/cooling rates between the isotherms.

The state of the art demonstrate that multi-objective optimization is one of the prevailing trends in composite manufacturing optimization. This is a logical progression from the research on single-objective optimization with constraints or the combination of multiple objectives in a weighted sum. The disadvantages of the latter strategy include hindering each objective's effectiveness, making it impossible to draw broad conclusions about each objective separately. By allowing two or more objectives to compete, using a pure multi-objective setting, liberates the designer from having to predict the benefits of the objective a priori. This competition

reveals the best trade-offs governing the problem. The process designer may have a wide range of design options to choose from if a MO optimization strategy is implemented. The Pareto-optimal front contains the best design points for various end applications, from which one can choose based on risk preferences and the associated process cost/time versus quality prioritization.

Furthermore, the complexity of the cure optimization problems drives the selection towards nature-inspired algorithms, especially GAs, which are capable of exploring a substantial part of the objective space without being stuck in local minima or maxima. Variability and robust optimization have also been studied, however this area still needs more research (STRUZZIERO et al., 2019).

3 METHODOLOGY

Facing the need to optimize the curing process of thick thermosetting polymers and composites, this work investigated two different approaches:

1. **A conversion rate driven (CRD) strategy**: which is a strategy based on the cure kinetics of the thermoset material that detects the instant when the average conversion rate of the sample reaches its maximum value and uses this data as a reference to reduce the total duration of the cure. This strategy was conceived by the authors of this work as a simple and fast way to find cure schedules that provide satisfactory results in terms of cure time. A similar study was not found in the literature.
2. **A multi-objective Genetic Algorithm (GA) optimization**: which is a well-established algorithm in the scientific community, being the most popular of the evolutionary algorithms (EAs). GA has been presented as a powerful solution to optimize manufacturing and curing processes of thermoset polymers taking into account the conflicting objectives that exist in this activity.

Both CRD strategy and GA optimization were implemented in MATLAB®, because of two mains reasons: it is a widely used and consolidated software to solve engineering problems; and it is capable to communicate with the finite element software used for the simulation of the curing process, COMSOL Multiphysics®, through the module COMSOL LiveLink for MATLAB®. The details of the methodology used for the numerical simulation and curing optimization were described in the sections below.

All simulations and optimizations were performed on an Intel® Core™ i5-8400 Desktop at 2.80 GHz with 8.00 GB of RAM.

After obtaining the results of the two approaches, CRD and GA, in order to evaluate the effectiveness of each method and its advantages and disadvantages, the solutions from both approaches were compared with each other and also with the generic cure schedule recommended by the thermoset manufacturer in the material datasheet.

3.1 NUMERICAL SIMULATION

Numerical simulations of the curing process were performed based on the work conducted by Paiva (2018), who successfully implemented a thermochemical simulation model of the curing process of a thermoset polymer in the finite element software COMSOL Multiphysics ®, validating it with many experimental results.

The simulation model of Paiva (2018) was generated from the replication of a model run on Abaqus FEA® provided by ENSTA Bretagne, while taking the studies of Rabearison (2009) and Rabearison et al. (2008; 2009) as a reference for the development of the cure investigation.

The curing of the thermosetting polymer matrix was implemented in COMSOL® and the simulations were performed with the coupling between the thermal and chemical physics. COMSOL Multiphysics® was the FEA software selected due to its high specialization in these kind of couplings.

3.1.1 Model geometry

The geometry investigated numerically in this work is displayed in Figure 25. It is a 2D-axissymetric geometry, corresponding to the thermoset resin system (in blue), cured in the cylindrical steel mold (in gray). The geometry of the resin system is a cylinder that has a diameter of 32 mm and a height of 60 mm, while the steel mold has an external diameter of 45 mm and a total height of 79 mm, with a vertical depth of 65 mm.

Figure 25 – 2D-axissymeric geometry used in the COMSOL cure simulation numerical model

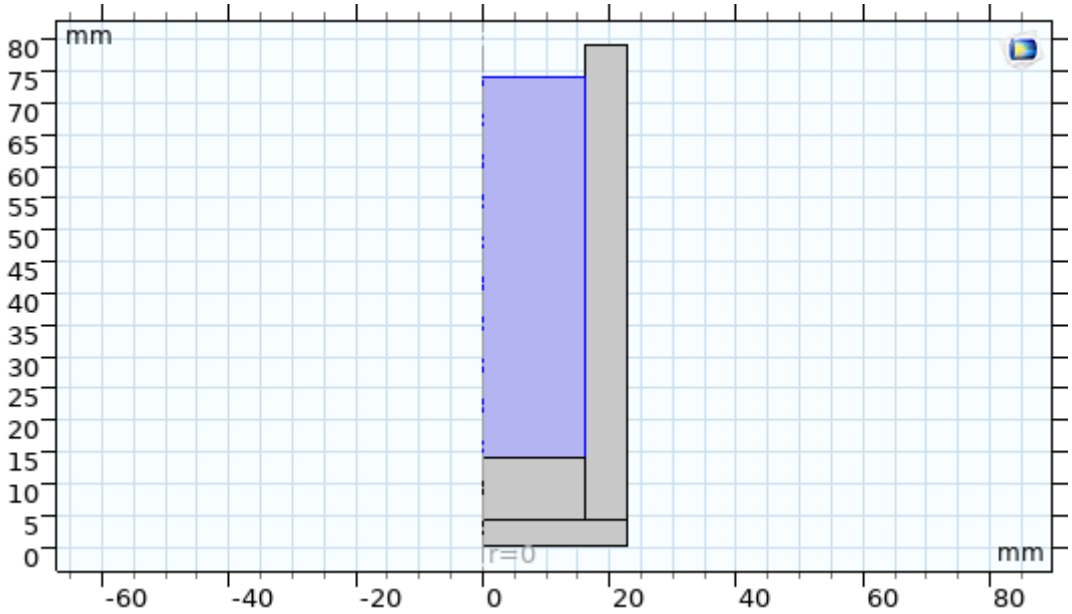

Source: The author (2022)

3.1.2 Materials and its properties

The resin system studied in this work is a three-component anhydride-epoxy system from Ciba. The blend consists of:

1) A bifunctional DGEBA-type epoxy (Araldite LY556, EEW=183-192 g/eq, n=0.3);
2) A tetra-functional anhydride hardener (methyl-tetrahydrophthalic anhydride HY 917, anhydride equivalent weight = 166g/eq); and
3) An accelerator (l-methyl imidazole DY 070).

The components are mixed in LY 556/HY 917/DY 070 weight ratio of 100/90/2, resulting in a stoichiometric epoxy-anhydride mixture. This system has been used in several publications, which provides adequate data as simulation parameters.

The variable epoxy material properties were established. Equations 20 to 28 give the specific heat capacity, thermal conductivity, and coefficient of thermal expansion as determined by the Rule of Mixtures (RABEARISON et al., 2009), as a function of properties for the uncured resin – $c_p(0,T)$, $k(0,T)$ – and the fully cured resin – $c_p(1,T)$, $k(1,T)$. These properties are given in ANNEXES A and B.

$$\boldsymbol{c_p(\alpha,T) = (1-\alpha)c_p(0,T) + \alpha\, c_p(1,T)\ [J/(g\,°C)]} \qquad (20)$$

$$c_p(0,T) = 1.8500 + 0.002625 * T[°C] \quad (21)$$

$$c_p(1,T) = 1.3125 + 0.004437 * T[°C], T < T_{g\infty} \text{ or } c_p(1,T) = c_p(0,T), T \geq T_{g\infty} \quad (22)$$

$$k(\alpha,T) = (1-\alpha)\,k(0) + \alpha\,k(1,T)\ [W/(m\,°C)] \quad (23)$$

$$k(0) = 0.188 \quad (24)$$

$$k(1,T) = -2.727\,10^{-4} * T[°C] + 3555.529 * 10^{-4} \quad (25)$$

$$\alpha_T(\alpha,T) = (1-\alpha)\alpha_T(0,T) + \alpha\,\alpha_T(1,T)\ [1/°C] \quad (26)$$

$$\alpha_T(0,T) = 5 * 10^{-4} \quad (27)$$

$$\alpha_T(1,T) = 450 * 10^{-6}, \quad T < Tg \text{ or } \alpha_T(1,T) = 450 * 10^{-6} + 4.1 * 10^{-6} * (T - Tg), \quad T \geq Tg \quad (28)$$

The density varies less than 10% throughout the curing; therefore, it was considered constant and assuming the value of 1170.6 kg/m³ (PAIVA, 2018). The steel mold that the epoxy was placed in had a density of 7800 kg/m^3, and respective thermal conductivity and specific heat capacities at 293 K of 24 W/(m.K) and 460 J/(kg.K), and at 773 K of 29 W/(m.K) and 540 J/(kg.K).

The glass transition temperature of the system T_g was modeled using DiBenedetto's equation (Equation 7), based on the glass transition temperatures for the uncured resin T_{g0} and fully cured resin $T_{g\infty}$, and an adjustable parameter λ, which can be found in Table 5.

Table 5 – Material properties related to glass transition

$Tg0$ [°C]	$Tg\infty$ [°C]	λ
-37	136	0.57

Source: Rabearison et al. (2011)

COMSOL interpolation, piecewise, and analytical functions were employed to add the variable parameters as input; no related programming language was required.

3.1.3 Cure kinetics model

The model used to describe the cure kinetics of the epoxy matrix was Kamal and Sourour's phenomenological model Kamal (KAMAL & SOUROUR, 1973) extended by Fournier et al. (1996), Equation 5, which includes the phenomenon of diffusion, as explained in a previous section. COMSOL® module *Domain ODEs and DAEs* was used to implement the cure kinetics model.

The cure kinetic parameters of the LY556 epoxy resin were identified by Rabearison et al. (2011), which were applied in the simulations and can be found in Table 6.

Table 6 – Cure kinetic parameters

A_1 [1/s]	1339879.17
A_2 [1/s]	21042820.69
E_1 [kJ/mol]	69.14
E_2 [kJ/mol]	72.62
m [-]	1
n [-]	2
α_f [-]	$4.0646\ 10^{-3}\ T[K] - 8.2434\ 10^{-1}$
b [-]	$7.1588\ 10^{-4}\ T[K] - 2.2816\ 10^{-1}$

Source: Rabearison et al. (2011)

Parameters α_f and b are limited to the temperature range 360 K to 420 K for which they were specified. Additionally, α_f is unaffected by temperature changes above 448.8 K because a physical limitation prevents the degree of cure from going above 100%. The avoidance of a null value for b is another limitation, which is why b is kept constant below 319 K and prevents indeterminacy in $f_d(\alpha)$.

3.1.4 Heat transfer equation (thermo-chemical coupling)

The heat transfer equation was modified to incorporate the equivalent heat flow produced by the exothermic curing reaction, bringing chemistry into the process (2). The resultant heat transfer equation, with temperature and degree of cure as dependent variables, is written as Equation (29):

$$\rho \boldsymbol{c_p} \frac{\boldsymbol{dT}}{\boldsymbol{dt}} = \boldsymbol{div}\{\boldsymbol{k}[\boldsymbol{grad}\, \boldsymbol{T}]\} + \boldsymbol{q} + \boldsymbol{\rho}\, \boldsymbol{\Delta Hr} \frac{\boldsymbol{d\alpha}}{\boldsymbol{dt}} \quad (29)$$

COMSOL® module *Heat Transfer* was applied to include the heat transfer equation and the thermo-chemical coupling.

3.1.5 Boundary conditions

Two boundary conditions were added to the heat transfer module: the heat flow imposed by the oven and the heat flow generated by the exothermic cure reaction.

The heat flow imposed by the oven (q) was considered to be only convection due to the considerably larger dimensions of the oven in comparison to the epoxy sample. It is expressed by Equation 30 with previously calculated coefficient of convection h (RABEARISON et al., 2008) shown in Table 7, and oven temperature T_e as:

$$\boldsymbol{q} = \boldsymbol{h}(\boldsymbol{T} - \boldsymbol{T_e}) \quad ((30)$$

Table 7 - Variation of the coefficient of heat transfer by convection with temperature

$T\ [K]$	$h\ [W/(m^2K)]$
300.779	147.0992149
318.15	80.46560193
353.15	48.69074624
373.15	38.73839524
423.15	26.45964679

Source: Rabearison (2008)

As to the heat flow from the chemical reaction, previous DSC experiments provided the total enthalpy of the complete reaction H_U as 355 ± 25 J/g (RABEARISON, 2009). Considering H_T as the enthalpy of the reaction at a given temperature, the heat flow from curing was defined by Equations 31 or 32, depending on the temperature value being below or above the glass transition:

$$\rho\, H_U \frac{d\alpha}{dt} = 1170600 * 330 * \frac{d\alpha}{dt}, \qquad T < T_g \tag{31}$$

$$\rho\, H_U \left(\frac{H_T}{H_U}\right)\frac{d\alpha}{dt} = 1170600 * 330 * (0.00243 * T[K] - 0.158) * d\alpha/dt, \quad T \geq T_g \tag{32}$$

3.1.6 Monitored variables for cure optimization

In order to perform the cure optimizations, it was created in the COMSOL model, operators that computed the maximum, minimum and average value of the variables of interest. This was important because the thick resin system exhibits highly heterogeneous properties throughout the cure and, therefore, it is not possible to get the properties of some point of the resin matrix and consider them as representants of the whole sample behavior.

The variables of interest for the cure optimization monitored in the domain of the resin sample were: degree of cure, temperature, conversion rate, gradient of degree of cure AGP and gradient of temperature AGP. The two last variables were defined in this work as the magnitude of the spatial gradients of degree of cure and temperature AGP, respectively. After the application of the operators, the most important variables for the correct implementation of the

CRD strategy and GA optimization are the ones explained below, because they are either to the objectives or to the restrictions of the algorithms:

1) **Minimum degree of cure reached by the sample at the end of cure**: this value must reach the degree of cure required by the application (CRD and GA optimization restriction);
2) **Maximum value throughout the cure of the volume average conversion rate**: this value and the time it occurs are the most important parameters for the CRD strategy, because they determine the duration of the first temperature plateau of the resulting cure schedule, reducing the total cure time, as explained in a previous section (CRD objective);
3) **Maximum temperature reached by the sample throughout the cure:** this value cannot exceed the material thermal degradation (CRD and GA optimization restriction);
4) **Maximum gradient of degree of conversion reached by the sample AGP:** this value must be minimized in order to avoid residual stress within the matrix and related problems (GA optimization objective). To ignore the gradients of degree of cure achieved before the gel point, a variable was created in COMSOL, using a condition in its expression that sets the variable value to zero if the gel point has not been reached, and, otherwise, copies the value of a variable that stores the gradient of degree of conversion. Then, the maximum gradient was computed from this new variable.
5) **Maximum gradient of temperature reached by the sample AGP:** this value must be minimized in order to avoid residual stress within the matrix and related problems (GA optimization objective). The same procedure executed to ignore the gradients of degree of cure achieved before the gel point was performed to ignore the gradients of temperature before gel point. That is, a variable was created in COMSOL, using a condition in its expression that sets the variable value to zero if the gel point has not been reached, and, otherwise, copies the value of a variable that stores the gradient of degree of temperature. Then, the maximum gradient was computed from this new variable.

The computation of the five variables listed above were performed on the epoxy domain, excluding a 3-mm-height cylindrical slice from the top, rather than in the whole epoxy domain, as shown in Figure 26.

Figure 26 – Region of the epoxy domain considered for computation of the optimization variables (in blue)

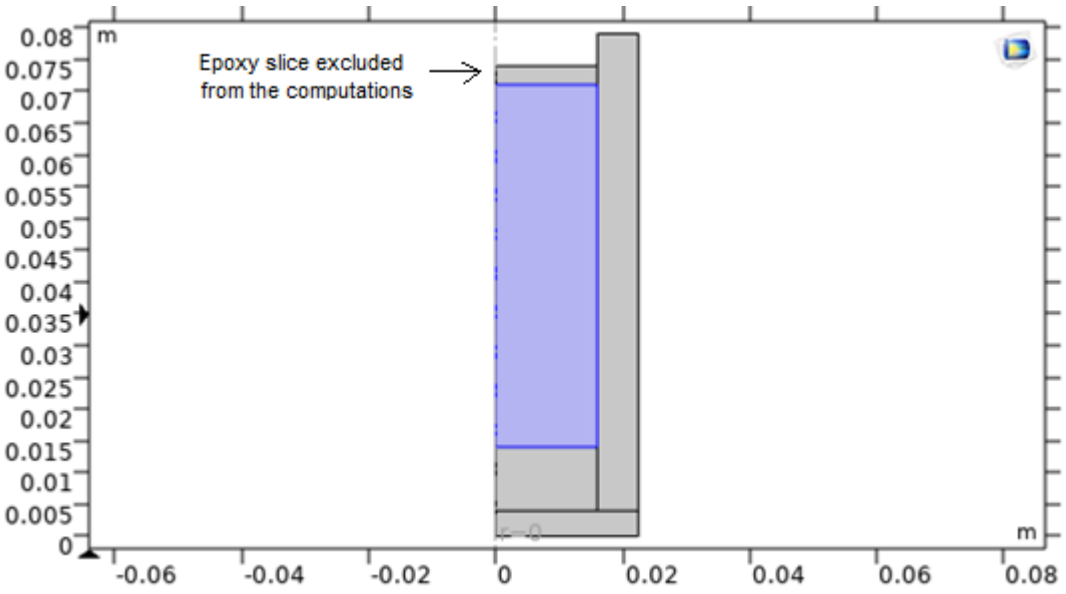

Source: The author (2022)

Figure 27 – Numerical singularity when computing the gradient of the degree of cure within the epoxy

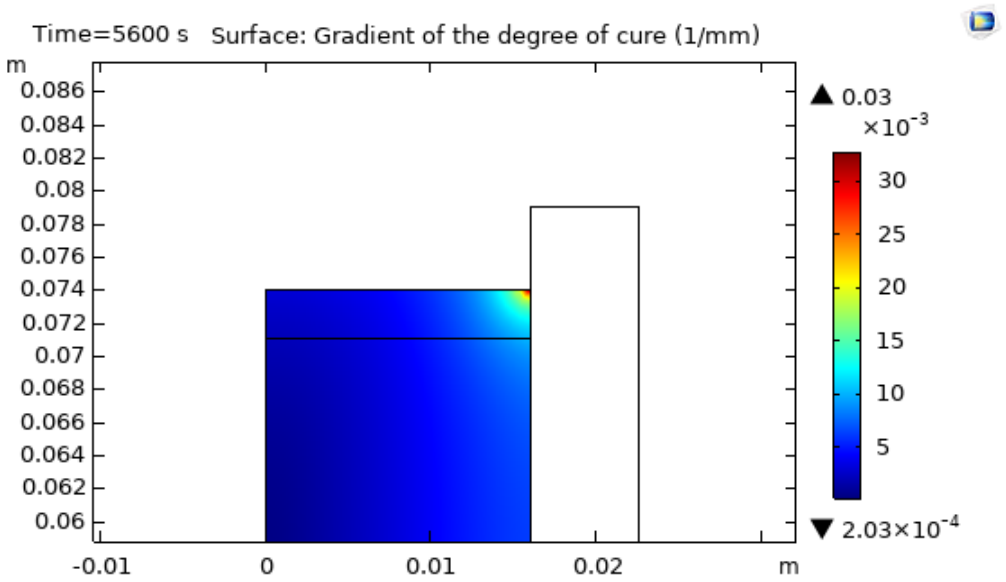

Source: The author (2022)

Figure 28 - Numerical singularity when computing the gradient of the temperature within the epoxy

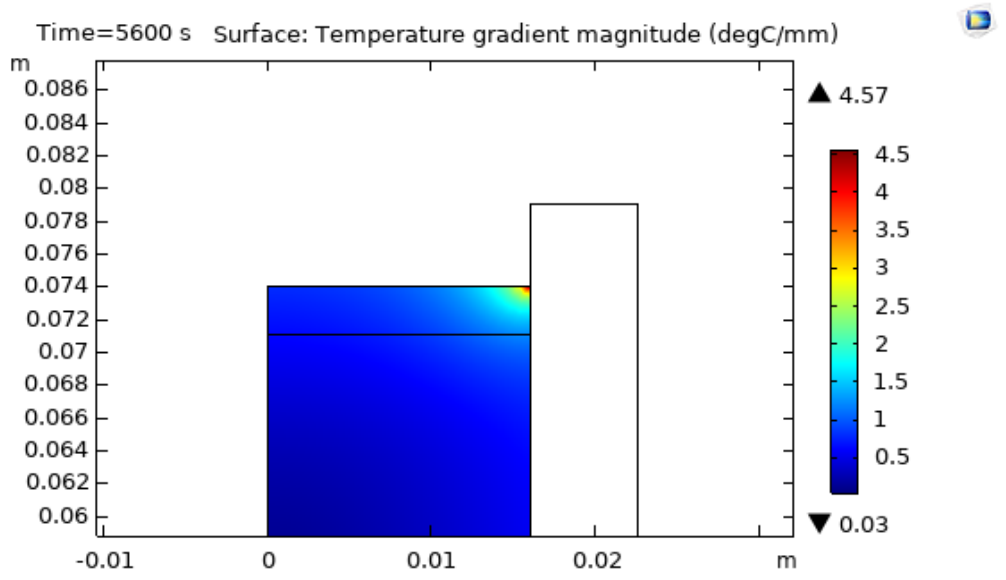

Source: The author (2022)

. In this figure, the blue region is the epoxy domain considered for the computations. This has been done due to a numerical singularity found on the upper right point of the epoxy 2D-axissymetric geometry, as displayed by Figure 27 and Figure 28, which resulted in convergence problems when computing the maximum gradients of degree of cure and

temperature on the whole epoxy domain. It was found that this singularity is related to the boundary condition of convection, because it disappears when simulating the same cure process with a solid cover right on top of the epoxy. By removing the singularity region, mesh convergence for the five variables was achieved.

Figure 26 – Region of the epoxy domain considered for computation of the optimization variables (in blue)

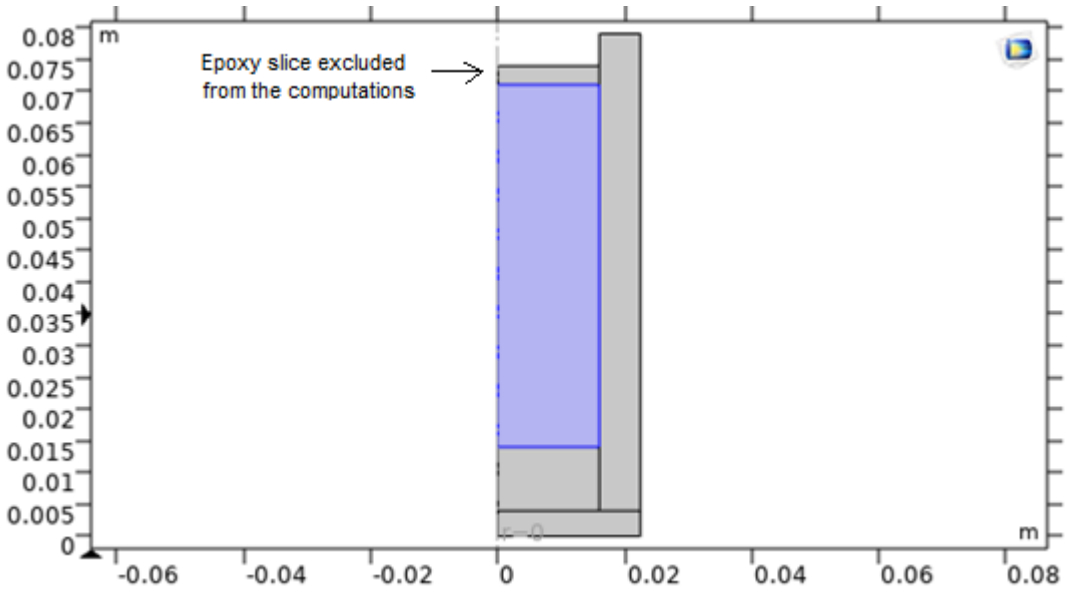

Source: The author (2022)

Figure 27 – Numerical singularity when computing the gradient of the degree of cure within the epoxy

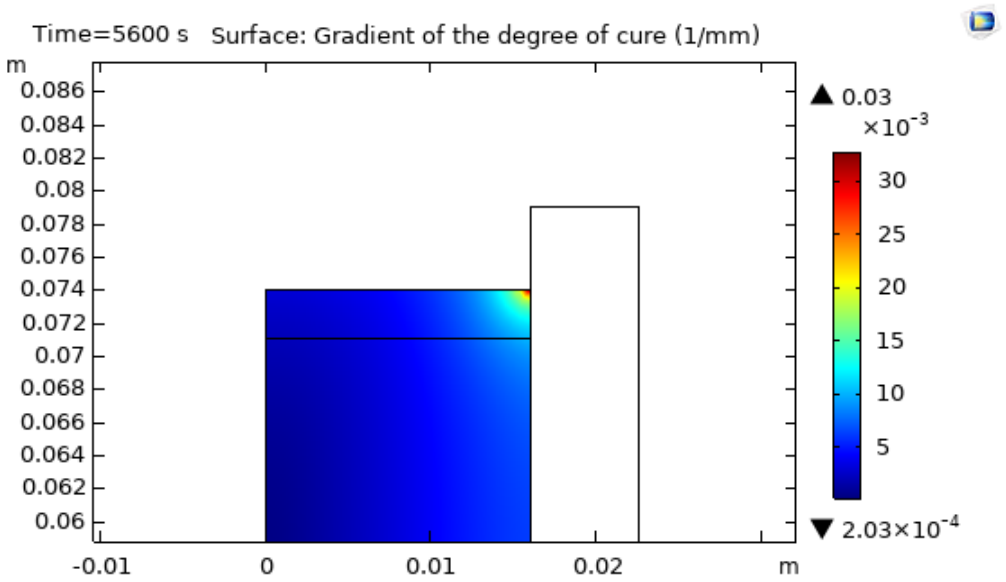

Source: The author (2022)

Figure 28 - Numerical singularity when computing the gradient of the temperature within the epoxy

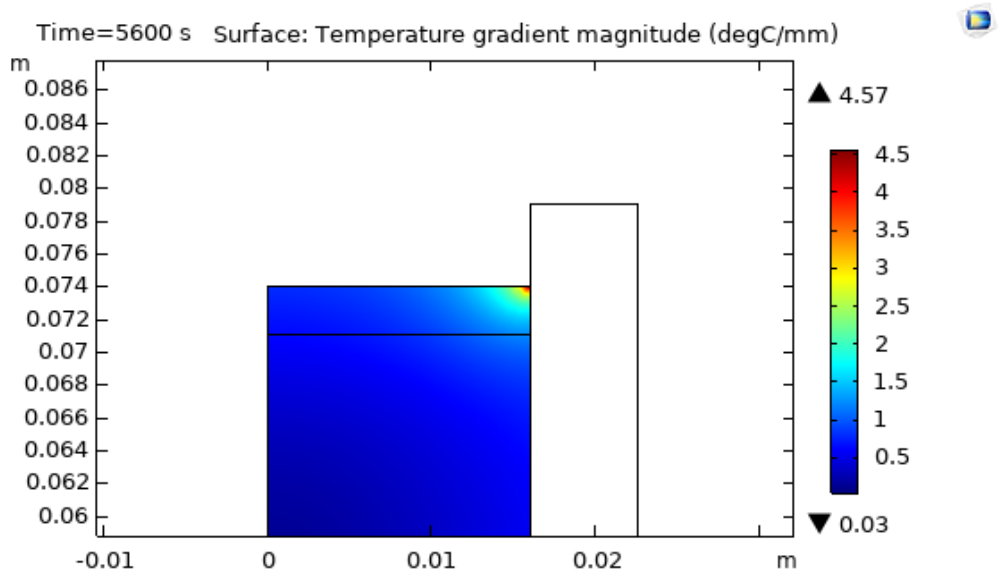

Source: The author (2022)

3.1.7 Mesh selection

In COMSOL, different physics interfaces can use different sets of shape functions. That is, each physics interface has its own unique *discretization* settings that govern what order shape functions are using for those dependent variables.

For the present study, both modules employed in the cure simulation model (COMSOL® modules *Heat Transfer* and *Domain ODEs and DAEs*) used second-order (quadratic) Lagrange elements as their default shape functions.

To gain trust in the results of the FE cure simulation model, the FE mesh was carefully analyzed through a mesh convergence study. The strategy used for the convergence study was the refinement by reducing the size of the elements, which is a simple and effective approach. The steps taken in the mesh convergence study were the following:

1) Ran the model with successively finer and finer meshes, using five element sizes predefined by COMSOL, which are called *Normal*, *Fine*, *Finer*, *Extra Fine* and *Extremely fine*, written here in the increasing order of refinement.
2) Compared the results between these different meshes. The results compared were the values obtained for the five variables of interest of the CRD strategy and GA cure optimization listed in Section 3.1.6.
3) Computed the differences between the normalized values of the variables;
4) Selected the mesh size that respected the error tolerance of 1.5% in relation to the next most refined size for all the variables.

The steps above were executed for three different element shape configurations: triangular elements in the whole geometry; quadrilateral elements in the whole geometry; and a combination of triangular elements (in the mold) and quadrilateral elements (in the resin). Considering the error tolerance and the simulation times, the best mesh configuration obtained and adopted for all cure simulations of the present work was: triangular elements in the whole geometry with *Extra Fine* mesh size, which resulted in 1781 elements, shown in Figure 29. As the shape function selected was quadratic, every mesh element contains 6 nodes. The results of the mesh convergence study performed with triangular elements can be found in the APPENDIX A.

Figure 29 – Mesh selected for the cure simulations

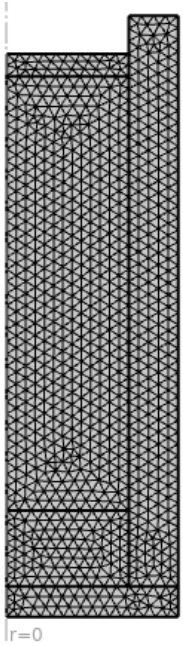

Source: The author (2022)

3.1.8 Timestep refinement

COMSOL Multiphysics are by default solved with an adaptive timestepping approach. This means that the software will automatically modify the timestep size to maintain the required relative tolerance. The default setting for this is “physics controlled”, but it was changed to “user controlled” and then lower relative tolerances were manually informed to perform the timestep refinement. Lowering the relative tolerance to smaller numbers results in smaller timesteps, which increases solution accuracy, and solving time. This was done using the triangular *Extra Fine* mesh selected in the previous step.

Through the timestep refinement study, the relative tolerance selected was 0.0001, which resulted in solutions with tolerable errors (below 1.5%) when compared to the solutions of a model with a maximum time step constraint of 1 s (which is extremely fine).

3.2 OPTIMIZATION APPROACHES

As stated previously, aiming to optimize the cure process of thick thermosets, this research work implemented two different approaches: the conversion rate driven (CRD) strategy and the multi-objective genetic algorithm (GA) optimization, following that order. Those approaches were investigated because they possess different characteristics and, therefore, each of them promised to have benefits over the other according to the application needs.

The common features selected for the two approaches are the following:

- **Two-step cure schedule**: both approaches search for a two-step cure schedule, as the one in Figure 30, with two plateaus at given temperatures *CT1* and *CT2*. This type of schedule was chosen because it is the standard cure cycle for thermoset resin composites;
- **Constant heating rate**: the heating rate from room temperature to CT1 and from CT1 to CT2 is fixed at 3°C/min for all cure schedules tested, as this rate is commonly used in the industry and higher values are difficult to achieve due to equipment capacity restrictions.
- **Restrictions for the minimum degree of cure at the end and maximum temperature reached by the sample throughout the cure**: All the cure schedules tested must meet two conditions to be considered a potential solution. The first one is that the whole thermoset must achieve the degree of conversion required by the application at the end of the cure process, since many properties of the material depend on this variable. As explained previously, it is not viable to reach 100% of cure as it would take too long to accomplish that due to mobility restrictions of the highly crosslinked polymers. Therefore, the application will dictate the minimum degree of cure that is acceptable, considering both material properties and manufacturing time. The second condition is that the maximum temperature reached by the sample during the cure cannot exceed the material degradation temperature (155°C), that is, it cannot be thermally degraded. Therefore, those two conditions were inserted into the COMSOL cure models employed in both strategies, CRD and GA, as stop conditions for the studies. When the simulation stopped because of thermal degradation, the study was dismissed. The opposite happens with the other stop

condition: when the minimum degree of cure is reached by the whole sample, the simulation study is stopped and saved as a viable solution for the problem.

Figure 30 – Two-step cure schedule used for the CRD and GA approaches, with its parameters of temperature and time

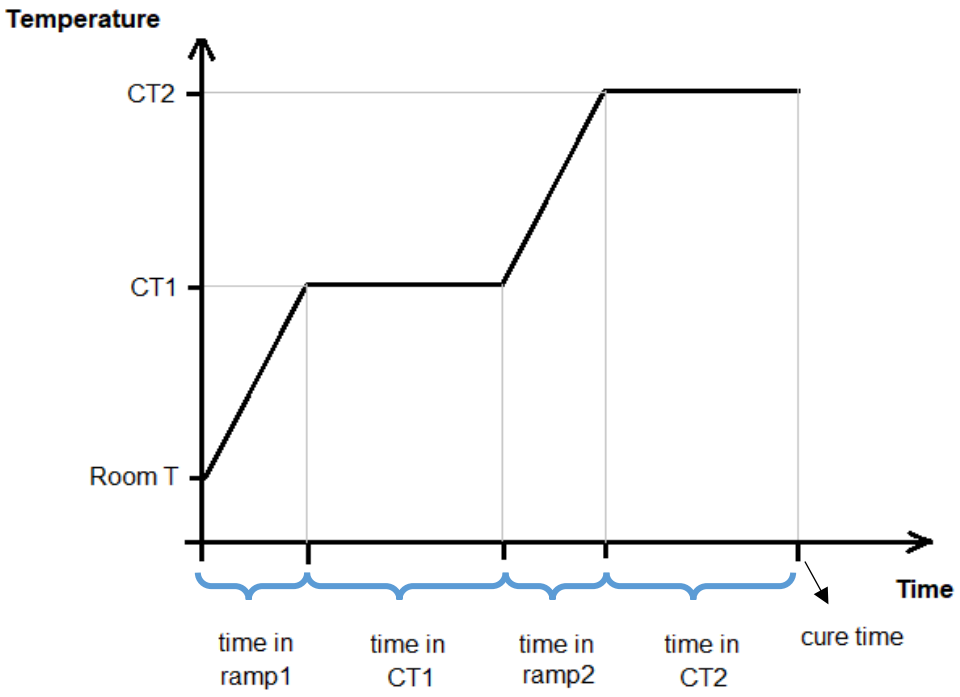

Source: The author (2022)

While the CRD strategy has a single objective, which is to minimize the cure time, the GA optimization aims to optimize three different objectives: (1) minimize the cure time; (2) minimize the maximum gradient of degree of cure reached by the material After Gel Point (AGP); and (3) minimize the maximum gradient of temperature AGP. The first GA objective is the same as the CRD strategy objective and is related to the increasing need to design fast manufacturing processes for thermosets and thermoset composites that meet the high demand for these materials in a multitude of applications. The last two GA objectives are associated to the quality of the cured product. It is widely acknowledged by the scientific community that high gradients of degree of cure and temperature within the thermoset material after the gel point results in a product with residual stresses and related problems, such as cracking, deformations, composite delamination and fiber ondulations (in the case of fiber-reinforced composites). Since no stresses are built up before gelation, the residual stress starts when the

degree of cure reaches 55% for the present resin system. Therefore, those intense gradients must be avoided once this point is reached.

There is clearly a trade-off between GA objectives 1 and 2, and between objectives 1 and 3. This is because when we increase the cure rate (and decrease the cure time) the intense thermal energy released by the exothermic cross-linking reaction has less time to be conducted out of the thick thermal insulating sample, which is in a rubbery or glass state after the gel point. As a result, high gradients of temperature and degree of cure arise inside of the material, with the highest temperatures and degree of conversion appearing in the central region of the specimen. As demonstrated through the literature review, multi-objective GA can successfully handle problems with this kind of conflicting goals, such as the trade-off between manufacturing time and product quality.

On the other hand, in cases that the most important concern is to minimize the cure time through fast simulations, the CRD strategy can be more appropriate then the GA algorithm. This is because the CRD algorithm is based on a simple concept of the cure kinetics and does not require the simulation of hundreds of different cure schedules to find good results, as is the case for the GA.

Having in mind that the CRD strategy has the benefit of being simple and fast, while the multi-objective GA has the advantage of considering the trade-off between different objectives, both strategies were implemented in MATLAB, connected to the same COMSOL cure simulation model. The use of the same COMSOL model allowed the authors to effectively compare the solutions provided from the two strategies in terms of the variables of interest, which are the following:

- **Cure schedule:** CT1, CT2, time in CT1, time in CT2;
- **Constrained variables:** maximum temperature reached during the cure, minimum degree of cure achieved at the end of the cure process;
- **Objective variables:** cure time, maximum gradient of degree of cure AGP and maximum gradient of temperature AGP.

Before executing the CRD strategy and the GA optimization, a cure schedule recommended by the manufacturer in the material's datasheet was simulated with the COMSOL model and the results obtained for the objective variables listed above were taken as a reference to judge the efficacy of the algorithms in finding optimal solutions. The manufacturer's recommended cure schedule (MRC) selected was a two-step cure cycle with CT1 = 80°C, CT2

= 140°C, time in CT1 = 4h and time in CT2 = 8h. The heating ramp adopted was, in accordance with the other cure simulations, 3°C/min.

As explained previously, the minimum degree of cure required for the sample depends on its application. In this research work, for the sake of evaluating the performance of the CRD strategy and GA optimization and being able to compare theirs results with the MRC, the minimum degree of cure required at the end of all cure schedules was set as the same degree of conversion provided by the MRC schedule, which was 85.4%. A detailed explanation of the CRD strategy and GA optimization is provided below.

3.2.1 Conversion Rate Driven strategy

The conversion rate-driven (CRD) strategy was designed in this research work with the objective of minimizing the cure time of thick thermosets, while making sure that the cured component achieves the minimum degree of cure required and is not thermally degraded. The implementation of this strategy was possible due to the numerical simulation of the cure process, which allows monitoring easily the evolution of many time-dependent variables of the curing, including the average conversion rate within the sample studied. Figure 31 shows the moment when the average conversion rate of the studied sample reaches its maximum value if cured for 2h at 80°C after a 20-min heating ramp of 3°C/min from room temperature.

Figure 31 – Average conversion rate of a sample cured at 80°C for 2h with an initial heating rate of 3°C/min and the time when this variable reaches its maximum value

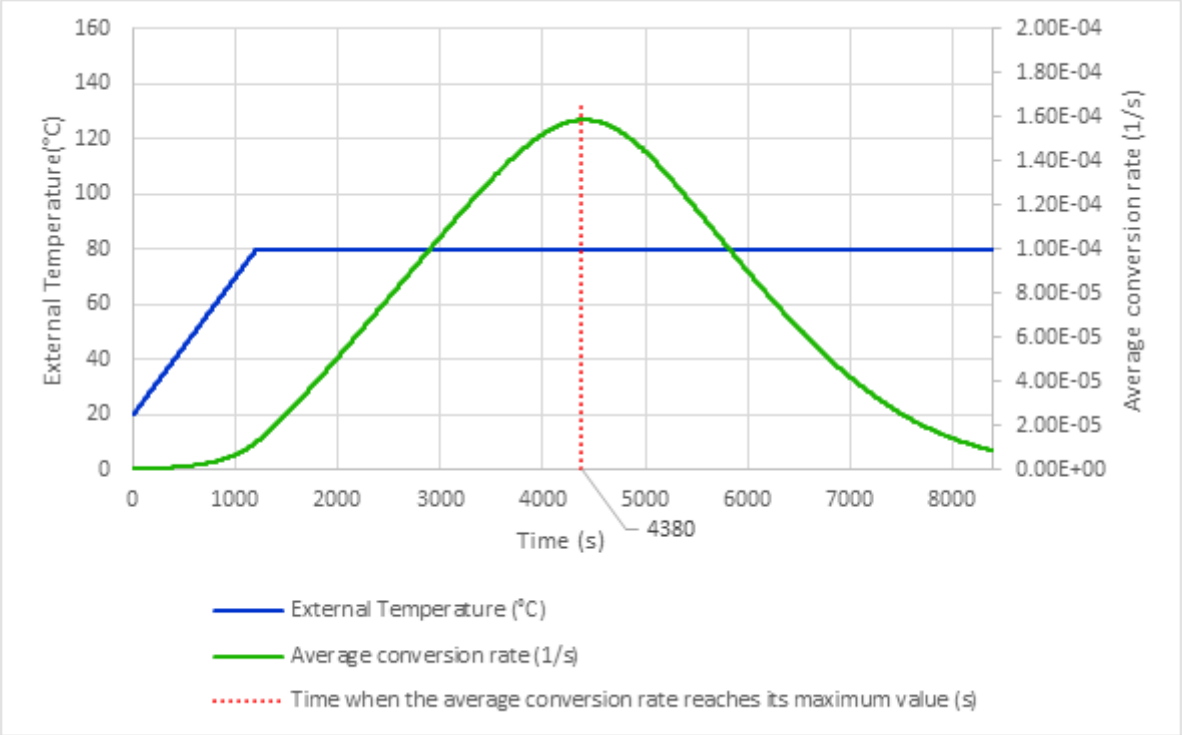

Source: The author (2022)

The leading idea of the strategy is to simulate the cure of a thermoset resin at a given temperature plateau (CT1) for some hours, as in Figure 31, and detect the time when the average conversion rate of the specimen reaches its maximum value, in order to set it as the time when the external temperature starts to increase from the first plateau (CT1) to the second one (CT2). That is, the CRD strategy defines the duration of the first temperature plateau (t_CT1) in a way that avoids wasting time on it once the conversion rate begins to decrease. For the case of Figure 31, following the CRD procedure, the first temperature plateau should end at 4380 s (73 min) and the second heating ramp should start towards CT2. This would result in a first temperature plateau of 53 min.

The duration of the second temperature plateau (t_CT2) is defined as the time when all points of the specimen reaches at least the minimum degree of cure required by the application. As an initial configuration, t_CT1 and t_CT2 were set as equal to 2 hours and 4 hours, respectively. However, the COMSOL model automatically stops the simulation study if one of the two conditions are met: (1) if the whole sample reaches the minimum required degree of cure or (2) if the degradation temperature is reached anywhere within the sample. This contributes to have short simulation times, as we do not need to wait until the end of the simulation if the sample is cured enough or if it is thermally degraded.

At first, the CRD was implemented directly in COMSOL, without the use of any additional software or script to automatize the procedure. Once the method was successfully completed in this way, aiming to be able to perform several different cure schedules for many combinations of CT1 and CT2 with the CRD strategy in an efficient mode, the strategy was completely automated by the development of a MATLAB script that runs in a loop. This automation allows the investigation of the behavior of a great number of cure schedules provided by the CRD results and select the best one for the objective of reducing the cure time.

The125evelopped MATLAB script configures and runs the COMSOL cure simulation model through the module COMSOL LiveLink for MATLAB®. The input parameters of the CRD strategy script and the values set for them are presented in Table 8. The cure schedules simulated with the strategy corresponds to the combinations of the temperatures CT1 and CT2 informed in vectors. The vector CT1 contains 16 temperatures and the vector CT2 has 3 temperatures. Thus, the total number of cure schedules simulated were 48. From a previous work (PAIVA, 2018), it was known that the sample would be thermally degraded if cured at CT1 = 100°C, that is why the upper limit for CT1 without thermally damaging the specimen was supposed to be around 95°C. The lower limit was set as 80°C to match the manufacturer's recommendation. The same idea was applied to CT2: the lower limit was defined as the temperature recommended by the manufacturer (140°C) and the upper limit was set as 150°C to avoid the thermal degradation that occurs at 155°C. A higher number of temperatures was set for CT1, when compared to CT2, because the CRD strategy acts mostly on the first temperature plateau and the main intention of running those simulations in mass was to investigate the behavior of the algorithm, in addition to finding the cure schedule that minimizes the cure time.

Table 8 – Input parameters of the CRD strategy script and the values set for them

PARAMETER NAME	PARAMETER DESCRIPTION	VALUE	UNIT
CT1	Vector of temperatures for the first plateau	[80;81;82;83;84;85;86;87;88;89;90;91;92;93;94;95]	[°C]
CT2	Vector of temperatures for the second plateau	[140;145;150]	[°C]
r	Heating rate for both ramps: from room temperature to CT1 and from CT1 to CT2	3	[°C/min]

t_CT1_0	Duration of the first temperature plateau in the first cure simulation, through which the time when the average conversion rate reaches its maximum value is detected	2	[h]
t_CT2_0	Maximum duration of the second temperature plateau	4	[h]
T_degrad	Material degradation temperature	155	[°C]
alpha_min_req	Minimum degree of cure required at the end of the cure	0.854	[1]

Source: The author (2022)

The complete MATLAB script developed for the CRD strategy can be found in APPENDIX B. The steps taken by the algorithm for a given combination of CT1 and CT2, considering that the thermal degradation does not occur, are roughly summarized below:

1. Initialize the plateau temperatures (CT1 and CT2) and the heating rate I;
2. Computes the duration of the heating ramps from room temperature to CT1 (t_ramp1) and from CT1 to CT2 (t_ramp2);
3. Simulate the cure of the sample with the following cure schedule: heating ramp from room temperature (20°C) to CT1 at the rate r + temperature plateau at CT1 for the time t_CT1_0;
4. Detect the time when the average conversion rate reaches its maximum value;
5. Set that time as the end of the first temperature plateau;
6. Computes the duration of the first temperature plateau (t_CT1), subtracting the time in the first heating ramp (t_ramp1);
7. Simulate the cure with a new schedule: heating ramp from room temperature (20°C) to CT1 at the rate r + temperature plateau at CT1 for the time t_CT1 + heating ramp from CT1 to CT2 at the rate r + temperature plateau at CT2 for the time t_CT2_0;
8. Get the minimum degree of cure within the sample at the end of the cure and the maximum temperature reached by the sample throughout the cure;

   If the material is cured enough and not thermally degraded:

9. Store the time of the end of the simulation as the cure time;
10. Compute the duration of the second temperature plateau (t_CT2), subtracting t_ramp1, t_CT1 and t_ramp2 from the cure time;

11. Get the maximum gradients of degree of cure and temperature reached by the sample AGP;
12. Print the results on the screen;
13. Saves COMSOL model.

For each cure schedule simulated, the computed values are stored by the script in a MATLAB structure named CRD, whose variables are listed in Table 9. Once the CRD strategy run was completed for the 48 cure schedules, the data of the structure was exported to an Excel spreadsheet in order to perform the results analysis. After each cure schedule simulation, the CRD script was programmed to save the COMSOL model as well, so that the model results could be further analyzed in the FEM software.

Table 9 – Fields of the MATLAB structure named CRD that stores the output of the simulations performed with the CRD strategy

STRUCTURE FIELD	FIELD DESCRIPTION	UNIT
CT1	Temperature of the first plateau	[°C]
CT2	Temperature of the second plateau	[°C]
t_CT1	Time in CT1	[s]
t_CT2	Time in CT2	[s]
t_CT1_min	Time in CT1	[min]
t_CT2_min	Time in CT2	[min]
t_ramp1	Time in the first heating ramp	[min]
t_ramp2	Time in the second heating ramp	[min]
T_max	Maximum temperature reached by the sample throughout the cure	[°C]
max_alphat	Historical maximum of the volume average conversion rate	[1/s]
t_max_alphat	Time when the volume average conversion rate reaches its maximum	[s]
last_min_alpha	Volume minimum degree of cure at the end of the cure	[1]
t_cure	Cure time	[s]
t_cure_min	Cure time	[min]
max_grad_alpha_AGP	Maximum gradient of degree of cure AGP	[1/mm]

max_grad_T_AGP	Maximum gradient of temperature AGP	[°C/mm]
S_min_alpha	Flag for the stop condition 1: sample cured enough	[1]
t_min_alpha	Time when the stop condition 1 is met	[s]
S_critic_T	Flag for the stop condition 2: thermal degradation	[1]
t_critic_T	Time when the stop condition 2 is met	[s]
t_cure_sim	Cure time computed by the simulation (without rounding to integer)	[s]

Source: The author (2022)

3.2.2 Genetic Algorithm optimization

As explained before, a genetic algorithm is a specific type of evolutionary algorithm, which evolves primal solutions ("individuals") into refined ones. It accomplishes this by choosing the solutions that are the most "fit" and changing their parameters to create brand-new, perhaps better solutions.

For the present optimization work, the "individual" is a two-step cure schedule as the one in Figure 30, which contains three "genes": the plateau temperatures CT1 and CT2 and the time in CT1. The time in CT2 was not included in the GA as a "gene" because it is not a parameter to be optimized, once its value is fully determined by the time when the whole sample reaches the minimum degree of cure required.

The multi-objective genetic algorithm was executed in MATLAB using the Genetic Optimization System Engineering Tool (GOSET) version 2.6 in conjunction with the previously described COMSOL cure simulation model. GOSET toolbox was chosen because it is a reliable free resource, trusted by the scientific community, that can be easily customized and applied in many problems. While GOSET was responsible for running the genetic algorithm operators that it contains in its library, it was left for the authors' of this research work to:

- Find the GA parameters that result in an effective multi-objective optimization. That is, find the GA parameters that lead to a diverse set of solutions, close to a Pareto-Optimal Front;

- Implement a MATLAB script that initialize the GOSET with the GA parameters, plot the solutions, and calls GOSET main optimization function, passing a fitness function handle as an argument;
- Implement a MATLAB fitness function, to compute the fitness of every cure schedule and check all the constraints, by executing the cure simulations in COMSOL through the COMSOL LiveLink for MATLAB and extracting the results of the variables of interest; and
- Invoke MATLAB's Parallel Processing Toolbox to use multiple cores to calculate the fitness of the population.

From the CRD strategy results, it was verified that the sample was thermally degraded for temperatures above 94° in the first plateau. Therefore, this temperature was configured as the upper limit for CT1 in the GA optimization. Besides, the minimum duration of the first plateau (t_CT1) provided by the CRD strategy, without thermally damaging the sample, was 32 min. In the hope of finding shorter cure times, with shorter temperature plateaus, the lower limit for the duration of CT1 was set as 10 min. The lower limits for CT1 and CT2 and the upper limit for CT2 were defined as equal to the parameters of the manufacturer's recommended cure schedule, while the upper limit for CT2 was set as 150°C, resulting in search spaces for the temperature plateaus that were almost the same of the CRD strategy, only excluding CT1 = 95°C. The full ranges configured by the three "genes" of the GA are presented in Table 10. The GA searches cure schedules whose genes have integer values within those ranges.

Table 10 – Lower and upper limits configured for the GA "genes"

Gene	Lower limit	Upper limit	Unit
CT1	80	94	[°C]
CT2	140	150	[°C]
Time in CT1	10	240	[min]

Source: The author (2022)

A parameter tuning of the standard GA configured in GOSET was conducted by trial-and-error. After performing many GA optimization runs, changing the number of generations,

individuals per gelation and some of the GA operators, a configuration that resulted in a diverse set of solutions for the Pareto-Optimal Front was obtained with 20 generations having 50 individuals/generation. That number of generations and individuals have also been considered satisfactory by other author's in the literature for different applications (GOLDBERG, 1989; DOLKUN et al., 2018). All the values selected as the GA parameters were stored in the GOSET structure named GAP, whose fields are shown in Table 11. Parameters that are not present in this table were set with the default GOSET value. The resulting GA was an elitist GA. Detailed explanations on the GA parameters used by GOSET can be found in its documentation (SUDHOFF, 2014).

Table 11 – Genetic Algorithm parameters and the values set for them in the GOSET Structure named GAP

GENETIC ALGORITHM PARAMETER	GOSET VARIABLE (STRUCTURE FIELD)	PARAMETER VALUE
No. of generations to evolve	GAP.fp_ngen	20
No. of chromosomes in initial population	GAP.fp_ipop	50
No. of chromosome in the population	GAP.fp_npop	50
No. of objective functions	GAP.fp_nobj	3
Objective to optimize	GAP.fp_obj	0 (Multi-objective optimization)
Diversity control algorithm	GAP.dc_alg	3
Diversity control space	GAP.dc_spc	1 (Parameter space)
Scaling algorithm	GAP.sc_alg	1
Selection algorithm	GAP.sl_alg	1 (Roulette wheel selection)
Death algorithm	GAP.dt_alg	3 (Tournament on fitness)
No. of individuals used in a death tournament	GAP.dt_nts	4
Percentage of pop. Replaced by children	GAP.mc_pp	0.6
Fraction of chromosomes involved in crossover	GAP.mc_fc	1
Crossover algorithm	GAP.mc_alg	6 (Random algorithms)

No. of gen. btw changing Algs for random crossover Alg	GAP.mc_gac	3
Probability of a total gene mutation	GAP.mt_ptgm	-
Initial value of GAP.mt_ptgm	GAP.mt_ptgm0	0.01
Final value of GAP.mt_ptgm	GAP.mt_ptgmf	0.001
Gene repair algorithm	GAP.gr_alg	Hard limiting (1)
No. of geographic regions the population is distributed	GAP.mg_nreg	1
Time between migrations in generations	GAP.mg_tmig	5
Probability of an individual to migrate	GAP.mg_pmig	0.1
Use parallel processing	GAP.ev_pp	true
Number of cores being used	GAP.ev_npg	6
Fraction of pop. Protected as elite for multi-objective optimization	GAP.el_fpe	-
Initial value of GAP.el_fpe	GAP.el_fpe0	0.2
Final value of GAP.el_fpe	GAP.el_fpef	0.8
Fraction of generations on which to execute the algorithm	GAP.rs_fea	0.5
Generation between reports	GAP.rp_gbr	1
List of objectives to make objective plots for	GAP.op_list	[1,2,3] (3 objectives)
Style for each objective	GAP.op_style	[1 1 1] (linear)
Sign of fitness for each objective	GAP.op_sign	[-1 -1 -1] (negative)
List of 2 or 3 objectives to be used in Pareto plot [ ]/[	GAP.pp_list	[1,2] -> (Pareto Plot 1); [2, 3] -> (Pareto Plot 2); [1,3] -> (Pareto Plot 3)
x-axis label	GAP.pp_xl	Curing time (s)' -> (Pareto Plot 1) ; 'Curing time (s)' -> (Pareto Plot 2) ; 'Max. gradient of degree of cure AGP (1/mm) -> (Pareto Plot 3)

y-axis label	GAP.pp_yl	Max. gradient of degree of cure AGP (1/mm)' -> (Pareto Plot 1) ; 'Max. gradient of temperature AGP (°C/mm)' -> (Pareto Plot 2) ; 'Max. gradient of temperature AGP (°C/mm)' -> (Pareto Plot 3)
Style for each objective	GAP.pp_style	[1,1,1] (linear)
Sign of fitness for each objective	GAP.pp_sign	[-1,-1,-1] (negative)
Row vector of minimum gene values	GAP.gd_min	[80 140 10]
Row vector of maximum gene values	GAP.gd_max	[94 150 240]
Row vector of gene types	GAP.gd_type	[1 1 1] (integer)
Row vector of chromosome ID number	GAP.gd_cid	[1 1 1]

Source: The author (2022)

For the scalarization of the fitness values in the multi-objective optimization problem, the normalized weight vector [0.4 0.3 0.3] was used, aiming to apply similar weights for the three different objectives. In order to exclude solutions that did not meet the optimization restrictions, a bad fitness value was attributed to every objective variable of them. The complete MATLAB script and fitness function developed for the GA optimization can be found in APPENDIX C and APPENDIX D, respectively.

As in the case of the CRD optimization, the results of the multi-objective optimization were stored in a MATLAB structure (the GOSET structure named GAS), and after that, exported do a spreadsheet in order to analyze better the results and compare them with the solutions provided by the CRD strategy and by the manufacturer.

4 RESULTS AND DISCUSSION

In this section, the results of the conversion rate driven strategy (CRD) and multi-objective genetic algorithm (GA) optimization are presented and discussed, taking the simulation results of the manufacturer's recommended cure schedule (MRC) as a reference for the analysis.

For each case, the best solution obtained is detailed and the values of the respective Cure schedule, constrained variables and objective variables are displayed. The heating ramp applied in all cases was 3°C/min. The results of every cure schedule simulated can be found in the APPENDIX E.

4.1 MANUFACTURER'S RECOMMENDED CURE SCHEDULE

The simulation of the manufacturer's recommended cure schedule (MRC) selected provided the results shown in Table 12. The minimum degree of cure reached at the end of the cure process was not 100%, but 85.4% instead, due to diffusion restrictions to the continuity of the reaction, which can still occur but at an extremely slow rate.

Table 12 – Parameters and results of the manufacturer's recommended cure schedule

Cure schedule				*Constrained variables*		*Optimization objective variables (to minimize)*			
						Objective 1		*Objective 2*	*Objective 3*
CT1 (°C)	**CT2 (°C)**	**Time in CT1 (min)**	**Time in CT2 (min)**	**Min. alpha – end of the cure**	**Max. T during the cure (°C)**	**Cure time (min)**	**Cure time (s)**	**Max. grad. Of alpha AGP (1/mm)**	**Max. grad. of T AGP (°C/mm)**
80	140	240	480	85.4%	140	760	45600	1.45E-02	1.76E+00

Source: The author (2022)

As for the maximum temperature reached by the sample during the cure, it was the same as the second plateau temperature (140 °C), staying away from the LY556 epoxy system thermal degradation temperature, which is 155 °C. That proves that the MRC schedule is thermally safe for the studied sample.

In order to analyze the thickness effect on the properties of the cured epoxy, Figures 32 and 34 were obtained from the simulation. They display the maximum, minimum and average

temperatures and degrees of conversion, as well as maximum gradients of temperature and degree of conversion AGP, reached by the sample during the cure. Two peaks can be observed in the maximum gradients of temperature and degree of conversion AGP. The first one occurs right after the gel point has been reached. This is related to heat provided at the first step of the cure schedule, associated with the exothermic polymerization reaction that takes place during the gelation period, from room temperature to the fist temperature plateau.

The exothermic aspect of the reaction is highlighted by the epoxy temperature rise above the external temperature displayed in Figure 32, and also by the temperature distribution within the epoxy shown in Figure 33, at the time when the temperature overshoot inside the thermoset reaches its maximum value. The second peak in the maximum gradients happens when the external temperature starts to increase again, from the first to the second temperature plateau, providing more thermal energy for the curing reaction occur and increase the crosslinking density of the sample. It is important to note that the first peak of the maximum gradient of temperature is less intense than the second one, while the opposite occurs with the peaks of the maximum gradient of degree of cure. This shows that these two variables are affected differently by the cure schedule and, thus, must be studied independently when optimizing the cure process.

Figure 32 – Temperatures and maximum gradients of temperature AGP reached by the sample during the cure, following the MRC schedule

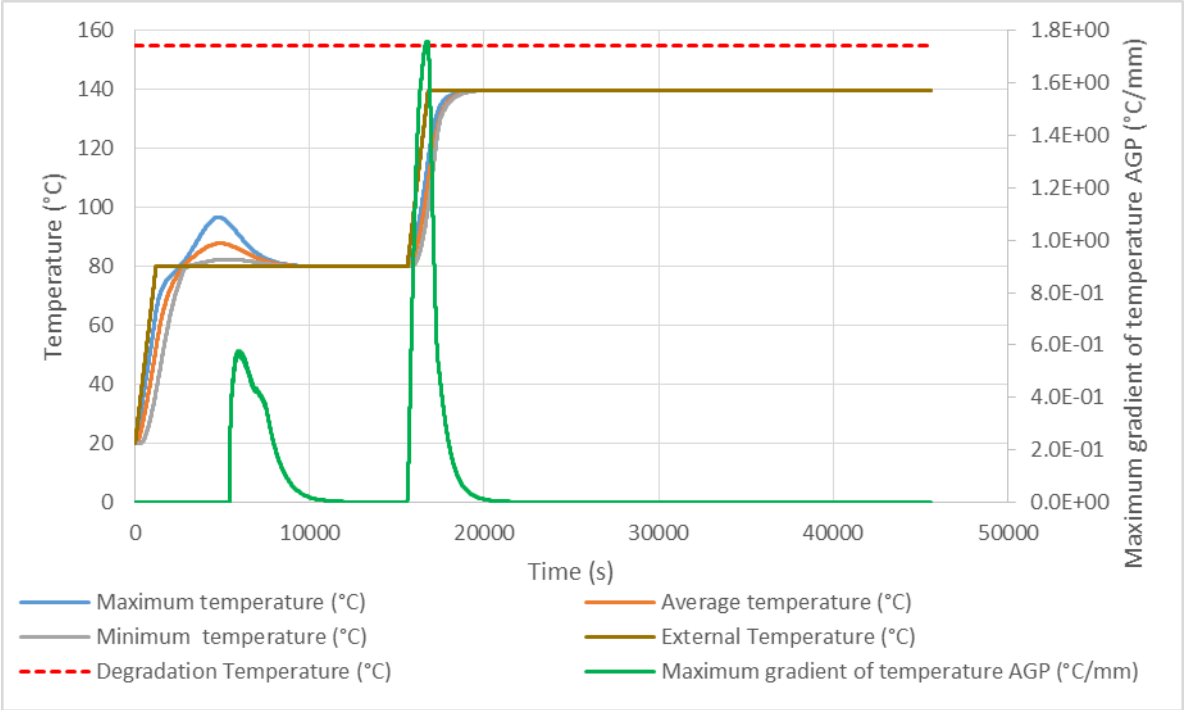

Source: The author (2022)

Figure 33 – Temperature distribution within the epoxy at the maximum temperature overshoot due to the intense exothermic heat

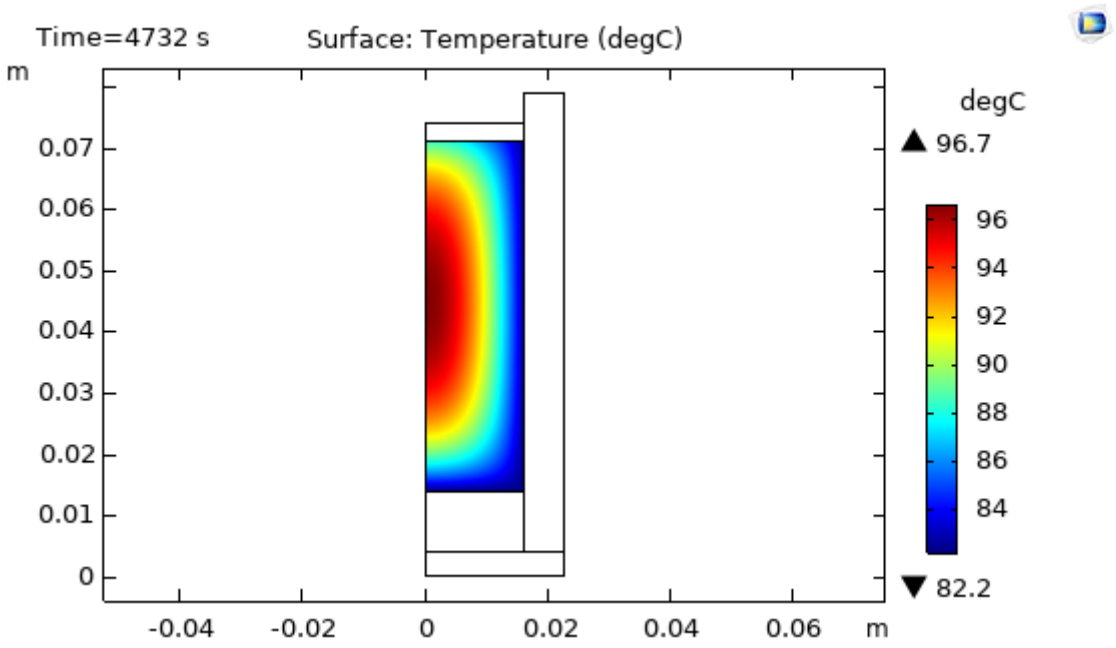

Source: The author (2022)

Figure 34 – Degrees of conversion and maximum gradients of degree of conversion AGP reached by the sample during the cure, following the MRC schedule

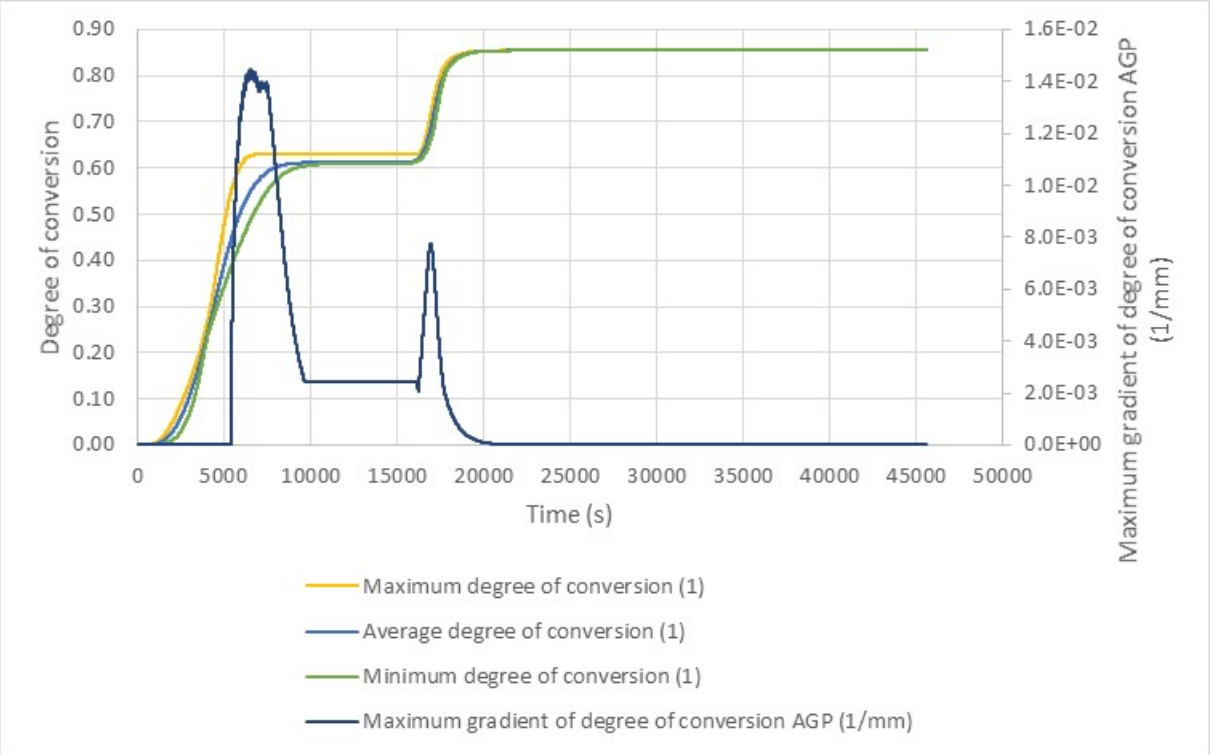

Source: The author (2022)

As the conversion rate increases with temperature, two peaks in this variable can also be observed during the heating ramps, as shown in Figure 35.

Figure 35 - Degrees of conversion and average conversion rate reached by the sample during the cure, following the MRC schedule

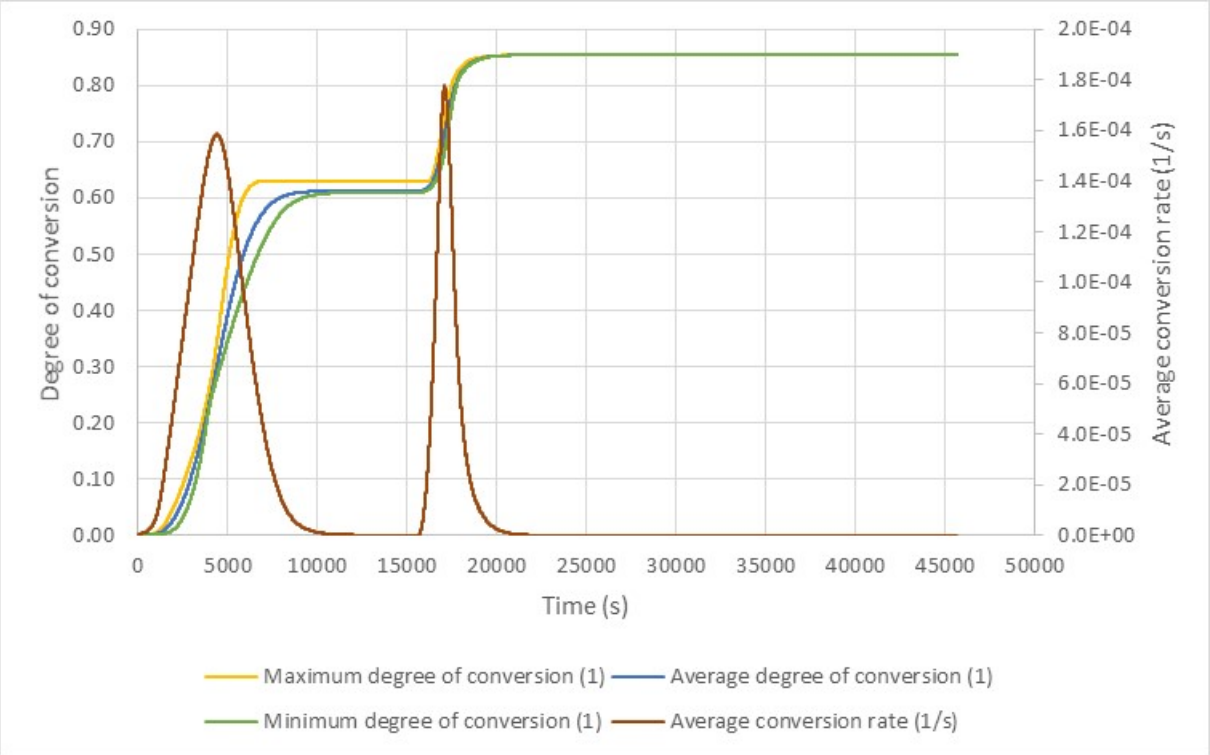

Source: The author (2022)

From Figure 34, it is evident that the this MRC schedule is too long for the specimen studied, because the sample reaches a uniform and stable degree of conversion (85.4%) before half the cure time has elapsed. So, for more than seven hours (25,200 s), the epoxy degree of conversion remains practically constant and homogeneous until the end of the cure, wasting time and energy in the manufacturing process.

In this context, the CRD strategy and multi-objective GA optimization promise to deliver cure schedules that take less time, and therefore, result in a lower cost of manufacturing when compared to a default MRC. Besides, multi-objective GA optimization also promises to find cure schedules that are not only more economic, but also that produce better quality thermosets and thermosetting matrix composites, by trying to minimize the gradients of temperature and degree of cure AGP that arise during the curing process, in addition to minimizing the curing time. The results obtained using both approaches were detailed in the following sections.

4.2 CONVERSION RATE-DRIVEN STRATEGY

As explained previously, the conversion rate-driven strategy was designed with the objective of minimizing the curing time of a sample, by tying the moment of completion of the first temperature plateau to the moment when the conversion rate of the sample is on the verge of starting to decrease, that is, when it reaches its maximum point.

Due to the automation of the strategy, it was possible to obtain several cure schedules in a single algorithm run, simply by providing as input the CT1 and CT2 temperatures, which were combined with each other to generate the cure schedules. The code returned the times of each temperature plateau, the values of the important variables (constrained and objective variables) and saved the simulation models so that a more sophisticated post-processing of the results of each cure schedule could be carried out.

In this study, 48 cure schedules were produced to be investigated through the CRD strategy, from the combinations of CT1 and CT2 provided:

1) CT1 = {80,81,82,83,84,85,86,87,88,89,90,91,92,93,94,95} °C and
2) CT2 = {140,145,150} °C.

However, it was found that curing the sample under study with CT1 = 95°C using the CRD strategy makes the material to reach its thermal degradation temperature (155 °C), which is not desired. Therefore, the three results obtained from the combination of CT1 = 95°C with CT2 = {140,145,150} °C were excluded from the feasible solution because they generated a thermally degraded specimen. Thus, only the 45 remaining combinations (cure schedules) were considered, whose results can be seen in APPENDIX E. Running the code took a total time of about 9 hours on the selected computer.

As expected, it was found that the fastest curing corresponds to the cure schedule with the maximum values for CT1 and CT2 among the selected temperatures, since the curing speed increases with temperature (and the thermal degradation limit is not hit). The durations of each plateau at these temperatures and the total cure time are the most important results of the CRD strategy, shown in Table 13. With the CRD strategy it was possible to reduce the MRC cure time from 12.7h (760 min) to just 1.6h (96 min), which is an impressive improvement of the process time.

In Table 13, the values obtained for the maximum gradients of temperature and degree of curing AGP obtained during the curing are also presented. It is observed that they are much

higher than those resulting from the MRC schedule, which raises a concern about the residual stresses that can be generated by the high levels of internal gradients.

With the CRD strategy, there is no time for the conversion rate to drop during the first temperature plateau, so the maximum gradients of degree of cure and temperature AGP that arise in the sample do not have time to subside by the heat conduction through the sample. Such behavior is highlighted by Figures 36, 37 and 38, which mostly show only one peak for the maximum temperature gradients, degree of curing and average conversion rate, but with higher values when compared to the MRC schedule.

Besides, from Table 13 and Figure 36, it can be seen that the best solution provided by the CRD strategy leads to a high peak of temperature within the sample during the curing, due to the fast curing with high temperatures for the two plateaus CT1 and CT2, almost reaching the material degradation temperature.

Table 13 – Best cure schedule found with the CRD strategy to minimize the cure time

Cure schedule				*Constrained variables*		*Optimization objective variables (to minimize)*			
						Objective 1		*Objective 2*	*Objective 3*
CT1 (°C)	**CT2 (°C)**	**Time in CT1 (min)**	**Time in CT2 (min)**	**Min. alpha - end of the cure**	**Max. T during the cure (°C)**	**Cure time (min)**	**Cure time (s)**	**Max. grad. of alpha AGP (1/mm)**	**Max. grad. of T AGP (°C/mm)**
94	150	32	21	85.5%	152	96	5780	4.52E-02	5.00E+00

Source: The author (2022)

Figure 36 - Temperatures and maximum gradients of temperature AGP reached by the sample during the cure, following the best cure schedule found with the CRD strategy to minimize the cure time

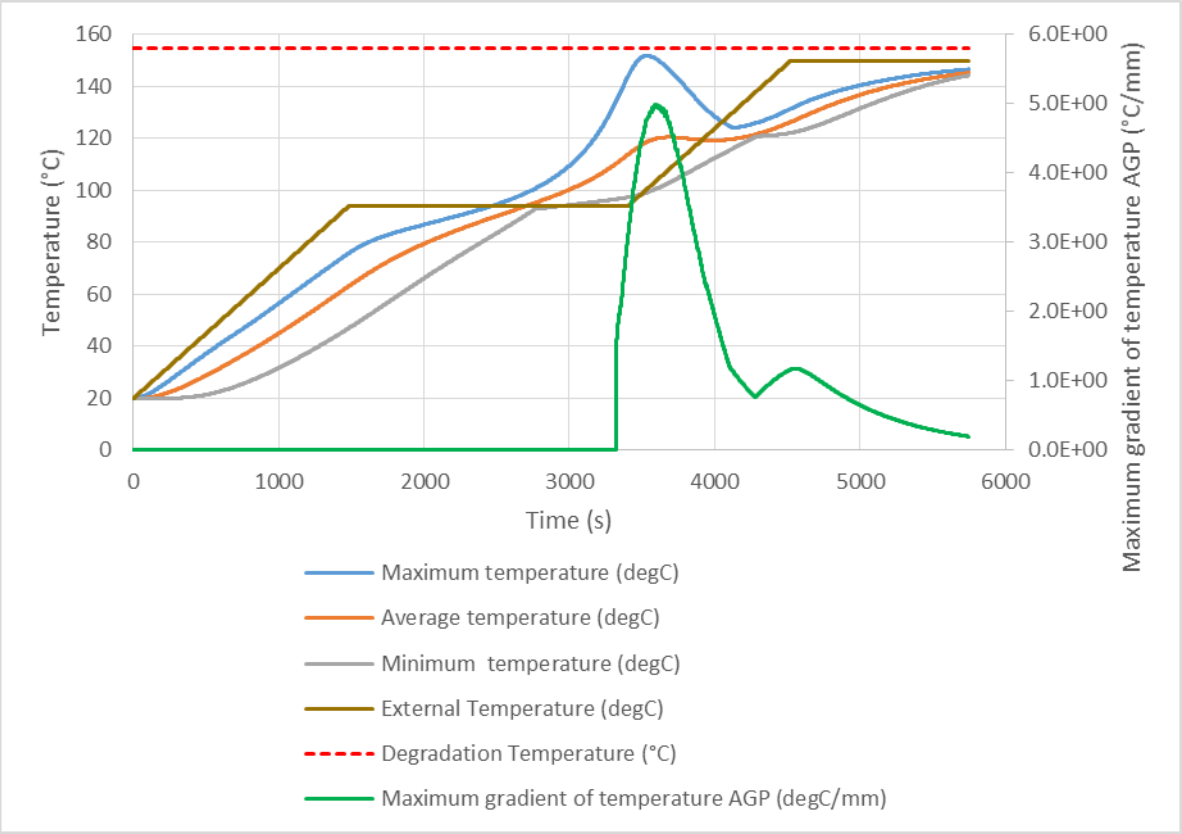

Source: The author (2022)

Figure 37 - Degrees of conversion and maximum gradients of degree of conversion AGP reached by the sample during the cure, following the best cure schedule found with the CRD strategy to minimize the cure time

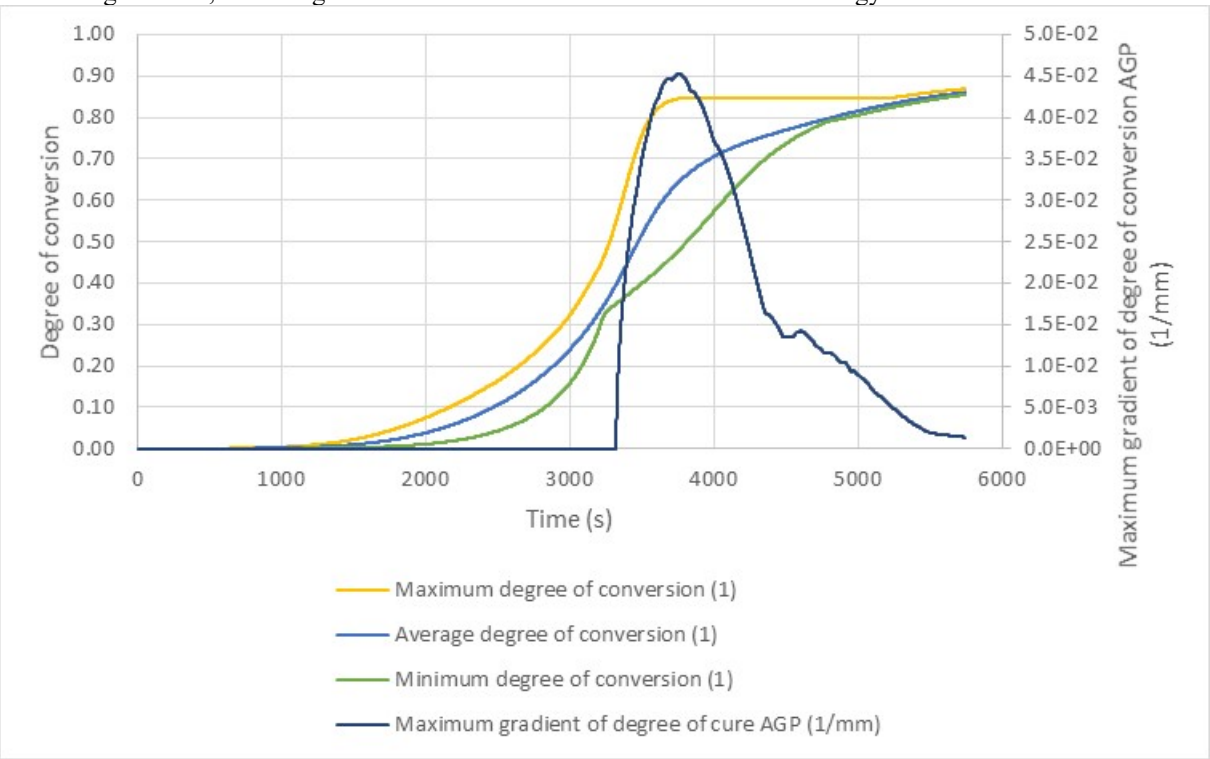

Source: The author (2022)

Figure 38 - Temperatures and average conversion rate reached by the sample during the cure, following the best cure schedule found with the CRD strategy to minimize the cure time

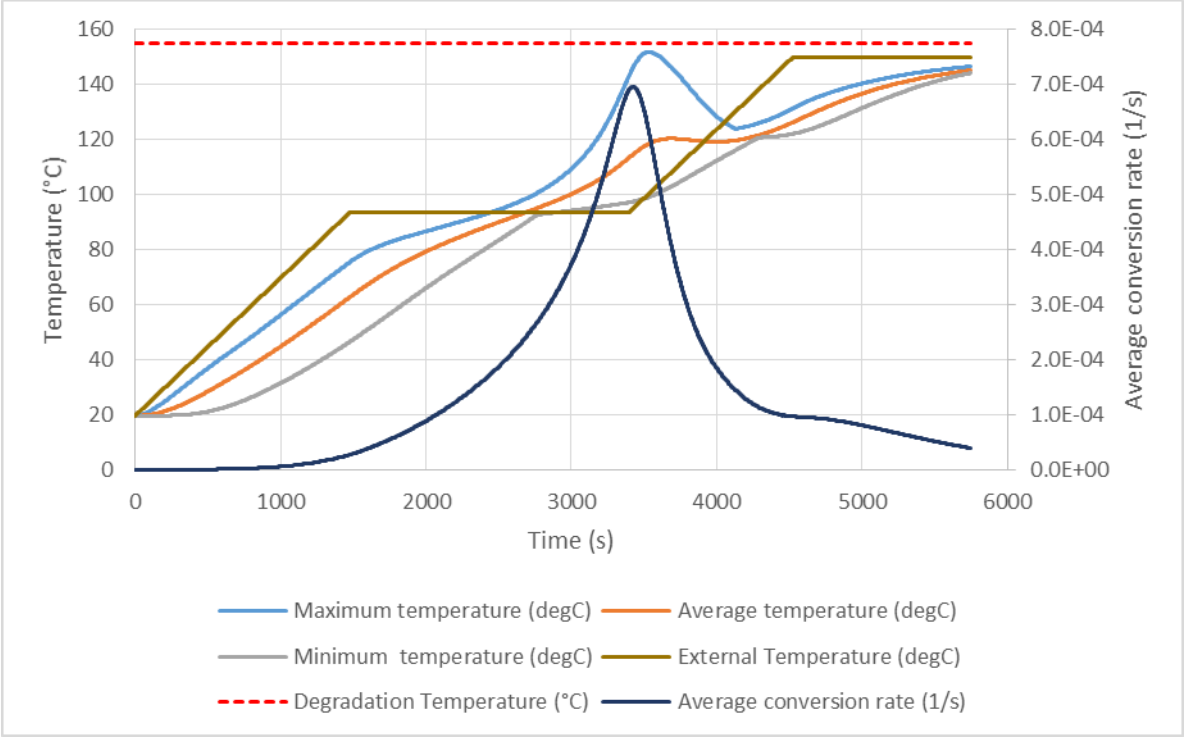

Source: The author (2022)

Investigating in more detail the cure times and gradients exhibited by the sample with the different cure schedules obtained by the CRD strategy, the following phenomena were observed:

a) The higher the **CT2**, the shorter the **time in CT2** and the **cure time** to reach a given degree of cure (Figures 39 and 42);

b) The higher the **CT1**, the shorter the **time in CT1** and the **cure time** to reach a given degree of cure (Figures 39 and 42);

c) The minimum values for the **maximum gradient of degree of cure AGP** and the **maximum gradient of temperature AGP** occur when **CT1** is around **84** and **85 °C**, respectively (Figures 40, 41, 43 and 44);

d) Low **CT2** has no benefits (for the variables studied). The higher the **CT2** the better, as long as the maximum temperature reached by the sample is below the material degradation temperature. That is, the higher the **CT2**, the shorter the **cure time**, while the **maximum gradient of degree of cure AGP** and the **maximum gradient of temperature AGP** remain the same (Figures 40, 41, 43 and 44).

Figure 39 – Variation of cure time with CT2 in the CRD strategy, for constant CT1

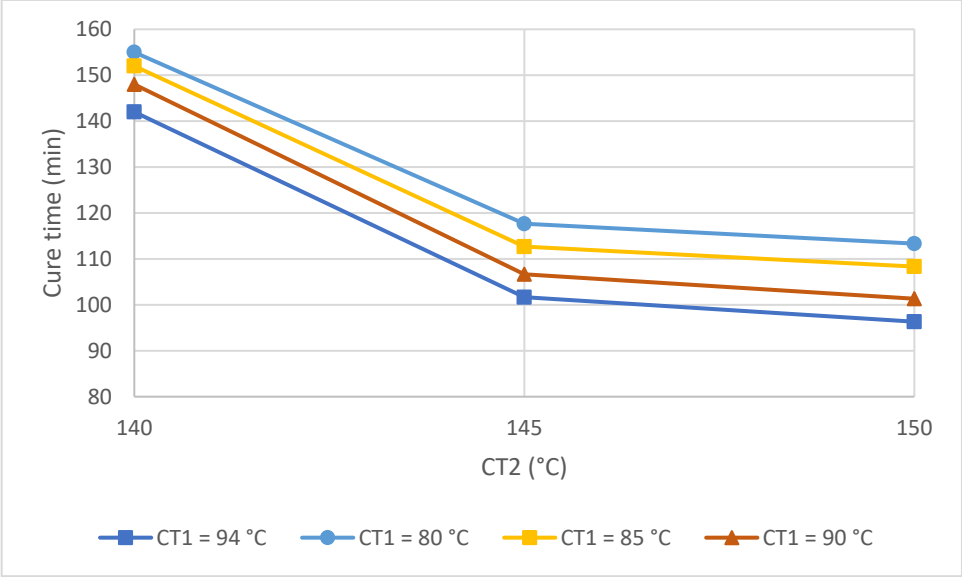

Source: The author (2022)

Figure 40 – Variation of the maximum gradient of degree of cure AGP with CT2 in the CRD strategy, for constant CT1

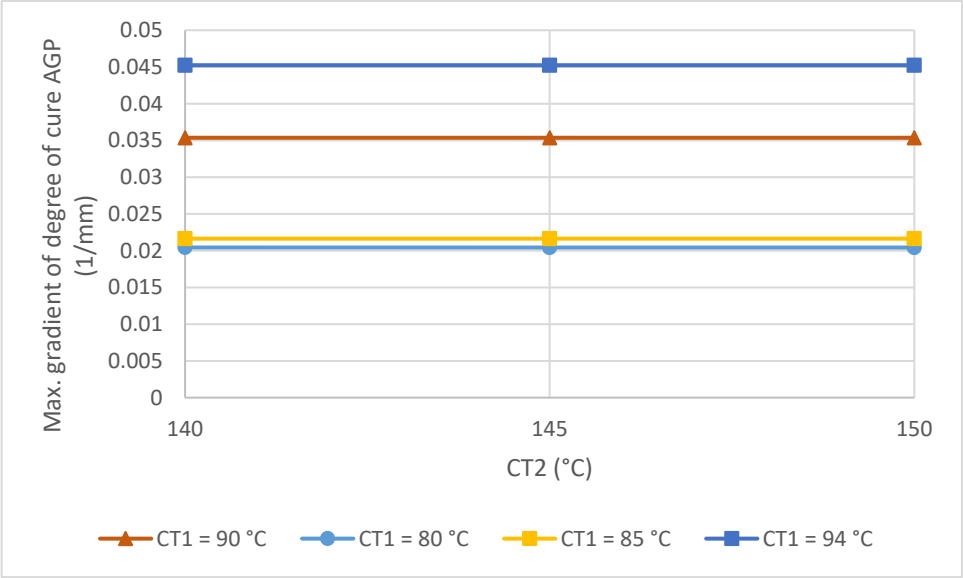

Source: The author (2022)

Figure 41 - Variation of the maximum gradient of temperature AGP with CT2 in the CRD strategy, for constant CT1

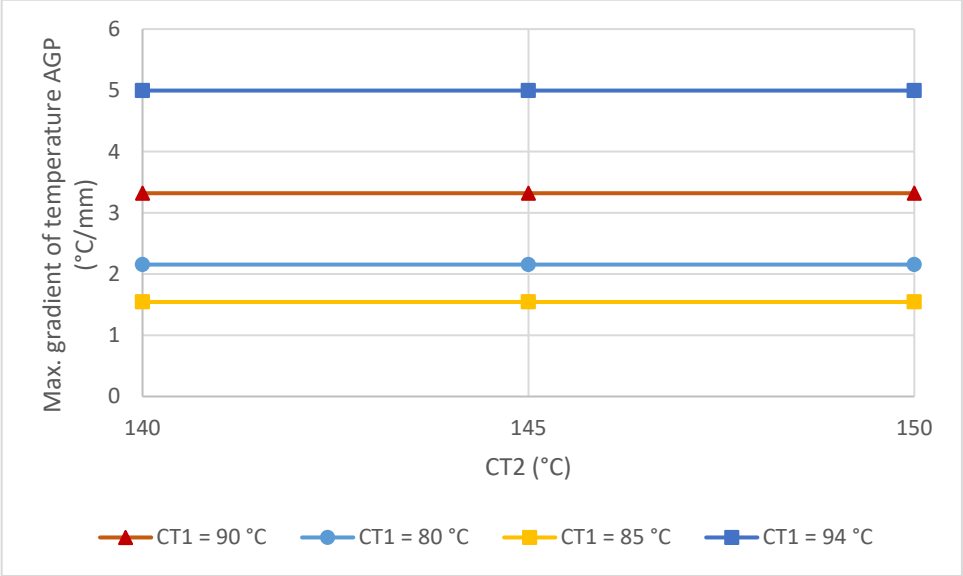

Source: The author (2022)

Figure 42 - Variation of cure time with CT1 in the CRD strategy, for constant CT2

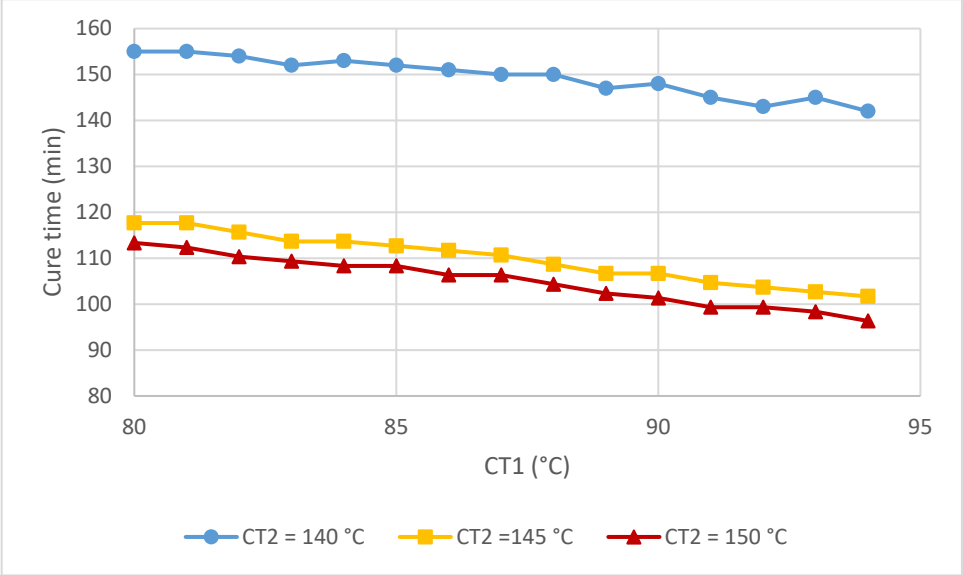

Source: The author (2022)

Figure 43 - Variation of the maximum gradient of degree of cure AGP with CT1 in the CRD strategy, for constant CT2

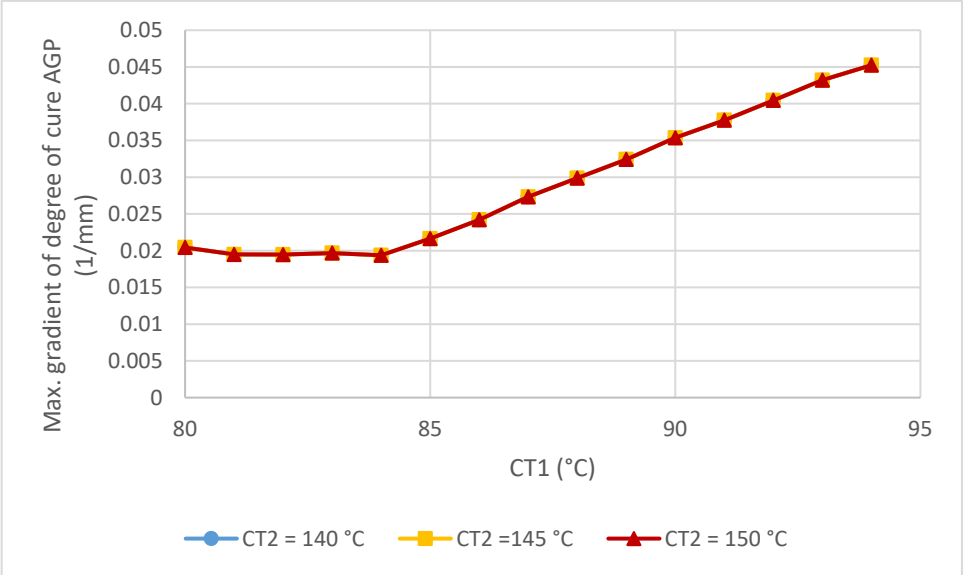

Source: The author (2022)

Figure 44 - Variation of the maximum gradient of temperature AGP with CT1 in the CRD strategy, for constant CT2

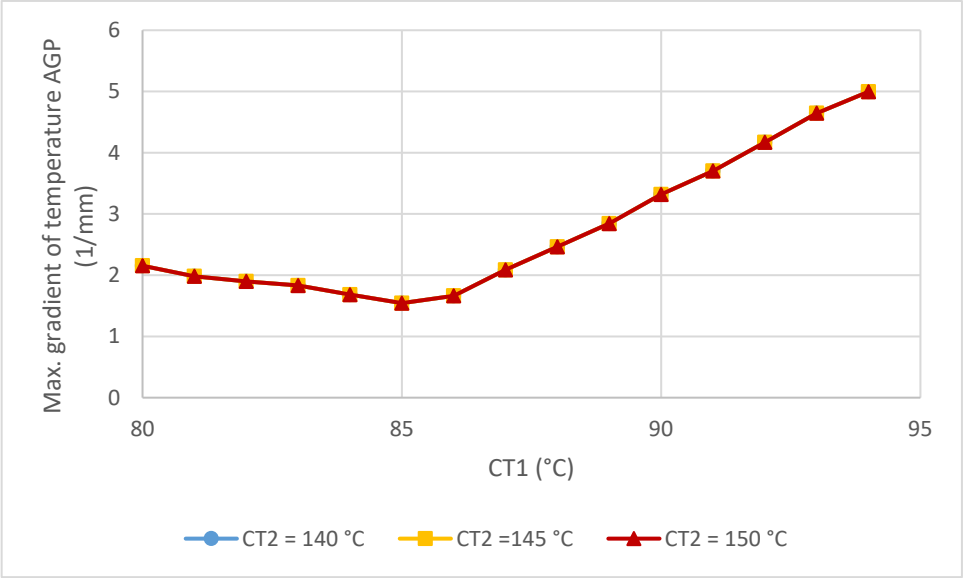

Source: The author (2022)

Evidently, the CRD strategy proved to be a very effective strategy for reducing the curing time of a thick epoxy matrix. The development of a code in MATAB linked to the finite element software COMSOL allowed the automatic execution of the simulation of several different cure schedules and their analysis according to the variables of interest: temperature, degree of cure, conversion rate, cure time and gradients of degree of cure and temperature AGP.

However, although the CRD strategy allows the verification of the maximum values of gradients of degree of cure and temperature reached by the matrix AGP, there is no routine in this algorithm that aims to reduce or minimize such gradients, while minimizing the curing time. For this reason, the Genetic Algorithm was selected as an additional solution to be studied, in order to optimize the curing process of thermoset matrices, as it can be programmed to be multi-objective and find cure schedules that tries to minimize simultaneously the curing time and the gradients of degree of cure and temperature AGP, finding a variety of cure schedules that are optimal for different applications with different requirements for the values of such variables.

4.3 GENETIC ALGORITHM

The execution of the GA for the multi-objective optimization of the cure schedule resulted in 31 different solutions (cure schedule), that is, 31 non-dominated solutions. The numerical values of all GA non-dominated results can be found in the APPENDIX E.

Figures 45, 46 and 47 show the combinations, 2 by 2, of the three optimization objectives. It is clear that Figure 45 and Figure 46 present variables that are in conflict with each other (when one increases, the other decreases). Therefore, the resulting curves correspond to a “front”, called the Pareto-Optimal Front.

Figure 45 - 2D Pareto-Optimal Front: Objective 2 x Objective 1

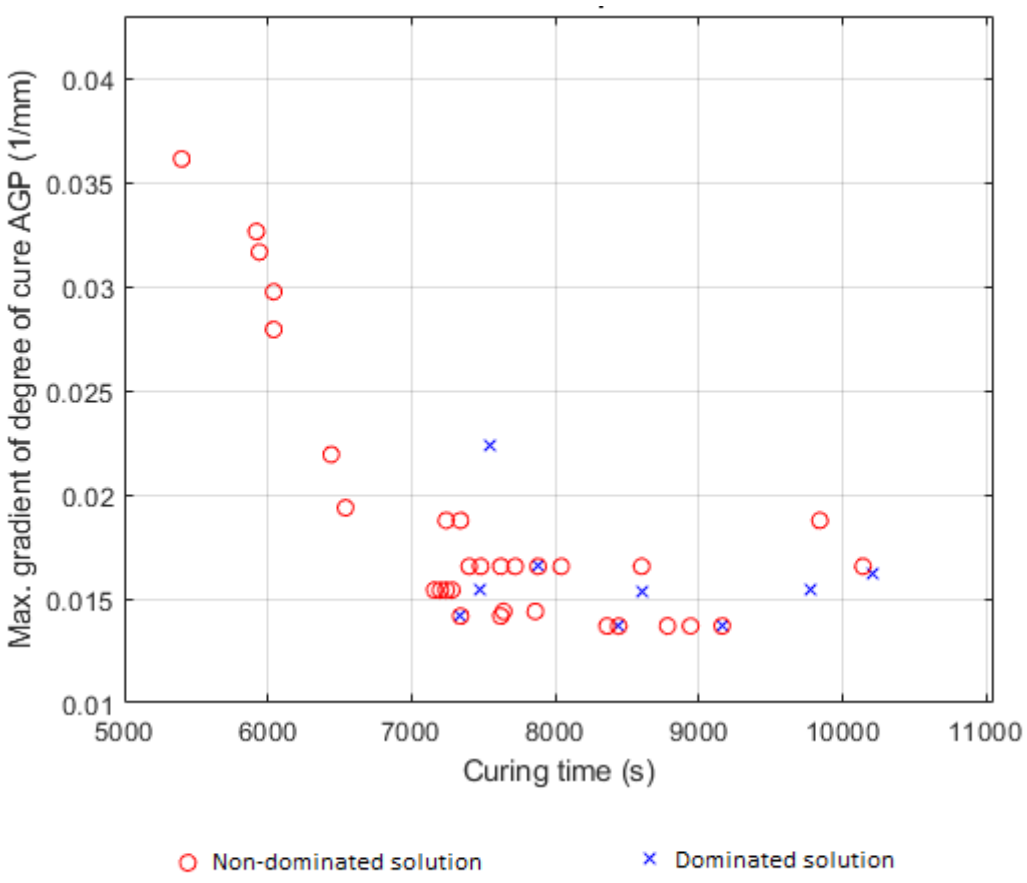

Source: The author (2022)

Figure 46 - 2D Pareto-Optimal Front: Objective 3 x Objective 1

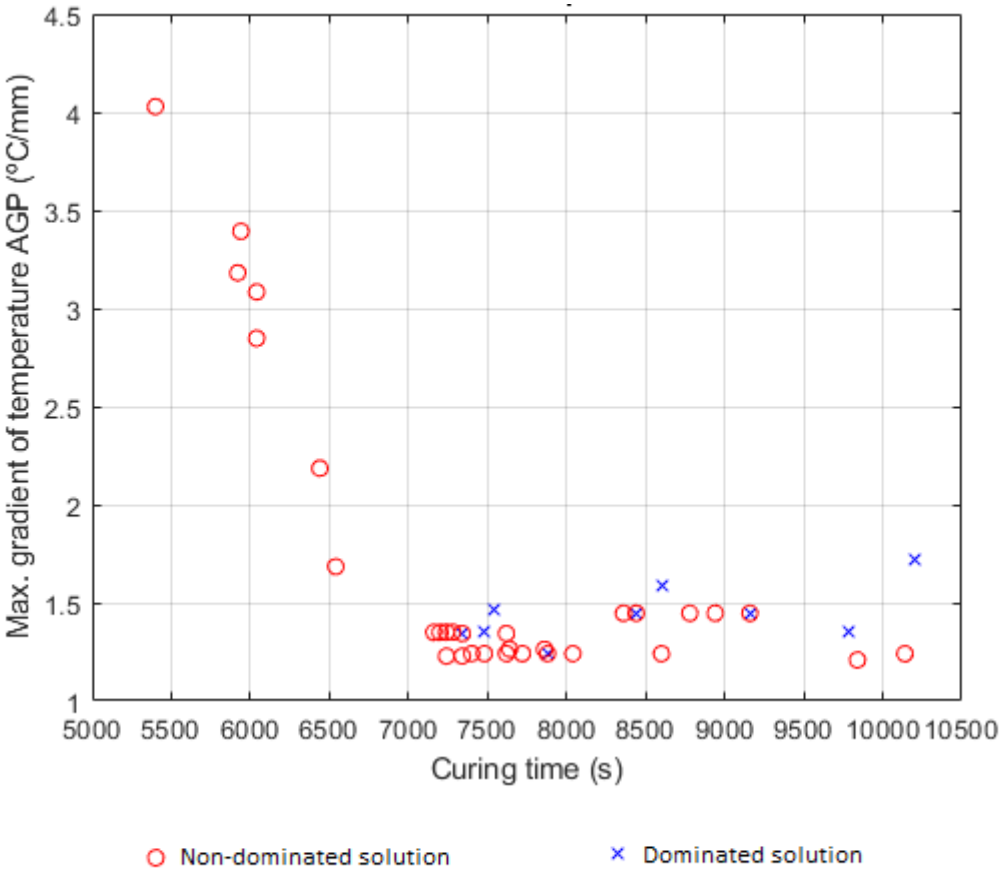

Source: The author (2022)

Figure 47, on the other hand, highlights two objectives that usually agree with each other, the gradients of degree of cure and temperature. This is because the degree of cure gradients are directly affected by the temperature gradients, so they both increase and decrease together.

Figure 47 - 2D Pareto-Optimal Front: Objective 3 x Objective 2

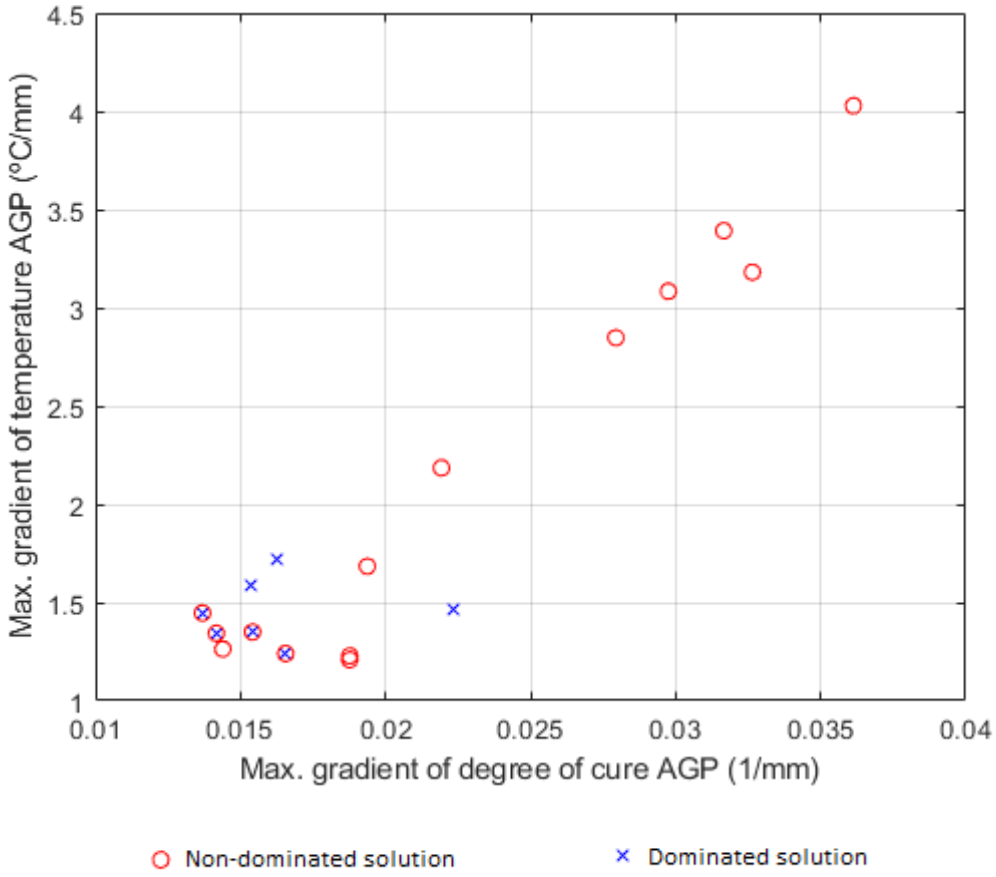

Source: The author (2022)

It was verified that, although the determined number of generations and individuals per generation was not high, the graphs obtained show a diverse set of solutions, which is highly beneficial in this multi-objective optimization, as there is no prior definition of which objective is more important. Thus, one can decide the weights of each objective after the optimization, depending on the application, and still obtain extremely satisfactory results due to the diversity of the solution set.

The solutions obtained for the optimization decision variables (or “genes”), which are the cure parameters CT1, CT2 and the time in CT1, can be seen graphically in Figure 48. Interestingly, the vast majority of solutions have lower values for CT1, close to its selected minimum limit, between 80 and 84°C, even those cure schedules that result in shorter curing times, contrary to the behavior of the CRD strategy, which raised CT1 to 94°C to obtain the shortest curing time, almost reaching the material's thermal degradation temperature. On the other hand, CT2 assumed values that were better distributed within its total range of

possibilities, but showing a greater tendency to be close to the maximum limit, between 145 and 150°C.

Figure 48 - 2D Pareto-Optimal Set: CT1 x time in CT1

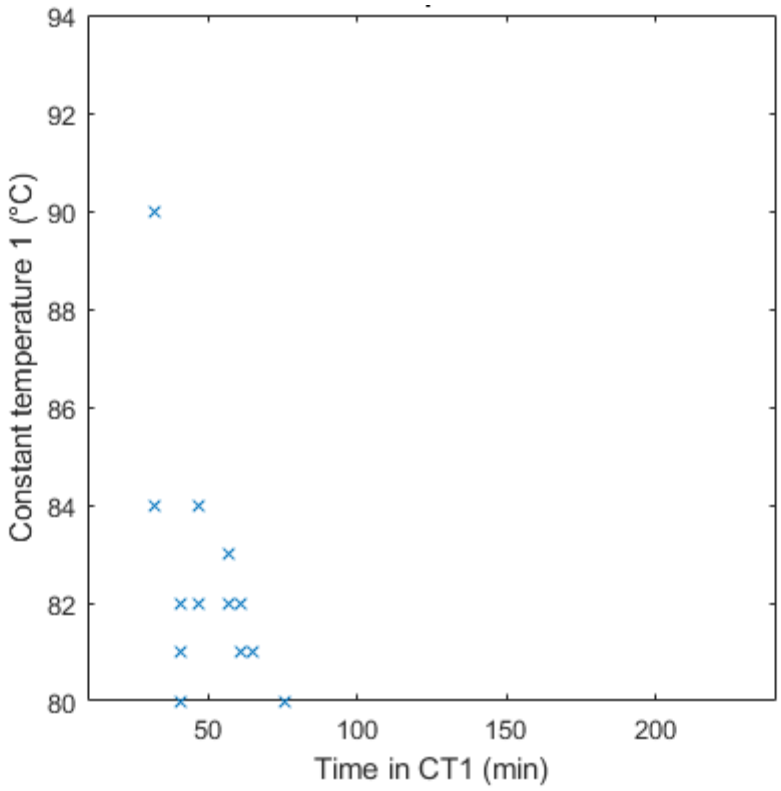

Source: The author (2022)

Figure 49 - 2D Pareto-Optimal Set: CT1 x CT21

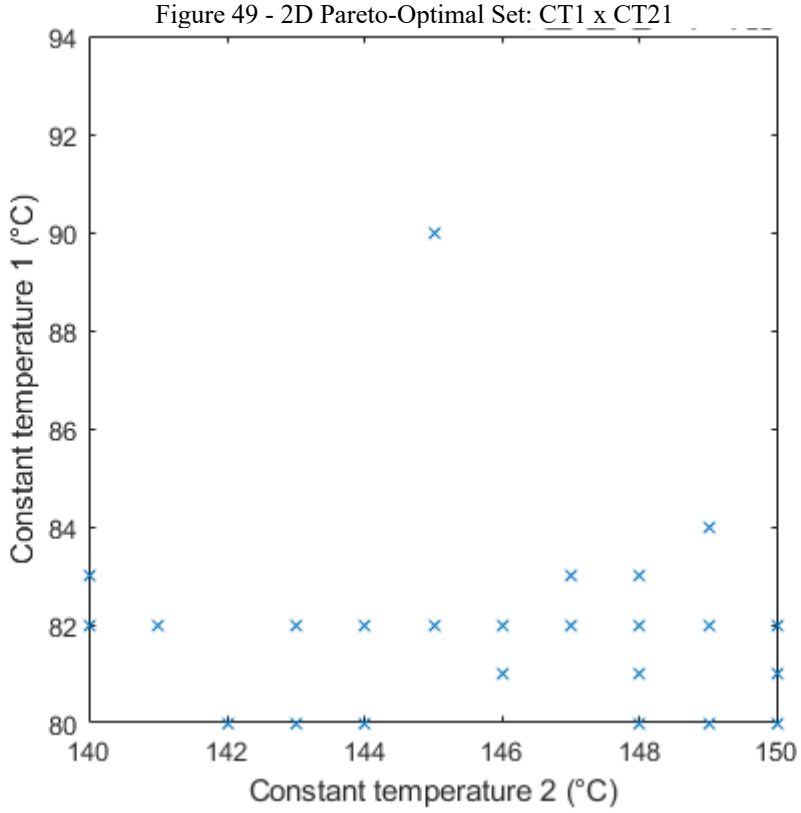

Source: The author (2022)

4.3.1 Objective 1

The best cure schedule provided by the GA optimization to minimize the cure time (objective 1) is presented in Table 14. With this solution, it was possible to reduce the MRC time from 12.7h (760 min) to just 1.5h (90 min), an incredible improvement in the cure time.

Table 14 - Best cure schedule found with the GA optimization to minimize the cure time

Cure schedule				*Constrained variables*		*Optimization objective variables (to minimize)*			
						Objective 1		*Objective 2*	*Objective 3*
CT1 (°C)	**CT2 (°C)**	**Time in CT1 (min)**	**Time in CT2 (min)**	**Min. alpha - end of the cure**	**Max. T during the cure (°C)**	**Cure time (min)**	**Cure time (s)**	**Max. grad. of alpha AGP (1/mm)**	**Max. grad. of T AGP (°C/mm)**
84	149	32	15	85.5%	154	90	5400	3.61E-02	4.03E+00

Source: The author (2022)

For this solution, the curve shapes of the conversion rate, gradients of degree of cure and temperature AGP, shown in Figures 50, 51 and 52, resemble the curve shapes of the best solution obtained by the CRD strategy aiming to minimize the cure time. This was completely expected as both cure schedules have the same goal. The cure time on the first plateau is very short compared to the MRC schedule, and equal to the CT1 time of the fastest MRC solution. So again what happens are virtually unique peaks in the conversion rate and in the gradients of degree of cure and temperature AGP, as these occur on the heating ramp from the first plateau to the second, a few minutes after the gel point has been reached, and there is no time for the conversion rate and maximum gradients AGP to stabilize before curing reaches the second plateau.

The levels reached by these three variables, however, are not as high as those observed in the MRC schedule, since the temperatures selected for both plateaus in the GA algorithm are lower, which is very advantageous to avoid residual stresses and related problems. It is also important to point out that, although the cure is extremely fast, it does not degrade the epoxy matrix (since it does not reach 155°C) and the spatial distribution of the degree of conversion at the end of the cure schedule is practically uniform, with a minimum degree of cure of 85.4°C, as in the case of the MRC schedule.

Figure 50 - Temperatures and maximum gradients of temperature AGP reached by the sample during the cure, following the best cure schedule found with the GA optimization to minimize the cure time

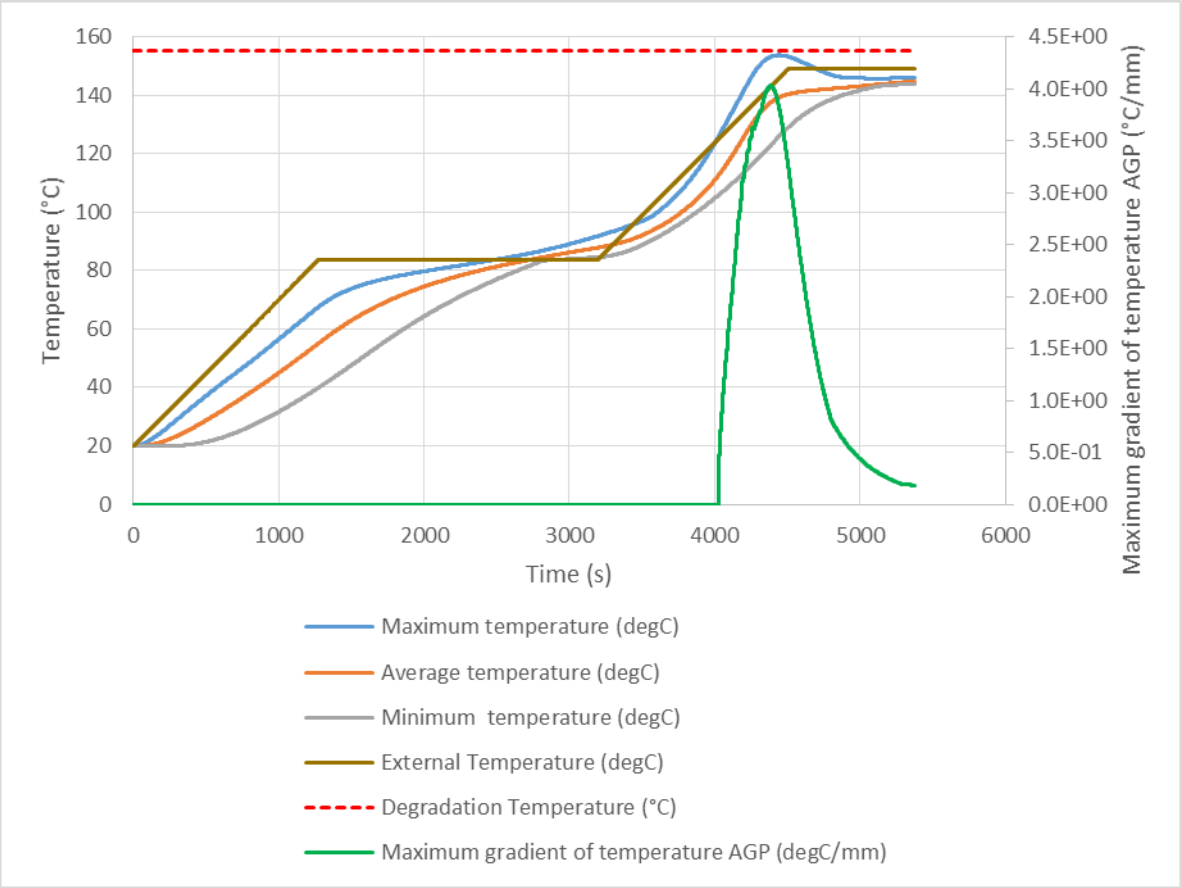

Source: The author (2022)

Figure 51 - Degrees of conversion and maximum gradients of degree of conversion AGP reached by the sample during the cure, following the best cure schedule found with the GA optimization to minimize the cure time

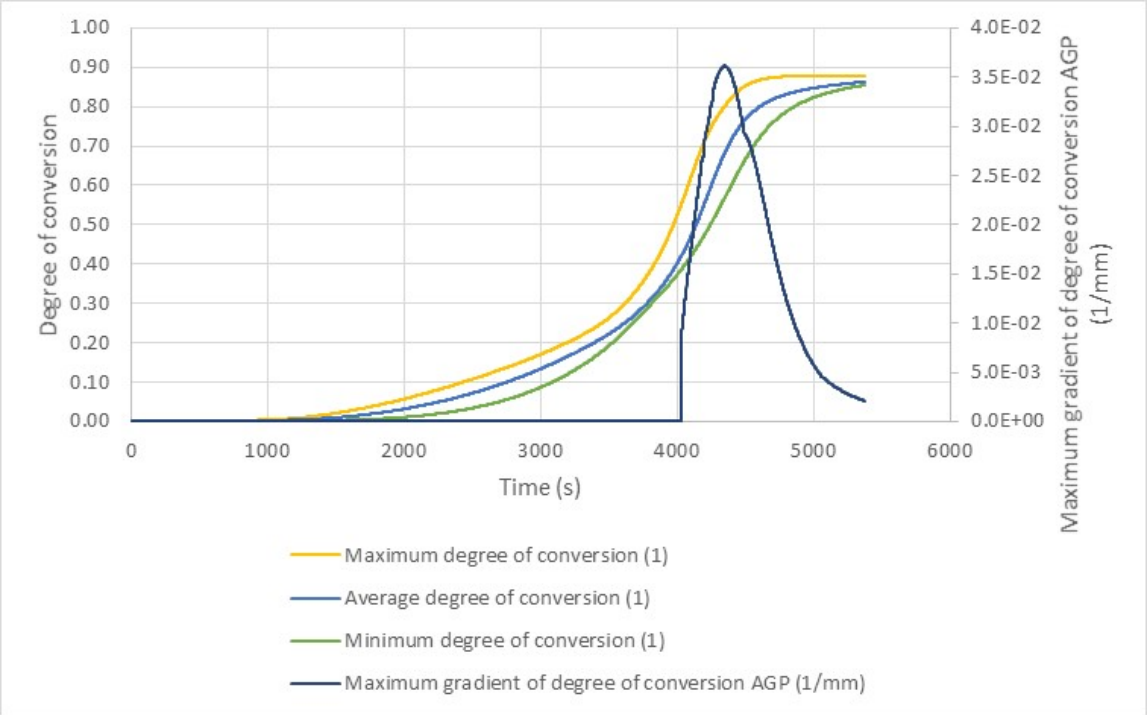

Source: The author (2022)

Figure 52 - Degrees of conversion and average conversion rate reached by the sample during the cure, following the best cure schedule found with the GA optimization to minimize the cure time

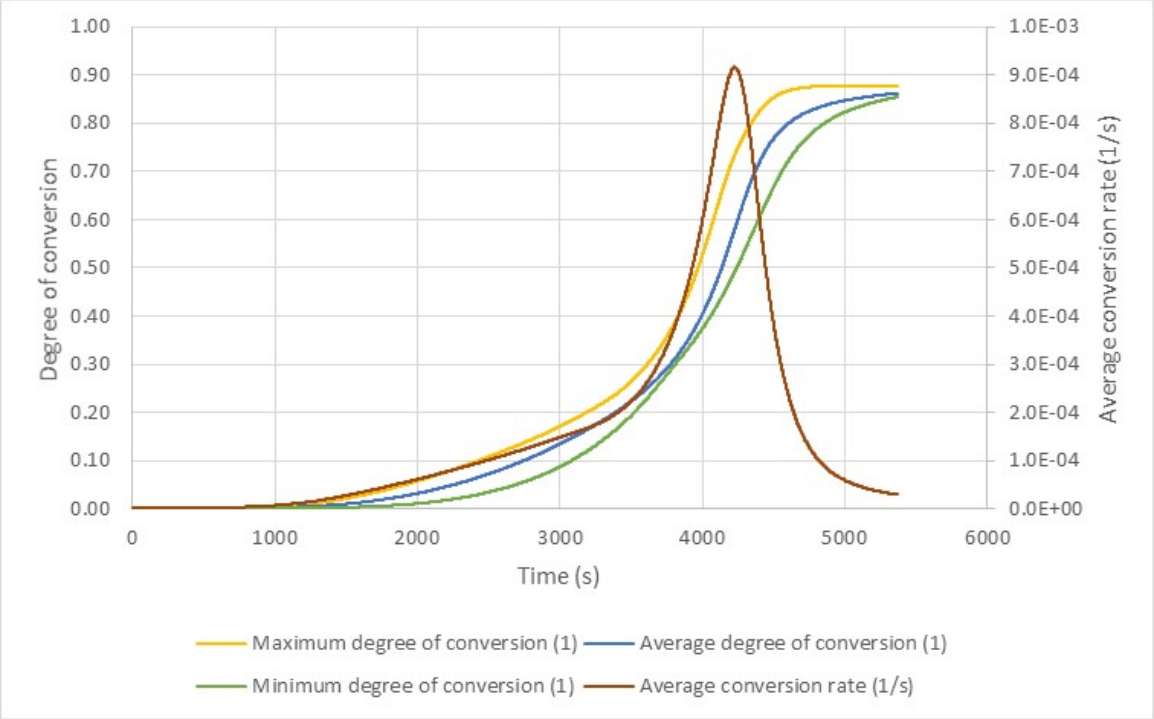

Source: The author (2022)

4.3.2 Objective 2

While reducing the cure time is very important for designing more efficient manufacturing processes, it is also necessary to ensure that the cured product achieves the quality required by its field of application. Minimizing the gradients of degree of cure and temperature developed by the epoxy matrix AGP material is one of the ways to obtain the desired quality. Considering only the minimization of the maximum gradient of degree of cure AGP (objective 2), Table 15 presents the optimal cure schedule found by the GA optimization.

Table 15 - Best cure schedule found with the GA optimization to minimize the maximum degree of cure AGP

Cure schedule				*Constrained variables*		*Optimization objective variables (to minimize)*			
						Objective 1		*Objective 2*	*Objective 3*
CT1 (°C)	**CT2 (°C)**	**Time in CT1 (min)**	**Time in CT2 (min)**	**Min. alpha - end of the cure**	**Max. T during the cure (°C)**	**Cure time (min)**	**Cure time (s)**	**Max. grad. of alpha AGP (1/mm)**	**Max. grad. of T AGP (°C/mm)**
80	150	76	20	85.5%	147	139	8360	1.37E-02	1.45E+00

Source: The author (2022)

For the cure schedule obtained, it can be seen from Figures 53 and 54 that the maximum gradient of degree of cure AGP starts to decrease as the external temperature begins to increase towards the second plateau. Thus, the heat flow supplied to the sample is responsible for increasing the gradient of the AGP cure degree again, generating a new peak, higher than the first one.

It is worth noting that the temperature set for the first plateau is the same as that of the MRC schedule, however, by ending this plateau just after the maximum gradient of degree of cure AGP starts to decrease, the cure can be much faster than that of the MRC, while the maximum value of the gradients of degree of cure reached AGP is approximately equal to the one obtained by the MRC.

Figure 53 - Temperatures and maximum gradients of temperature AGP reached by the sample during the cure, following the best cure schedule found with the GA optimization to minimize the maximum gradient of degree of cure AGP

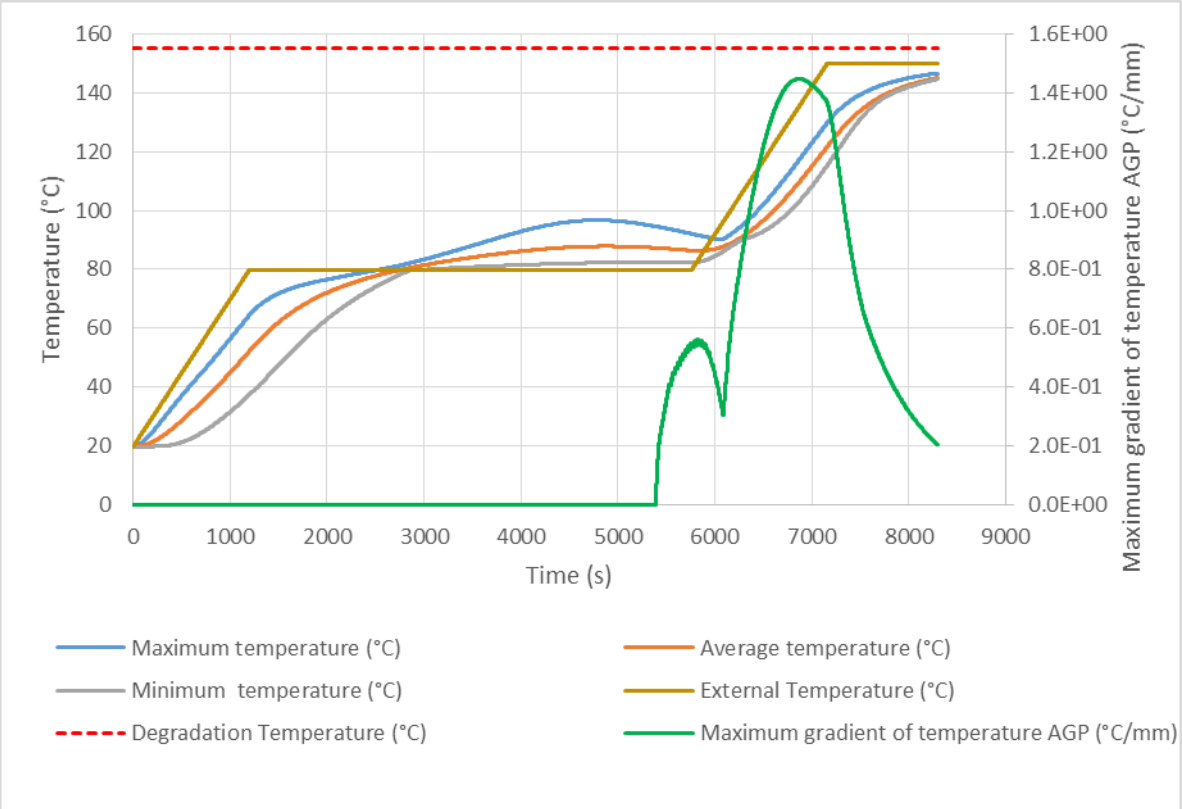

Source: The author (2022)

Figure 54 - Degrees of conversion and maximum gradients of degree of conversion AGP reached by the sample during the cure, following the best cure schedule found with the GA optimization to minimize the maximum gradient of degree of cure AGP

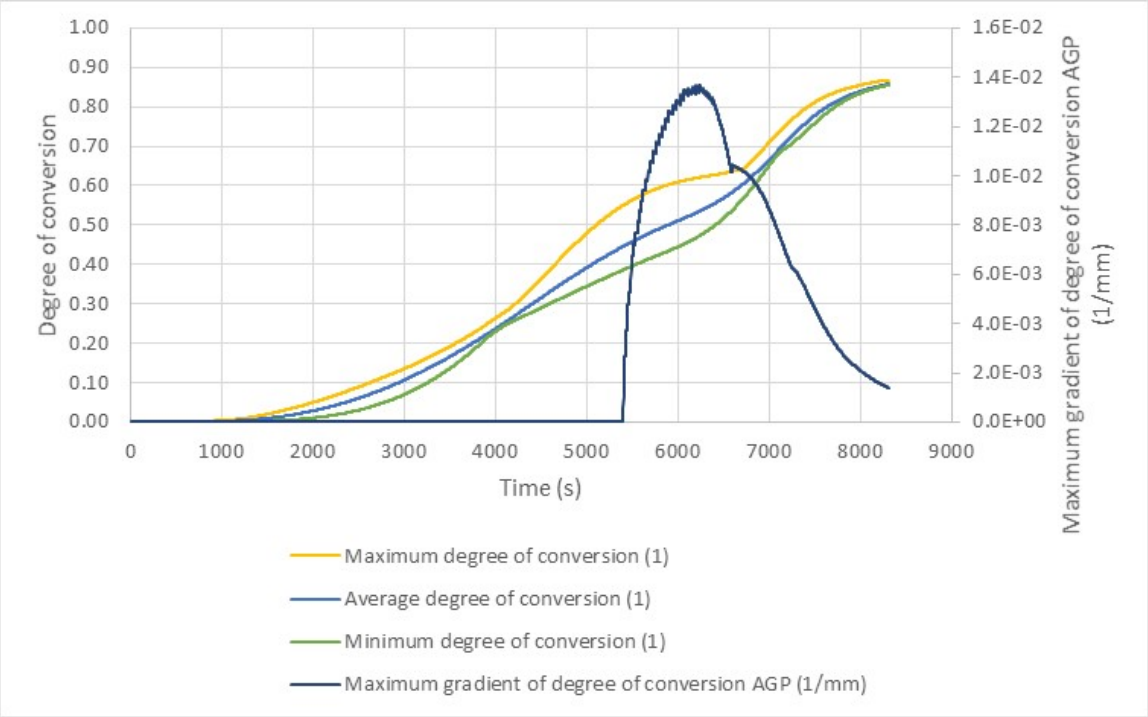

Source: The author (2022)

Figure 55 - Degrees of conversion and average conversion rate reached by the sample during the cure, following the best cure schedule found with the GA optimization to minimize the maximum gradient of degree of cure AGP

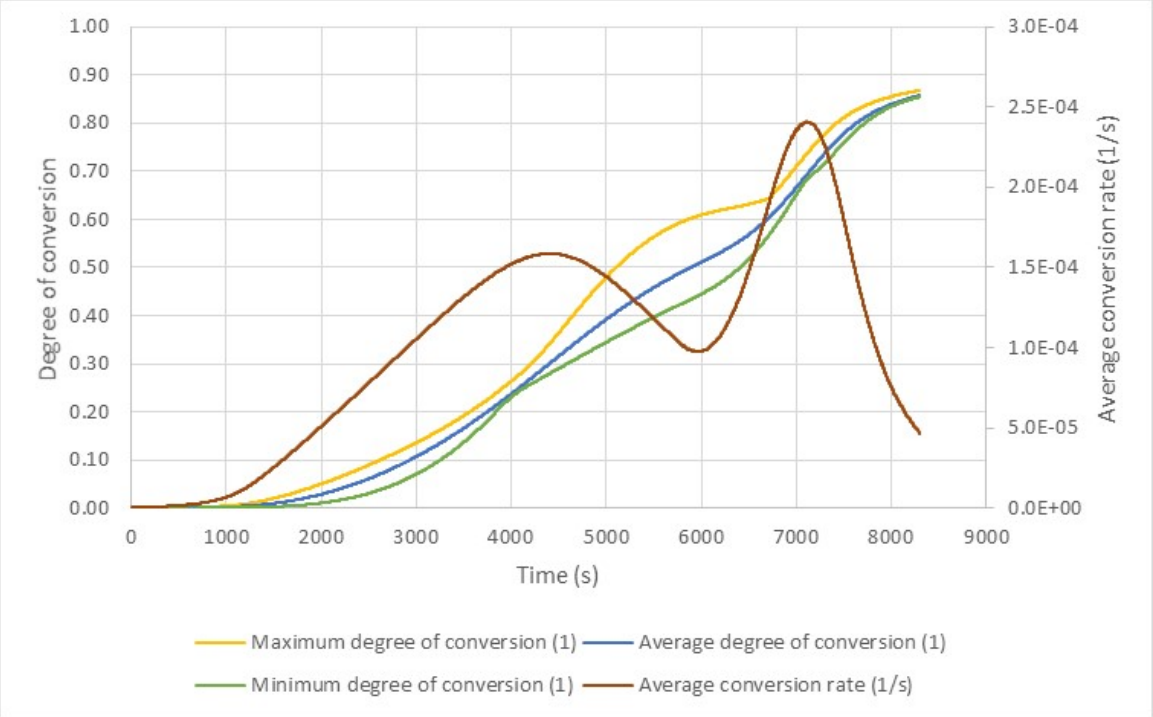

Source: The author (2022)

4.3.3 Objective 3

Considering only the minimization of the maximum gradient of temperature reached by the specimen AGP (objective 3), Table 16 presents the optimal cure schedule determined by the GA optimization.

Table 16 - Best cure schedule found with the GA optimization to minimize the maximum temperature AGP

Cure schedule				*Constrained variables*		*Optimization objective variables (to minimize)*			
						Objective 1		*Objective 2*	*Objective 3*
CT1 (°C)	**CT2 (°C)**	**Time in CT1 (min)**	**Time in CT2 (min)**	**Min. alpha - end of the cure**	**Max. T during the cure (°C)**	**Cure time (min)**	**Cure time (s)**	**Max. grad. of alpha AGP (1/mm)**	**Max. grad. of T AGP (°C/mm)**
83	140	57	67	85.4%	140	164	9840	1.88E-02	1.21E+00

Source: The author (2022)

The behavior of the variables in this optimal cure schedule is similar to that of the cure schedule that minimizes the maximum gradient of degree of cure AGP (objective 2), as presented in Figures 56, 57 and 58. One of the differences from the previous cure schedule is that this phenomenon occurs at the very end of the first plateau at a faster rate, as CT1 was selected with a higher value. Another important difference is that, as the external temperature increases towards the second plateau, the heat supplied by the environment and the heat generated by the exothermic reaction within the thick sample result in temperature gradients that occur in two peaks and lead to a higher (historical) global maximum value for the gradient of temperature AGP when compared to the previous cure schedule. One explanation for this is that the temperature selected for the second plateau is 10 °C lower.

In relation to the MRC schedule, there was also a good reduction in the maximum gradient of degree of cure AGP, from 1.76 to 1.21 °C/mm.

Figure 56 - Temperatures and maximum gradients of temperature AGP reached by the sample during the cure, following the best cure schedule found with the GA optimization to minimize the maximum gradient of temperature AGP

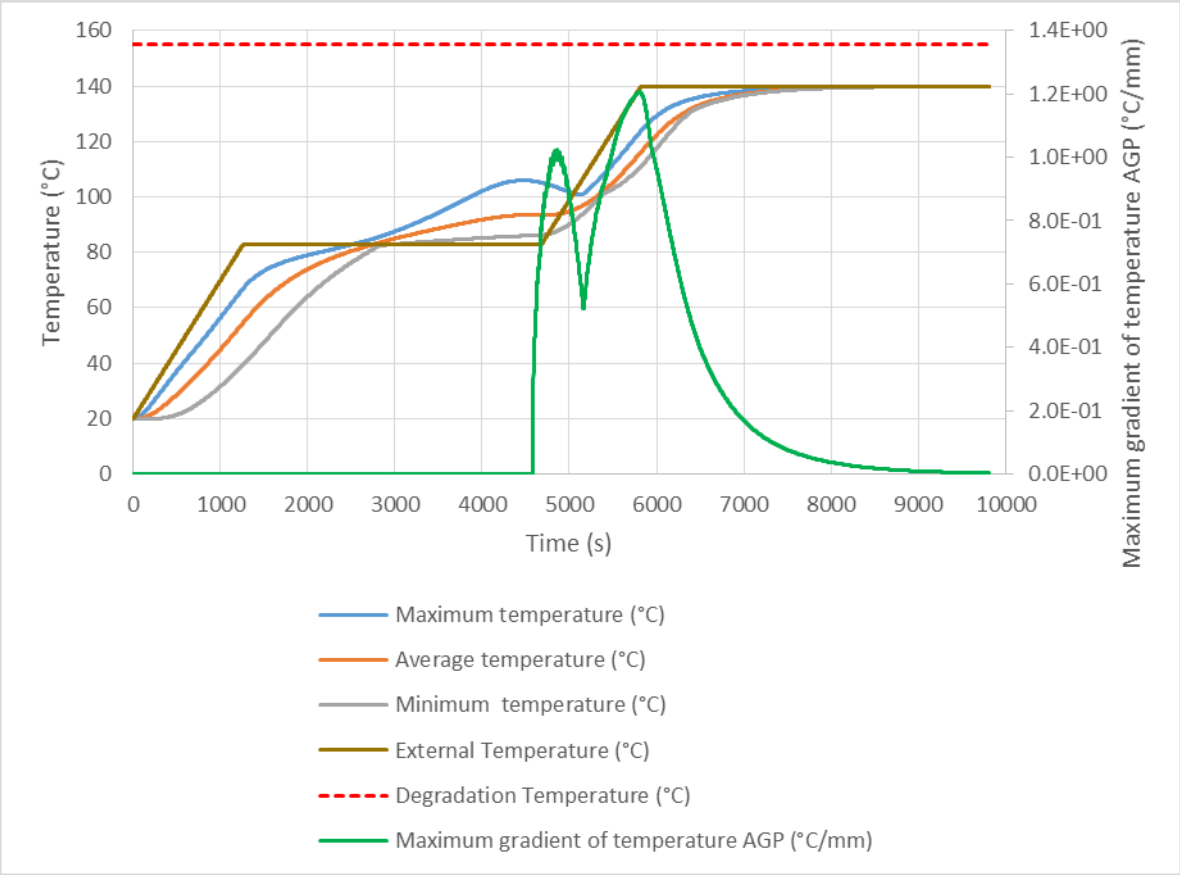

Source: The author (2022)

Figure 57 - Degrees of conversion and maximum gradients of degree of conversion AGP reached by the sample during the cure, following the best cure schedule found with the GA optimization to minimize the maximum gradient of temperature AGP

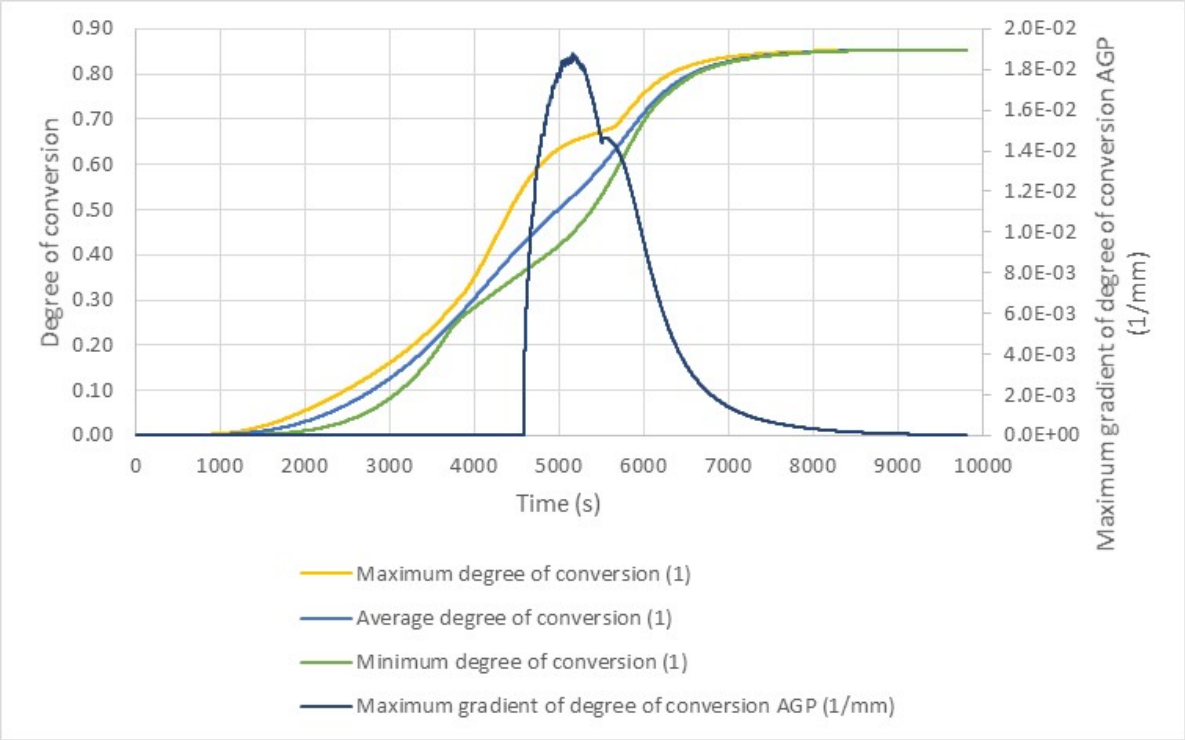

Source: The author (2022)

Figure 58 - Degrees of conversion and average conversion rate reached by the sample during the cure, following the best cure schedule found with the GA optimization to minimize the maximum gradient of temperature AGP

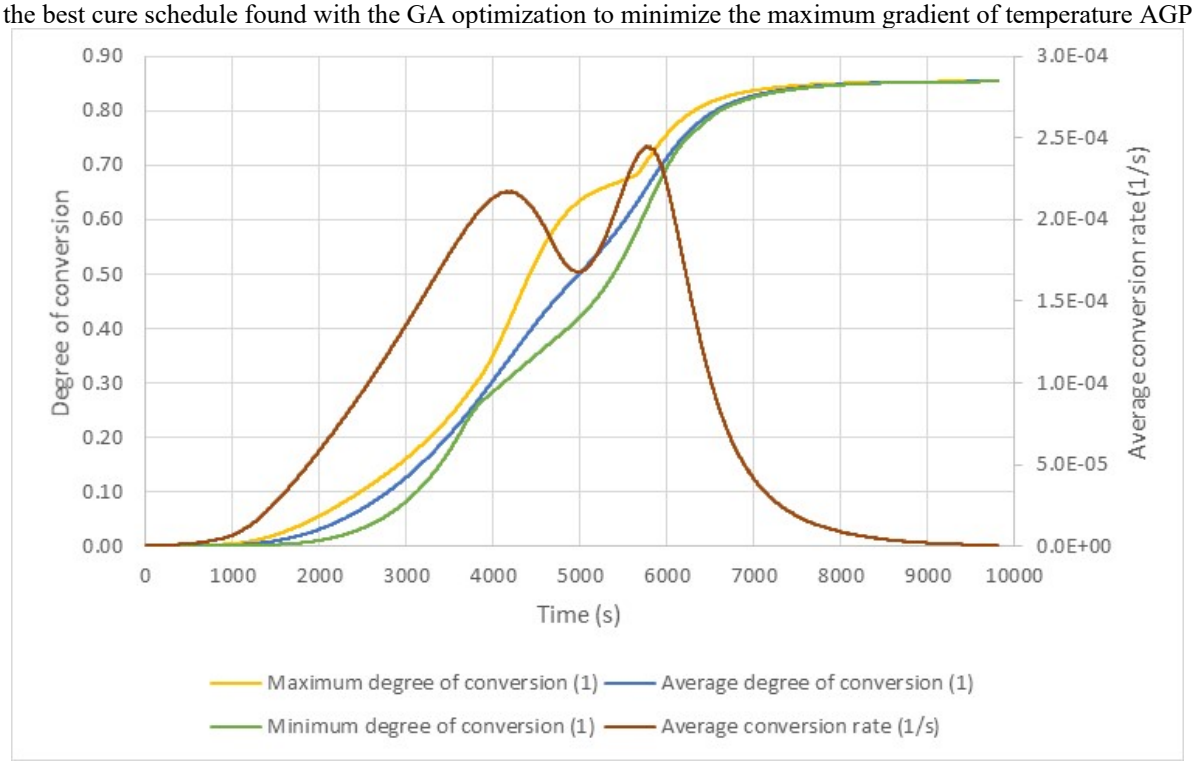

Source: The author (2022)

4.3.4 Weighted objectives

So far, the optimal solutions provided by GA optimization that minimize each objective separately have been presented. However, in real life applications, it is necessary to take into account the tradeoff that exists between the different objectives and the weight that each of them has in a specific application of the thermoset polymer.

It is of utmost importance that the selected temperature profile satisfies a number of criteria which include the minimum residual stresses, minimum cure cycle time, no thermal degradation and high degree of cure.

The need to have available a set of solutions that optimize the cure schedule considering different objectives for the manufacturing process and are optimal for different cases is the main motivation for the development of multi-objective optimization based on a population of solutions, such as GA.

Therefore, we will illustrate the selection of one of the non-dominant solutions provided by GA taking into consideration the requirements of a fictitious application. For the sake of comparison, in the selection of the solution, more emphasis will be put on the reduction of the gradients of degree of cure and temperature, in the same way done by YUAN et al. (2021). Thus, the weights of each objective are defined as follows:

- Objective 1 (cure time): Weight 0.2;
- Objective 2 (maximum gradient of degree of cure AGP): Weight 0.4;
- Objective 3 (maximum gradient of temperature AGP): Weight 0.4.

Such weights are then applied to the normalized and opposite values of each objective, to obtain the sum of those results in the fitness value. Normalization of the value of each objective is necessary so that different scales of the objective values do not impact the decision. Besides, the opposite value of each objective is used as we are working with three objectives that must be minimized and what we are calculating by weighing the normalized solutions and summing them is how fit they are for the application. That is, the lower the objective values, the higher the fitness value (f) must be, which is calculated using the expression below:

$$f = \mathbf{W_{obj1}} * (-Value_{obj1}) + \mathbf{W_{obj2}} * (-Value_{obj2}) + \mathbf{W_{obj3}} * (-Value_{obj3})$$

Where $\mathbf{W_{obj1}}$, $\mathbf{W_{obj2\ and}}$ $\mathbf{W_{obj3}}$ are the weights of the objectives 1, 2 and 3, respectively. And $Value_{obj1}$, $Value_{obj2}$, $Value_{obj3}$ are the values obtained for the objectives 1, 2 and 3 variables, respectively.

Then, the best cure schedule obtained by the GA optimization that maximizes the fitness, considering the weights informed above, is presented in Table 17.

Table 17 - Best cure schedule found with the GA optimization that maximizes the solution fitness, applying the weights 0.2, 0.4 and 0.4 for objectives 1, 2 and 3, respectivly

Cure schedule parameters				*Constrained variables*		*Optimization objective variables (to minimize)*			
						Objective 1		*Objective 2*	*Objective 3*
CT1 (°C)	**CT2 (°C)**	**Time in CT1 (min)**	**Time in CT2 (min)**	**Min. alpha - end of the cure**	**Max. T during the cure (°C)**	**Cure time (min)**	**Cure time (s)**	**Max. grad. of alpha AGP (1/mm)**	**Max. grad. of T AGP (°C/mm)**
81	150	65	19	85.5%	147	127	17%	99%	72%

Source: The author (2022)

YUAN et al. (2021) implemented a NSGA-II cure optimization model, which possess optimization objectives, restrictions and decision variables similar to the ones selected for this research work. As previously reported at the state of the art section, the optimal solution found by YUAN et al. (2021) from the Pareto-optimal set, considering the weights informed above, reduced the maximum gradient of degree of cure by 17%, decreased the maximum gradient of temperature by 46%, and cut down the cure time by 31%. When compared to the optimal result of the present work, which provided reductions of 1%, 18% and 83% in the respective objectives, it is easy to see that the optimization performed by YUAN et al. (2021) was much more effective in decreasing the differences of the degree of cure and temperature found within the thermoset component. On the other hand, the present work was much better in improving the cure time. Although these two optimizations have similar parameters, there are still many differences between them, such as the definition of gradients of degree of cure and temperature, the number of decision variables, the thickness of the sample studied, the material composition, the elitist GA parameters, etc. So, one cannot expect that the results from both optimization works be the same.

4.4 COMPARISON BETWEEN THE SOLUTIONS

In order to better evaluate the results obtained for both the CRD strategy and the multi-objective GA optimization, the solutions were presented together in Table 18 and the values found for the objectives were expressed in relative terms to the values obtained by the MRC. For the CRD strategy, the result that minimizes the curing time was indicated, which is the focus of this algorithm. For GA, solutions that minimize individually each of the three objectives (curing time, maximum gradient of degree of cure AGP and maximum gradient of temperature AGP) were listed:

Table 18 – Results of the CRD strategy and GA optimization: values of the objective variables presented in relation to the MRC schedule results

	Cure schedule parameters				*Constrained variables*		*Optimization objective variables (to minimize)*		
							Objective 1	*Objective 2*	*Objective 3*
Solution	**CT1 (°C)**	**CT2 (°C)**	**Time in CT1 (min)**	**Time in CT2 (min)**	**Min. alpha - end of the cure**	**Max. T during the cure (°C)**	**Cure time (%)**	**Max. grad. of alpha AGP (%)**	**Max. grad. of T AGP (%)**
MRC	80	140	240	480	85.4%	140	100%	100%	100%
CRD	94	150	32	21	85.5%	152	13%	312%	284%
GA OBJ. 1	84	149	32	15	85.5%	154	12%	249%	229%
GA OBJ. 2	80	150	76	20	85.5%	147	18%	94%	82%
GA OBJ. 3	83	140	57	67	85.4%	140	22%	129%	69%

Source: The author (2022)

It is clear from Table 18 that both the CRD and GA strategies are extremely effective in reducing the cure time of the studied sample, with incredible reductions of 87 and 88% of the total cure time recommended by the manufacturer, respectively. Without surprise, these high reductions in the cure time ended up more than doubling the values obtained for the gradients of degree of cure and temperature AGP in the GA cure schedule, and approximately tripling these gradients in the CRD solution.

The best solution found through the GA optimization to minimize objective 2, which reduced by 6% the maximum gradient of degree of cure AGP of the MRC schedule, also generated considerable reductions in the values of the two other objectives obtained by the MRC. Therefore, this cure schedule can be regarded as the best alternative solution to the MRC schedule among the four presented in Table 18, if the purpose is to improve the manufacturer's results in all objectives.

As for objective 3, a great reduction of 31% of the maximum gradient of temperature of AGP was obtained by the GA, however increasing in 29% the maximum gradient of degree of cure AGP, in relation to the MRC.

The evolution of the maximum gradients of degree of conversion and temperature AGP reached by the sample during the cure for the five cure schedules shown in Table 18 were presented in a superimposed way in the plots of Figures 59 and 60. This type of plots allow an easier comparison of the solutions found for the 3 objectives and a better understanding of the curing phenomena that has been discussed so far. The horizontal axis of the graphs of both figures ends at 25,000 s, because from this moment on, only the manufacturer's cure schedule continues to run, but with all the variables stabilized (they no longer suffer any noticeable variation during the cure, which ends in 45,600 s). Therefore, plotting the final part of the MRC would not bring any additional information.

Figure 59 - Cure time and maximum gradient of temperature AGP of the MRC schedule and the best solutions given by the CRD strategy and GA optimization

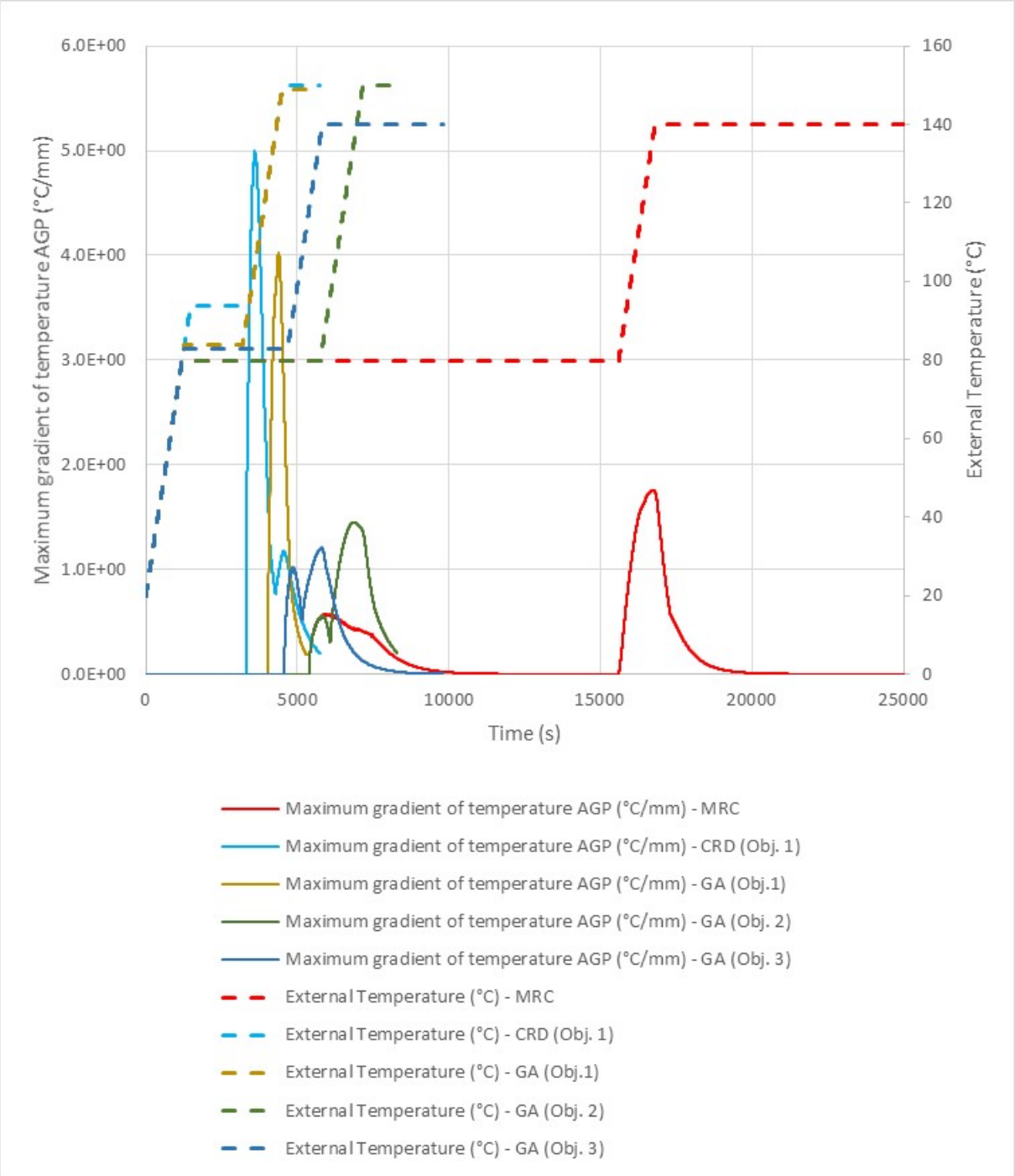

Source: The author (2022)

Figure 60 - Cure time and maximum gradient of degree of cure AGP of the MRC schedule and the best solutions given by the CRD strategy and GA optimization

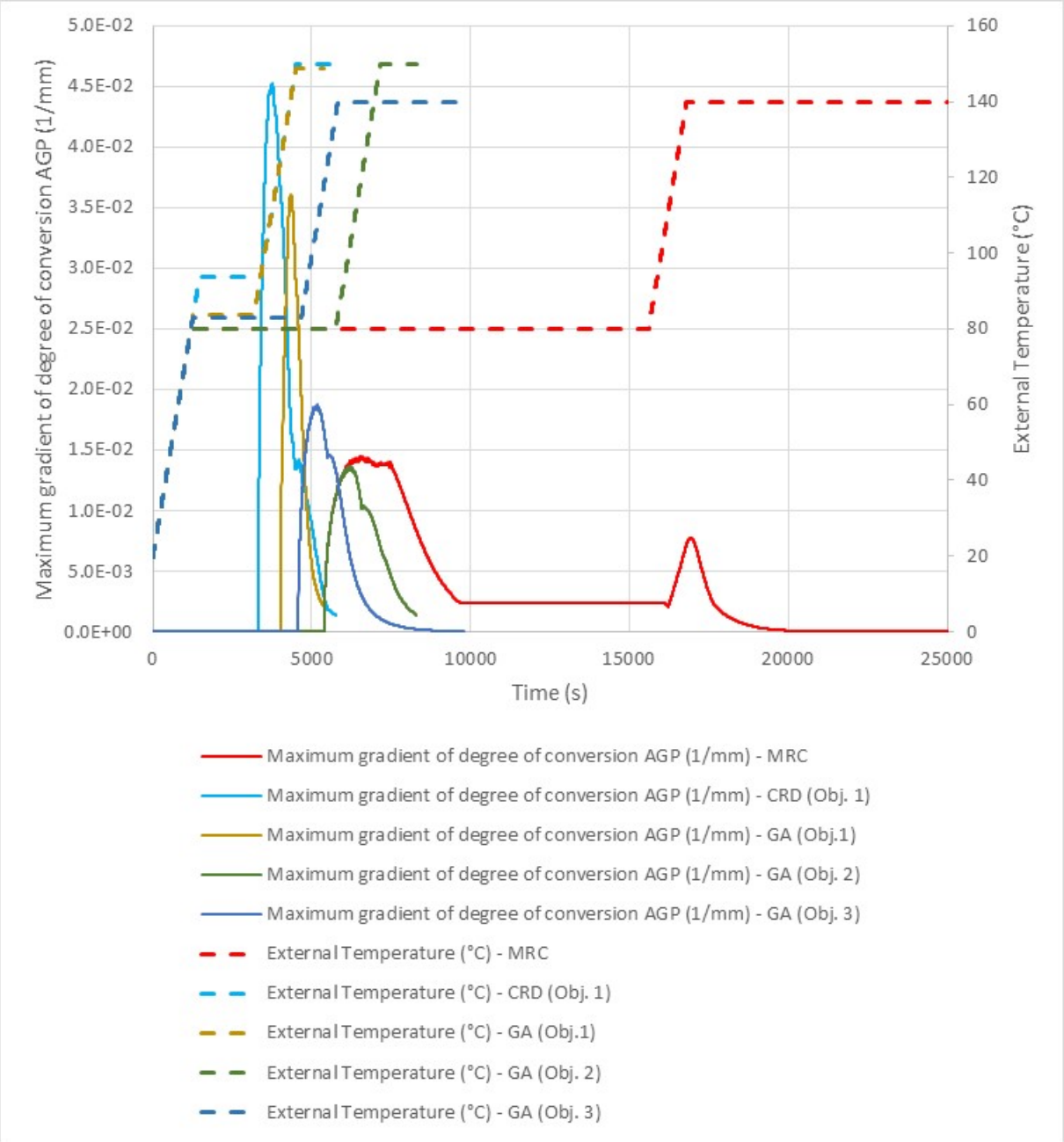

Source: The author (2022)

Analyzing all the feasibles solutions obtained by the CRD strategy and the non-dominant solutions found by the GA, which add up to the 76 cure schedules that are tabulated in APPENDIX E and plotted in Figures 61, 62 and 63, the following observations were made:

- **For objective 1** (minimize cure time): All the 76 cure schedules obtained by both methods are better than the MRC schedule. The best solution was provided

by GA. A very interesting aspect of the optimal result obtained by GA for objective 1 is that it shows that it is possible to obtain faster cures than the CRD, using lower temperature plateaus with shorter durations, and ensuring that the sample will have the required minimum degree of cure without being thermally degraded.

- **For objective 2** (minimize the maximum gradient of degree of cure AGP): GA resulted in 9 cure schedules that are better than the one recommended by the manufacturer. CRD strategy could not improve the MRC schedule results for this objective.
- **For objective 3** (minimize the maximum gradient of temperature AGP): The best solution was provided by GA. CRD strategy provided 9 cure schedules schedules that are better than the MRC schedule, while GA provided an even higher number of better solutions: 25 cure schedules.

Figure 61 – Maxixum gradient of degree of cure AGP vs. cure time for the CRD strategy feasible solutions and GA non-dominated solutions

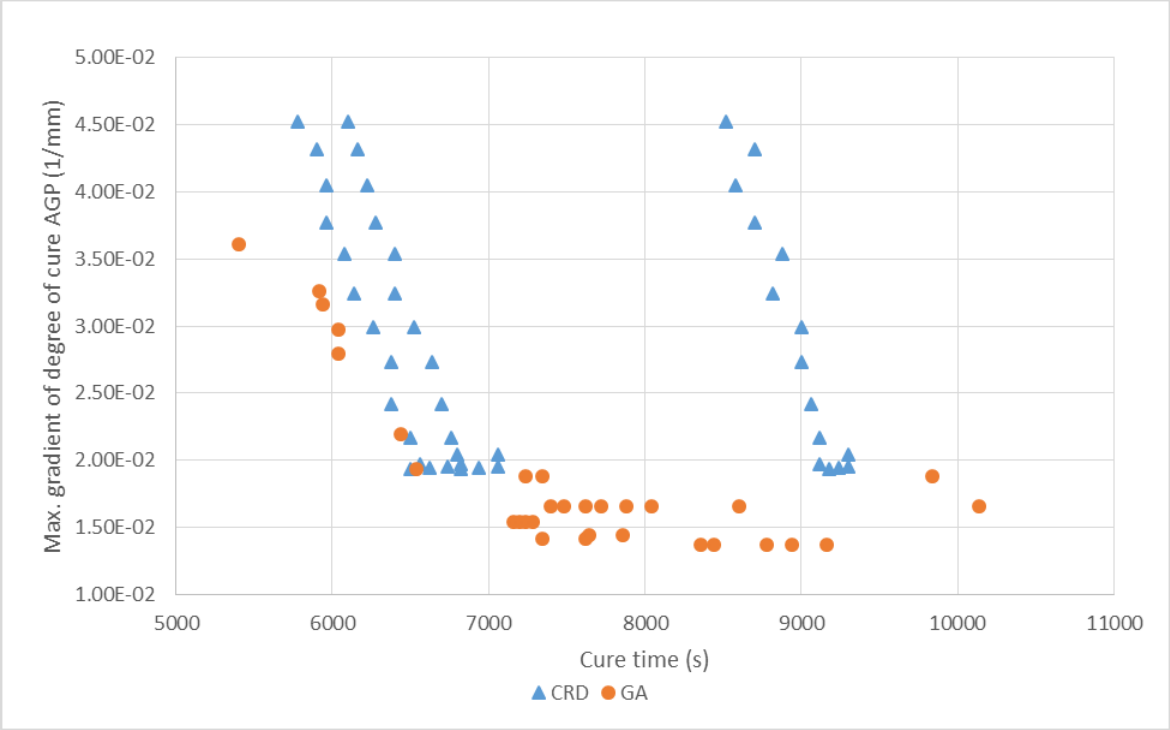

Source: The author (2022)

Figure 62 - Maxixum gradient of temperature AGP vs. cure time for the CRD strategy feasible solutions and GA non-dominated solutions

Source: The author (2022)

Figure 63 - Maxixum gradient of degree of cure AGP vs. maxixum gradient of temperature AGP for the CRD strategy feasible solutions, GA non-dominated solutions, and MRC schedule

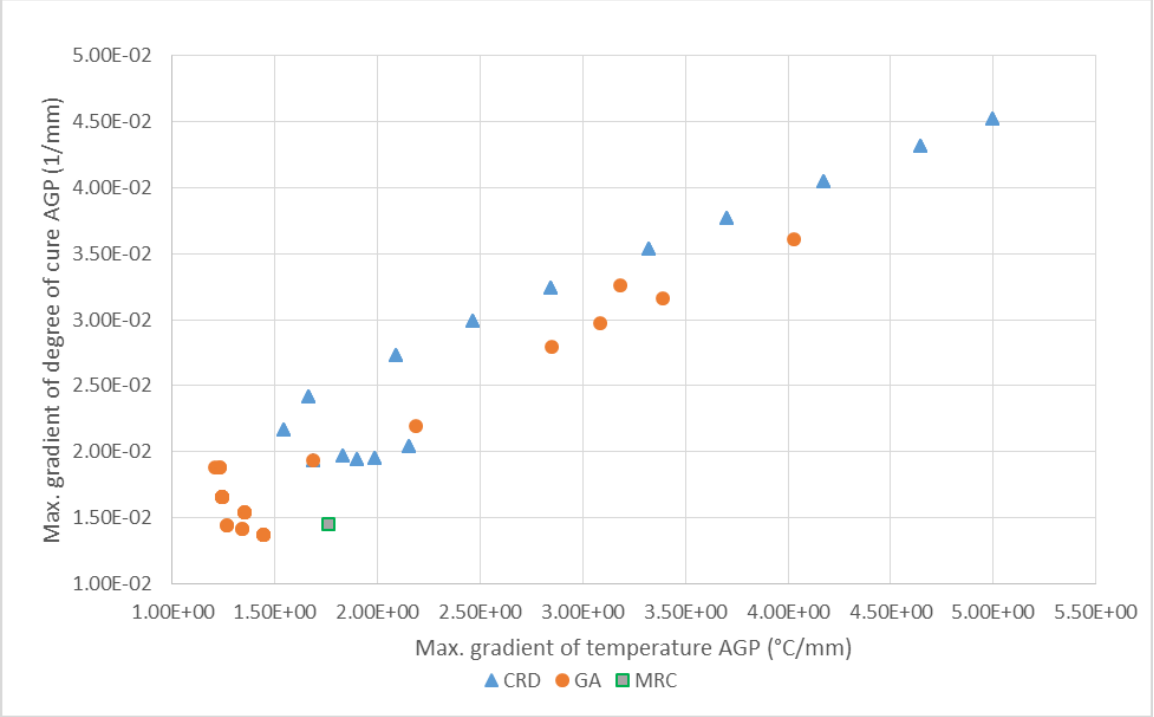

Source: The author (2022)

With the configuration selected in this work for the GA, the computational time to run the algorithm was around 103 hours = 4.3 days. While to run the CRD strategy using the same computer, the running time was around 9 hours. These results show that the CRD approach has the benefit to be based on a simple aspect of the thermoset cure kinetics, providing fast results. On the other hand, the multi-objective GA has the advantage of considering the real world trade-off between manufacturing speed and product quality, being capable of finding cure schedules that reduce internal gradients that arise during the cure process (and thus, reduce the residual stresses), in addition to reducing the cure time.

5 CONCLUSIONS

The present work successfully simulated and optimized the cure schedule of a thick thermoset, through two different methods: an authorial method based on the cure kinetics, called Conversion Rate Driven (CRD) strategy; and a multi-objective Genetic Algorithm (GA). Both methods were implemented in MATLAB and commanded the cure simulation models running in COMSOL through the COMSOL LiveLink for MATLAB.

A manufacturer's recommended cure (MRC) schedule was also simulated and it was verified that it is highly ineffective for the materials, geometries and boundary conditions studied, as the cure time was extremely overestimated, which in real world would lead to high manufacturing costs. This confirmed the need for the cure optimization and served as the basis for the analysis of the CRD strategy and GA optimization results.

An easy implementation of the multi-objective GA was possible due to use of the free MATLAB-based software package GOSET, which delivered a diverse Pareto-Optimal front, with 31 non-dominated solutions (cure schedules) that could meet the needs of different composite manufacturing applications, considering the trade-off between three different objectives: minimize the cure time, minimize the gradient of degree of cure AGP and minimize the gradient of temperature AGP. The automation of the CRD strategy through the development of a script in MATLAB allowed finding many feasible cure schedules, 45 in total, in a single algorithm run. As this strategy was developed with a single objective (minimize the cure time), a single solution was selected from the as the optimal one.

Both CRD and GA approaches were extremely effective in minimizing the cure time of a thick thermoset matrix. They are both excellent tools if the most important goal in an application is to increase the speed of the thermoset fabrication process, while assuring that the minimum degree of cure required for the resulting polymer is reached and that thermal degradation does not occur. It is important to highlight that each of the methods, CRD and GA, has its advantages and disadvantages in relation to the other.

As advantages of the multi-objective GA in this work, we have that:

- The algorithm seeks to find solutions that minimize all objectives at the same time. Thus, the optimal solution found by the multi-objective GA to minimize the curing time also resulted in values for the other two objectives that are better than those obtained by the CRD strategy, since this strategy only focuses on the

curing time. Besides, this algorithm managed to improve all 3 objective variables over the MRC.

- In addition to presenting the minimum curing time, the shortest cure schedule found by the GA also has lower temperatures for both plateaus, when compared to the CRD solution, which facilitates the manufacturing process.

On the other hand, the main advantage of the CRD strategy is that it is based on the kinetics of the curing process and takes less time to run than the GA, which needs to simulate hundreds of cures or more to obtain reliable solutions. With the parameters selected for the algorithms in this work, The CRD approach took around 91% less time than the GA to run, using the same computer.

Although GA requires high computational resources to run in a feasible time, it gives highly satisfactory results. The literature has been reporting that its performance can be largely improved when it is combined with other optimization or heuristic techniques. Therefore, this algorithm hybridization is left here as a future work suggestion.

6 FUTURE WORKS SUGGESTIONS

From the present work, many research paths can be followed in order to advance in the study of thermosets and composites cure optimization. Some of them are suggested below:

- Reproduce experimentally the best cure schedules obtained by the CRD strategy and multi-objective GA optimization and check the integrity and mechanical behavior of the cured samples.
- Perform the cure optimization of the whole thermoset resin composite, considering the interactions between the polymer matrix and the reinforcements, since possible failures may occur due to thermal mismatches between the matrix and reinforcements, fiber undulations, delaminations, etc.
- Study cure schedules with a higher number of temperature plateaus (three or four, for example) and see the impact on the optimization objectives: cure time and internal gradients AGP.
- Initialize the multi-objective GA optimization with solutions provided by the CRD strategy, instead of initializing it randomly, seeking to improve the optimization performance.
- Hybrid Optimization: combine the multi-objective GA optimization with a local search method to increase its performance.
- Run the GA optimization or the hybrid optimization with a higher number of generations and individuals per generation, using a cluster (parallel computing) to achieve good results in shorter times.
- Implement a multiphysics cure simulation model that takes into consideration the coupling between the thermal, chemical and mechanical aspects of the curing, in order to directly compute the residual stress generated by the internal gradients that appear during the cure process and assess how they affect the final product properties. Then, optimize the cure process taking the maximum residual stresses observed within the sample either as a constrained variable or as an objective to be minimized.
- Study the effect of the cooling stage of the cure schedule on the generations of internal gradients and residual stresses.

- Execute a robust cure optimization, taking into account the variability of the optimization parameters (decision variables).

7 SCIENTIFIC CONTRIBUTIONS

The scientific contributions that were made by the authors of the present work, related to this research, are presented below:

- Presented at the 5th Brazilian Conference on Composite Materials (BCCM5) and published in the Conference Proceedings the work entitled “Exotherm issues predictions during the curing of a thick epoxy matrix and effects on elastic properties”;
- Submitted to the journal Materials Research (on-line ISSN: 1980-5373) the paper entitled “Exotherm issues predictions during the curing of a thick epoxy matrix and effects on elastic properties”;
- Presented at the 14th International Conference on Advanced Computational Engineering and Experimenting (ACEX 2021) the work entitled “A thermal degradation modelling for exothermal effects on the specs of thick epoxies: Experiments vs physico chemical coupled approaches”;
- Presented at the 15th International Conference on Advanced Computational Engineering and Experimenting (ACEX 2022) the work entitled “A novel cure optimization strategy for thick thermosets based on thermal damage risks and curing time optimization: application to mechanical properties”;
- Submitted to the journal Advanced Engineering Materials (online ISSN: 1527-2648) the paper entitled “A thermal degradation modelling for exothermal effects on the elastic modulus of thick epoxies: Experiments vs physico-chemical coupled simulations”.

REFERENCES

ABOUHAMZEH, M. et al. **Closed form expression for residual stresses and warpage during cure of composite laminates**. Composite Structures, v. 133, p. 902-910, 2015.

ADOMANIS, Bryan; BURCKEL, D. Bruce; MARCINIAK, Michael. **COMSOL Multiphysics® Implementation of a Genetic Algorithm Routine for Metasurface Optimization**. Proceedings of the 2017 COMSOL Conference in Boston. 2017.

ADVANI, Suresh G.; HSIAO, Kuang-Ting. **Manufacturing techniques for polymer matrix composites (PMCs)**. Elsevier, 2012.

AGIUS, S. L. et al. **Rapidly cured epoxy/anhydride composites: Effect of residual stress on laminate shear strength**. Composites Part A: Applied Science and Manufacturing, v. 90, p. 125-136, 2016.

ALBERT, Carolyne; FERNLUND, Göran. **Spring-in and warpage of angled composite laminates**. Composites Science and Technology, v. 62, n. 14, p. 1895-1912, 2002.

ALEKSENDRIĆ, Dragan; CARLONE, Pierpaolo; ĆIROVIĆ, Velimir. **Optimization of the temperature-time curve for the curing process of thermoset matrix composites**. Applied Composite Materials, v. 23, n. 5, p. 1047-1063, 2016.

AL-SALAMI, Nada MA. **Evolutionary algorithm definition**. American J. of Engineering and Applied Sciences, v. 2, n. 4, p. 789-795, 2009.

ANDERSON, Ted L. **Fracture Mechanics—Fundamentals and Applications**. 3rd edn. CRC. 2005.

ANTONUCCI, Vincenza et al. **Cure-induced residual strain build-up in a thermoset resin**. Composites Part A: Applied Science and Manufacturing, v. 37, n. 4, p. 592-601, 2006.

ARAFATH, Abdul Rahim Ahamed. **Efficient numerical techniques for predicting process-induced stresses and deformations in composite structures**. Ph.D. Thesis, The University of British Columbia, Vancouver, BC, Canada, 2007.

ASKELAND, D. R.; FULAY, P. P.; WRIGHT, W. J. **The Science and Engineering of Materials**. 6th Ed. Boston: Cengage Learning, 2011. 956 p.

ASKELAND, D. R.; WRIGHT, W. J. **Ciência e engenharia dos materias**. São Paulo: Cengage Learning, 2014.

BAILLEUL, J.-L. et al. **Inverse algorithm for optimal processing of composite materials**. Composites Part A: Applied Science and Manufacturing, v. 34, n. 8, p. 695-708, 2003.

BARAN, Ismet et al. **A review on the mechanical modeling of composite manufacturing processes**. Archives of computational methods in engineering, v. 24, n. 2, p. 365-395, 2017.

BARBERO, Ever J. **Finite element analysis of composite materials using Abaqus**. Boca Raton, EUA: CRC Press, 2013.

BAUER, Ronald S. **Epoxy resin chemistry**. ACS Symposium Series No.114, American Chemical Society, Washington, DC, US. 1979.

BELLINI, Costanzo; SORRENTINO, Luca. **Analysis of cure induced deformation of CFRP U-shaped laminates**. Composite Structures, v. 197, p. 1-9, 2018.

BERINS, Michael (Ed.). **Plastics engineering handbook of the society of the plastics industry**. Springer Science & Business Media, 1991.

BIAGIOTTI, J.; PUGLIA, D.; KENNY, J. M. **A Review on Natural Fibre-Based Composites-Part I**. Journal of Natural Fibers, 1:2, p. 37-68. 2008. DOI: http://dx.doi.org/10.1300/J395v01n02_04.

BLEST, D. C. et al. **Curing simulation by autoclave resin infusion**. Composites Science and Technology, v. 59, n. 16, p. 2297-2313, 1999.

BOGETTI, T. A.; GILLIPSE, J. W. **Process-induced stress and deformation in thick-section thermoset composite laminates**. Journal of composite materials, v. 26, n. 5, p. 626-660, 1992.

BOGETTI, T. A.; GILLIPSE, J. W. **Processing-induced stress and deformation in thick section thermosetting composite laminates**. CCM report. University of Delaware, August, p. 89-21, 1989.

CALLISTER, W. D.; RETHWISCH, D. G. **The structure of crystalline solids. Materials science and engineering: an introduction**. New York: John Wiley & Sons, Inc, p. 38-79, 2007.

CALLISTER, William D. **An introduction: material science and engineering**. New York, v. 106, p. 139, 2007.

CALLISTER, William D. **Ciência e Engenharia de Materiais: Uma Introdução**. 7ª Ed. Rio de Janeiro: LTC, 2008. 589 p.

CAPEHART, T. W.; MUHAMMAD, Nouman; KIA, Hamid G. **Compensating thermoset composite panel deformation using corrective molding**. Journal of composite materials, v. 41, n. 14, p. 1675-1701, 2007.

CARLONE, Pierpaolo; PALAZZO, Gaetano S. **A simulation based metaheuristic optimization of the thermal cure cycle of carbon-epoxy composite laminates**. In: AIP Conference Proceedings. American Institute of Physics, 2011. p. 5-10.

CARLONE, Pierpaolo; PALAZZO, Gaetano S. **Composite laminates cure cycle optimisation by meta-heuristic algorithms**. International Journal of Materials and Product Technology, v. 46, n. 2-3, p. 106-123, 2013.

CARLONE, Pierpaolo; PALAZZO, Gaetano S. **Thermo-chemical and rheological finite element analysis of the cure process of thick carbon-epoxy composite laminates**. International Journal of Material Forming, v. 2, n. 1, p. 137-140, 2009.

CENTEA, Timotei; GRUNENFELDER, Lessa K.; NUTT, Steven R. **A review of out-of-autoclave prepregs–Material properties, process phenomena, and manufacturing considerations**. Composites Part A: Applied Science and Manufacturing, v. 70, p. 132-154, 2015.

CHAKRADEO, Sarvesh S.; HENDRE, Aishwarya S.; DESHPANDE, Shantanu U. **Generalized theory for hybridization of evolutionary algorithms**. In: 2014 IEEE International Conference on Computational Intelligence and Computing Research. IEEE, 2014. p. 1-5.

CHONG, Edwin KP; ZAK, Stanislaw H. **An introduction to optimization**. 3. ed. John Wiley & Sons, 2008.

CINAR, K. et al. **Modelling manufacturing deformations in corner sections made of composite materials**. Journal of Composite Materials, v. 48, n. 7, p. 799-813, 2014.

CINAR, K. **Process modelling for distortions in manufacturing of fibre reinforced composite materials**. 2014. Tese de Doutorado. Ph. D. thesis, Bogazici University.

CIRISCIOLI, Peter R.; SPRINGER, George S.; LEE, Woo Il. **An expert system for autoclave curing of composites**. Journal of Composite Materials, v. 25, n. 12, p. 1542-1587, 1991.

CLIFFORD, S. et al. **Thermoviscoelastic anisotropic analysis of process induced residual stresses and dimensional stability in real polymer matrix composite components**. Composites Part A: Applied Science and Manufacturing, v. 37, n. 4, p. 538-545, 2006.

COELLO, Carlos A. Coello et al. **Evolutionary algorithms for solving multi-objective problems**. New York: Springer, 2014.

COELLO, Carlos A. Coello. **An introduction to evolutionary algorithms and their applications**. In: International Symposium and School on Advancex Distributed Systems. Springer, Berlin, Heidelberg, 2005. p. 425-442.

COHERENT MARKET INSIGHTS. **Polymer Matrix Composites Market Analysis**. 2022. Available at: https://www.coherentmarketinsights.com/market-insight/polymer-matrix-composites-market-560. Access in: 09 Aug 2022.

COMSOL INC. **Automatic Time Step and Order Selection in Time-Dependent Problems**, 2019f. Available at https://www.comsol.com/blogs/automatic-time-step-and-order-selection-in-time-dependent-problems/. Access in 22 Oct 2019.

COMSOL INC. **COMSOL Multiphysics® Simulation Software Understand, Predict, and Optimize**, 2019c. Available at https://www.comsol.com/comsol-multiphysics. Access in 15 Aug 2019.

COMSOL INC. **Controlling the Time Dependent solver timesteps**, 2019e. Available at https://www.comsol.com/support/knowledgebase/1254. Access in 17 Oct 2019.

COMSOL INC. **Download COMSOL software documentation**, 2019a. Available at https://br.comsol.com/documentation. Access in 10 Aug 2019.

COMSOL INC. **Finite Element Mesh Refinement: Definitions and Techniques**, 2019b. Available at https://www.comsol.com/multiphysics/mesh-refinement. Access in 15 Aug 2019.

COMSOL INC. **Introduction to LiveLink for MATLAB - COMSOL Documentation**, 2021. Available at https://doc.comsol.com/5.6/doc/com.comsol.help.llmatlab/IntroductionToLiveLinkForMATLAB.pdf. Access in 30 jan 2021.

COMSOL INC. **Run COMSOL Multiphysics® Simulations with MATLAB®,** 2020. Available at: https://www.comsol.com/livelink-for-matlab. Access in: 12 Aug 2020.

COMSOL INC. **Understanding, and changing, the element order – Knowledge base**, 2019d. Available at https://www.comsol.com/support/knowledgebase/1270. Access in 12 Sep 2019.

COSTA, Michelle L.; REZENDE, Mirabel C.; PARDINI, Luiz C. **Métodos de estudo da cinética de cura de resinas epóxi**. Polímeros, v. 9, p. 37-44, 1999.

COSTA, V. A. F.; SOUSA, A. C. M. **Modeling of flow and thermo-kinetics during the cure of thick laminated composites**. International Journal of Thermal Sciences, v. 42, n. 1, p. 15-22, 2003.

DAI, Jianfeng; XI, Shangbin; LI, Dongna. **Numerical analysis of curing residual stress and deformation in thermosetting composite laminates with comparison between different constitutive models**. Materials, v. 12, n. 4, p. 572, 2019.

DE JONG, Kenneth Alan. **An analysis of the behavior of a class of genetic adaptive systems**. University of Michigan, 1975.

DE JONG, Kenneth; FOGEL, David B.; SCHWEFEL, Hans-Paul. **A history of evolutionary computation**. Handbook of Evolutionary Computation A, v. 2, p. 1-12, 1997.

DEB, K. **Multi-Objective Optimization using Evolutionary Algorithms**, John Wiley & Sons, Inc., 2001.

DEB, K; KUMAR, A. **Real-coded genetic algorithms with simulated binary crossover: Studies on multi-modal and multi-objective problems**. Complex Systems, v. 9, n. 6, p. 431-454. 1995.

DIBENEDETTO, A. T. **Prediction of the glass transition temperature of polymers: a model based on the principle of corresponding states**. Journal of Polymer Science Part B: Polymer Physics, v. 25, n. 9, p. 1949-1969, 1987.

DING, A.; Li, S.;Wang, J.; Ni, A. **A new analytical solution for spring-in of curved composite parts. Composites Science and Technology**, v. 142, p. 30-40, 2017.

DOLKUN, Dilmurat et al. **Optimization of cure profile for thick composite parts based on finite element analysis and genetic algorithm**. Journal of Composite Materials, v. 52, n. 28, p. 3885-3894, 2018.

DRZAL, L. T. **Epoxy Resins and Composites II**. Advanced Polymer Science Series, Springer-Verlag, Berlin, Germany, p. 75, 1986.

DUSEK, K.; ILAVSKI, M.; LUNAK, S. **Curing of epoxy resins. I. Statistics of curing of diepoxides with diamines**. In: Journal of polymer science: Polymer Symposia. New York: Wiley Subscription Services, Inc., A Wiley Company, 1975. p. 29-44.

EOM, Yongsung et al. **Time-cure-temperature superposition for the prediction of instantaneous viscoelastic properties during cure**. Polymer Engineering & Science, v. 40, n. 6, p. 1281-1292, 2000.

ERSOY, Nuri et al. **Development of spring-in angle during cure of a thermosetting composite**. Composites Part A: Applied Science and Manufacturing, v. 36, n. 12, p. 1700-1706, 2005.

ERSOY, Nuri et al. **Modelling of the spring-in phenomenon in curved parts made of a thermosetting composite**. Composites Part A: Applied Science and Manufacturing, v. 41, n. 3, p. 410-418, 2010.

FERNLUND, G. et al. **Experimental and numerical study of the effect of cure cycle, tool surface, geometry, and lay-up on the dimensional fidelity of autoclave-processed**

composite parts. Composites part A: applied science and manufacturing, v. 33, n. 3, p. 341-351, 2002.

FISH, Jacob. **Um primeiro curso em elementos finitos**. Rio de Janeiro: LTC, 2009.

FOURMAN, Michael P. **Compaction of symbolic layout using genetic algorithms**. In: Proceedings of the 1st international conference on genetic algorithms. 1985. p. 141-153.

FOURNIER, Jérôme et al. **Changes in molecular dynamics during bulk polymerization of an epoxide− amine system as studied by dielectric relaxation spectroscopy**. Macromolecules, v. 29, n. 22, p. 7097-7107, 1996.

GOLBERG, David E. **Genetic algorithms in search, optimization, and machine learning**. Addion wesley, v. 1989, n. 102, p. 36, 1989.

GOLDBERG, David Edward. **Genetic Algorithms in Search, Optimization & Machine Learning.** 401pp. Addison-Wesley, 1989.

GOLDBERG, David Edward. **The design of innovation: Lessons from and for competent genetic algorithms**. Boston: Kluwer Academic Publishers, 2002.

GOODMAN, S. H.; DODIUK, H. **Handbook of Thermoset Plastics**. 2014.

GOPAL, Ajith K.; ADALI, Sarp; VERIJENKO, Viktor E. **Optimal temperature profiles for minimum residual stress in the cure process of polymer composites**. Composite Structures, v. 48, n. 1-3, p. 99-106, 2000.

GUTOWSKI, Timothy George Peter; GUTOWSKI, Timothy George Peter (Ed.). **Advanced composites manufacturing**. New York: Wiley, 1997.

HAHN, H. T. **Effects of residual stresses in polymer matrix composites**. Journal of the Astronautical Sciences, v. 32, p. 253-267, 1984.

HOJJATI, M.; HOA, S. V. **Curing simulation of thick thermosetting composites**. Composites Manufacturing, v. 5, n. 3, p. 159-169, 1994.

HOLLAND, John H. **Adaptation in natural and artificial systems: an introductory analysis with applications to biology, control, and artificial intelligence**. MIT press, 1992.

HORIE, K. et al. **Calorimetric investigation of polymerization reactions. III. Curing reaction of epoxides with amines**. Journal of Polymer Science Part A-1: Polymer Chemistry, v. 8, n. 6, p. 1357-1372, 1970.

HUTTON, David V. **Fundamentals of finite element analysis**. New York, EUA: McGraw-Hill, 2004.

ITO, Koichi; AKAGI, Shinsuke; NISHIKAWA, Masaaki. **A multiobjective optimization approach to a design problem of heat insulation for thermal distribution piping network systems**. In: Journal of Mechanisms, Transmissions and Automation in Design (Transactions of the ASME), 1983. p. 206–213.

JAHROMI, Parisa Eghbal; SHOJAEI, Akbar; REZA PISHVAIE, S. Mahmoud. **Prediction and optimization of cure cycle of thick fiber-reinforced composite parts using dynamic artificial neural networks**. Journal of reinforced plastics and composites, v. 31, n. 18, p. 1201-1215, 2012.

JANG, B. Z. **Fracture behavior of fiber-resin composites containing a controlled interlaminar phase (CIP)**. Science and Engineering of Composite Materials, v. 2, n. 1, p. 29-48, 1991.

JOCHUM, Ch. et al. **A cut-off fracture approach for residual stress estimation in thick epoxies**. Materialwissenschaft und Werkstofftechnik, Vol. 47, Issue 5-6, 2016. p. 530-538.

JOCHUM, Ch. et al. **Cure multiphysic couplings effects on the dynamic behaviour of a thick epoxy**. The 19th International Conference on Composite Materials. Montreal, Canada, 2013.

JOCHUM, Ch. et al. **Estimation of the residual stress state generated during the curing of a thick epoxy matrix by pulsed laser**. 16th European Conference on Composite Materials, Seville, Spain, 2014.

JOCHUM, Ch. **Thermosetting laminates quality: from fiber waviness to FEM cure modeling**. Habilitation à Diriger des Recherches, ENSIETA, 2009.

JOCHUM, Ch.; GRANDIDIER, J. C.; POTIER-FERRY, M. **Modeling approach of microbuckling mechanism during cure in a carbon epoxy laminate**. The 12th Conference on Composite Materials, Paris, France, 1999.

JOCHUM, Ch.; GRANDIDIER, J. C.; SMAALI, M. A. **Experimental study of long T300 carbon fibre undulations during the curing of LY556 epoxy resin**. Composites Science and Technology, Vol. 67, 2007. p. 2633-2642.

JOCHUM, Ch.; GRANDIDIER, J. C.; SMAALI, M. A. **Proposal for a long-fibre microbuckling scenario during the cure of a thermosetting matrix**. Composites: Part A, Vol. 39, 2008. p. 19-28.

JOCHUM, Ch; GRANDIDIER, J. C. **Microbuckling elastic modelling approach of a single carbon fibre embedded in an epoxy matrix**. Composites science and technology, v. 64, n. 16, p. 2441-2449, 2004.

JOHNSTON, Andrew A. **An integrated model of the development of process-induced deformation in autoclave processing of composite structures**. 1997. Tese de Doutorado. University of British Columbia.

KAM, Tai-Yan; LAI, F. M.; SHER, H. F. **Optimal paramerers for curing graphite/epoxy composite laminates**. Journal of materials processing technology, v. 48, n. 1-4, p. 357-363, 1995.

KAMAL, M. R.; SOUROUR, S. **Kinetics and thermal characterization of thermoset cure**. Polymer Engineering & Science, v. 13, n. 1, p. 59-64, 1973.

KAPPEL, Erik. **Forced-interaction and spring-in–relevant initiators of process-induced distortions in composite manufacturing**. Composite Structures, v. 140, p. 217-229, 2016.

KAPPEL, Erik; STEFANIAK, Daniel; HÜHNE, Christian. **Process distortions in prepreg manufacturing–an experimental study on CFRP L-profiles**. Composite Structures, v. 106, p. 615-625, 2013.

KENNEDY, Graeme J.; HANSEN, Jorn S. **The hybrid-adjoint method: a semi-analytic gradient evaluation technique applied to composite cure cycle optimization**. Optimization and Engineering, v. 11, n. 1, p. 23-43, 2010.

LEE, Henry; NEVILLE, Kris. **Handbook of epoxy resins**. McGraw-Hill, New York, NY, USA, 1967.

LI, Chun et al. **In-situ measurement of chemical shrinkage of MY750 epoxy resin by a novel gravimetric method**. Composites Science and Technology, v. 64, n. 1, p. 55-64, 2004.

LI, Min et al. **Optimal curing for thermoset matrix composites: thermochemical considerations**. Polymer Composites, v. 22, n. 1, p. 118-131, 2001.

LI, Yuan-Long et al. **A primary theoretical study on decomposition-based multiobjective evolutionary algorithms**. IEEE Transactions on Evolutionary Computation, v. 20, n. 4, p. 563-576, 2015.

LIU, Chao; SHI, Yaoyao. **An improved analytical solution for process-induced residual stresses and deformations in flat composite laminates considering thermo-viscoelastic effects**. Materials, v. 11, n. 12, p. 2506, 2018.

LIU, Jing; CHI, Yaxiong; ZHU, Chen. **A dynamic multiagent genetic algorithm for gene regulatory network reconstruction based on fuzzy cognitive maps**. IEEE Transactions on Fuzzy Systems, v. 24, n. 2, p. 419-431, 2015.

LORD, S. J.; STRINGER, L. G. **A modelling approach for predicting residual stresses and distortions in polymer composites**. In: 17th International Conference on Composite Materials. Edinburgh. 2009.

MATSUZAKI, Ryosuke et al. **Multi-objective curing optimization of carbon fiber composite materials using data assimilation and localized heating**. Composites Part A: Applied Science and Manufacturing, v. 119, p. 61-72, 2019.

MAWARDI, A.; PITCHUMANI, R. **Optimal temperature and current cycles for curing of composites using embedded resistive heating elements**. J. Heat Transfer, v. 125, n. 1, p. 126-136, 2003.

MAZUMDAR, S. K. **Composites Manufacturing: Materials, Product and Process Engineering**. Boca Raton: CRC Press, 2002. 416 p.

MCCRUM, Norman Gerard et al. **Principles of polymer engineering**. Oxford University Press, USA, 1997.

MIDDLETON, Don H. (Ed.). **Composite materials in aircraft structures**. John Wiley & Sons, 1990.

MIRACLE, D. B.; DONALDSON, S. L. **ASM Handbook: Composites**. v. 21. Metals Park, EUA: ASM International, 2001.

MSALLEM, Youssef Abou; JACQUEMIN, Frédéric; POITOU, Arnaud. **Residual stresses formation during the manufacturing process of epoxy matrix composites: resin yield stress and anisotropic chemical shrinkage**. International journal of material forming, v. 3, n. 2, p. 1363-1372, 2010.

MUZUMDAR, Shailesh V.; JAMES LEE, L. **Chemorheological analysis of unsaturated polyester-styrene copolymerization**. Polymer Engineering & Science, v. 36, n. 7, p. 943-952, 1996.

NOCEDAL, Jorge; WRIGHT, Stephen J. (2nd Ed.). **Numerical optimization**. New York, NY: Springer New York, 2006.

OLIVIER, Ph; COTTU, J. P. **Optimisation of the co-curing of two different composites with the aim of minimising residual curing stress levels**. Composites science and technology, v. 58, n. 5, p. 645-651, 1998.

OSYCZKA, Andrzej. **Evolutionary algorithms for single and multicriteria design optimization**. Heidelberg: Physica-Verlag, 2002.

PAGANO, Rogério L. et al. **Proposal of an optimum cure cycle for filament winding process using a hybrid neural network-first principles model**. Polymer composites, v. 35, n. 7, p. 1377-1387, 2014.

PAIVA, Vivianne Marie Bruère de Carvalho. **A multiphysics numerical simulation of the curing process of a thermosetting polymer resin**. 2018. Dissertação de Mestrado. Universidade Federal de Pernambuco.

PANTELELIS, N.; VROUVAKIS, Th; SPENTZAS, K. **Cure cycle design for composite materials using computer simulation and optimisation tools**. Forschung im Ingenieurwesen, v. 67, n. 6, p. 254-262, 2003.

PATHAM, Bhaskar. **COMSOL® Implementation of a viscoelastic model with cure-temperature-time superposition for predicting cure stresses and springback in a thermoset resin**. In: Excerpt from the proceedings of the COMSOL conference. 2009.

PATHAM, Bhaskar. **Multiphysics simulations of cure residual stresses and springback in a thermoset resin using a viscoelastic model with cure-temperature-time superposition**. Journal of applied polymer science, v. 129, n. 3, p. 983-998, 2013.

PIERRICK, Hamel et al. **Klystron efficiency optimization based on a genetic algorithm**. In: 2019 International Vacuum Electronics Conference (IVEC). IEEE, 2019. p. 1-2.

PILLAI, V.; BERIS, A. N.; DHURJATI, P. **Heuristics guided optimization of a batch autoclave curing process**. Computers & chemical engineering, v. 20, n. 3, p. 275-294, 1996.

PILLAI, V.; BERIS, A. N.; DHURJATI, P. **Implementation of model-based optimal temperature profiles for autoclave curing of composites using a knowledge-based system**. Industrial & engineering chemistry research, v. 33, n. 10, p. 2443-2452, 1994.

PITCHUMANI, Rangarajan; YAO, Shi-Chune. **Non-dimensional analysis of an idealized thermoset composites manufacture**. Journal of composite materials, v. 27, n. 6, p. 613-636, 1993.

RABEARISON, N. **Elaboration d'un outil numérique dédié à la simulation du procédé de fabrication des matériaux composites à résine thermodurcissable - prédiction des contraintes internes**. 2009. 172 p. Thesis (Doctorate in Mécaniques des matériaux et structures) – École Doctorale SICMA, Université de Bretagne Occidentale, France, 2009.

RABEARISON, N.; JOCHUM, Ch.; GRANDIDIER, J. C. **A cure kinetics, diffusion controlled and temperature dependent, identification of the Araldite LY556 epoxy**. Journal of Materials Science, v. 46, n. 3, p. 787-796, 2011.

RABEARISON, N.; JOCHUM, Ch.; GRANDIDIER, J. C. **A FEM coupling model for properties prediction during the curing of an epoxy matrix**. Computational Materials Science. Vol. 45, p. 715-724, 2009.

RABEARISON, N.; JOCHUM, Ch; GRANDIDIER, J. C. **A finite element coupling model for internal stress prediction during the curing of thick epoxy composites**. In: The 9th International Conference on Flow Processes in Composite Materials, Montreal, Canada, 2008.

RATNA, Debdatta. **Epoxy composites: impact resistance and flame retardancy**. iSmithers Rapra Publishing, 2007.

RATNA, Debdatta. **Handbook of thermoset resins**. Shawbury, UK: ISmithers, 2009.

RUIZ, Edu; TROCHU, F. **Comprehensive thermal optimization of liquid composite molding to reduce cycle time and processing stresses**. Polymer composites, v. 26, n. 2, p. 209-230, 2005.

RUIZ, Edu; TROCHU, F. **Multi-criteria thermal optimization in liquid composite molding to reduce processing stresses and cycle time.** Composites Part A: Applied Science and Manufacturing, v. 37, n. 6, p. 913-924, 2006.

SAFARABADI, M.; SHOKRIEH, M. M. **Understanding residual stresses in polymer matrix composites**. In: Residual stresses in composite materials. Woodhead Publishing, 2014. p. 197-232.

SALOMI, A. et al. **Spring-in angle as molding distortion for thermoplastic matrix composite**. Composites Science and technology, v. 68, n. 14, p. 3047-3054, 2008.

SCHAFFER, J. David. **Multiple objective optimization with vector evaluated genetic algorithms**. In: Proceedings of the First International Conference of Genetic Algorithms and Their Application. 1985. p. 93-100.

SCHAFFER, James David. **Some experiments in machine learning using vector evaluated genetic algorithms (artificial intelligence, optimization, adaptation, pattern recognition)**. 1984. Tese de Doutorado. Vanderbilt University.

SKORDOS, Alexandros A.; PARTRIDGE, Ivana K. **Inverse heat transfer for optimization and on-line thermal properties estimation in composites curing**. Inverse Problems in Science and Engineering, v. 12, n. 2, p. 157-172, 2004.

SMAALI, M. A. **Contribution à l'étude expérimentale du phénomène d'ondulation d'une fibre de carbone noyée dans une résine thermodurcissable tout au long de la cuisson**. 2005. 216 p. Thesis (Doctorate in Mécanique des Solides, des Matériaux, des Structures et des Surfaces) - Sciences pour l'Ingénieur, École Nationale Supérieure de Mécanique et d'Aérotechnique & Faculté des Sciences Fondamentales et Appliquées, France, 2005.

STRUZZIERO, G.; SKORDOS, A. A. **Multi-objective optimisation of composites cure using genetic algorithms**. In: ECCM15-15th European conference on composite materials. Venice, Italy. 2012.

STRUZZIERO, G.; SKORDOS, A. A. **Multi-objective optimisation of the cure of thick components**. Composites Part A: Applied Science and Manufacturing, v. 93, p. 126-136, 2017.

STRUZZIERO, G.; TEUWEN, J. E. **Optimal cure cycles for manufacturing of thick composite parts using multi-objective genetic algorithms**. In: ECCM18–18th European conference on composite materials. Athens, Greece. 2018.

STRUZZIERO, Giacomo; TEUWEN, Julie JE; SKORDOS, Alexandros A. **Numerical optimisation of thermoset composites manufacturing processes: A review**. Composites Part A: Applied Science and Manufacturing, v. 124, p. 105499, 2019.

SUBBIAH, A.; LALDIN, O. **Genetic algorithm based multi-objective optimization of electromagnetic components using COMSOL® and MATLAB®**. In: COMSOL Conference Proceedings. 2016.

SUDHOFF, S. D. **Genetic Optimization System Engineering Tool (GOSET) Version 2.6 Manual 2014** [Online]. 2014. Available at

https://engineering.purdue.edu/ECE/Research/Areas/PES/Software/genetic-optimization-toolbox-2.6. Access in 05 Fev 2021.

SUDHOFF, Scott D. **Power magnetic devices: a multi-objective design approach**. John Wiley & Sons, 2021.

SUDHOLT, Dirk. **Parallel evolutionary algorithms**. In: Handbook of Computational Intelligence, University of Sheffield, UK, 2007.

SUN, Chengfo; ZHOU, Haiyan; CHEN, Liqing. **Improved differential evolution algorithms**. In: 2012 IEEE International Conference on Computer Science and Automation Engineering (CSAE). IEEE, 2012. p. 142-145.

SURATNO, Basuki R.; YE, Lin; MAI, Yiu-Wing. **Simulation of temperature and curing profiles in pultruded composite rods**. Composites Science and Technology, v. 58, n. 2, p. 191-197, 1998.

TAVAKOL, Behrouz et al. **Prediction of residual stresses and distortion in carbon fiber-epoxy composite parts due to curing process using finite element analysis**. Journal of Applied Polymer Science, v. 128, n. 2, p. 941-950, 2013.

TEIJIN CARBON. **Applications**. 2022. Available at: https://www.teijincarbon.com/applications/. Access in: 15 Jul 2022.

TEIMOURI, V.; SAFARABADI, M. **Semi-analytical study of thick polymer composites behavior during curing process**. Engineering Solid Mechanics, v. 7, n. 3, p. 205-216, 2019.

TIFKITSIS, Konstantinos I. et al. **Stochastic multi-objective optimisation of the cure process of thick laminates**. Composites Part A: Applied Science and Manufacturing, v. 112, p. 383-394, 2018.

VAFAYAN, Mehdy et al. **Development of an optimized thermal cure cycle for a complex-shape composite part using a coupled finite element/genetic algorithm technique**. Iranian Polymer Journal, v. 24, n. 6, p. 459-469, 2015.

VIKHAR, Pradnya A. **Evolutionary algorithms: A critical review and its future prospects**. In: 2016 International conference on global trends in signal processing, information computing and communication (ICGTSPICC). IEEE, 2016. p. 261-265.

WANG, R-M.; ZHENG, S-R.; ZHENG, Y-P. **Polymer matrix composites and technology**. Beijing: Woodhead Publishing, 2011. 555 p.

WHITE, S. R.; HAHN, H. T. **Cure cycle optimization for the reduction of processing-induced residual stresses in composite materials**. Journal of Composite Materials, v. 27, n. 14, p. 1352-1378, 1993.

WHITE, S. R.; HAHN, H. T. **Mechanical property and residual stress development during cure of a graphite/BMI composite**. Polymer Engineering & Science, v. 30, n. 22, p. 1465-1473, 1990.

WHITLEY, Darrell. **An overview of evolutionary algorithms: practical issues and common pitfalls.** Information and software technology, v. 43, n. 14, p. 817-831, 2001.

WISNOM, M. R. et al. **Curing stresses in thick polymer composite components**. Part i: analysis. In: 12th International Conference on Composite Materials, Paris, July. 1999. p. 859.

WISNOM, M. R. et al. **Mechanisms generating residual stresses and distortion during manufacture of polymer–matrix composite structures**. Composites Part A: Applied Science and Manufacturing, v. 37, n. 4, p. 522-529, 2006.

WISNOM, Michael R.; POTTER, Kevin D.; ERSOY, Nuri. **Shear-lag analysis of the effect of thickness on spring-in of curved composites**. Journal of composite materials, v. 41, n. 11, p. 1311-1324, 2007.

WOLPERT, David H.; MACREADY, William G. **Coevolutionary free lunches**. IEEE Transactions on evolutionary computation, v. 9, n. 6, p. 721-735, 2005.

WOLPERT, David H.; MACREADY, William G. **No free lunch theorems for optimization**. IEEE transactions on evolutionary computation, v. 1, n. 1, p. 67-82, 1997.

WRIGHT, Ralph E. **Thermosets, reinforced plastics, and composites**. Handbook of Plastics, Elastomers, and Composites, p. 109-188, 2002.

WUCHER, B. et al. **Tooling geometry optimization for compensation of cure-induced distortions of a curved carbon/epoxy C-spar**. Composites Part A: Applied Science and Manufacturing, v. 56, p. 27-35, 2014.

YU, Xinjie; GEN, Mitsuo. **Introduction to evolutionary algorithms**. Springer Science & Business Media, 2010.

YUAN, Zhenyi et al. **Multi-objective approach to optimize cure process for thick composite based on multi-field coupled model with RBF surrogate model**. Composites Communications, v. 24, p. 100671, 2021.

ZBIGNIEW, Michalewicz. **Genetic Algorithms + Data Structures = Evolution Programs**. Third, revised and extended edition. Berlin: Springer-Verlag, 1999.

ZENG, Yujiao; SUN, Yanguang. **Comparison of multiobjective particle swarm optimization and evolutionary algorithms for optimal reactive power dispatch problem**. In: 2014 IEEE Congress on Evolutionary Computation (CEC). IEEE, 2014. p. 258-265.

ZHU, Q.; GEUBELLE, P.H.; Li, M.; TUCKER, C.L. **Dimensional accuracy of thermoset composites: simulation of process-induced residual stresses**. Journal of composite materials, v. 35, n. 24, p. 2171-2205, 2001.

ZITZLER, Eckart**. Evolutionary algorithms for multiobjective optimization: Methods and applications**. Ithaca: Shaker, 1999. Ph. D. Thesis, Zurich, Switzerland: Swiss Federal Institute of Technology (ETH) (Dissertation ETH No. 13398).

APPENDIX A – MESH CONVERGENCE STUDY RESULTS

	MESH SIZES				
VARIABLE	**Normal**	**Fine**	**Finer**	**Extra Fine**	**Extremely Fine**
Min. degree of cure reached by the sample at the end of cure (1)	-3.22%	-1.25%	0.00%	0.00%	0.00%
Max. temperature reached by the sample throughout the cure (°C)	0.26%	0.22%	-0.01%	0.01%	0.00%
Max. gradient of temperature reached by the sample AGP (°C/mm)	23.70%	23.93%	5.75%	0.60%	0.00%
Max. gradient of degree of conversion reached by the sample AGP (1/mm)	532.46%	581.76%	-0.51%	1.50%	0.00%
Max. value of the volume average conversion rate throughout the cure (1/s)	8.41%	7.29%	-1.24%	0.38%	0.00%
SIMULATION TIME	502	502	518	588	936
NUMBER OF ELEMENTS	236	236	591	1783	7086

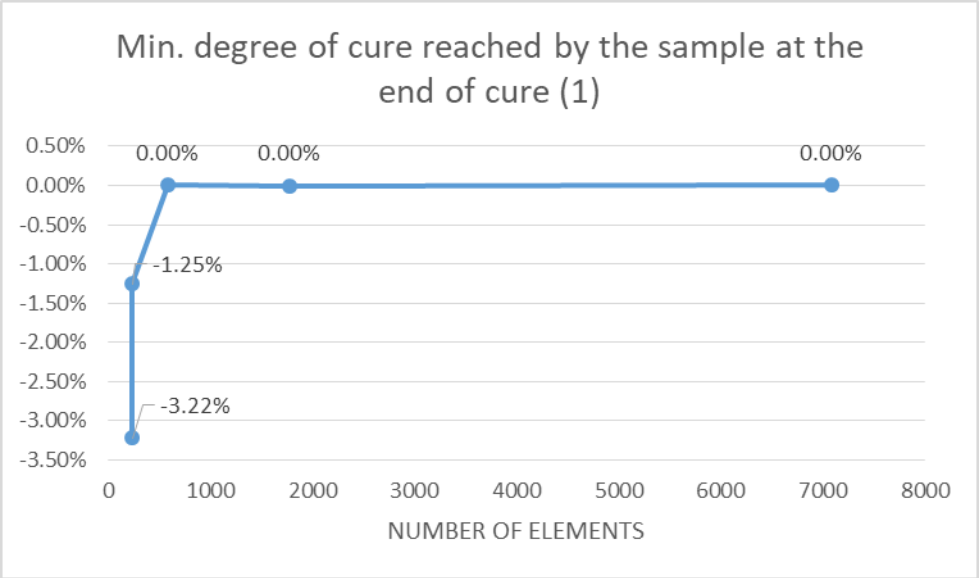

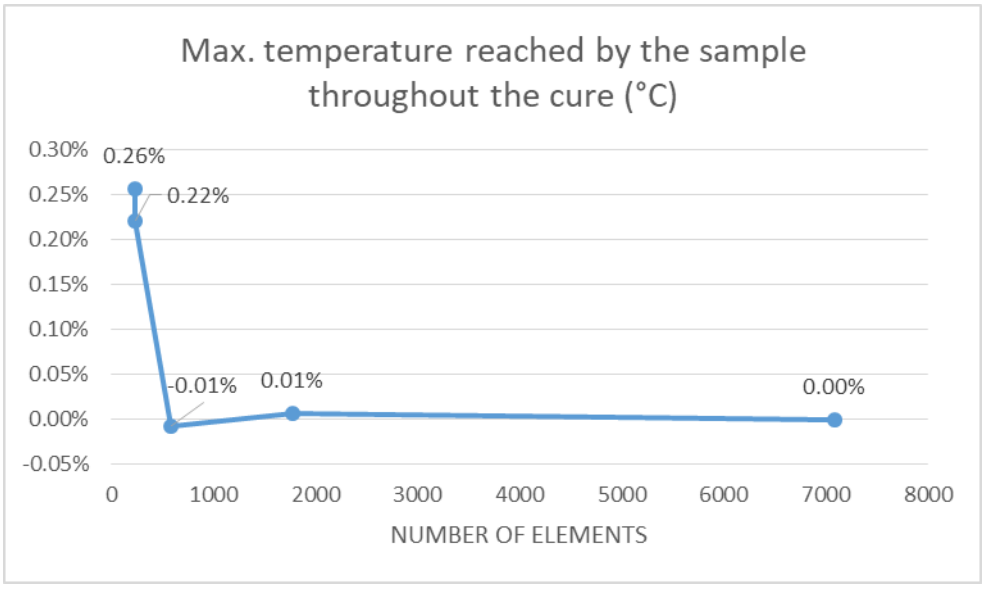
Max. temperature reached by the sample throughout the cure (°C)
0.30%
0.25%
0.20%
0.15%
0.10%
0.05%
0.00%
-0.05%
0.26%
0.22%
-0.01%
0.01%
0.00%
0
1000
2000
3000
4000
5000
6000
7000
8000
NUMBER OF ELEMENTS

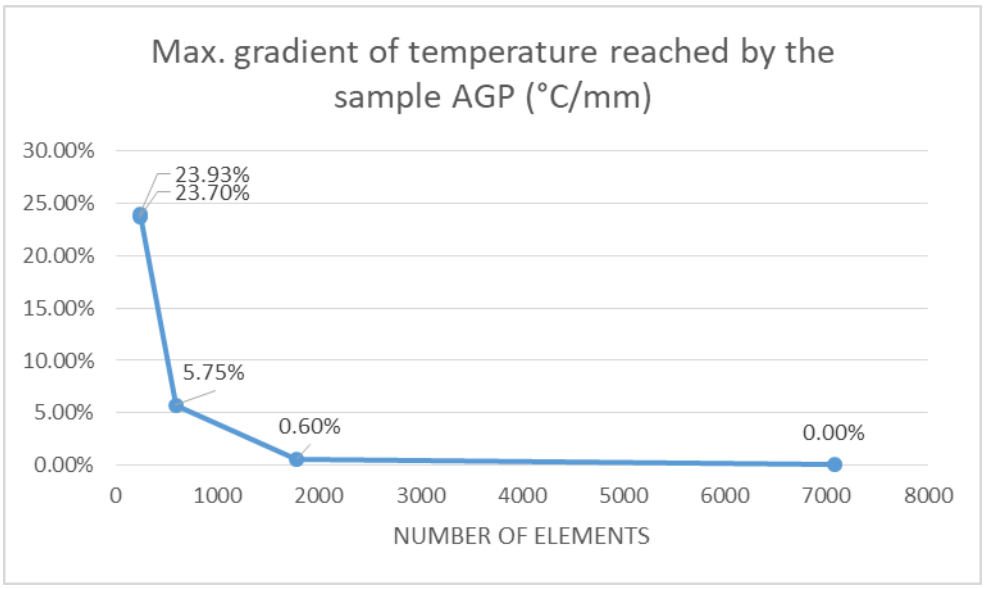
Max. gradient of temperature reached by the sample AGP (°C/mm)
30.00%
25.00%
20.00%
15.00%
10.00%
5.00%
0.00%
23.93%
23.70%
5.75%
0.60%
0.00%
0
1000
2000
3000
4000
5000
6000
7000
8000
NUMBER OF ELEMENTS

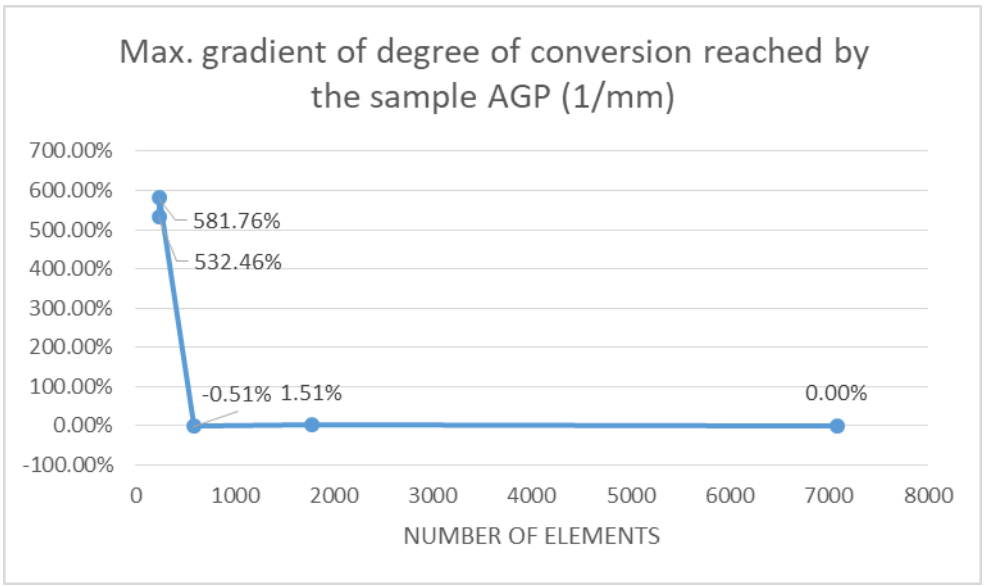
Max. gradient of degree of conversion reached by the sample AGP (1/mm)
700.00%
600.00%
500.00%
400.00%
300.00%
200.00%
100.00%
0.00%
-100.00%
581.76%
532.46%
-0.51%
1.51%
0.00%
0
1000
2000
3000
4000
5000
6000
7000
8000
NUMBER OF ELEMENTS

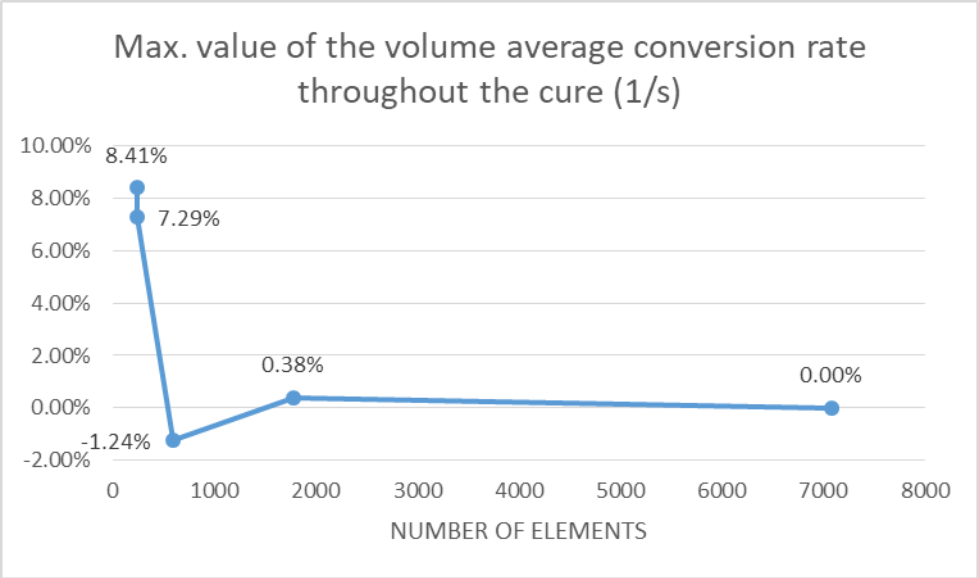
Max. value of the volume average conversion rate throughout the cure (1/s)
10.00%
8.00%
6.00%
4.00%
2.00%
0.00%
-2.00%
8.41%
7.29%
-1.24%
0.38%
0.00%
0
1000
2000
3000
4000
5000
6000
7000
8000
NUMBER OF ELEMENTS

APPENDIX B – MATLAB SCRIPT FOR THE CONVERSION RATE DRIVEN (CRD) STRATEGY

```
% CONVERSION RATE DRIVEN (CRD) STRATEGY
import com.comsol.model.util.*

% Start to measure the elapsed time
tic;

% Initialize CT1 = [80;81;82;...;95]
CT1_i = 80; %[°C]
CT1_f = 95; %[°C]
step = 1;   %[°C]
CT1 = (CT1_i:step:CT1_f)';
[n_CT1,~] = size(CT1);

% Initialize CT2 = [140;145;150]
CT2_i = 140; %[°C]
CT2_f = 150; %[°C]
step = 5;    %[°C]
CT2 = (CT2_i:step:CT2_f)';
[n_CT2,~] = size(CT2);

% Initialize the duration of the first temperature plateau in the first cure↙
simulation,...
...through which the time when the average conversion rate reaches its maximum value↙
is detected
t_CT1_0 = 2*3600;  %[s] -> 2[h]

% Initialize the maximum duration of the second temperature plateau
t_CT2_0 = 4*3600;  %[s] -> 4[h]

% Initialize the heating rate
r = 3;    %[°C/min]

% Initialize the degradation temperature
T_degrad = 155;    %[°C]

% Initialize the minimum degree of cure required at the end of the cure
alpha_min_req = 0.854;

% Folder that stores the model
folder = 'C:\Users\User\Documents\COMSOL\CURE OPTIMIZATION\CONVERSION RATE DRIVEN\With↙
MATLAB\'; %

% Create a structure to store the CRD strategy parameters and results
CRD = struct('CT1',zeros(n_CT1,n_CT2),'CT2',zeros(n_CT1,n_CT2),'t_CT1',zeros(n_CT1,↙
n_CT2)...
,'t_CT2',zeros(n_CT1,n_CT2),'t_CT1_min',zeros(n_CT1,n_CT2),'t_CT2_min',zeros(n_CT1,↙
n_CT2),'t_ramp1',zeros(n_CT1,n_CT2),'t_ramp2',zeros(n_CT1,n_CT2)...
,'T_max',zeros(n_CT1,n_CT2),'max_alphat',zeros(n_CT1,n_CT2),'t_max_alphat',zeros↙
(n_CT1,n_CT2)...
,'last_min_alpha',zeros(n_CT1,n_CT2),'t_cure',zeros(n_CT1,n_CT2),'t_cure_min',zeros↙
(n_CT1,n_CT2),'max_grad_alpha_AGP',zeros(n_CT1,n_CT2)...
,'max_grad_T_AGP',zeros(n_CT1,n_CT2),'S_min_alpha',zeros(n_CT1,n_CT2),'t_min_alpha',↙
zeros(n_CT1,n_CT2)...
,'S_critic_T',zeros(n_CT1,n_CT2),'t_critic_T',zeros(n_CT1,n_CT2),'t_cure_sim',zeros↙
(n_CT1,n_CT2));

% Create an object to the simulation model exported to the COMSOL Multiphysics Server
model = mphopen('C:\Users\User\Documents\COMSOL\CURE OPTIMIZATION\CONVERSION RATE↙
DRIVEN\With MATLAB\COMSOL_CRD_cure_optimization');
model.hist.disable % If you run a model in a loop you do not need to store the model↙
```

```
history because it contains the same operations as
           % many times as you have iterations in the loop. The solution is to disable↙
the history recording

for k = 1:n_CT1 % Loop over all CT1 temperatures
    disp("Start of cure schedule configuration");
    % Initialize cure schedule parameters
    CRD.CT1(k,:) = CT1(k);
    CRD.t_CT1(k,:) = t_CT1_0;      %[s]
    CRD.t_CT2(k,:) = 0;
    CRD.t_ramp1(k,:) = (CRD.CT1(k,1)-20)/r*60;     %[s]
    CRD.t_ramp2(k,:) = 0;

    % Set up cure schedule parameters in COMSOL
    model.param.set('CT1', CRD.CT1(k,1)+"+273[K]", 'Constant temperature 1');    %[K]
    model.param.set('t_CT1', CRD.t_CT1(k,1)+"[s]", 'Duration of temperature 1'); %[s]
    model.param.set('t_CT2', CRD.t_CT2(k,1)+"[s]", 'Duration of temperature 2'); %[s]
    model.param.set('t_ramp1', CRD.t_ramp1(k,1)+"[s]", 'ramp duratin 1');        %[s]
    model.param.set('t_ramp2', CRD.t_ramp2(k,1)+"[s]", 'ramp duration 2');       %[s]

    % RUN THE MODEL AND SHOW PROGRESS
    ModelUtil.showProgress(true);
    model.study('std1').run();

    % Compute the maximum T reached by the sample until the end of the first plateau
    probe1 = mphtable(model,'tbl1');
    CRD.T_max(k,:) = max(probe1.data(:,4));  %[°C]

    if CRD.T_max(k,1) < 155 % Check if the degradation temperature has been reached
        % Get the maximum conversion rate and the time when it happens
        [CRD.max_alphat(k,:),index_max_alphat] = max(probe1.data(:,2));
        CRD.t_max_alphat(k,:) = probe1.data(index_max_alphat,1);

        % Compute the duration of the first plateaou (t_CT1)
        CRD.t_CT1(k,:) = round((CRD.t_max_alphat(k,1) - CRD.t_ramp1(k,1))/60)*60; %[s]

        % Proceeds to set up the second plateaou
        for j = 1:n_CT2 % Loop over all CT2 temperatures

            % Compute the parameters of the second plateou
            CRD.CT2(k,j) = CT2(j);
            CRD.t_CT2(k,j) = t_CT2_0;
            CRD.t_ramp2(k,j) = (CRD.CT2(k,j)-CRD.CT1(k,j))/r*60;    %[s]

            % Set up cure temperature profile parameters in COMSOL
            model.param.set('CT2', CRD.CT2(k,j)+"+273[K]", 'Constant temperature 2');↙
%[K]
            model.param.set('t_CT1', CRD.t_CT1(k,j)+"[s]", 'Duration of temperature↙
1'); %[s]
            model.param.set('t_CT2', CRD.t_CT2(k,j)+"[s]", 'Duration of temperature↙
2'); %[s]
            model.param.set('t_ramp2', CRD.t_ramp2(k,j)+"[s]", 'ramp duration 2');↙
%[s]

            % RUN THE MODEL AND SHOW PROGRESS
            ModelUtil.showProgress(true);
            model.study('std1').run();

            % Compute the maximum T reached by the sample until the end of the first↙
plateau
```

```
            probe1 = mphtable(model,'tbl1');
            CRD.last_min_alpha(k,j) = probe1.data(end,3);
            CRD.T_max(k,j) = max(probe1.data(:,4));  %[°C]

            fprintf('\nMininum degree of cure at the end = %.4f\n',CRD.last_min_alpha↙
(k,j)); % Print the min. alpha reached at the end
            fprintf('Maximum temperature = %.1f °C\n',CRD.T_max(k,j)); % Print the↙
max. T reached

            if CRD.T_max(k,j) < T_degrad && CRD.last_min_alpha(k,j) >= alpha_min_req %↙
Check if the sample is not thermally degraded and enough cured

                % Compute the duration of the second plateaou (t_CT2) in min
                CRD.t_cure_sim(k,j) = probe1.data(end,1);
                CRD.t_CT2(k,j) = ceil((CRD.t_cure_sim(k,j) - CRD.t_ramp1(k,j) -...
                    CRD.t_CT1(k,j) - CRD.t_ramp2(k,j))/60)*60; %[s]

                % Compute total cure duration
                CRD.t_cure(k,j) = CRD.t_ramp1(k,j) + CRD.t_CT1(k,j) + CRD.t_ramp2(k,j)↙
+ CRD.t_CT2(k,j);  %[s]

                %Compute the durations in minutes
                CRD.t_CT1_min(k,j) = CRD.t_CT1(k,j)/60;
                CRD.t_CT2_min(k,j) = CRD.t_CT2(k,j)/60;
                CRD.t_cure_min(k,j) = CRD.t_cure(k,j)/60;

                % Compute T and degree of cure gradients AGP
                CRD.max_grad_alpha_AGP(k,j) = max(probe1.data(:,5));  %[1/mm]
                CRD.max_grad_T_AGP(k,j) = max(probe1.data(:,6));  %[°C/mm]

                % Save COMSOL model
                base_filename = sprintf('CRD_cure_optimization - CT1_%d°C - CT2_%d°C',↙
CRD.CT1(k,j),CRD.CT2(k,j));
                filename = fullfile(folder, base_filename);
                mphsave(model,filename);

                % Print the results on the screen
                fprintf('\nCT1 = %d °C\n',CRD.CT1(k,j));
                fprintf('CT2 = %d °C\n',CRD.CT2(k,j));
                fprintf('Time in CT1 = %d min\n',CRD.t_CT1_min(k,j));
                fprintf('Time in CT2 = %d min\n',CRD.t_CT2_min(k,j));
                fprintf('Curing time = %d s = %.1f min\n',CRD.t_cure(k,j),CRD.↙
t_cure_min(k,j));
                fprintf('Max. gradient of degree of cure AGP = %.3d 1/mm\n',CRD.↙
max_grad_alpha_AGP(k,j));
                fprintf('Max. gradient of temperature AGP = %.3d °C/mm\n',CRD.↙
max_grad_T_AGP(k,j));
            end
            probe2 = mphtable(model,'tbl2');
            CRD.S_min_alpha(k,j) = probe2.data(end,2); % Get the flag state for the↙
stop condition of min. alpha
            CRD.t_min_alpha(k,j) = probe2.data(end,3); % Get the time when the stop↙
condition of min. alpha was met
            CRD.S_critic_T(k,j) = probe2.data(end,4); % Get the flag state for the↙
stop condition of thermal degradation
            CRD.t_critic_T(k,j) = probe2.data(end,5); % Get the time when the stop↙
condition of thermal degradation was met
        end
    else
        fprintf('\nMaximum temperature = %.1f °C\n',CRD.T_max(k,1)); % Print the max.↙
```

```
T reached
    end
        fprintf("\nEnd of cure schedule simulation\n\n");
end

% Measure and save the elapsed time
running_time = toc; % [s]
```

APPENDIX C – MATLAB SCRIPT FOR THE MULTI-OBJECTIVE GENETIC ALGORITHM (GA) OPTIMIZATION

```
% Start to measure the elapsed time
tic;

% Invoke MATLAB's Parallel Processing Toolbox to use multiple cores to calculate the↙
fitness of the population
GAP.ev_pp = true;
GAP.ev_npg = 6; % Number of cores being used

% Initialize the GA parameters
GAP = gapdefault(3,0,50,20);

GAP.rp_gbr = 1; % Number of generations between reports

GAP.dc_alg = 3; % Diversity control algorithm 3
% GAP.dc_nt = 10; % Diversity control test population size (for algorithm 4)
GAP.sl_alg = 1; % Activate roulette wheel selection
GAP.dt_alg = 3; % The parent to be replaced is determined via the tournament based on↙
the aggregate fitness value
GAP.mc_alg = 6; % Set the crossover method as random
GAP.rs_fea = 0.5; % Fraction of generations on which to execute the random search↙
algorithm

% Plotting parameters
% OBJECTIVE PLOT
GAP.op_list = [1,2,3]; % objectives list for objective plots
GAP.op_style = [1,1,1];
GAP.op_sign = [-1,-1,-1];
GAP.dp_type = 2;

% PARETO PLOT (1)
GAP.pp_list = [1,2]; % objectives list for Pareto plot
GAP.pp_style = [1,1,1];
GAP.pp_xl = 'Curing time (s)';
GAP.pp_yl = 'Max. gradient of degree of cure AGP (1/mm)';
GAP.pp_sign = [-1,-1,-1]; % sign of fitness for each objective
% (1=positive,-1=negative)
GAP.pp_axis = []; % axis limits for Pareto plot

% PARETO PLOT (2)
GAP.pp_list2 = [1,3]; % objectives list for Pareto plot
GAP.pp_style2 = [1,1,1];
GAP.pp_xl2 = 'Curing time (s)';
GAP.pp_yl2 = 'Max. gradient of temperature AGP (°C/mm)';
GAP.pp_sign2 = [-1,-1,-1]; % sign of fitness for each objective
% (1=positive,-1=negative)
GAP.pp_axis2 = []; % axis limits for Pareto plot

% PARETO PLOT (3)
GAP.pp_list3 = [2,3]; % objectives list for Pareto plot
GAP.pp_style3 = [1,1,1];
GAP.pp_xl3 = 'Max. gradient of degree of cure AGP (1/mm)';
GAP.pp_yl3 = 'Max. gradient of temperature AGP (°C/mm)';
GAP.pp_sign3 = [-1,-1,-1]; % sign of fitness for each objective
% (1=positive,-1=negative)
GAP.pp_axis3 = []; % axis limits for Pareto plot

% Gene setup
%                CT1    CT2 t_CT1
%           gene   1      2     3
GAP.gd_min = [    80    140    10   ];
```

```
GAP.gd_max = [    94    150   240   ];
GAP.gd_type = [    1      1     1   ];
GAP.gd_cid = [     1      1     1   ];

% Perform optimization
[P,GAS,best,f]= gaoptimize(@cure_fitness_3obj_3param_AGP_custom_GAP,GAP);

% Plot final solutions
figure()
plot(best(3,:),best(1,:),'x');
axis([10 240 80 94]);
ylabel('Constant temperature 1 (°C)');
xlabel('Time in CT1 (min)');
axis square;
title('Pareto-Optimal Set');

figure()
plot(best(2,:),best(1,:),'x');
axis([140 150 80 94]);
ylabel('Constant temperature 1 (°C)');
xlabel('Constant temperature 2 (°C)');
axis square;
title('Pareto-Optimal Set');

% Measure and save the elapsed time
running_time = toc; % [s]
```

APPENDIX D – MATLAB FUNCTION THAT COMPUTES THE FITNESS OF A CURE SCHEDULE FOR THE MULTI-OBJECTIVE GENETIC ALGORITHM (GA) OPTIMIZATION

```
function [f] = cure_fitness_3obj_3param_AGP_custom_GAP(x)
% tic;
disp("Start of fitness computation");

import com.comsol.model.util.*
% Computes the fitness of the chromosome cure parameters (genes) using
% COMSOL LiveLink with MATLAB

% Optimization objectives:
%   1 - (min) curing time;
%   2 - (min) max grad alpha AGP;
%   3 - (min) max grad T AGP.

% Optimization restrictions:
%   1 - hist max T < 155 °C;
%   2 - last min alpha >= 85.4%.

t_CT2 = 240;    % Preliminar time in CT2 [min] -> 4h (it may be shorter if the min↙
degree of cure is rechead sooner)
r = 3;          % Heating rate [°C/min]
T_deg = 155;    % Temperature of degradation start [°C]
alpha_min_req = 0.854;  % Minimum alpha required at the end of the cure
alpha_min_req2 = 0.800; % A second value for the minimum alpha used to improve the↙
efficiency of the algorithm

% Compute COMSOL simulation parameters
CT1 = x(1);     % Optimization parameter 1 - Constant Temperature 1 [°C]
CT2 = x(2);     % Optimization parameter 2 - Constant Temperature 2 [°C]
t_CT1 = x(3);   % Optimization parameter 3 - Time in CT1 [min]

t_ramp1 = (CT1-20)/r;   % Time in heating ramp from room T to CT1 [min]
t_ramp2 = (CT2-CT1)/r;  % Time in heating ramp from room CT1 to CT2 [min]

fprintf('\nConstant Temperature 1 = %d °C\n',CT1);
fprintf('Constant Temperature 2 = %d °C\n',CT2);
fprintf('Time in CT1 = %d min\n',t_CT1);
% fprintf('Time in CT2 = %d min\n',t_CT2);
% fprintf('Curing time = %d s = %.1f min\n',t_cure,t_cure/60);

% Create an object to the simulation model exported to the COMSOL Multiphysics Server
model = mphopen('C:\Users\User\Documents\COMSOL\COMSOL 5.6\CURE OPTIMIZATION\GENETIC↙
ALGORITHM\COMSOL_GA_cure_optimization');
%{
If you run a model in a loop you do not need to store the model history because it↙
contains
 the same operations as  many times as you have iterations in the loop. The solution↙
is to
disable the history recording, as done below
%}
model.hist.disable;

% Set up COMSOL simulation parameters
model.param.set('CT1', CT1+"+273[K]", 'Constant temperature 1');        %[°C]
model.param.set('CT2', CT2+"+273[K]", 'Constant temperature 2');        %[°C]
model.param.set('t_CT1', t_CT1+"[min]", 'Duration of temperature 1'); %[min]
model.param.set('t_CT2', t_CT2+"[min]", 'Duration of temperature 2'); %[min]
model.param.set('t_ramp1', t_ramp1+"[min]", 'ramp duratin 1');         %[min]
model.param.set('t_ramp2', t_ramp2+"[min]", 'ramp duration 2');        %[min]

% Run the model and show progress
```

```
ModelUtil.showProgress(true);
model.study('std1').run();

%% COMSOL simulation results
probe1 = mphtable(model,'tbl1');
last_alpha_min = probe1.data(end,3); % Last mininum degree of cure within the sample↙
[1];
T_max = max(probe1.data(:,4)); % Historical maximum T within the sample %[°C]

fprintf('\nMaximum temperature = %.1f °C\n',T_max);
fprintf('Mininum degree of cure in the end = %.4f\n',last_alpha_min);

if T_max < T_deg && last_alpha_min >= alpha_min_req
    % Compute the duration of the second plateaou (t_CT2) in min
    t_cure_sim = probe1.data(end,1); %[s]
    t_CT2 = ceil(t_cure_sim/60 - t_ramp1 -...
        t_CT1 - t_ramp2); %[min]

    % Compute total cure duration
    if t_CT2 >= 0
        t_cure = (t_ramp1 + t_CT1 + t_ramp2 + t_CT2)*60;  %[s]
    else
        t_CT2 = 0;
        t_ramp2 = ceil(t_cure_sim/60 - t_ramp1 -...
        t_CT1); %[min]
        t_cure = (t_ramp1 + t_CT1 + t_ramp2)*60;  %[s]
    end
    fprintf('Time in CT2 = %d min\n',t_CT2);

    % Compute the objectives
    f(1,1) = -t_cure; % curing time [s]
    f(2,1) = -max(probe1.data(:,5));  % Historical maximum gradient of degree of cure↙
After Gelation Point within the sample (AGP) [1/mm]
    f(3,1) = -max(probe1.data(:,6));  % Historical maximum gradient of temperature AGP↙
within the sample [degC/mm]
    fprintf('\nCuring time = %d s = %.1f min\n',-f(1,1),-f(1,1)/60);
    fprintf('Max. gradient of degree of cure AGP = %.3d 1/mm\n',-f(2,1));
    fprintf('Max. gradient of temperature AGP = %.3d °C/mm\n',-f(3,1));
else
    if T_max < T_deg && last_alpha_min >= alpha_min_req2
        f(1,1) = -31500;  % curing time higher than the recommended by the↙
manufacturer (with r = 3°C/min) [s]: 4h (@80°C) + 20 min (ramp1) + 4h (@140°C)+ 20 min↙
(ramp2) = 31200 s
        f(2,1) = -1; % Random extremely high grad_alpha_AGP [1/mm]
        f(3,1) = -10; % Random extremely high grad_T_AGP [°C/mm]
    else
        f(1,1) = -38000;  % curing time higher than the recommended by the↙
manufacturer (with r = 3°C/min) [s]: 4h (@80°C) + 20 min (ramp1) + 4h (@140°C)+ 20 min↙
(ramp2) = 31200 s
        f(2,1) = -1.2; % Random extremely high grad_alpha_AGP [1/mm]
        f(3,1) = -12; % Random extremely high grad_T_AGP [°C/mm]
    end
end

end
```

APPENDIX E – RESULTS OF THE MANUFACTURER'S RECOMMENDED CURE SCHEDULE, CONVERSION RATE DRIVEN STRATEGY AND MULTI-OBJECTIVE GENETIC ALGORITHM OPTIMIZATION

Method	CT1 (°C)	CT2 (°C)	Time in CT1 (min)	Time in CT2 (min)	Min. alpha - end of the cure	Max. T during the cure (°C)	Cure time (min)	Cure time (s)	Max. grad. of alpha AGP (1/mm)	Max. grad. of T AGP (°C/mm)
MRC	80	140	240	480	85.4%	140	760	45600	1.450400E-02	1.758738E+00
GA	84	149	32	15	85.5%	154	90	5400	3.613083E-02	4.028064E+00
GA	90	145	32	25	85.5%	143	99	5920	3.264634E-02	3.181300E+00
GA	80	149	41	15	85.5%	152	99	5940	3.166027E-02	3.392312E+00
GA	82	148	41	17	85.5%	145	101	6040	2.793968E-02	2.847233E+00
GA	81	148	41	17	85.5%	147	101	6040	2.975206E-02	3.084031E+00
GA	82	150	47	17	85.5%	146	107	6440	2.193098E-02	2.185444E+00
GA	84	149	47	19	85.5%	146	109	6540	1.937290E-02	1.683725E+00
GA	82	150	57	19	85.5%	147	119	7160	1.541973E-02	1.349670E+00
GA	82	149	57	20	85.5%	146	120	7200	1.541972E-02	1.349673E+00
GA	82	148	57	21	85.5%	145	121	7240	1.541972E-02	1.349672E+00
GA	83	148	57	21	85.4%	145	121	7240	1.876637E-02	1.228392E+00
GA	82	147	57	22	85.5%	145	121	7280	1.541973E-02	1.349670E+00
GA	81	150	61	18	85.5%	147	122	7340	1.417046E-02	1.343327E+00
GA	83	147	57	23	85.5%	145	122	7340	1.876637E-02	1.228361E+00
GA	82	150	61	19	85.4%	147	123	7400	1.655796E-02	1.240613E+00
GA	82	148	61	21	85.5%	145	125	7480	1.655795E-02	1.240615E+00
GA	81	146	61	24	85.5%	144	127	7620	1.417045E-02	1.343325E+00
GA	82	146	61	24	85.5%	144	127	7620	1.655795E-02	1.240617E+00

GA	81	150	65	19	85.5%	147	127	7640	1.439326E-02	1.263197E+00
GA	82	145	61	26	85.4%	143	129	7720	1.655795E-02	1.240615E+00
GA	81	146	65	24	85.4%	144	131	7860	1.439326E-02	1.263195E+00
GA	82	144	61	29	85.5%	143	131	7880	1.655796E-02	1.240613E+00
GA	82	143	61	32	85.5%	142	134	8040	1.655795E-02	1.240617E+00
GA	80	150	76	20	85.5%	147	139	8360	1.369253E-02	1.446501E+00
GA	80	148	76	22	85.5%	145	141	8440	1.369253E-02	1.446497E+00
GA	82	141	61	42	85.4%	141	143	8600	1.655796E-02	1.240046E+00
GA	80	144	76	29	85.5%	143	146	8780	1.369253E-02	1.446501E+00
GA	80	143	76	32	85.5%	142	149	8940	1.369253E-02	1.446499E+00
GA	80	142	76	36	85.4%	141	153	9160	1.369253E-02	1.446496E+00
GA	83	140	57	67	85.4%	140	164	9840	1.876637E-02	1.208578E+00
GA	82	140	61	68	85.4%	140	169	10140	1.655795E-02	1.240050E+00
CRD	94	150	32	21	85.5%	152	96	5780	4.524162E-02	4.996324E+00
CRD	93	150	34	21	85.5%	148	98	5900	4.320814E-02	4.646478E+00
CRD	91	150	36	20	85.5%	147	99	5960	3.775106E-02	3.702488E+00
CRD	92	150	35	21	85.5%	147	99	5960	4.045397E-02	4.170036E+00
CRD	90	150	38	20	85.5%	147	101	6080	3.537003E-02	3.319597E+00
CRD	94	145	32	28	85.5%	152	102	6100	4.524162E-02	4.996324E+00
CRD	89	150	39	20	85.5%	147	102	6140	3.241552E-02	2.843575E+00
CRD	93	145	34	27	85.4%	148	103	6160	4.320814E-02	4.646478E+00
CRD	92	145	35	27	85.5%	144	104	6220	4.045397E-02	4.170036E+00
CRD	88	150	41	20	85.5%	147	104	6260	2.988124E-02	2.464465E+00
CRD	91	145	36	27	85.4%	143	105	6280	3.775106E-02	3.702488E+00
CRD	86	150	44	19	85.5%	147	106	6380	2.420268E-02	1.663500E+00

CRD	87	150	43	20	85.5%	147	106	6380	2.732556E-02	2.088699E+00
CRD	89	145	39	26	85.4%	143	107	6400	3.241552E-02	2.843575E+00
CRD	90	145	38	27	85.5%	143	107	6400	3.537003E-02	3.319597E+00
CRD	84	150	47	18	85.5%	146	108	6500	1.937288E-02	1.683724E+00
CRD	85	150	46	19	85.5%	147	108	6500	2.164025E-02	1.543725E+00
CRD	88	145	41	26	85.5%	143	109	6520	2.988124E-02	2.464465E+00
CRD	83	150	48	18	85.5%	146	109	6560	1.967349E-02	1.832096E+00
CRD	82	150	50	17	85.5%	146	110	6620	1.946504E-02	1.898448E+00
CRD	87	145	43	26	85.5%	143	111	6640	2.732556E-02	2.088699E+00
CRD	86	145	44	26	85.5%	143	112	6700	2.420268E-02	1.663500E+00
CRD	81	150	52	17	85.4%	146	112	6740	1.949057E-02	1.982924E+00
CRD	85	145	46	25	85.5%	143	113	6760	2.164025E-02	1.543725E+00
CRD	80	150	53	17	85.5%	147	113	6800	2.043112E-02	2.154546E+00
CRD	83	145	48	24	85.4%	143	114	6820	1.967349E-02	1.832096E+00
CRD	84	145	47	25	85.5%	143	114	6820	1.937288E-02	1.683724E+00
CRD	82	145	50	24	85.5%	143	116	6940	1.946504E-02	1.898448E+00
CRD	80	145	53	23	85.5%	143	118	7060	2.043112E-02	2.154546E+00
CRD	81	145	52	24	85.5%	143	118	7060	1.949057E-02	1.982924E+00
CRD	94	140	32	70	85.4%	152	142	8520	4.524162E-02	4.996324E+00
CRD	92	140	35	68	85.4%	143	143	8580	4.045397E-02	4.170036E+00
CRD	91	140	36	69	85.4%	140	145	8700	3.775106E-02	3.702488E+00
CRD	93	140	34	71	85.4%	148	145	8700	4.320814E-02	4.646478E+00
CRD	89	140	39	68	85.4%	140	147	8820	3.241552E-02	2.843575E+00
CRD	90	140	38	70	85.4%	140	148	8880	3.537003E-02	3.319597E+00
CRD	87	140	43	67	85.4%	140	150	9000	2.732556E-02	2.088699E+00

CRD	88	140	41	69	85.4%	140	150	9000	2.988124E-02	2.464465E+00
CRD	86	140	44	67	85.4%	140	151	9060	2.420268E-02	1.663500E+00
CRD	83	140	48	64	85.4%	140	152	9120	1.967349E-02	1.832096E+00
CRD	85	140	46	66	85.4%	140	152	9120	2.164025E-02	1.543725E+00
CRD	84	140	47	66	85.4%	140	153	9180	1.937288E-02	1.683724E+00
CRD	82	140	50	64	85.4%	140	154	9240	1.946504E-02	1.898448E+00
CRD	80	140	53	62	85.4%	140	155	9300	2.043637E-02	2.154546E+00
CRD	81	140	52	63	85.4%	140	155	9300	1.949057E-02	1.982924E+00

ANNEX A – EPOXY RESIN'S SPECIFIC HEAT CAPACITY (RABEARISON, 2009)

α	T $[K]$	c_p $[J/(kg.K)$
0	293	1902.5
1	293	1401.25
0	303	1928.75
1	303	1445.625
0	313	1955
1	313	1490
0	323	1981.25
1	323	1534.375
0	333	2007.5
1	333	1578.75
0	343	2033.75
1	343	1623.125
0	353	2060
1	353	1667.5
0	363	2086.25
1	363	1711.875
0	373	2112.5
1	373	1756.25
0	383	2138.75
1	383	1800.625
0	393	2165
1	393	1845
0	403	2191.25
1	403	1889.375

α	T $[K]$	c_p $[J/(kg.K)$
0	413	2217.5
1	413	2217.5
0	423	2243.75
1	423	2243.75
0	433	2270
1	433	2270
0	443	2296.25
1	443	2296.25
0	453	2322.5
1	453	2322.5
0	463	2348.75
1	463	2348.75
0	473	2375
1	473	2375
0	483	2401.25
1	483	2401.25
0	493	2427.5
1	493	2427.5
0	503	2453.75
1	503	2453.75
0	513	2480
1	513	2480
0	523	2506.25
1	523	2506.25

ANNEX B – EPOXY RESIN'S THERMAL CONDUCTIVITY (RABEARISON, 2009)

α	T [K]	k [$W/(m.K)$]
0	293	0.188
1	293	0.350099
0	303	0.188
1	303	0.347372
0	313	0.188
1	313	0.344645
0	323	0.188
1	323	0.341918
0	333	0.188
1	333	0.339191
0	343	0.188
1	343	0.336464
0	353	0.188
1	353	0.333737
0	363	0.188
1	363	0.33101
0	373	0.188
1	373	0.328283
0	383	0.188
1	383	0.325556
0	393	0.188
1	393	0.322829
0	403	0.188
1	403	0.320102

α	T [K]	k [$W/(m.K)$]
0	413	0.188
1	413	0.317375
0	423	0.188
1	423	0.314648
0	433	0.188
1	433	0.311921
0	443	0.188
1	443	0.309194
0	453	0.188
1	453	0.306467
0	463	0.188
1	463	0.30374
0	473	0.188
1	473	0.301013
0	483	0.188
1	483	0.298286
0	493	0.188
1	493	0.295559
0	503	0.188
1	503	0.292832
0	513	0.188
1	513	0.290105
0	523	0.188
1	523	0.287378